eman ta zabal zazu
Universidad del País Vasco
Euskal Herriko Unibertsitatea
KIMIKA ZIENTZIEN FAKULTATEA
FACULTAD DE CIENCIAS QUÍMICAS
CFM
Materials Physics Center
Centro de Física de Materiales

Dynamics of biological and non-biological aqueous solutions – Evidence of coupling between the motions of water and solutes

PhD Thesis Submitted by

Izaskun Combarro Palacios

to the

University of the Basque Country

Supervised by

Dr. *Silvina Cerveny Murcia*

Dr. *Ángel Alegría Loinaz*

Donostia – San Sebastián, May 2017

ABSTRACT

Proteins are the main structural and functional polymers in living organisms. They fulfill a wide range of functions due to their structural heterogeneity and therefore describing the functions of proteins is equivalent to describing several biological phenomena. Briefly some proteins constitute the structure of tissues, while others catalyze the metabolic reactions and carry vitamins, minerals, oxygen and fuels. Proteins are synthesized as a sequence of amino acids joined linearly and they adopt a complex three-dimensional structure when performing their biological functions. Nevertheless, the "working protein" consists not only of the folded chain of amino acids; they are surrounded by a hydration shell and embedded in a bulk solvent. The hydration shell of a protein is very important for the conformation, the three-dimensional structure and for the functionality. In fact, proteins lack biological activity in absence of sufficient hydration water. In part, the necessity of the surrounding solvent to carry the functions has been explained by the plasticizing effect on proteins, which leads to the increase in flexibility of the protein backbone, and therefore it can acquire its ultimate and biologically active structure. Therefore, to properly understand how a protein works, it is essential to first clear up the dynamics of the solvent molecules surrounding protein, mainly water, and how this water affects the dynamics of the latter.

The number of studies related with hydrated proteins is numerous but despite of this, the role of water is not clear enough. Water fluctuations could "slave" the protein dynamics or the water could facilitate the protein dynamics. Many experimental and computational studies have demonstrated that, above the glass transition temperature, the protein motions follow the same temperature dependence as the surrounding water molecules being the fluctuations of the protein about 10^3 - 10^6 times slower than that of water. According to this, a coupling between the protein and the solvent dynamics is observed, describing the motion of proteins as being "slaved" to that of the solvents surrounding the protein molecules.

The major problem of the dynamical studies on proteins is related to the low solubility degree of these macromolecules. Due to this, to obtain a proper protein solution, a large quantity of

water is necessary which crystallizes on cooling, masking the dielectric signal of the protein itself and hindering the dynamic study. Therefore, most studies are carried out on hydrated powders instead of well-diluted solutions which represent more realistic cases.

In this thesis, we try to overcome this problem by studying small peptides since they share many properties with proteins but they also have higher solubility. Among the 20 amino acids in animal proteins, lysine is the most soluble one and, in aqueous solutions does not crystallize up to high water contents. Therefore, lysine was chosen as the basic component of the peptides analyzed in this work.

We first report the dynamical results of ε-polylysine (25 – 35 lysine residues) aqueous solutions. This molecule has a precise conformation in aqueous solutions as proteins have. Our study allow us to develop a reliable methodology to analyze the dynamics of ε-polylysine in aqueous solutions even in the case that a strong conductivity masks the relevant dynamical processes. Moreover, this methodology can be used to analyze the response of all the materials we analyze in this thesis (mainly peptides, synthetic polymers and polysaccharides) as well as the dynamics of proteins. The dynamical results for ε-polylysine aqueous solutions are presented and discussed in the Chapter IV. Due to the high solubility of this molecule, the results are reported for solutions over a wide range of water contents and different pH values.

Then, in the Chapter V, we analyze the crucial role of water in the dynamics of *n*-lysine oligomers (n = 3, 4 and 10). Data for ε-PLL, n = 32, are also included for comparison. Although these small peptides do not show any biological function, they adopt a specific conformation and studying their dynamics in aqueous solutions it is possible to obtain additional insights for the dynamics of protein solutions. The results presented here show that the previously observed coupling between protein and solvent dynamics is preserved even if the protein is replaced by short chains of these single amino acids. This implies that solvent slaved motions are not unique for proteins, and they can be also present in all types of solute molecules which need the movements of the surrounding solvent to overcome the enthalpy barrier to relax.

Finally, in the Chapter VI, we studied whether the slaving phenomenon is only observed in biological solutions or it can be also observed in non-biological systems as synthetic polymers or polysaccharides. We analyse what are the main characteristics that are necessary to observe the slaving behaviour and we concluded that one important characteristic is related to the water concentration dependence of the glass transition temperature. Based on this, we have chosen to study poly(vinyl pyrrolidone), a synthetic polymer with a high T_g value in the dry state, and some polysaccharides as sucrose and dextran. In all these cases, we find that the slaving behaviour is clearly observed. According to this finding, we can conclude that the "slaving behaviour", previously observed in proteins can be extended to non-biological system.

Key-words: Water – peptide / protein dynamics, slaving phenomenon, water plasticization, glass transition temperature, lysine, *n*-lysine oligomers, ε-polylysine, synthetic polymers, PVP, polysaccharides, sucrose and dextran.

RESUMEN

Las proteínas son los principales polímeros estructurales y funcionales en los seres vivos. Cumplen un amplio abanico de funciones gracias a su gran heterogeneidad estructural. Describir las funciones de las proteínas equivale a describir en términos moleculares todos los fenómenos biológicos pero, brevemente, podríamos decir que algunas proteínas constituyen la estructura de los tejidos, mientras otras funcionan en la catálisis de reacciones metabólicas o el transporte de vitaminas, minerales, oxígeno y combustibles. Las proteínas son sintetizadas como una secuencia de aminoácidos unidos en una estructura lineal, pero adoptan estructuras tridimensionales complejas para realizar las funciones biológicas previamente mencionadas. La mayoría de los libros de texto muestran las proteínas en una única conformación, sin su envoltura de hidratación y sin el disolvente en el que están disueltas, y mucho menos se mencionan las fluctuaciones de estos. Pero lo cierto es que las proteínas son sistemas dinámicos que interactúan fuertemente con su entorno. De hecho, el propio disolvente es el que potencia los movimientos y los cambios de conformación de la proteína, aportando flexibilidad a la estructura de la molécula para que esta pueda adquirir la estructura final y biológicamente activa. De acuerdo con esto, para comprender correctamente cómo funciona una proteína, primeramente, es esencial primero comprender la dinámica de las moléculas del solvente que la rodean, y cómo este afecta a la dinámica de la proteína.

El número de estudios relacionados con la dinámica de las proteínas es numeroso, sin embargo, existe una gran discusión en la literatura, ya que hasta la fecha no está claro si las fluctuaciones del solvente (principalmente agua) gobiernan la dinámica de las proteínas, o si tanto la proteína y la dinámica del agua se están afectando mutuamente. Muchos trabajos experimentales y computacionales han demostrado que por debajo de la temperatura de transición vítrea (T_g), los movimientos de la proteína siguen la misma dependencia con la temperatura que las moléculas de agua que la rodean, aunque 10^3 - 10^6 veces más lentos con respecto al agua. De acuerdo con estos resultados, se puede definir un acoplamiento entre la dinámica de la proteína y la dinámica del disolvente, describiendo el movimiento de las proteínas como “esclavizado’’ al movimiento del disolvente que las rodea.

El principal problema de los estudios que tratan la dinámica de las proteínas en soluciones acuosas viene dado por el grado de solubilidad de estas macromoléculas. Su escasa capacidad para disolverse en el medio solvente hace que para adquirir una adecuada solución proteica sea necesaria una gran cantidad de agua, la cual cristaliza a bajas temperaturas, enmascarando la señal dieléctrica de la propia proteína y dificultando el estudio dinámico. Es por ello que para evitar esta cristalización, la mayoría de los estudios se llevan a cabo con proteínas muy poco hidratadas (lo que se conoce como polvos hidratados) en lugar de soluciones proteicas diluidas. Sin embargo, los estudios dinámicos de polvos hidratados no representan casos realistas, y por lo tanto, no suponen un medio para el estudio y entendimiento adecuado sobre su funcionalidad.

Con el fin de resolver este problema, nosotros proponemos estudiar péptidos en lugar de grandes macromoléculas como son las proteínas, ya que estos comparten muchas propiedades con las proteínas pero con la ventaja de que su solubilidad es mayor. Entre los 20 aminoácidos que forman parte de las proteínas, la lisina es el más soluble, y al disolverlo en agua las soluciones no muestran cristalización hasta altos grados de hidratación. Por ello, este amino acido fue elegido como el componente básico de los péptidos analizados en este trabajo.

En primer lugar se presentan los resultados de la dinámica de las soluciones acuosas de ε-polilisina (ε-PLL, compuesto por 25 – 35 residuos de lisina). Esta molécula, al igual que las proteínas, adquiere una conformación precisa en soluciones acuosas. Este estudio nos ha permitido desarrollar una metodología fiable para analizar la dinámica de la ε-polilisina en soluciones acuosas, incluso en los casos en los cuales una fuerte conductividad enmascara los procesos dinámicos más relevantes. Esta metodología es útil para analizar la respuesta dieléctrica de todos los materiales que analizamos en esta tesis, así como la dinámica de las proteínas. Los resultados para las soluciones acuosas de ε-polilisina a distintos contenidos de agua y distintos valores pH son presentados y discutidos en el Capítulo IV.

Posteriormente, en el Capítulo V, analizamos el papel crucial del agua en la dinámica de distintos oligómeros de *n*-lisina (siendo n = 3, 4, 10). En este capítulo también se incluyen los resultados obtenidos para la ε-polilisina a modo de comparativa. Aunque estos pequeños péptidos no muestran ninguna función biológica, sí adoptan una conformación específica y al

estudiar su dinámica en soluciones acuosas, es posible obtener información adicional sobre la dinámica de las soluciones proteicas. Los resultados presentados en este capítulo muestran que el acoplamiento previamente observado entre la dinámica de la proteína y la del disolvente se mantiene incluso si la proteína es reemplazada por cadenas cortas de un único aminoácido. Esto implica que los movimientos del soluto "esclavos'' con el disolvente no son únicos para las proteínas, y que también están presentes en aquellas moléculas de soluto que necesitan la dinámica en el disolvente circundante para superar la barrera de entalpía y así relajar.

Por último, en el capítulo VI, estudiamos si el fenómeno de "esclavización'' es exclusivo de soluciones biológicas o si también puede observarse en sistemas no biológicos como son los polímeros sintéticos o los polisacáridos. Analizamos cuáles son las principales características necesarias para observar este comportamiento de "esclavitud'' y concluimos que una característica importante está relacionada con la dependencia de la temperatura de transición vítrea al contendido de agua. En base a este hecho, decidimos estudiar poli(vinilpirrolidona) (PVP), un polímero sintético con un alto valor de T_g en estado de no hidratación, y algunos polisacáridos como la sacarosa y el dextrano. En todos estos casos, encontramos que el comportamiento de "esclavitud'' se observa claramente, de manera que de acuerdo con este hallazgo, podemos concluir que el fenómeno de "esclavización'', previamente observado en las proteínas puede extenderse a sistemas no biológico.

Palabras clave: Dinámica de agua y péptidos / proteínas, dinámica "esclavizada", el agua como plastificante, lisina, oligómeros de lisina, ε-polylysina, polímeros sintéticos, PVP, polisacáridos, sacarosa y dextrano.

Table of Contents

Page

CHAPTER V: COUPLING BETWEEN THE MOTIONS OF WATER AND PEPTIDES

CHAPTER VI: WATER PLASTICIZATION VS SLAVING PHENOMENA

CHAPTER VII: CONCLUDING REMARKS

APPENDIX

CHAPTER I

INTRODUCTION TO THE BASIS OF LIFE PROCESSES: AMINO ACIDS, PROTEINS AND WATER

In this chapter, we introduce the most relevant concepts of proteins. We analyze the structure of amino acids and their linking mechanism for protein synthesis, and we describe ε-polylysine, the main molecule studied in this thesis. Then, due to the importance of water in protein functions, we describe the structure of the water molecule and its different physical states, and we conclude with a brief summary of the main benefits of its analogous properties.

1. AMINO ACIDS

Amino acids are the building blocks of proteins, and hence protein structure and reactivity are dependent on the sequence of the incorporated amino acids. There are approximately 300 amino acids present in various animal, plant and microbial systems, but only 20 amino acids are encoded by DNA to appear in proteins. Those 20 amino acids are simultaneously alike and different, as they all share a common backbone but have different side chains, each with different chemical properties. Each amino acid has a central carbon, called the α-carbon, to which four different groups are attached: a basic amino group (NH_2), an acidic carboxyl group (COOH), a hydrogen atom (H) and a distinctive side chain (R)[1] (see Figure I. 1).

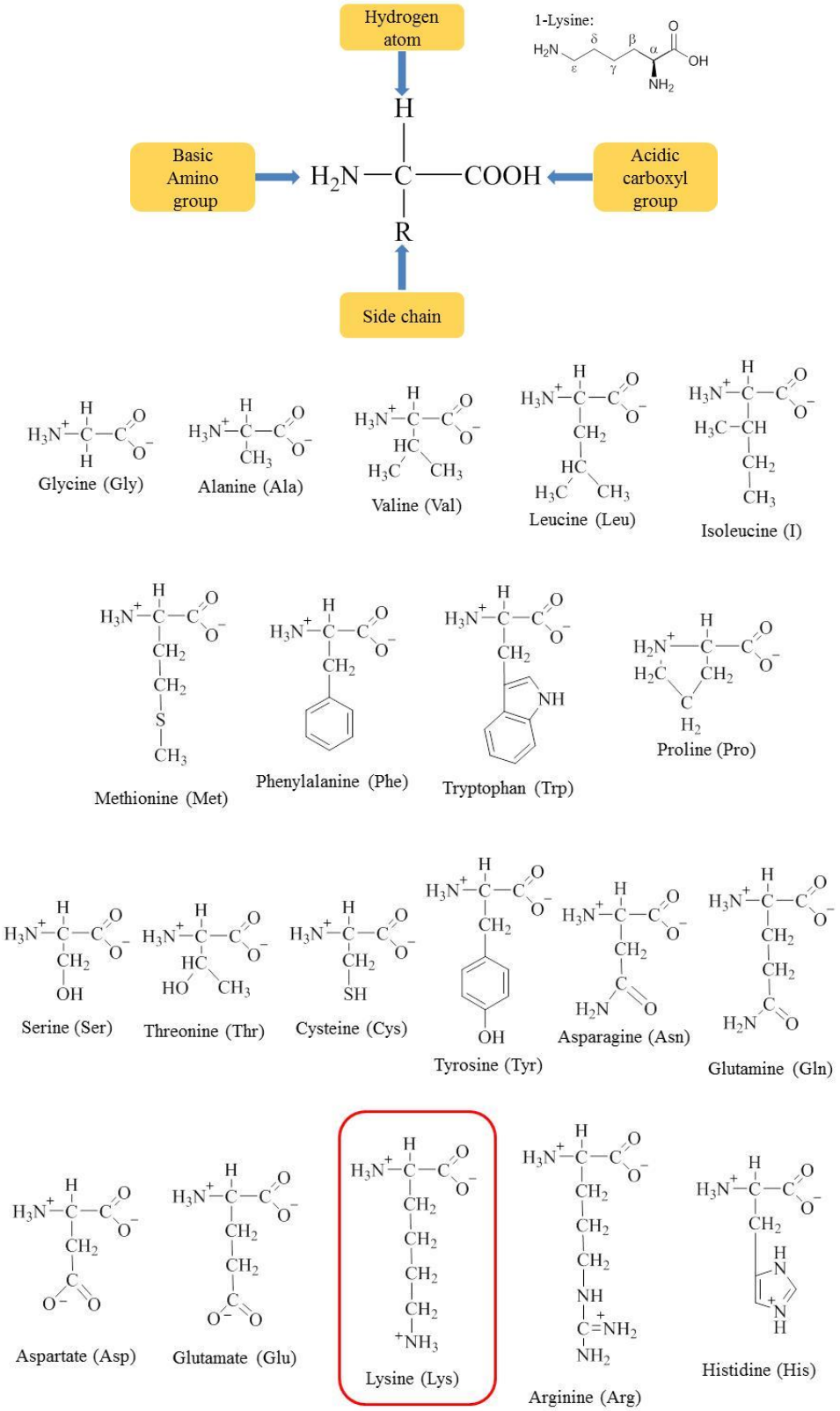

Figure I. 1. Molecular structures of amino acids, containing an α-amino group, an α-carboxyl group and a side chain bound to the α-carbon atom. The side chain of lysine, with a red border, consists of a long flexible backbone of four CH_2 groups and a terminal ε-amino group.

As mentioned, the properties of each amino acid are dependent on its side chain; therefore, the 20 amino acids in proteins encoded by DNA are usually classified according to the charge state of their side chain functional groups[1]. For example, lysine, which contains a protonated amino group attached to the terminal ε-carbon of the side chain, is a basic amino acid at neutral pH and therefore is positively charged[1]. Amino acids can also be classified based on the polarity (hydrophilicity) of their side chains. According to this second classification, lysine is defined as an hydrophilic amino acid due to its polar side chain, which includes a nitrogen atom involved in hydrogen bonding to water and other polar groups[1].

Lysine, which is the building block of the peptides studied in this thesis, is considered an essential amino acid for humans because it cannot be synthesized in the human body, so it has to be supplied by nutrition[2-4]. Its lack in the human body can generate some problems, as it is necessary for many biological processes:

- Lysine is the first limiting amino acid needed to digest food proteins; with too little, proteins in food are not properly assimilated by the body[4].
- It builds proteins in the muscles and collagen, the main component of connective tissue. The strength and elasticity of ligaments and tendons depend on lysine. Moreover, it is an essential part of the prevention and treatment of osteoporosis because it promotes the absorption of calcium from food and its incorporation into bone tissue[4].
- Lysine intercepts lipoprotein(a) (LP(a)) and prevents from depositing on arterial walls[4]. Therefore, this amino acid can reduce high blood pressure, one of the main causes of heart attacks and strokes.
- It inhibits the action of collagenase enzymes that dissolve the shell of the cancer constraining its metastasis. Thus, the use of lysine in combination with other substances can inhibit or block the spread of cancer[4].
- Lysine can enhance the secretion of thyroid hormones in the elderly, which helps to prevent senile immunodeficiency. This amino acid is very important for the efficient operation of the brain, and its deficiency may impair short-term memory and the ability to concentrate[4].
- On the other hand, lysine also plays a key role in several neurodegenerative human diseases such as Alzheimer's disease. It participates in a combination of hydrophobic and

electrostatic interactions that leads to the formation of protein aggregates: amyloid fibrils[5,6]. Thus, lysine promotes the reversion of the highly evolved biologically functional forms of proteins into an alternative and unwelcome structural state[7] that is believe to drive many neurodegenerative human diseases.

- Among more aesthetic purposes, lysine is used by bodybuilders for the combined effect of increasing muscle volume and strength, since it promotes the release of growth hormone[4]. Furthermore, scientists have linked the presence of lysine to the absorption of iron and zinc. This property has a positive effect on hair growth, and thus, lysine supplementation reduces the rate of hair loss and makes it thicker[4].

2. PROTEINS

In proteins, the α-carboxyl group of one amino acid is linked to the α-amino group of the next amino acid, forming an amide bond (also called peptide bond) and eliminating a water molecule during the reaction (see Figure I. 2). When the resulting molecules consist of between 2 and 50 amino acids, they are called peptides, whereas proteins are made up of 50 to 2000 amino acid residues[1]. As the mean molecular mass of an amino acid residue is approximately 110 Dalton units (Da), the molecular mass of proteins is between 5500 and 220,000 Da[1].

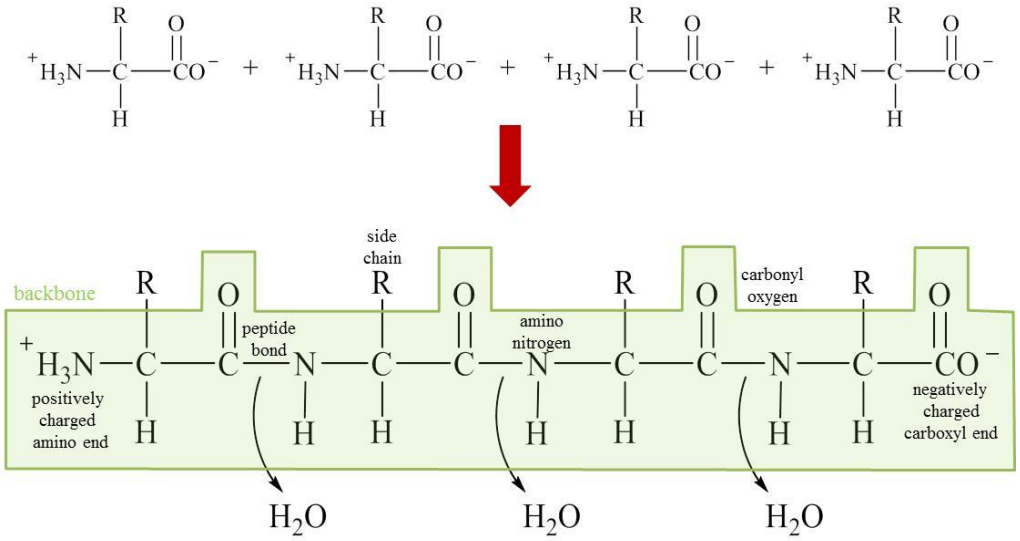

Figure I. 2. Amide bond or peptide bond formation.

As shown in Figure I. 2, in a protein, the backbone α-amino group of the N-terminal amino acid is positively charged, and the backbone α-carboxyl group of the C-terminal amino acid is negatively charged. All other backbone charges are neutralized by peptide bond formation. As the α-amino and α-carboxyl groups that form the backbone of the protein do not contribute to the charge of the protein, it depends only on the side chain functional groups of the amino acids, and the balance of side chain charges determines the net charge of the molecule. Based on the side chain functional group, proteins rich in lysine, such as the peptides studied in this thesis, are basic in solution due to protonated amino group positive charge[1].

Nevertheless, the importance of the amino acids side chains extends still further. They have a profound effect on the physical and chemical properties of proteins, as they have different tendencies to participate in interactions with each other and with water. These differences profoundly influence their contributions to protein stability and thus to the final folded 3D structure[8]. The four levels of protein structure are shown in Figure I. 3. The **primary structure** of a protein is simply its amino acid sequence. The final shape of a protein is encoded in this primary structure, so it is the sequence of amino acids in a protein that determines its final 3D structure[8]. The **secondary structure** of a protein refers to the three-dimensional structure. The most common secondary structures are α-helices or β-sheets. These two structures are stabilized by hydrogen bonding between backbone atoms; side chains are not involved in protein secondary structure[8]. The α-helix is a rod-like structure with the protein chain tightly coiled and the side chains of the amino acids extending outward from the axis of the spiral. Each oxygen of the carbonyl C=O group is hydrogen-bonded to the hydrogen of the amide C-N group that is four residues away along the same chain. Thus, there are on average 3.6 amino acid residues per turn of the helix, and the helix winds in a right-handed (clockwise) manner in almost all natural proteins[1].

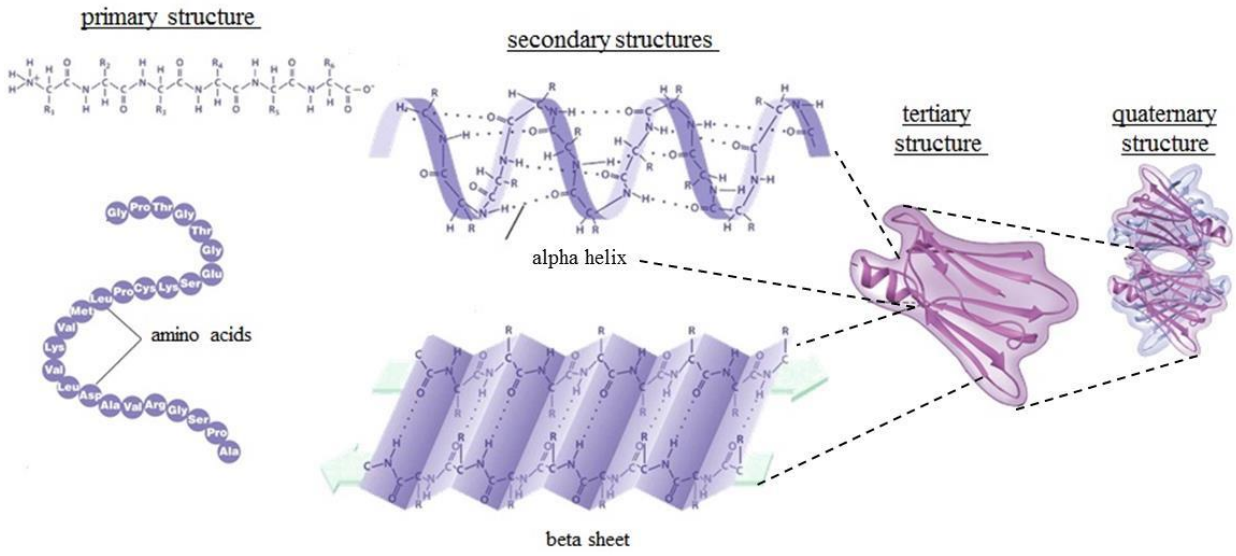

Figure I. 3. Typical protein representation from primary to quaternary structure.

If the hydrogen bonds are formed laterally between peptide bonds, the polypeptide sequences are arrayed parallel or antiparallel to one another in what is commonly called a β-pleated sheet[1]. The β-pleated sheet is an extended structure, as opposed to the coiled α-helix. The parallel β-sheet is characterized by two peptide strands running in the same direction, held together by hydrogen bonding between the strands[1]. If the polypeptide chains run in the opposite direction, they form an antiparallel β-sheet[1] (see differences in Figure I. 4). Each hydrogen bonded ring in a parallel β-sheet contains 12 atoms, and the hydrogen bonds holding together the two peptide chains are not at 180 degree angles to one another. However, in an antiparallel β-sheet, the number of atoms in the hydrogen bonded rings alternates between 14 and 10, and the hydrogen bonds are linear[9,10]. For this reason, antiparallel β-sheets are more stable than parallel β-sheets. Finally, a β-turn structure is usually defined by four amino acids turning back on themselves[10,11] (see Figure I. 4).

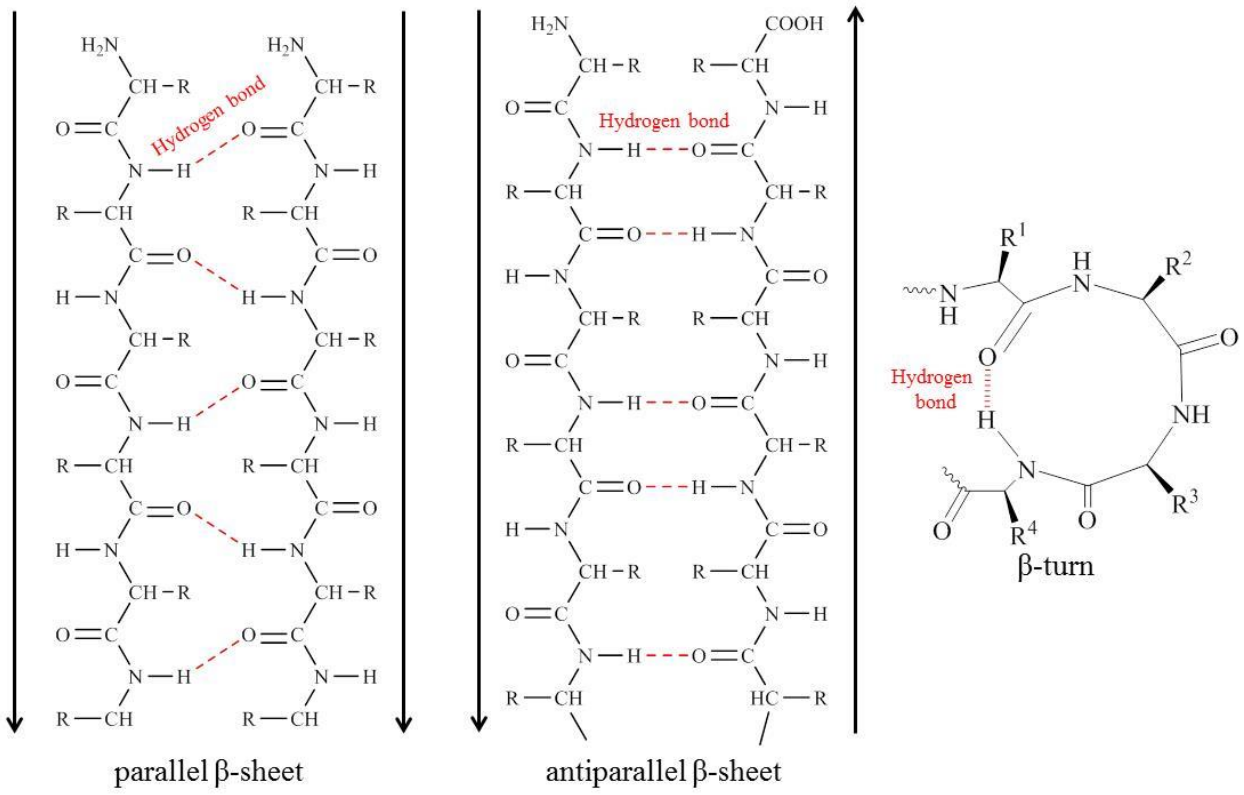

Figure I. 4. Parallel and antiparallel *β*-sheet and *β*-turn structures.

The **tertiary structure** refers to the three-dimensional, folded and biologically active conformation of a protein[1]. This structure reflects the overall shape of the molecule and generally consists of several smaller folded units[1]. Figure I. 3 shows a typical representation of the tertiary structure of a protein, which can be thought of as a collection of *α*-helices and strands of *β*-sheets connected by loops. It is stabilized mainly by a combination of many non-covalent interactions including hydrophobic forces, hydrogen bonds between polar atoms, ionic interactions between charged side chains and Van der Waals forces. Covalent sulfide bonds can also increase the stability of some proteins[1].

The **quaternary structure** of a protein refers to protein complexes composed of more than one protein chain, assembled to function as complex molecular machines[1]. Hemoglobin is a good example of a protein with quaternary structure, made up of two alpha chains and two beta chains[8].

The native state of a protein is defined as the conformation that possesses a minimum energy reached under folding conditions, in which the protein is stable and performs its action[12]. The folding amount or number of conformations necessary to find this minimum energy is huge: for example, for a protein consisting of 100 amino acids, if each amino acid can assume, for instance, three different conformations, there are 3^{100} or 1047 states available[12]. The native state is characterized by a low entropy because all protein atoms are maintained by mutual interaction in a well-defined geometry[12]. The intramolecular enthalpy is also relatively low because many attractive interactions are satisfied[12]. And finally, the solvent molecules surrounding the folded protein in its native state are not involved in interactions with the hydrophobic protein interior[12].

Upon alteration to the protein solution environment, such as an increase in temperature, change in the solvent pH or addition of a chemical denaturant, such as urea, to the protein solution, the protein unfolds and adopts a much more complex and heterogeneous ensemble of conformations, which is called the denatured or unfolded state[12]. Under strong unfolding conditions, a high percentage of the secondary structure is lost, and the unfolded state assumes a random coil structure[12] (see Figure I. 5). Nevertheless, it is difficult to define the structural properties of the denatured state, since it depends strongly on the unfolding conditions[12]. The denatured state is characterized by high conformational entropy because native interactions are lost, and the residues are free to assume a large set of arrangements[12]. The intramolecular enthalpy may also be higher because of the loss of native interactions[12], and the solvent molecules come into contact with hydrophobic parts of the protein chain that were buried in the native state[12]. This fact causes water molecules to assume more ordered conformations to minimize the contact with nonpolar groups, which reduces the entropy of the solvent relatively to the folded state[12]. Therefore, entropy is a driving force for folding, and when restoring the folding conditions, the spontaneous refolding of a denatured protein is usually initiated: the molecule is able to find the native state spontaneously. In essence, the denaturation is usually reversible, as the protein spontaneously returns to the original native structure when the folding conditions are restored; however, this case may not hold for some large multi-domain proteins, which cannot refold without assistance[12].

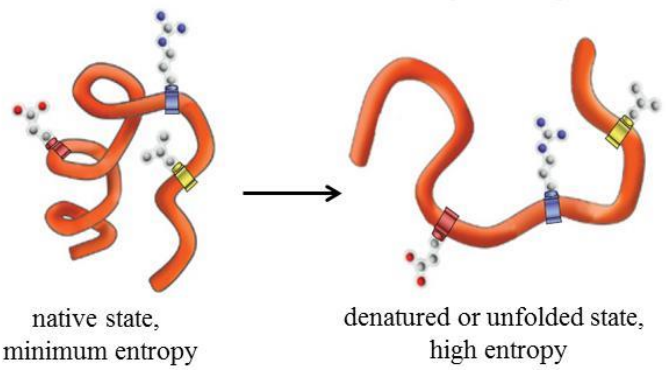

Figure I. 5. The protein acquires an unfolded conformation, going from a low- to a high-energy state.

The folded conformation of a protein is a very important factor, as this structure determines the protein function. According to their function, proteins can be categorized as **defense proteins** (specialized proteins involved in defending the body from antigens: they travel through the bloodstream to identify bacteria, viruses, and other foreign intruders; once antibodies detect these antigens, they immobilize them, and later, they are destroyed by white blood cells[13]), **transport proteins** (carrier proteins that move molecules from one place to another around the body: hemoglobin is an example, transporting oxygen through the blood via red blood cells[13]), **enzymes** or **catalyst proteins** (proteins that facilitate or speed up biochemical reactions: for example, pepsin is a digestive enzyme that works in the stomach to break down proteins in food[13]), **regulatory proteins** (cellular or physiological activity is regulated by some proteins as hormones: insulin is an example, regulating the glucose metabolism by controlling the blood-sugar concentration[14]), **nutrients and storage proteins** (found in many plant seeds, these proteins are vital for the growth and survival of the germinating seedling[14]), **contractile proteins** (proteins responsible for movement, providing cells and organisms with the ability to contract, to change conformation or to move about[14]), and **structural proteins** (proteins that serve as supporting filaments to give biological structures strength, support and protection, such as keratin and collagen: keratin strengthens protective coverings such as skin, hair, fingernails, feathers, horns, and beaks; collagen is the chief constituent of tendons and cartilage, as it is a fibrous protein with a very high tensile strength; leather, for example, consists of almost pure collagen[14]).

2.1. Introduction to ε-polylysine and comparison with proteins

The term polyamide covers a large variety of polymer compounds with their constituents linked by amide bonds[15]. They can be grouped into two categories: one group in which the polyamides consists of only one type of monomers, called homopolyamides (or homopolyamino acids if the building blocks are amino acids)[15-18], and another group that consists of polyamides with different constituents in their chains, for example, proteins[15,18-21].

To date, the number of amino acids and proteins discovered and synthetized is enormous. However, only four homopolyamino acids, namely, γ-polyglutamic acid (γ-PGA), γ-polydiaminobutanoic acid (γ-PAB), polydiaminopropionic acid (PDAP) and ε-polylysine (ε-PLL), have been found in nature[22]. The last, which is studied in this thesis, was found in 1977 during the culture filtration of a Japanese soil sample[21,23-32] and verified to be a homopolyamino acid consisting only of the essential amino acid lysine[26]. It consists of 25 to 35 lysine residues connected between the α-carboxyl group and the ε-amino group[15-19,21,23,24,27,28,30-43]. It is a highly water-soluble polymer[16-19,21,23,29,32,34,40,41,43-45] with an isoelectric point of approximately pH 9[17,21,23]. ε-Polylysine has hydrophobic methylene groups on the inside and hydrophilic carboxyl and amino groups on the outside of the molecule[46]. It is a strongly basic homopolyamino acid due to the positively charged amino groups in water[19,33,46,47].

As a homopolyamino acid, ε-polylysine differs from proteins in the following aspects:

- Proteins are synthesized following information in DNA that directs the placement of the amino acids[21]. In ε-polylysine the amide linkage is not between the α-amino and α-carboxyl groups typical of peptide bonds, but is instead between the ε-amino and α-carboxyl group (see Figure I. 6).

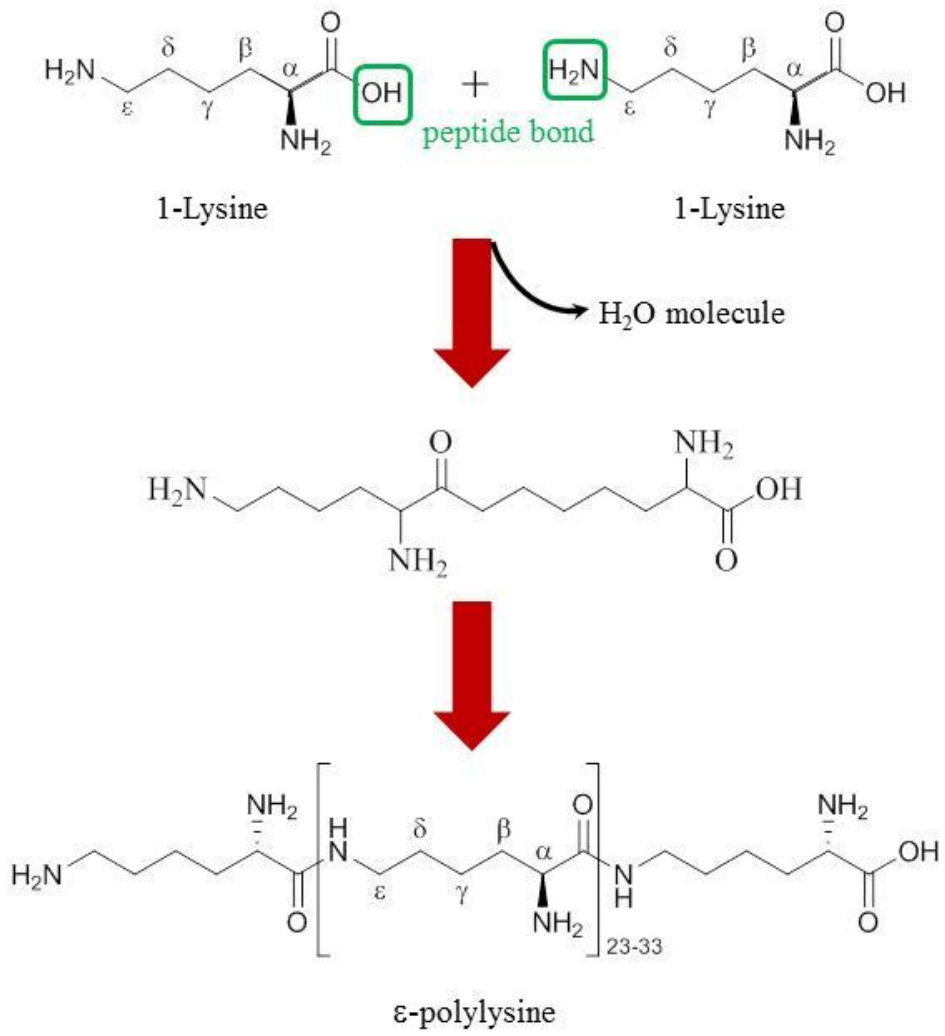

Figure I. 6. Peptide bond formation between *ε*-amino and *α*-carboxyl group in *ε*-polylysine.

- As previously mentioned, unlike proteins in which a variety of amino acids are present, homopolyamino acids such as *ε*-PLL are polyamides composed of a single type of amino acid. Thus, while proteins show a specific amino acid sequence along their backbone, homopolyamides do not[21].
- Upon amide linkage, protein backbones show the following sequence: NH_3^+-CH_2-CH_2-NH-CH_2-CH_2-NH-…-CH_2-CH_2-COO^-, while the sequence in *ε*-polylysine's backbone is: NH_3^+-CH_2-CH_2-CH_2-CH_2-CH_2-CH_2-NH-CH_2-CH_2-CH_2-CH_2-CH_2-CH_2-NH-…-CH_2-CH_2-CH_2-CH_2-CH_2-CH_2-COO^-. Thus, the backbone of *ε*-PLL differs from protein backbone in the number of carbon atoms in the main chain.

- Finally, proteins in general have exact length, whereas homopolyamides show a remarkable variation in molecular weight[15]. This variation is important for *ε*-PLL, as its antimicrobial activity depends primarily upon its molecular size. On this basis, it has been found that molecules with more than nine lysine residues show considerable potential to inhibit the growth of microorganisms, but with only eight lysine residues, *ε*-PLL exhibits negligible antimicrobial activity[16,17,36,48].

For all these reasons, when dissolved in water *ε*-PLL solution should be classified as an ordinary solution, similar to aqueous solutions of synthetic polymers (such as PVME, PVP). Nevertheless, despite the mentioned differences, *ε*-PLL and proteins also have some similarities that allow us to compare them. The main one is that both proteins and our *ε*-polylysine exhibit a well-defined three-dimensional structure (typically *α*-helix or *β*-sheet for proteins, and only the latter for *ε*-PLL[18,25,27-29,40,41,45,49,50]). In proteins, the amino acid sequence, together with environmental conditions (e.g., hydration level, pH…), determines their three-dimensional shapes and thus their biological functions. In the case of *ε*-polylysine, although it has a specific structure (*β*-sheet), it does not show any biological activity. Nevertheless, its properties as a biodegradable material and an edible substance that can be completely digested by the body, being nontoxic toward humans and the environment[16,17,19,21,28,34,40,41,46,47], give it huge potential, and it is being investigated for applications in several fields including food, medicine and pharmaceuticals, biotechnology and other industries.

Most of the applications of *ε*-PLL have focused on its use as a food preservative [16,17,19,21,23,24,28,29,31-36,38,39,41,42,46,47] in multiple foods of the oriental diet, such as sliced fish, fish sushi, Nimono (Japanese daily dishes), boiled rice, soups, noodles, cooked vegetables, sukiyaki (Japanese beef steak), potato salad, steamed cake and custard cream[21]. *ε*-PLL also shows potential applications in bioelectronics as a coating material for biochips and biosensors[17,19,21,28,50]. In medicine, it is used in micro/nanocapsules for drug delivery[17,19,21,28,50] and gene delivery carriers[17,19,21], as a glucose sensor[17] and as an anticancer agent enhancer[19]. Conjugated with anticancer drugs, it is used to treat human leukemias, sarcomas, and other forms of neoplastic diseases[17,28]. Finally, it has also been used to construct numerous products such as multi-array sensors, optical read/write discs and nanoscale electronic/photonic circuits[17,28].

3. THE WATER MOLECULE

Water has always fascinated humas, as we need to live near fresh water to survive. Early civilizations knew the importance of rain and annual flooding to avoid drought and hunger, so they made it an important part of their religions. The Ancient Greek philosophers proposed water as one of the four elements, together with fire, earth and air, that made up the world, with water being particularly important for life. In the XVIII century, the scientist Henry Cavendish (1731 - 1810) discovered hydrogen (calling it phlogiston or inflammable air) and reported that it produced water when reacted with oxygen (called dephlogisticated air). He thereby established water as a compound, not an element. Later, in 1781, Cavendish discovered water's composition; two parts hydrogen to one part oxygen. This composition was confirmed in 1800, when the amounts of hydrogen and oxygen produced by the electrolysis of water were measured by Johan Ritter (1776 - 1810)[51]. At present, water research remains extremely active, with much continuing controversy.

3.1. Water molecule structure

Water is a tiny molecule with the molecular formula of H_2O, consisting of two light hydrogen atoms attached to an oxygen atom. Each hydrogen atom has a nucleus, consisting of a single positively charged proton, surrounded by a single negatively charged electron. The oxygen atom has a nucleus consisting of eight positively charged protons and eight uncharged neutrons, surrounded by a cloud of eight negatively charged electrons. Those eight outer electrons are often shown as pairs of dots, as in Figure I. 7 a. The eight positive charges in the oxygen nucleus attract all these electrons strongly relative to the single positive charges on each of the hydrogen atoms. This attraction leaves the hydrogen atoms partially denuded of electrons, and hence partially positively charged, while the oxygen atom is partially negatively charged, see Figure I. 7 b. In this representation, the pairs of electrons between the oxygen and hydrogen atoms represent the O-H covalent bonds. Figure I. 7 also shows the bent structure of the water molecule (V-shaped) (c) and its two mirror planes of symmetry (d).

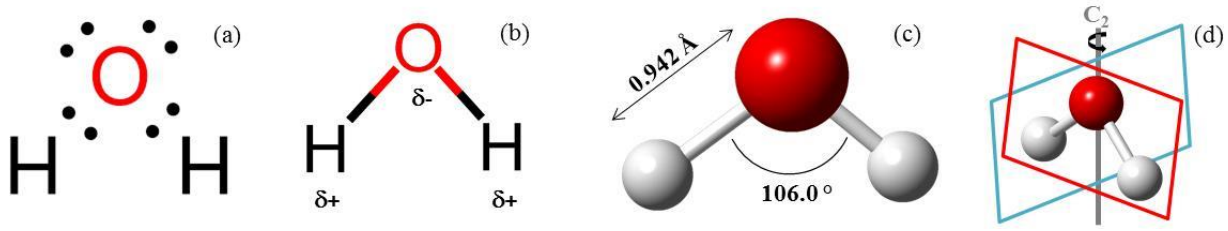

Figure I. 7. Different representations for the water molecule: (a) electro distribution, (b) charge distribution, (c) dimensions of the V-shaped molecule and (d) molecule mirror planes symmetry.

Due to the presence of these charges and the bent nature of the molecule, the center of the positive charge (halfway between the two hydrogen atoms) does not coincide with the center of the negative charge (on the oxygen atom). This charge transfer from the hydrogen atoms towards the oxygen atom creates the polarity of the water molecule, resulting in a molecular dipole moment from the center of negative charge to the center of positive charge. The electron density distribution for water is shown in Figure I. 8 (red and blue colors showing the negatively and positively charged surfaces, respectively), with the average electron density around the oxygen atom being approximately 10x the average electron density around the hydrogen atoms.

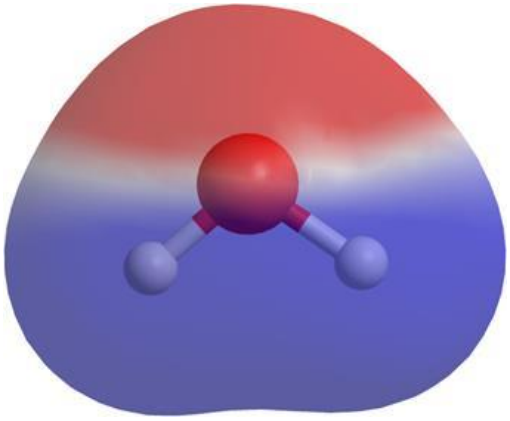

Figure I. 8. Approximate shape and charge distribution of water.

The opposite charges on the oxygen and hydrogen atoms cause different water molecules to attract each other. Thus, when the hydrogen atoms of one water molecule are attracted towards the oxygen atom of a neighboring water molecule, a hydrogen bond is formed. Thus, hydrogen atoms are not only covalently attached to their oxygen atoms but also attracted towards other nearby oxygen atoms by hydrogen bonds (see Figure I. 9).

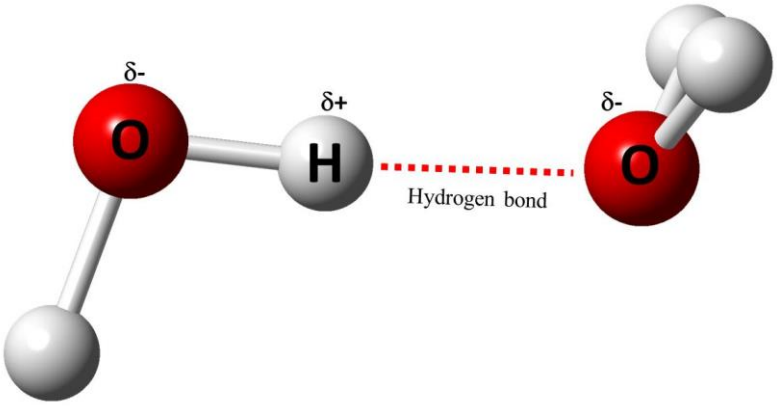

Figure I. 9. Hydrogen bond (red dashed line) between two water molecules.

Each water molecule can form two hydrogen bonds involving their hydrogen atoms, plus two further hydrogen bonds utilizing the hydrogen atoms attached to neighboring water molecules. These four hydrogen bonds optimally arrange themselves tetrahedrally around each water molecule, as found in ordinary ice (see Figure I. 10). The hydrogen bond is a weak bond, never stronger than approximately a twentieth of the strength of the O-H covalent bond. It is strong enough, however, to be maintained during thermal fluctuations at and below ambient temperatures. This attraction, together with the high density of molecules due to their small size, produces a great cohesive effect within liquid water, and it is the strong tetrahedrally placed hydrogen bond network that results in water's physical properties[51].

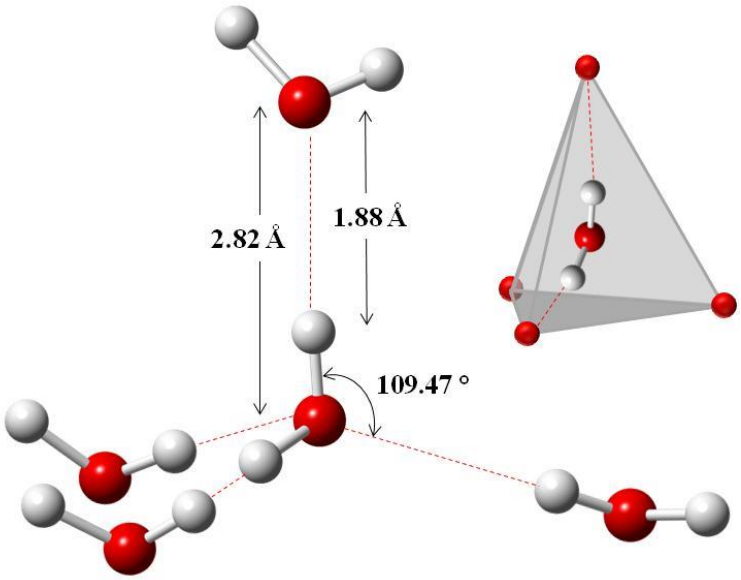

Figure I. 10. Tetrahedral arrangement of four hydrogen bonds, shown as red discontinuous lines.

3.2. Phase diagram of water

Phase diagrams show the preferred physical states of matter at different temperatures and pressures. Within each phase, the material is uniform with respect to its chemical composition and physical state. Figure I. 11 shows the water phase diagram[51]. At typical temperature and pressure on Earth (marked by an E in Figure I. 11), water is a liquid, but it becomes solid (ice) if its temperature is lowered below 273 K and gaseous (vapor) if its temperature is raised above 373 K, at the same pressure.

Each line on a phase diagram, called a phase line, represents a phase boundary and gives the conditions where two phases may stably coexist in any relative proportions. Here, a slight change in temperature or pressure may cause the phases to change abruptly from one physical state to the other. As shown in Figure I. 11, the phase diagram of water is complex, with a number of liquid-vapor, liquid-solid, vapor-solid and solid-solid phase transitions.

Where three phase lines join, there is a triple point (TP). Here, the three phases coexist stably at equilibrium, but may abruptly and totally change into each other given a slight change in temperature or pressure. As shown in Figure I. 11, the water phase diagram includes some triple points: for example, under the singular conditions of temperature and pressure where liquid water, gaseous water and hexagonal ice coexist stably, there is a triple point (red circle denoted as TP). Here, the boiling point of water and the melting point of ice are equal.

Finally, a critical point (CP) occurs at the end of a phase line where the properties of the two phases become indistinguishable from each other. The water phase diagram includes one, or possibly two, critical points. The first critical point is found at high temperatures at the end of the liquid-gas phase line (red circle marked as CP_1 in Figure I. 11). Here, liquid water is hot enough and gaseous water is under sufficient pressure that their densities are identical. At temperatures above the critical temperature, a gas cannot be liquefied.

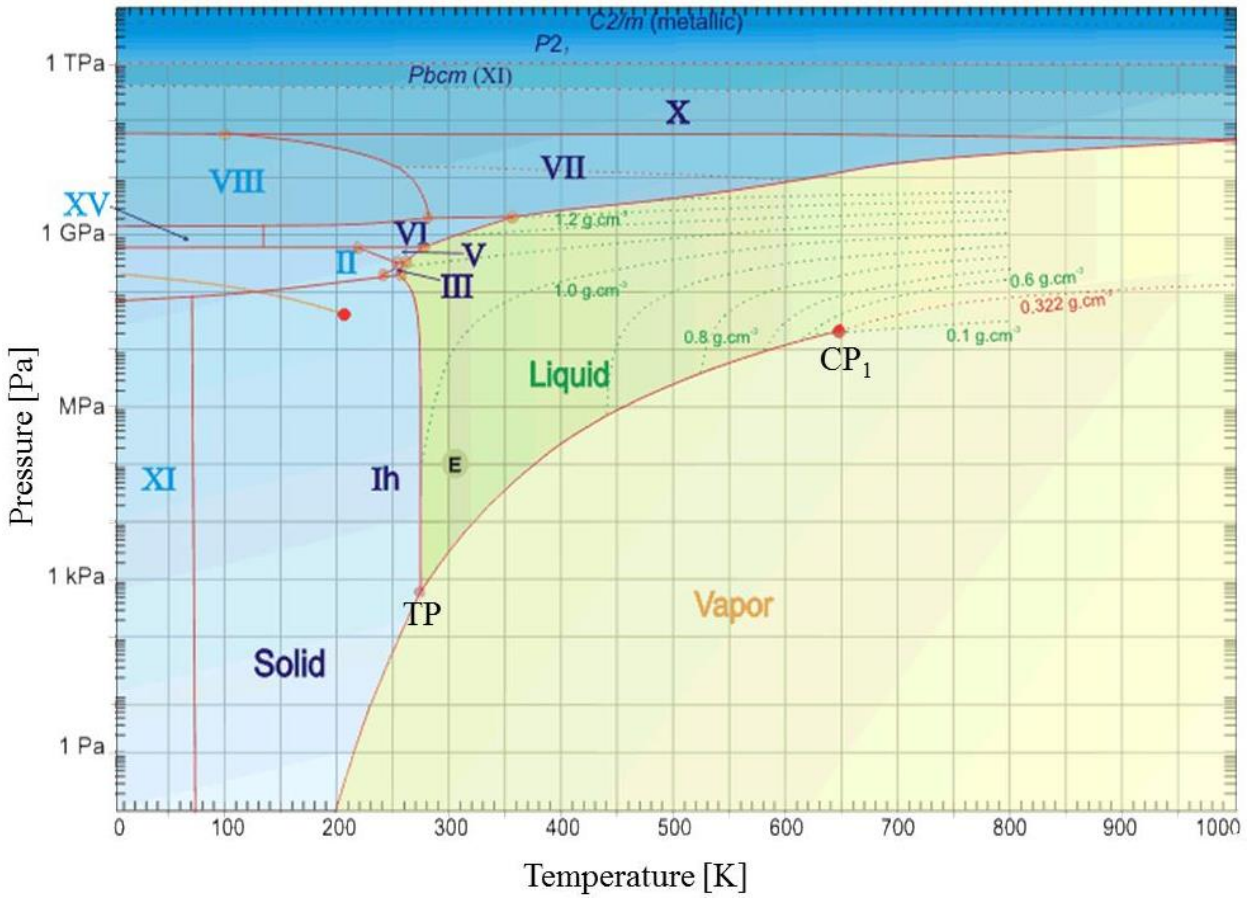

Figure I. 11. Water phase diagram[51] including phase lines and triple and critical points. In the solid state, water has more than 15 crystalline forms, of which hexagonal ice (Ih) is the most abundant.

In the 1970s, Speedy and Angell suggested the existence of a second critical point (CP_2) at approximately 230 K that could explain many of the anomalous properties of water[52]. They proposed that if water could be supercooled without crystallization, it might reach a liquid-liquid transition between low-density liquid (LDL) and high-density liquid water (HDL) at the second critical point where the two liquid water phases differing only in density merge. Figure I. 12 shows the water phase diagram[53] at low temperatures where this second critical point is displayed. Figure I. 12 also shows how the structure of liquid water changes to high-density amorphous ice (HDA) when it is cooled at high pressures and to low-density amorphous ice (LDA) when cooled at low pressures. Unfortunately, the second critical point is difficult to study, as it lies in the "no man's land'' temperature range, where water crystallizes before this second critical point can be reached. At the present time, there is no clear experimental report that establishes the existence of this second critical point, and thus there is substantial controversy in the literature regarding this hypothesis[54-56].

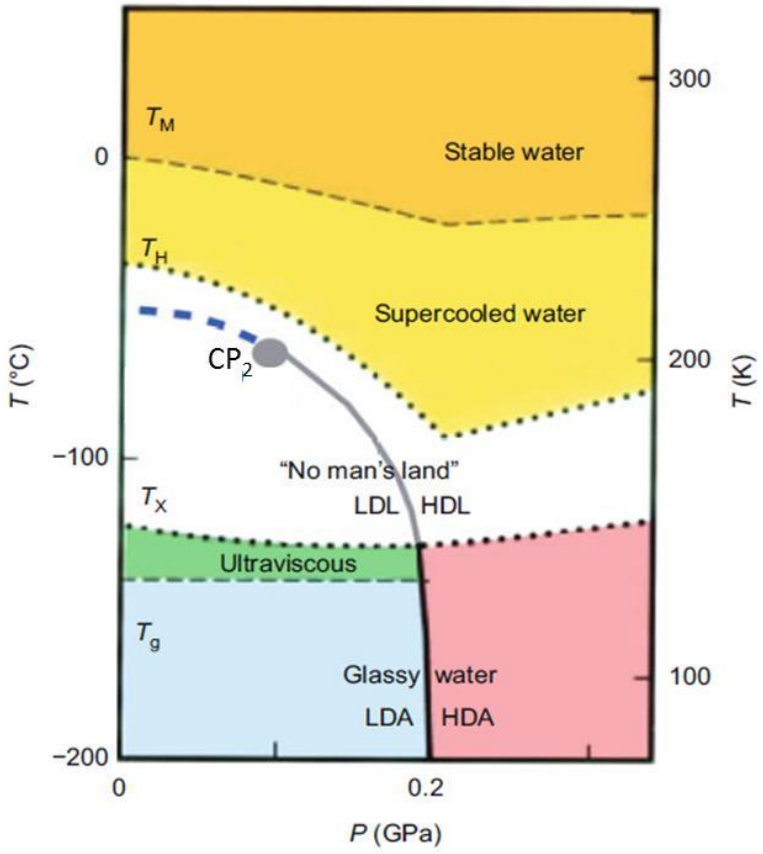

Figure I. 12. Water's various phases at different temperatures and pressures[53].

Another debated point is the glass transition (T_g) of amorphous water. There is a long history of research on its value[57,58]. The generally accepted view is that the onset glass transition for water occurs at approximately 136 K. This value was reported based on calorimetric determination by Johari, Hallbrucker and Mayer in 1987[57,59]. However, in 2002, Angell and coworkers[57,60,61] questioned the validity of a T_g near 136 K for water by suggesting that the feature observed by differential scanning calorimetry is not the T_g endotherm but a "shadow-T_g peak" or "sub-T_g peak" appearing in the 0.7 T_g to 0.8 T_g range in the DSC scan of some glasses. On this basis, Angell proposed that the T_g of water is between 165 and 180 K and is unobservable[57,60]. In response, Johari provided several criteria to distinguish a sub-T_g peak from a T_g endotherm by different DSC features and concluded that the endothermic feature observed for glassy water cannot be regarded as a sub-T_g peak[57,62]. Nevertheless, the controversy on the location of T_g of water continued with the latest argument of Angell and coworkers[57,63], who defined the glass transition in water as an order-disorder transition that occurs in the range from 150 to 250 K, and

the criticism of its premise by Johari et al[57]. The glass transition temperature in water still remains uncertain, with conflicting values reported in the literature.

3.3. Supercooled water

Supercooling is the process of lowering the temperature of a liquid or a gas below its freezing point without becoming a solid[64]. Liquid water cooled below its normal freezing point normally remains liquid for a few degrees below 273 K[51,64] and then forms solid hexagonal ice. If it is very pure and cooled quickly (supercooling at ~ 100 K/min), the liquid water may supercool further, to approximately 231 K or even lower temperatures (227 K) at higher pressures or shorter times[51]. This value is the nucleation temperature (T_N) and is the starting point of the "no man´s land", in the sense that water cannot be liquid below T_N but inevitably becomes ice.

In addition, very pure liquid water can be cooled in milliseconds (hyperquenched at ~ 10^5 K/min) below the "no man´s land" temperature range or by compressing ordinary ice at low temperatures to prevent the spontaneous nucleation of crystals. By hyperquenching liquid water, an amorphous state of water (called glassy water) is obtained, which is distinguished from regular ice by a lack of long-range order in its molecular arrangement[65]. However, amorphous water crystallizes on heating at approximately 150 K[65].

Thus, between 150 and 231.15 K, there is no bulk liquid water, as crystallization occurs, and these two temperatures define the "no man´s land" temperature region (see Figure I. 13).

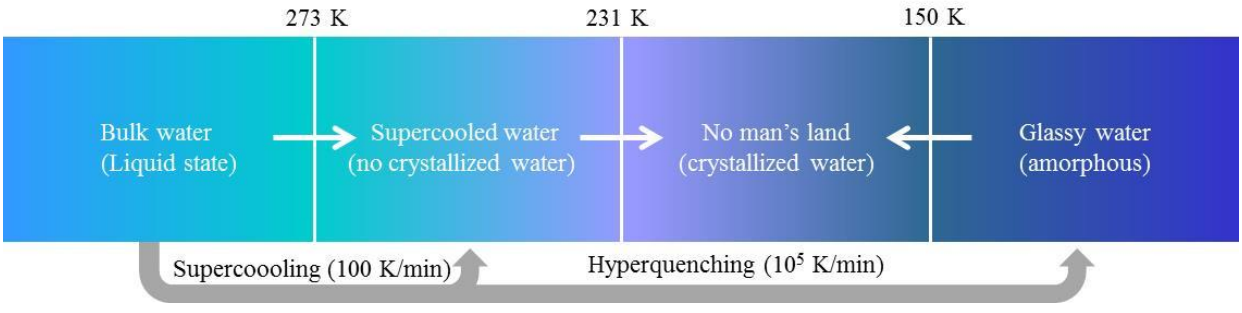

Figure I. 13. Water phases at different temperatures.

3.4. Benefits of the anomalous properties of water

Although it appears to be a simple molecule, water has a highly complex and anomalous character due to its inter-molecular hydrogen bonding[51,66]. No other material is so commonly found as a solid, liquid and gas. Moreover, as a gas, water is one of the lightest known; as a liquid, it is much denser than expected; and as a solid, it is much lighter than expected compared to its liquid form[51].

It has often been stated that life depends on these anomalous properties of water[51]. For example, the high cohesion between molecules gives it a high freezing and melting point, allowing us and our planet to be bathed in liquid water[51]. Water also plays a crucial role in the Earth mantle by reducing friction between moving rocks. Furthermore, it decreases their melting point and density, encouraging the movement of the tectonic plates and both volcanic and seismic activities (earthquakes)[51]. As far as the human body is concerned, the large heat capacity and the high thermal conductivity contribute to thermal regulation and prevent local temperature fluctuations, thus controlling our body temperature[51]. Moreover, the high latent heat of evaporation makes water resistant to evaporation and dehydration[51]. Finally, it has unique hydration properties towards important biological macromolecules (particularly proteins and nucleic acids) that determine their three-dimensional structures and hence their biological functions.

4. REFERENCES

1 Baynes, J. W. D. M. H. *Medical Biochemistry*. 4th edn, (Saunders-Elsevier, 2014).

2 Mehta, B. M. & Deeth, H. C. Blocked Lysine in Dairy Products: Formation, Occurrence, Analysis, and Nutritional Implications. *Comprehensive Reviews in Food Science and Food Safety* **15**, 206-218, doi:10.1111/1541-4337.12178 (2016).

3 Tome, D. & Bos, C. Lysine requirement through the human life cycle. *Journal of Nutrition* **137**, 1642S-1645S (2007).

4 CalivitaInternational. *This essential lysine*, <http://www.fit-leader.com/eng-articles/lysine.shtml> (

5 Cerveny, S. & Swenson, J. Dynamics of supercooled water in a biological model system of the amino acid L-lysine. *Physical Chemistry Chemical Physics* **16**, 22382-22390, doi:10.1039/c4cp02487g (2014).

6 Sinha, S., Lopes, D. H. J. & Bitan, G. A Key Role for Lysine Residues in Amyloid beta-Protein Folding, Assembly, and Toxicity. *Acs Chemical Neuroscience* **3**, 473-481, doi:10.1021/cn3000247 (2012).

7 Hoang, T. X. *et al.* Common attributes of native-state structures of proteins, disordered proteins, and amyloid. *Proceedings of the National Academy of Sciences of the United States of America* **103**, 6883-6888, doi:10.1073/pnas.0601824103 (2006).

8 3D-MolecularDesigns. *From Amino Acids to Proteins in 4 Easy Steps*, <http://www.3dmoleculardesigns.com/3DMD-Files/AASK/PDFs/AASKTeacherNotes1-8-15.pdf> (

9 Van der Maarel, J. R. C. *Introduction to biopolymer physics*. (World Scientific Publishing Co. Pte. Ltd, 2008).

10 Branden, C. T., J. *Introduction to protein structure*. 2 edn, (Garland Science, Taylor & Frances Group, 1991).

11 Chou, P. Y. & Fasman, G. D. Prediction of beta-turns. *Biophysical journal* **26**, 367-383 (1979).

12 Giulia, M. *Role of electrostatics explored with molecular dynamics simulations for protein stability and folding*, (2006).

13 Bailey, R. *Protein Function*, <https://www.thoughtco.com/protein-function-373550> (2017).

14 Adnan, A. *Biological functions of proteins*, <http://www.biotecharticles.com/Others-Article/Biological-Functions-of-Proteins-453.html> (2010).

15 Shi, F., Xu, Z. & Cen, P. Microbial production of natural poly amino acid. *Science in China Series B: Chemistry* **50**, 291-303, doi:10.1007/s11426-007-0061-5 (2007).

16 Hamano, Y. Occurrence, biosynthesis, biodegradation, and industrial and medical applications of a naturally occurring ε-poly-L-lysine. *Bioscience, biotechnology, and biochemistry* **75**, 1226-1233, doi:10.1271/bbb.110201 (2011).

17 Pandey, A. K. & Kumar, A. Improved microbial biosynthesis strategies and multifarious applications of the natural biopolymer ε-poly-L-lysine. *Process Biochemistry* **49**, 496-505, doi:10.1016/j.procbio.2013.12.009 (2014).

18 Singh, M. *et al.* Phonon Dispersion and Heat Capacity in Microbial Poly(ε-L-lysine)(M-ε-PL). *Polymer Journal* **40**, 503-512, doi:10.1295/polymj.PJ2007184 (2008).

19 Shukla, S. C., Singh, A., Pandey, A. K. & Mishra, A. Review on production and medical applications of ε-polylysine. *Biochemical Engineering Journal* **65**, 70-81, doi:10.1016/j.bej.2012.04.001 (2012).

20 Oppermann-Sanio, F. B. & Steinbuchel, A. Occurrence, functions and biosynthesis of polyamides in microorganisms and biotechnological production. *Naturwissenschaften* **89**, 11-22, doi:10.1007/s00114-001-0280-0 (2002).

21 Bankar, S. B. & Singhal, R. S. Panorama of poly-ε-lysine. *RSC Advances* **3**, 8586, doi:10.1039/c3ra22596h (2013).

22 Xu, Z. X. *et al.* Systematic unravelling of the biosynthesis of poly (L-diaminopropionic acid) in Streptomyces albulus PD-1. *Scientific reports* **5**, doi:10.1038/srep17400 (2015).

23 Yoshida, T. & Nagasawa, T. ε-Poly-L-lysine: microbial production, biodegradation and application potential. *Applied microbiology and biotechnology* **62**, 21-26, doi:10.1007/s00253-003-1312-9 (2003).

24 Hiraki, J. *et al.* Use of ADME studies to confirm the safety of ε-polylysine as a preservative in food. *Regulatory Toxicology and Pharmacology* **37**, 328-340, doi:10.1016/s0273-2300(03)00029-1 (2003).

25 Jia, S. *et al.* Computational study on the conformation and vibration frequencies of beta-sheet of ε-polylysine in vacuum. *International journal of molecular sciences* **10**, 3358-3370, doi:10.3390/ijms10083358 (2009).

26 Shima, S. & Sakai, H. Polylysine produced by streptomices. *Agricultural and Biological Chemistry* **41**, 1807-1809 (1977).

27 Maeda, S., Sasaki, C. & Kunimoto, K. K. in *Nmr Spectroscopy of Polymers: Innovative Strategies for Complex Macromolecules* Vol. 1077 *ACS Symposium Series* (eds H. N. Cheng, T. Asakura, & A. D. English) 317-335 (2011).

28 Shih, I. L., Shen, M. H. & Van, Y. T. Microbial synthesis of poly(ε-lysine) and its various applications. *Bioresource technology* **97**, 1148-1159, doi:10.1016/j.biortech.2004.08.012 (2006).

29 Maeda, S. *et al.* Structural investigation of microbial poly(ε-L-lysine) derivatives with azo dyes by solid-state C-13 and N-15 NMR. *Polymer Bulletin* **53**, 259-267, doi:10.1007/s00289-004-0330-9 (2005).

30 Sasaki, C. *et al.* Aggregation behavior of dabsylated poly(ε-L-lysine) in aqueous DMSO solution. *Polymer Bulletin* **57**, 747-756, doi:10.1007/s00289-006-0643-y (2006).

31 Chang, Y., McLandsborough, L. & McClements, D. J. Interactions of a cationic antimicrobial (ε-polylysine) with an anionic biopolymer (pectin): an isothermal titration calorimetry, microelectrophoresis, and turbidity study. *Journal of agricultural and food chemistry* **59**, 5579-5588, doi:10.1021/jf104299q (2011).

32 Li, Y.-Q., Han, Q., Feng, J.-L., Tian, W.-L. & Mo, H.-Z. Antibacterial characteristics and mechanisms of ε-poly-lysine against Escherichia coli and Staphylococcus aureus. *Food Control* **43**, 22-27, doi:10.1016/j.foodcont.2014.02.023 (2014).

33 Zhang, L. M. *et al.* Physical, mechanical and antimicrobial properties of starch films incorporated with ε-poly-L-lysine. *Food chemistry* **166**, 107-114, doi:10.1016/j.foodchem.2014.06.008 (2015).

34 Jia, S. R. *et al.* Fractionation and characterization of ε-poly-l-lysine from Streptomyces albulus CGMCC 1986. *Food Science and Biotechnology* **19**, 361-366, doi:10.1007/s10068-010-0051-9 (2010).

35 Nishikawa, M. & Ogawa, K. Inhibition of ε-poly-L-lysine biosynthesis in Streptomycetaceae bacteria by short-chain polyols. *Applied and environmental microbiology* **72**, 2306-2312, doi:10.1128/AEM.72.4.2306-2312.2006 (2006).

36 Hamano, Y. *et al.* ε-Poly-L-lysine peptide chain length regulated by the linkers connecting the transmembrane domains of ε-Poly-L-lysine synthetase. *Applied and environmental microbiology* **80**, 4993-5000, doi:10.1128/AEM.01201-14 (2014).

37 Kito, M., Takimoto, R., Yoshida, T. & Nagasawa, T. Purification and characterization of an ε-poly-L-lysine-degrading enzyme from an ε-poly-L-lysine-producing strain of Streptomyces albulus. *Archives of microbiology* **178**, 325-330, doi:10.1007/s00203-002-0459-6 (2002).

38 Kito, M., Onji, Y., Yoshida, T. & Nagasawa, T. Occurrence of ε-poly-L-lysine-degrading enzyme in ε-poly-L-lysine-tolerant Sphingobacterium multivorum OJ10: purification and characterization. *Fems Microbiology Letters* **207**, 147-151, doi:10.1016/s0378-1097(01)00571-7 (2002).

39 Yamanaka, K. *et al.* Mechanism of ε-poly-L-lysine production and accumulation revealed by identification and analysis of an ε-poly-L-lysine-degrading enzyme. *Applied and environmental microbiology* **76**, 5669-5675, doi:10.1128/AEM.00853-10 (2010).

40 Maeda, S., Oumae, S., Kaneko, S. & Kunimoto, K.-K. Formation of carbamates and cross-linking of microbial poly(ε-l-lysine) studied by 13C and 15N solid-state NMR. *Polymer Bulletin* **68**, 745-754, doi:10.1007/s00289-011-0580-2 (2011).

41 Maeda, S., Fujiwara, Y., Sasaki, C. & Kunimoto, K.-K. Structural analysis of microbial poly(ε-L-lysine)/poly(acrylic acid) complex by FT-IR, DSC, and solid-state 13C and 15N NMR. *Polymer Journal* **44**, 200-203, doi:10.1038/pj.2011.108 (2011).

42 Bankar, S. B., Chaudhary, S. A. & Singhal, R. S. Purification and characterization of poly-ε-lysine from Streptomyces noursei NRRL 5126. *Journal of Scientific & Industrial Research* **73**, 33-40 (2014).

43 Shih, I. L., Van, Y. T. & Shen, M. H. Biomedical applications of chemically and microbiologically synthesized poly(glutamic acid) and poly(lysine). *Mini-Reviews in Medicinal Chemistry* **4**, 179-188, doi:10.2174/1389557043487420 (2004).

44 Maeda, S., Chizuru Sasaki, C. & Kunimoto, K. Characterization of Microbial Poly(ε-L-lysine) and Its Derivatives by Solid-State NMR. *American Chemical Society* (2011).

45 Maeda, S., Kunimoto, K.-K., Sasaki, C., Kuwae, A. & Hanai, K. Characterization of microbial poly (ε-l-lysine) by FT-IR, Raman and solid state 13C NMR spectroscopies. *Journal of Molecular Structure* **655**, 149-155, doi:10.1016/s0022-2860(03)00218-7 (2003).

46 Hiraki, J. *et al.* Use of ADME studies to confirm the safety of ε-polylysine as a preservative in food. *Regulatory Toxicology and Pharmacology* **37**, 328-340, doi:10.1016/s0273-2300(03)00029-1 (2003).

47 Yu, H., Huang, Y. & Huang, Q. Synthesis and characterization of novel antimicrobial emulsifiers from ε-polylysine. *Journal of agricultural and food chemistry* **58**, 1290-1295, doi:10.1021/jf903300m (2010).

48 Shima, S., Matsuoka, H., Iwamoto, T. & Sakai, H. Antimicrobial action of ε-poly-lysine. *Journal of Antibiotics* **37**, 1449-1455 (1984).

49 Lee, H.-H. *et al.* Synthesis and Conformation of Monodispersed Oligo(ε-L-Lysine)mers Studied by Cd and IR Spectroscopies. *Spectroscopy Letters* **28**, 177-190, doi:10.1080/00387019508010070 (1995).

50 Shukla, S. C., Singh, A., Pandey, A. K. & Mishra, A. Review on production and medical applications of ε-polylysine. *Biochemical Engineering Journal* **65**, 70-81, doi:10.1016/j.bej.2012.04.001 (2012).

51 Chaplin, M. *Water structure and science* <http://www1.lsbu.ac.uk/water/> (2000).

52 Speedy, R. J. & Angell, C. A. Isothermal compressibility of supercooled water and evidence for a thermodynamic singularity at -45ºC *Journal of Chemical Physics* **65**, 851-858, doi:10.1063/1.433153 (1976).

53 Sun, Z. R., Sun, G., Chen, Y. X. & Xu, L. M. Liquid-liquid phase transition in water. *Science China-Physics Mechanics & Astronomy* **57**, 810-818, doi:10.1007/s11433-014-5451-z (2014).

54 Liu, L., Chen, S. H., Faraone, A., Yen, C. W. & Mou, C. Y. Pressure dependence of fragile-to-strong transition and a possible second critical point in supercooled confined water. *Physical review letters* **95**, doi:10.1103/PhysRevLett.95.117802 (2005).

55 Swenson, J. Comment on "Pressure dependence of fragile-to-strong transition and a possible second critical point in supercooled confined water. *Physical review letters* **97**, doi:10.1103/PhysRevLett.97.189801 (2006).

56 Cerveny, S., Colmenero, J. & Alegria, A. Comment on "Pressure dependence of fragile-to-strong transition and a possible second critical point in supercooled confined water". *Physical review letters* **97**, 189802, doi:10.1103/PhysRevLett.97.189802 (2006).

57 Capaccioli, S. & Ngai, K. L. Resolving the controversy on the glass transition temperature of water? *Journal of Chemical Physics* **135**, doi:10.1063/1.3633242 (2011).

58 Debenedetti, P. G. Supercooled and glassy water. *Journal of Physics-Condensed Matter* **15**, R1669-R1726, doi:10.1088/0953-8984/15/45/r01 (2003).

59 Johari, G. P., Hallbrucker, A. & Mayer, E. The glass liquid transition of hyperquenched water *Nature* **330**, 552-553, doi:10.1038/330552a0 (1987).

60 Angell, C. A. Liquid fragility and the glass transition in water and aqueous solutions. *Chemical Reviews* **102**, 2627-2649, doi:10.1021/cr000689q (2002).

61 Yue, Y. Z. & Angell, C. A. Clarifying the glass-transition behaviour of water by comparison with hyperquenched inorganic glasses. *Nature* **427**, 717-720, doi:10.1038/nature02295 (2004).

62 Johari, G. P. Calorimetric features of high-enthalpy amorphous solids and glass-softening temperature of water. *Journal of Physical Chemistry B* **107**, 9063-9070, doi:10.1021/jp030009y (2003).

63 Angell, C. A. Insights into phases of liquid water from study of its unusual glass-forming properties. *Science* **319**, 582-587, doi:10.1126/science.1131939 (2008).

64 Cavagna, A. Supercooled liquids for pedestrians. *Physics Reports-Review Section of Physics Letters* **476**, 51-124, doi:10.1016/j.physrep.2009.03.003 (2009).

65 Mishima, O. & Stanley, H. E. The relationship between liquid, supercooled and glassy water. *Nature* **396**, 329-335 (1998).

66 Stokely, K., Mazza, M. G., Stanley, H. E. & Franzese, G. Effect of hydrogen bond cooperativity on the behavior of water. *Proceedings of the National Academy of Sciences of the United States of America* **107**, 1301-1306, doi:10.1073/pnas.0912756107 (2010).

CHAPTER II

INTRODUCTION TO WATER AND PROTEIN DYNAMICS

In this chapter, we analyze the importance of water for the functionality of proteins, and we also review previous results on proteins dynamics in the literature. A common problem in these studies is that proteins have low solubility and therefore cannot be studied in dilute solutions, as water crystallizes. Finally, we address the main objectives of this thesis, proposing an alternative way of studying protein dynamics by exploring aqueous solutions of highly soluble small peptides.

1. THE IMPORTANCE OF WATER DYNAMICS IN PROTEIN FUNCTION

Proteins fold into three-dimensional structures that depend on the primary sequence of the amino acids. This folding mechanism requires flexible, exchangeable and extensible linkages, and water-mediated hydrogen bonding is perfectly suited for this purpose. Water hydrates the peptide backbone and maneuvers it through its secondary structural assembly towards its ultimate and unique active structure[1]. Thus, the motion of water molecules is of great biological importance in that it enables and determines protein mobility; it also permits proton transfer along the protein surface and allows proteins to associate and dissociate, facilitating a large number of biochemical processes[2,3].

This fact clearly implies that protein functions depend on the degree of hydration, h, defined as the weight ratio of water to protein. Dehydrated biomolecules have strongly suppressed dynamics and exhibit no biological activity[3-9]. At minimum, a spanning network of hydrogen-bonded water molecules that covers most of the surface of an enzyme is required for enzyme activity. The function of a protein begins when the hydration level reaches approximately $h \approx 0.2$ g of water/g of protein[2,7-9]. With a further increase in hydration, the protein dynamics (essential for function) is increased, and the protein achieves full function in solution, at equal amounts of

water and protein ($h \approx 1$ g of water/g of protein)[2,5,8,9]. This type of water, named ‘‘biological water”[10,11], has been found to be strongly connected not only to the functionality and flexibility but also to the stability and dynamics of biomolecules[9].

In summary, the function of a protein is dependent not only on the amino acid sequence, which determines its three-dimensional shape, but also on both its dynamics (motions of the protein itself, such as vibrations, rotations, and transitions between substrates[12,13]) and motions in the solvent. Therefore, to study the functionality of a protein, one must first understand the dynamics of the surrounding water molecules and how this water affects the dynamics of the protein.

2. FUNDAMENTALS OF PROTEIN DYNAMICS

2.1. Energy landscape

Proteins can be considered as nanomachines that perform some functions. They consequently must possess at least two different states, like a switch that can be open or closed. Myoglobin (Mb), for example, can have a bound dioxygen (MbO_2 or MbCO) or not (deoxy Mb), giving the molecule two possible distinct states: ligand bound and unbound[14]. Moreover, there is a spectrum of conformations in either state, called conformational substates (CSs)[14]. Conformational substates are specified by the coordinates of every atom of the protein, and they form the scaffold for protein motions[14-16]. The energy landscape is thus a construct in a high-dimensional conformation space with approximately 10^4 coordinates[15]. It describes the potential energy (E_c) of the protein as a function of conformational coordinates of all atoms[14]. As an example, the organization of the CSs for MbCO is shown in Figure II. 1. Substates are conformational minima described by points in this space. Different proteins likely exhibit different sets of conformational states, but general concepts are probably common to all.

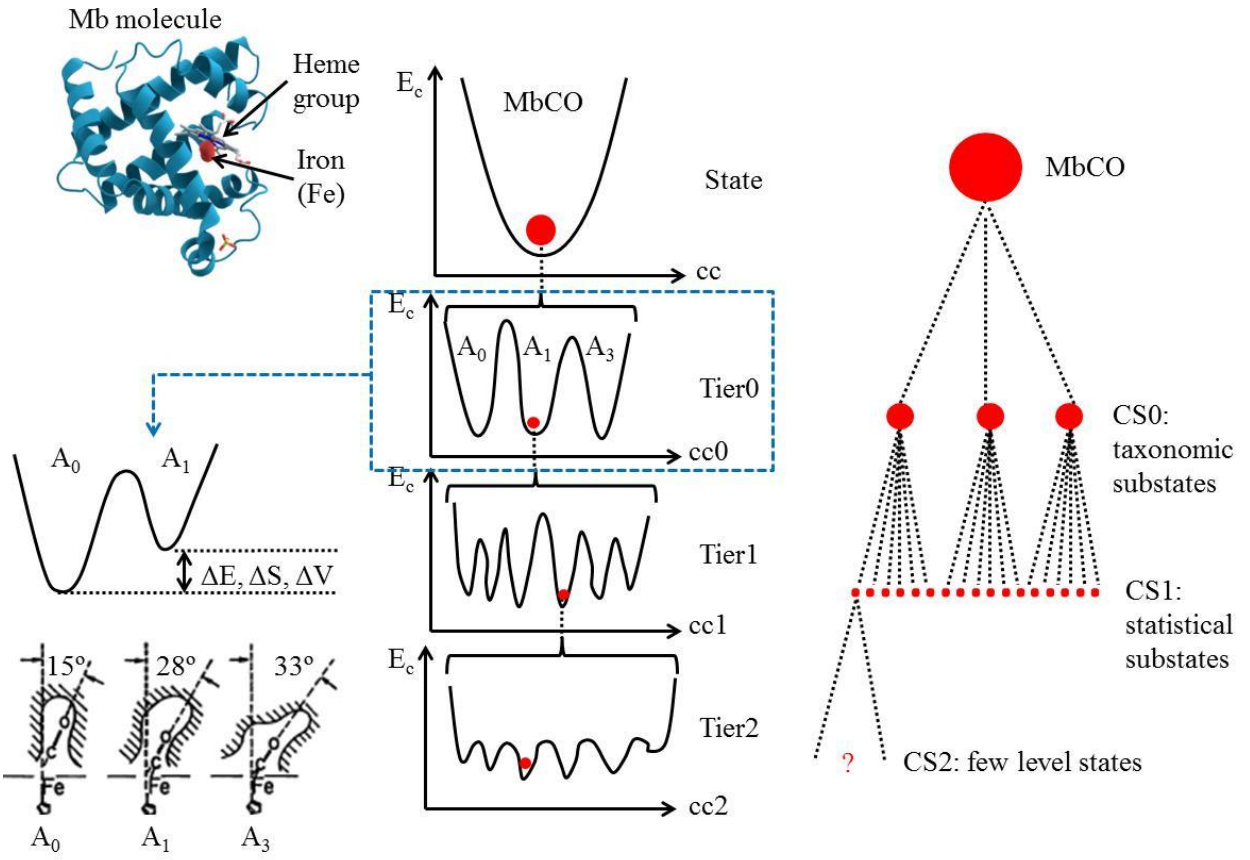

Figure II. 1. The structure of MbCO and the overall picture of the conformational energy *Ec* as a function of a conformational coordinate, *cc*.

Figure II. 1 implies that the CSs can be classified into a hierarchy. They are organized into tiers characterized by the magnitude of the barriers between them[15]. CSi in Figure II. 1 denotes the substates in the i^{th} tier in the organization. The top row depicts MbCO in the convectional conception, with a unique structure corresponding to a unique energy valley. Nevertheless, there are valleys within valleys within valleys in the energy landscape, which are classified into a number of tiers[16,17].

Accordingly, the second row depicts three substrates in tier 0 (CS0). Those substates, called A_0, A_1, and A_3, possess different enthalpies, entropies and volumes. They are separated by the largest barriers, and their properties, for instance, structure, function, and reaction rates, can be determined individually[15]. In the case of MbCO, the A_0, A_1, A_3 substates all have the same primary amino acid sequence but differ in structure at least due to the difference in the orientation of the bound CO with respect to the heme[14,15,17] (see Figure II. 1). The dependence on

external parameters also varies: for instance, at low pH, A_0 dominates, whereas at high pH, A_1 does[15,17]. The ratio depends strongly on pressure and temperature[17]. The CS0 tier for MbCO is functionally important. In the substate A_0, myoglobin acts as an enzyme, while in A_1 Mb stores and transports dioxygen[15-17]. The function of A_3, if any, is not known[15]. Thus, if a simple protein such as myoglobin possesses two different functions, one can hypothesize that many proteins may have multiple substates with different functions, to be switched on when needed[17].

Each substate can assume a very large number of different conformations, mainly because of different orientations of the amino acid side chains[15]. Thus, in each substate of tier 0, there are many substates of tier 1, which are conformational minima and characterized by very small barriers[15]. This situation is shown in Figure II. 1, where the existence of a second tier of substates (CS1) in each of the preceding tiers (CS0) is described by the inhomogeneous broadening of the individual stretch bands. Note that the plot of *Ec* versus conformational coordinate1 (*cc1*) for tier 1 is oversimplified, as the number of valleys in *Ec1* is extremely large. The same applies to lower tiers such as CS2.

The tiers can be characterized as taxonomic, statistical and few-level tiers[17]. In the top tier, CS0, a taxonomic approach (a particular description, identification and classification) is fruitful, but for lower tiers such as CS1, the substates are so numerous that they cannot be characterized individually; therefore, a statistical viewpoint is needed[15,17]. This perspective requires new concepts, and one no longer talks about specific energy but about the statistics of the energy landscape. The lowest tiers, such as CS2 in MbCO, are classified as few-level substates[17].

Protein motions are jumps between substates; the very fast processes are transitions among local conformational minima and the slower processes (e.g., slaved motions) are jumps between statistical and taxonomic substates[15]. This description elucidates the relation of the energy landscape to protein function. Considering myoglobin, at temperatures above 250 K, the binding of CO becomes exponential over time, implying that some barriers between substates prevent transitions at low temperature but permit them above 250 K[17].

2.2. Review of protein dynamics

A very large number of experiments in many different systems (such as polymers, glass forming systems, and so on) demonstrate that two main classes of relaxation processes occur, distinguished by their time and temperature dependence: the so called α- and β-relaxations. The slower one is called the structural α-relaxation, and the faster one is the secondary or β-relaxation. The main characteristic of the α-fluctuations is the Vogel – Fulcher – Tammann-like (VFT) temperature dependence, whereas β-relaxations follow an Arrhenius temperature dependence[17].

Most protein functions stop below 200 K, and it has often been claimed that below this temperature, proteins undergo only harmonic motions[17]. However, internal motions, for instance the transit of small molecules from one cavity to another, occur well below 200 K, and some enzymatic reactions have also been observed to occur below this temperature[17]. Therefore, the study of protein dynamics at low temperatures is important not only for learning about the physics of these processes but also because the results are relevant if extrapolated to biological temperatures. In this section, we review the previous studies on protein dynamics, mainly using BDS, based on the works of N. Shinyashiki et al[18], A. Panagopoulou et al[19], and S. Khodadadi and A. P. Sokolov[20].

N. Shinyashiki et al studied Bovine Serum Albumin (BSA) at two water contents (80 and 60 wt%) by BDS. The dielectric spectra were quite complicated, but they identified three major relaxations, from the fastest to the slowest, processes I, II and III. Figure II. 2 shows the temperature dependences of these processes[18]. For comparison, the relaxation time of pure ice obtained by N. Shinyashiki et al and G. P. Johari et al[21] are also included.

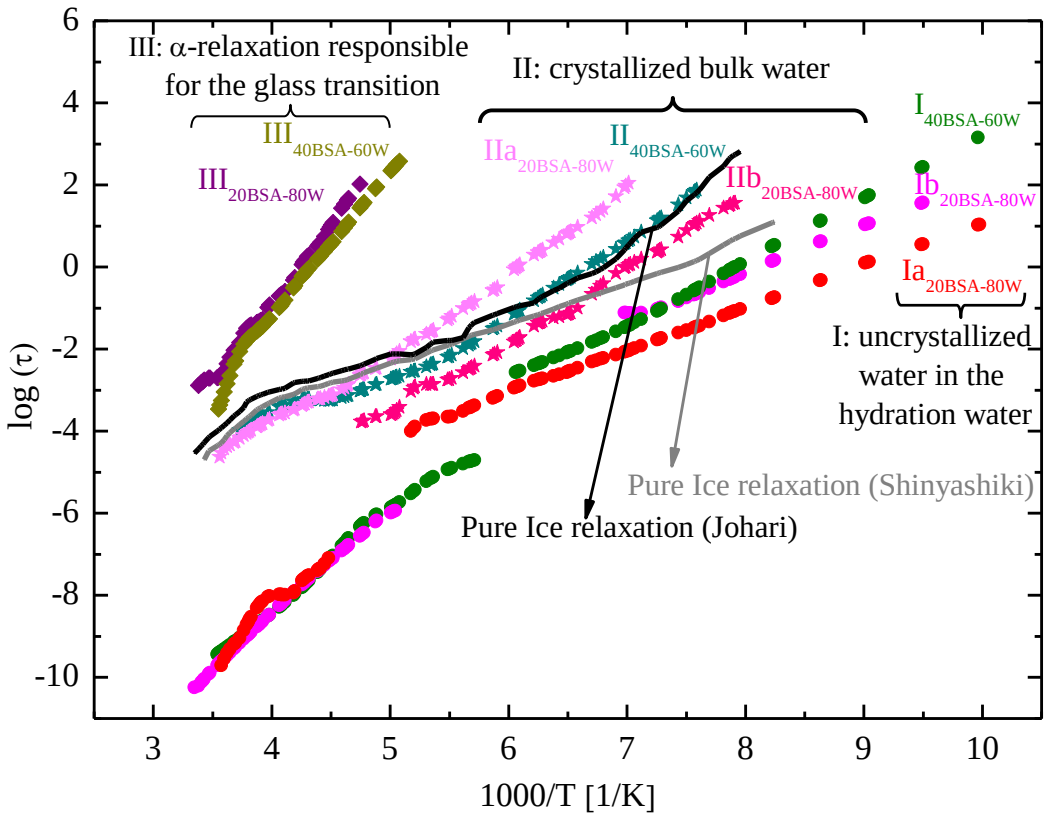

Figure II. 2. Plots of relaxation times for 20 and 40 wt% BSA-water mixtures against reciprocal temperatures of processes $Ia_{20BSA\text{-}80W}$ (red circles), $Ib_{20BSA\text{-}80W}$ (magenta circles), $I_{40BSA\text{-}60W}$ (olive circles), $IIa_{20BSA\text{-}80W}$ (light magenta starts), $IIb_{20BSA\text{-}80W}$ (pink starts), $II_{40BSA\text{-}60W}$ (dark cyan stars), $III_{20BSA\text{-}80W}$ (purple diamonds) and $III_{40BSA\text{-}60W}$ (dark yellow diamonds). Grey and black lines denote the relaxation times of pure ice obtained by N. Shinyashiki et al and G. P. Johari et al, respectively.

According to the authors[18], the relaxation times of the fastest processes, Ia and Ib, in the samples with c_w = 80 wt% were comparable, having almost the same activation energies, and therefore originated from same molecular mechanism. Moreover, those relaxation times, together with process I observed in BSA at c_w = 60 wt%, were similar to the relaxation of water in many aqueous mixtures[22-27] previously identified as the Johari–Goldstein β-relaxation of water. Thus, process I (in both samples) was defined as a β-relaxation of uncrystallized water in BSA aqueous solutions. This process showed a crossover from Arrhenius to non-Arrhenius T-dependence with increasing temperature at T_g. According to the authors, such a change in the temperature dependence of the secondary relaxation of water has also been found in many aqueous mixtures (as water in mixtures with glycerol, ethylene glycol, ethylene glycol oligomers, poly(ethylene glycol), propanol, poly(vinyl pyrro1idone), poly(vinylmethylether), fructose[22,23]), in the dynamics of myoglobin solvated by water/glycerol mixtures[2,26] and in a variety of neat glass-

formers (e.g., tert-butyilpyridine dissolved in tristyrene solvent or 2-picoline mixed with tristyrene[24,25,27]).

Due to the similarities of process II with the relaxation of pure ice, the authors attributed this process to the dynamics of crystallized bulk water in BSA – water mixtures. When comparing the relaxation times for pure ice obtained from N. Shinyashiki et al with the ones published by G. P. Johari et al[21], the data agreed well at temperatures above 170 K. However, the differences became larger with decreasing temperature below 170 K. Nevertheless, N. Shinyashiki et al attributed these small differences to impurities or thermal history.

The slowest process, called as III, showed temperature dependence similar to a Vogel – Fulcher – Tammann form. The temperature at which this process reached 100 s agreed well with the glass transition temperature observed by calorimetric measurements. Thus, process III was related to the molecular motion responsible for the glass transition of the hydrated BSA system. Furthermore, due to the same temperature dependence of processes III and I above T_g, N. Shinyashiki et al established that the secondary relaxation of water and the structural relaxation of the hydrated BSA (the α-relaxation) were coupled or connected to each other as inseparable processes. Consequently, they described the glass transition temperature of the solvated protein as "slaved" by the β-relaxation of the solvent. Nevertheless, the dielectric strength of the process III was too large to be due solely to local chain motions of the protein, so they attributed this effect to the contribution of interfacial polarization and/or the effect of an internal electric field.

On the other hand, A. Panagopoulou et al studied the same protein (BSA) by BDS at a wide range of hydration levels ($7 \leq c_w\,[\text{wt\%}] \leq 40$). Figure II. 3 shows the temperature dependence of the relaxation time for the hydrated BSA[19].

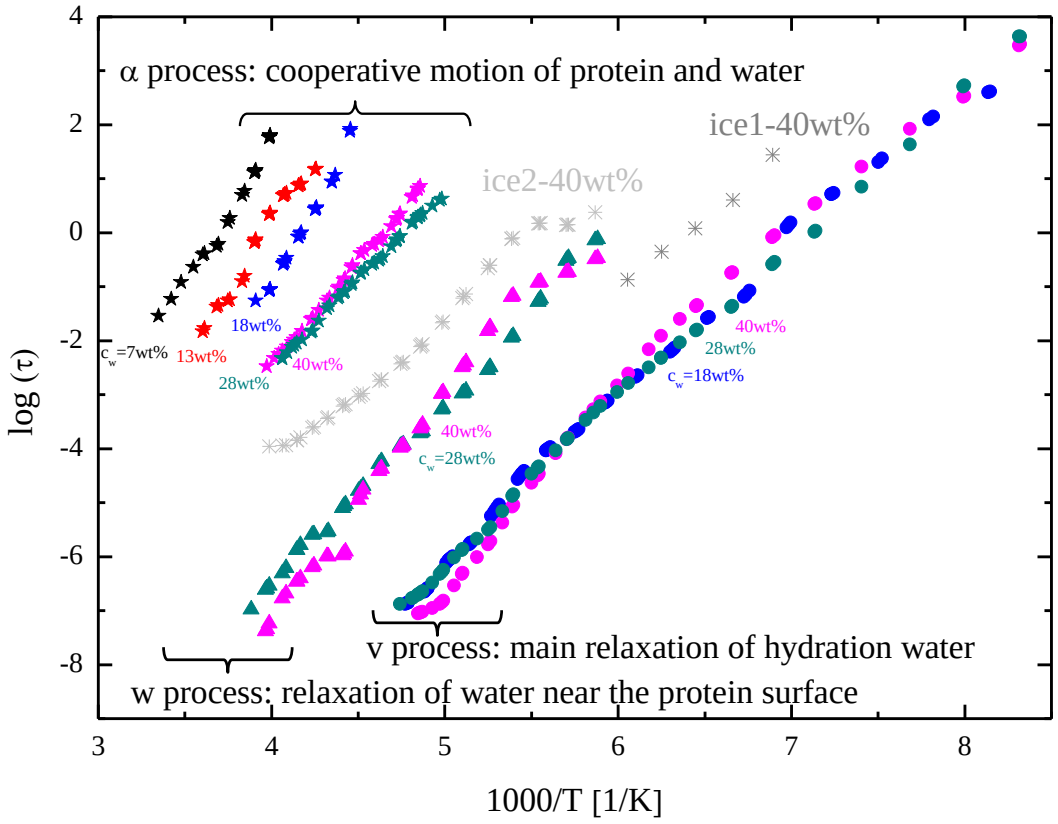

Figure II. 3. Temperature dependence of the relaxation time for the different relaxation processes in hydrated BSA.

In agreement with N. Shinyashiki et al[18], the authors found the "*v* relaxation" to be the main relaxation of water molecules. According to the authors, this relaxation is due to water molecules interacting with protein polar groups that can rotate and translate similarly to bulk water[19,28]. The relaxation denoted as *w* was only observed for the most hydrated samples (c_w = 28 and 40 wt%). The solution with the highest hydration level showed crystallization of water during cooling, unlike the sample c_w = 28 wt%, which showed no crystallization. Thus, as the "*w* relaxation" remained the same for both samples, the authors related this process to water molecules near the protein surface. However, nowadays its origin is not fully clear, and there is a certain controversy concerning this relaxation. Processes called ice1 and ice2 in Figure II. 3 were interpreted as ice relaxations since they only appear in the spectra of sample with c_w = 40 wt%. Finally, the authors defined the slowest process as the protein α-relaxation in agreement with N. Shinyashiki et al[18]. They assigned this process to the movement of polar groups rather than water molecules alone by the observation of this relaxation in the dry sample. They also observed a strong plasticization of the α-relaxation with the addition of water up to 28 wt%. The further addition of water caused

no change in the time scale of the α-relaxation, as the position of the data for the 40 wt% sample followed the same trace as for 28 wt%. Moreover, the T_g value was found to decrease significantly with the addition of water. Taking into account all these observations and previous works in the literature[18,29-31], A. Panagopoulou et al related this process to the glass transition in hydrated proteins, which is highly connected to water, leading to a cooperative motion of protein chains and water molecules.

S. Khodadadi and A. P. Sokolov[20] proposed the following hierarchy of protein dynamics (see Figure II. 4) at temperatures above the glass transition based on several experimental techniques including Broadband Dielectric Spectroscopy (BDS), Neutron Scattering (NS) and Nuclear Magnetic Resonance (NMR) measurements, as well as Molecular Dynamic Simulations (MDS).

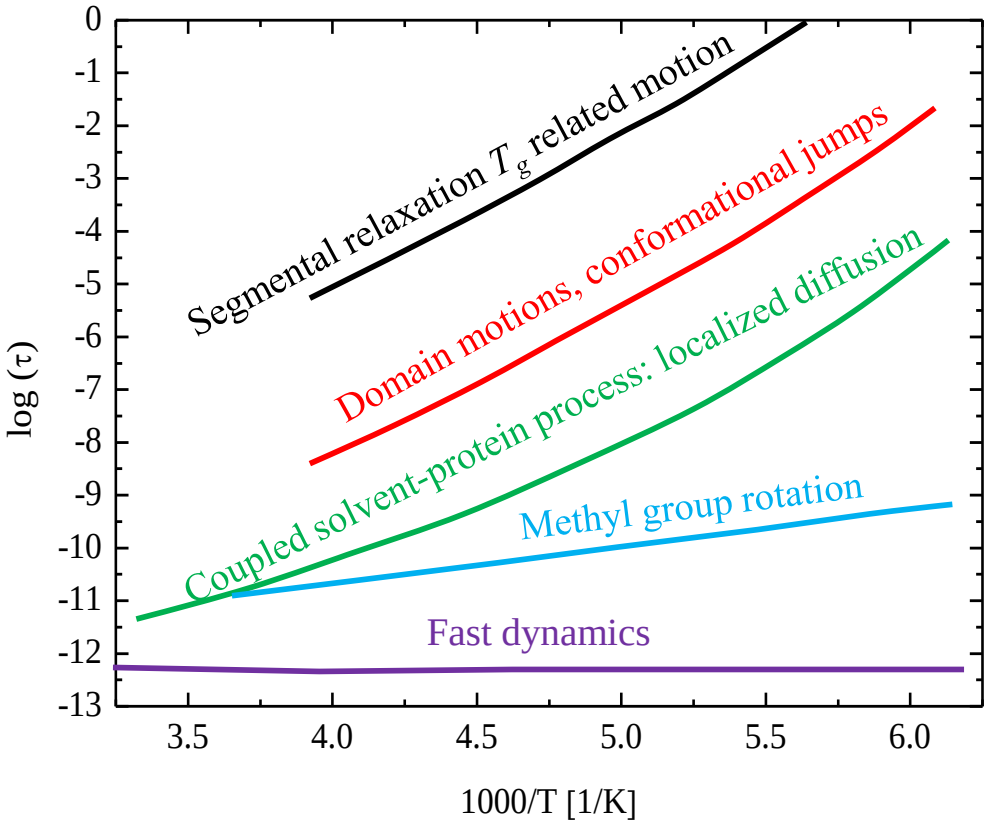

Figure II. 4. Proposed hierarchy of protein dynamics.

According to the authors, at a time scale of approximately 1 picosecond or even faster, small fluctuations are observed. This fast dynamic may present some rattling in a cage formed by

neighboring structural units or fast dynamics in the solvent[20,32]. Methyl group dynamics appear on time scales of several ps[20] and seem to facilitate protein dynamics even at very low temperatures or hydration levels. Finally, although it is not shown in Figure II. 4, the translational and rotational dynamics of hydration water also appear on the same time scale of 10 - 50 ps[20]. According to the authors, these dynamics have much stronger temperature dependence than the methyl groups, leading to a VFT temperature dependence of the relaxation times.

Localized protein fluctuations appear on the sub nanosecond time scale and present conformational fluctuations of residues, side groups and the protein backbone[20]. The VFT temperature dependence of this relaxation suggests a strong coupling with the dynamics of the hydration water. Thus, authors suggested that the time scale of this process is dictated by the behavior of hydration water together with the internal flexibility of the protein. The coupling of the solvent-protein process dependence with the hydration level is so strong that the authors confirmed its suppression in dry proteins or even in proteins placed in glassy matrices[20,33-37].

Moreover, the process has an inflexion point in its temperature dependence near T_g. As the relaxation time of this process does not reach 10^2 s at T_g, authors concluded that the relaxation was not the main relaxation responsible for the glass transition and classified it as a secondary relaxation. Nevertheless, they proposed that this process might be a precursor for slower protein dynamics, in particular, for motions directly involved in proteins functions.

As shown in Figure II. 4, the next process appears in the nanosecond time scale. Its time scale shows a VFT behavior similar to the VFT dependence of the sub nanosecond process, but it is slower than the latter by approximately 10^2 or 10^3 times. The relaxation depends strongly on the protein hydration level, even more than the sub-nanosecond process, and the authors related its origin to protein domain motions[20]. Moreover, according to the authors, this relaxation could be the precursor for conformational jumps that occur on the nanosecond time scale. Thus, both processes, the sub nanosecond and nanosecond relaxations, involve mostly side group motions in the protein core and surface, but S. Khodadadi and A. P. Sokolov considered them as secondary relaxations in biomolecules.

Finally, the authors related the slowest relaxation appearing on the microsecond time scale to the protein structural relaxation[20]. As observed in Figure II. 4, this process has a slightly non-Arrhenius temperature dependence, and a strong dependence on the hydration level. The characteristic energy barriers controlling this process are comparable to the barriers characteristic for peptide backbone rotations (50 – 100 kJ/mol). As backbone motions are the key for the segmental dynamics in proteins, and the microsecond process seems to presents backbone motions, authors suggested that this relaxation might be related to the main structural relaxation of proteins and thus, to the glass transition temperature of hydrated proteins. Furthermore, the authors suggested that this process might be the most directly related to protein functions, folding and other biologically relevant processes, including, as mentioned, the glass transition. Unfortunately, very little is currently known about this process. Studies on this process are complicated due to several reasons. First, modern Neutron Scattering Spectroscopy cannot reach this time, and only a few simulations have been performed at long enough times to equilibrate the system and detect the process. Second, Dielectric Spectroscopy reveals an anomalously large amplitude of this process[18,19]. So, as authors conclude, more studies are required to shed light on this process.

2.3. The slaving mechanism

As mentioned, there is great interest in understanding the role of the solvent in protein dynamics, and the interplay between the solvent (usually water) and the protein is mostly supported by spectroscopy studies[2,5,8,9,13,15,28]. Nevertheless, due to the complexity of the dynamics, it remains a tricky subject, and there is a large literature debate on whether hydration water is driven by peptide dynamics or it drives peptide dynamics. However, experimental[2,13,31] and computational studies of Molecular Dynamics Simulations[38,39] over a broad range of temperatures have indicated that the protein motions are mainly determined by the water dynamics. The protein follows the solvent and not the other way around, leading to the concept of "slaving." The first experimental data deal with ideal mixtures of glass forming systems, which showed that the secondary relaxation of the component and the cooperative relaxation involving the same component were so strongly correlated in properties that they could not be considered separately[18,24,25]. Since the properties of hydrated proteins and binary mixtures of

glass forming systems are similar, the theoretical understanding observed in binary mixtures of glass forming systems was transferred to hydrated proteins describing their motion as being "slaved" to the surrounding solvent. It should be mentioned that recent studies of other biological materials such as lipid membranes have indicated that certain types of motions in these materials are also "solvent slaved"[40], suggesting that the concept "solvent slaving" is not unique for proteins and glass forming systems. Moreover, H. Jansson et al[8] investigated the relation between solvent and protein dynamics, comparing how solvents of different viscosities and dynamical properties affect the protein dynamics. They studied the dynamics of hemoglobin in three different solvents such as water, methanol and glycerol, and observed that the glycerol and methanol samples both showed "slaving-like behavior", even though hemoglobin is not a working protein in these solvents. This finding supports the idea that "solvent slaving" may be a general phenomenon for molecular motions in certain solutions, existing even for nonfunctional proteins and other molecules.

The fact that protein motions are "slaved" by the solvent implies that the protein fluctuations (α-relaxations) exhibit the same, or very similar, non-Arrhenius temperature dependence to the relaxation in the surrounding solvent at temperatures above the glass transition, although at different time scales. This idea also comes from the observation that the glass transition temperature of the protein depends crucially on the solvent. Experimental data from many sources[4,18,29-31] indicate that both the protein and the water participate in the glass transition mechanism, eliminating any doubt as to whether the glass transition originates from the motions of atoms in the protein itself, the motions of the solvent, or the collective motions of both components. Nevertheless, as mentioned, the coupling between protein and solvent dynamics does not mean that the solvent relaxation and its associated protein motions occur on the same timescale. Protein relaxation processes usually occur at lower frequencies than the ones observed for the slaving-water relaxation process. Accurately, protein fluctuations are typically 10^3 - 10^6 times slower, which is because many solvent fluctuations are necessary to cause all the steps for a large-scale conformational changes of the protein[2,12].

2.4. Actual problems in proteins dynamics studies and a summary of our proposal

As mentioned above, Dielectric Spectroscopy is a very efficient tool to analyze the dynamics of proteins in a broad temperature and frequency range. The major problem in protein dynamics studies is that due to water crystallization, hydrated protein powders must be studied[33,34,41-43] instead of solutions. The reason lies in the low solubility of proteins. To achieve dilute aqueous solutions, a large quantity of water is needed, which in the case of Broadband Dielectric Spectroscopy generates major disadvantages. First, large contributions of direct current conductivity (dc) and electrode polarization to the dielectric response masks the solute relaxation and often renders interpretation of the low-frequency data ambiguous[29,43]. Second, at high water contents, the solvent crystallizes at low temperatures (aqueous solvent unavoidably crystallizes below 235 K), masking the solute relaxation on one hand and preventing the study of the dynamics of amorphous water at low temperatures on the other[43].

To avoid these problems, proteins are usually studied in a hydrated powder form, i.e., at low water concentrations, which offers specific advantages compared with measurements in solution. The conductivity and electrode polarization contributions are suppressed or absent at low water concentrations[29], and ice formation can be avoided at all temperatures for h values up to approximately 0.4, at h g of water per g of proteins[44]. Nevertheless, this point originates the most important drawback, as proteins in their hydrated powder form do not represent real situations. Proteins are usually found in nature in solution[42,45]. Living cells, for example, contain approximately 70 wt% water[46,47], so the inability to study proteins in dilute solutions limits the understanding of their biological function and activity.

Thus, to overcome all these difficulties, we propose the study of peptides instead of large macromolecules. Solutions of small peptides share many properties of protein solutions but have the advantage that they can be diluted in aqueous solutions. Thus, to obtain a hierarchy of the dynamics of small biological aqueous solutions and identify the origin of the different relaxations, *n*-lysine oligomers solvated in water were studied by BDS. Lysine is one of the most soluble amino acids, and it does not crystallize in solutions up to hydration levels of 40 wt%[44], which is why we decided to study peptides based on this building block. Chapter IV describes

and collects the results of the different Dielectric Spectroscopy studies performed on ε-polylysine (n = 32 lysine residues) water systems ($30 \leq c_w$ [wt%] ≤ 45 and $7 \leq$ pH ≤ 10). This study allows us to develop an experimental methodology to analyze the complex dielectric data and thus define the molecular origin of each process. Moreover, the coupling between the solute and the solvent dynamics has, as far as we are aware, not been observed for any other water mixtures than protein and lipid membrane solutions. Accordingly, we extended those studies to smaller molecules of lysine peptides. Therefore, we discuss the role of water in *n*-lysine oligomers dynamics (n = 3, 4, 10 and 32) in Chapter V. The dielectric data showed that the oligomers' glass transition related dynamics was determined by water dynamics, as is typical for solvated proteins. Moreover, ε-PLL – water system is an ordinary aqueous solution (note that ε-PLL it is not a peptide as n = 3 to 10 lysine oligomers), so this finding implies that the role of water in protein or peptide dynamics can be extended to other systems where water determines the solute fluctuations.

Accordingly, we also studied the slaving concept in other non-biological systems. For that purpose, in Chapter VI, the coupling between the solvent and a synthetic polymer (polyvinyl pyrrolidone (PVP)) and some polysaccharides (sucrose and dextran) was analyzed. The dynamics of these systems was compared with the previously studied *n*-lysine oligomer solutions and with an aqueous solution of a synthetic glass-forming liquid (tripropylene glycol, 3PG). In the latter case, the water acts as a plasticizer as in typical aqueous systems, while in *n*-lysine, PVP and dextran aqueous solutions, a coupling between the water and the solute dynamics was confirmed. Thus, through this comparison, we extended the slaving behavior to solutions other than proteins.

3. REFERENCES

1 Chaplin, M. Opinion - Do we underestimate the importance of water in cell biology? *Nature Reviews Molecular Cell Biology* **7**, 861-866, doi:10.1038/nrm2021 (2006).

2 Swenson, J., Jansson, H., Hedström, J. & Bergman, R. Properties of hydration water and its role in protein dynamics. *Journal of Physics: Condensed Matter* **19**, 205109, doi:10.1088/0953-8984/19/20/205109 (2007).

3 Rupley, J. A. & Careri, G. Protein hydration and function. *Advances in Protein Chemistry* **41**, 37-172 (1991).

4 Jansson, H. & Swenson, J. The protein glass transition as measured by dielectric spectroscopy and differential scanning calorimetry. *Biochimica et biophysica acta* **1804**, 20-26, doi:10.1016/j.bbapap.2009.06.026 (2010).

5 Khodadadi, S. *et al.* Dynamics of biological macromolecules: not a simple slaving by hydration water. *Biophysical journal* **98**, 1321-1326, doi:10.1016/j.bpj.2009.12.4284 (2010).

6 Frauenfelder, H., Fenimore, P. W. & McMahon, B. H. Hydration, slaving and protein function. *Biophysical chemistry* **98**, 35-48, doi:10.1016/s0301-4622(02)00083-2 (2002).

7 Gabel, F. *et al.* Protein dynamics studied by neutron scattering. *Quarterly Reviews of Biophysics* **35**, 327-367, doi:10.1017/s0033583502003840 (2002).

8 Jansson, H., Bergman, R. & Swenson, J. Relation between solvent and protein dynamics as studied by dielectric spectroscopy. *Journal of Physical Chemistry B* **109**, 24134-24141, doi:10.1021/jp052418v (2005).

9 Frauenfelder, H. *et al.* A unified model of protein dynamics. *Proceedings of the National Academy of Sciences of the United States of America* **106**, 5129-5134, doi:10.1073/pnas.0900336106 (2009).

10 Pal, S. K. & Zewail, A. H. Dynamics of water in biological recognition. *Chemical Reviews* **104**, 2099-2123, doi:10.1021/cr020689l (2004).

11 Despa, F. in *Cell Injury: Mechanisms, Responses, and Repair* Vol. 1066 *Annals of the New York Academy of Sciences* (eds R. C. Lee, F. Despa, & K. J. Hamann) 1-11 (2005).

12 Cerveny, S., Combarro-Palacios, I. & Swenson, J. Evidence of Coupling between the Motions of Water and Peptides. *Journal of Physical Chemistry Letters* **7**, 4093-4098, doi:10.1021/acs.jpclett.6b01864 (2016).

13 Fenimore, P. W., Frauenfelder, H., McMahon, B. H. & Young, R. D. Bulk-solvent and hydration-shell fluctuations, similar to alpha- and beta-fluctuations in glasses, control protein motions and functions. *Proceedings of the National Academy of Sciences of the United States of America* **101**, 14408-14413, doi:10.1073/pnas.0405573101 (2004).

14 Frauenfelder, H., Sligar, S. G. & Wolynes, P. G. The energy landscape and motions of proteins. *Science* **254**, 1598-1603, doi:10.1126/science.1749933 (1991).

15 Fenimore, P. W., Frauenfelder, H., McMahon, B. H. & Parak, F. G. Slaving: Solvent fluctuations dominate protein dynamics and functions. *Proceedings of the National Academy of Sciences of the United States of America* **99**, 16047-16051, doi:10.1073/pnas.212637899 (2002).

16 Frauenfelder, H., McMahon, B. H., Austin, R. H., Chu, K. & Groves, J. T. The role of structure, energy landscape, dynamics, and allostery in the enzymatic function of

myoglobin. *Proceedings of the National Academy of Sciences of the United States of America* **98**, 2370-2374, doi:10.1073/pnas.041614298 (2001).

17 Frauenfelder, H. *The Physics of Proteins: An Introduction to Biological Physics and Molecular Biophysics*. (Springer, 2010).

18 Shinyashiki, N. *et al.* Glass Transitions in Aqueous Solutions of Protein (Bovine Serum Albumin). *Journal of Physical Chemistry B* **113**, 14448-14456, doi:10.1021/jp905511w (2009).

19 Panagopoulou, A., Kyritsis, A., Shinyashiki, N. & Pissis, P. Protein and Water Dynamics in Bovine Serum Albumin-Water Mixtures over Wide Ranges of Composition. *Journal of Physical Chemistry B* **116**, 4593-4602, doi:10.1021/jp2105727 (2012).

20 Khodadadi, S. & Sokolov, A. P. Protein dynamics: from rattling in a cage to structural relaxation. *Soft matter* **11**, 4984-4998, doi:10.1039/c5sm00636h (2015).

21 Johari, G. P. & Whalley, E. The dielectric properties of ice in the range 272-133-K. *Journal of Chemical Physics* **75**, 1333-1340, doi:10.1063/1.442139 (1981).

22 Capaccioli, S., Ngai, K. L. & Shinyashiki, N. The Johari-Goldstein beta-relaxation of water. *Journal of Physical Chemistry B* **111**, 8197-8209, doi:10.1021/jp071857m (2007).

23 Shinyashiki, N. *et al.* Relaxation processes of water in the liquid to glassy states of water mixtures studied by broadband dielectric spectroscopy. *Journal of Physics: Condensed Matter* **19**, 205113, doi:10.1088/0953-8984/19/20/205113 (2007).

24 Capaccioli, S. & Ngai, K. L. Relation between the alpha-relaxation and Johari-Goldstein beta-relaxation of a component in binary miscible mixtures of glass-formers. *Journal of Physical Chemistry B* **109**, 9727-9735, doi:10.1021/jp044893j (2005).

25 Kessairi, K., Capaccioli, S., Prevosto, D., Lucchesi, M. & Rolla, P. Relaxation dynamics in tert-butylpyridine/tristyrene mixture investigated by broadband dielectric spectroscopy. *Journal of Chemical Physics* **127**, doi:10.1063/1.2784190 (2007).

26 Ngai, K. L., Capaccioli, S. & Shinyashiki, N. The protein "glass" transition and the role of the solvent. *Journal of Physical Chemistry B* **112**, 3826-3832, doi:10.1021/jp710462e (2008).

27 Frontzek, A. V., Strokov, S. V., Embs, J. P. & Lushnikov, S. G. Does a dry protein undergo a glass transition? *The journal of physical chemistry. B* **118**, 2796-2802, doi:10.1021/jp4104905 (2014).

28 Ngai, K. L., Capaccioli, S., Ancherbak, S. & Shinyashiki, N. Resolving the ambiguity of the dynamics of water and clarifying its role in hydrated proteins. *Philosophical Magazine* **91**, 1809-1835, doi:10.1080/14786435.2010.523716 (2011).

29 Panagopoulou, A. *et al.* Glass Transition and Dynamics in Lysozyme-Water Mixtures Over Wide Ranges of Composition. *Food Biophysics* **6**, 199-209, doi:10.1007/s11483-010-9201-0 (2011).

30 Panagopoulou, A. *et al.* Glass transition and dynamics in BSA-water mixtures over wide ranges of composition studied by thermal and dielectric techniques. *Biochimica Et Biophysica Acta-Proteins and Proteomics* **1814**, 1984-1996, doi:10.1016/j.bbapap.2011.07.014 (2011).

31 Jansson, H., Bergman, R. & Swenson, J. Role of solvent for the dynamics and the glass transition of proteins. *Journal of Physical Chemistry B* **115**, 4099-4109, doi:10.1021/jp1089867 (2011).

32 Sakai, V. G. *et al.* Solvent effects on protein fast dynamics: implications for biopreservation. *Soft matter* **9**, 5336-5340, doi:10.1039/c3sm50492a (2013).

33 Roh, J. H. *et al.* Influence of hydration on the dynamics of lysozyme. *Biophysical journal* **91**, 2573-2588, doi:10.1529/biophysj.106.082214 (2006).

34 Khodadadi, S., Pawlus, S. & Sokolov, A. P. Influence of Hydration on Protein Dynamics: Combining Dielectric and Neutron Scattering Spectroscopy Data. *Journal of Physical Chemistry B* **112**, 14273-14280, doi:10.1021/jp8059807 (2008).

35 Paciaroni, A., Cinelli, S. & Onori, G. Effect of the environment on the protein dynamical transition: A neutron scattering study. *Biophysical journal* **83**, 1157-1164 (2002).

36 Nickels, J. D. *et al.* Dynamics of Protein and its Hydration Water: Neutron Scattering Studies on Fully Deuterated GFP. *Biophysical journal* **103**, 1566-1575, doi:10.1016/j.bpj.2012.08.046 (2012).

37 Tsai, A. M., Neumann, D. A. & Bell, L. N. Molecular dynamics of solid-state lysozyme as affected by glycerol and water: A neutron scattering study. *Biophysical journal* **79**, 2728-2732 (2000).

38 Tarek, M. & Tobias, D. J. Role of protein-water hydrogen bond dynamics in the protein dynamical transition. *Physical review letters* **88**, doi:10.1103/PhysRevLett.88.138101 (2002).

39 Vitkup, D., Ringe, D., Petsko, G. A. & Karplus, M. Solvent mobility and the protein 'glass' transition. *Nature Structural Biology* **7**, 34-38 (2000).

40 Berntsen, P., Svanberg, C. & Swenson, J. Interplay between Hydration Water and Headgroup Dynamics in Lipid Bilayers. *Journal of Physical Chemistry B* **115**, 1825-1832, doi:10.1021/jp110899j (2011).

41 Lusceac, S. A. *et al.* NMR and dielectric studies of hydrated collagen and elastin: Evidence for a delocalized secondary relaxation. *Journal of Non-Crystalline Solids* **357**, 655-663, doi:10.1016/j.jnoncrysol.2010.07.035 (2011).

42 Pagnotta, S. E., Cerveny, S., Alegria, A. & Colmenero, J. The dynamical behavior of hydrated glutathione: a model for protein-water interactions. *Physical Chemistry Chemical Physics* **12**, 10512-10517, doi:10.1039/c003493b (2010).

43 Nakanishi, M. & Sokolov, A. P. Protein dynamics in a broad frequency range: Dielectric spectroscopy studies. *Journal of Non-Crystalline Solids* **407**, 478-485, doi:10.1016/j.jnoncrysol.2014.08.057 (2015).

44 Cerveny, S. & Swenson, J. Dynamics of supercooled water in a biological model system of the amino acid L-lysine. *Physical Chemistry Chemical Physics* **16**, 22382-22390, doi:10.1039/c4cp02487g (2014).

45 Gaspar, A. M., Appavou, M. S., Busch, S., Unruh, T. & Doster, W. Dynamics of well-folded and natively disordered proteins in solution: a time-of-flight neutron scattering study. *European Biophysics Journal with Biophysics Letters* **37**, 573-582, doi:10.1007/s00249-008-0266-3 (2008).

46 Cooper, G. M. *The cell: A molecular approach*. 2 edn, (Sinauer Associates, 2000).

47 Alberts, B. *et al. Molecular biology of the cell*. Vol. 4 (Garland Science, 2002).

CHAPTER III

MATERIALS AND EXPERIMENTAL TECHNIQUES

1. MATERIALS

In this section we present the materials under study and the protocols used to prepare the samples.

1.1. Oligomers of lysine aqueous solutions

Oligomers of lysine (*n*-lysine, n = 3, 4 and 10) from Sigma Aldrich Chemical Co. Inc. (n = 3 and 4) and Byomatic (n = 10) were used without any further purification. The oligomers molecular structures are shown in Figure III.1.

We prepared solutions at different water concentrations (c_w) ranging from 5 to 45 wt%, as show Table III. 1, using ultrapure water from Aldrich Chemical Co. Inc. The solutions were left under continuous stirring in order to achieve homogeneity. After one week, a yellowish translucent solution was obtained in samples with 45 to 35 wt%. When decreasing the water content down to c_w = 30 wt% the solutions turned opaque and acquired a gel-like consistency. Finally, at extremely low water contents, $c_w \leq 20$ wt%, lysine oligomer - water mixtures were in the form of hydrated powders.

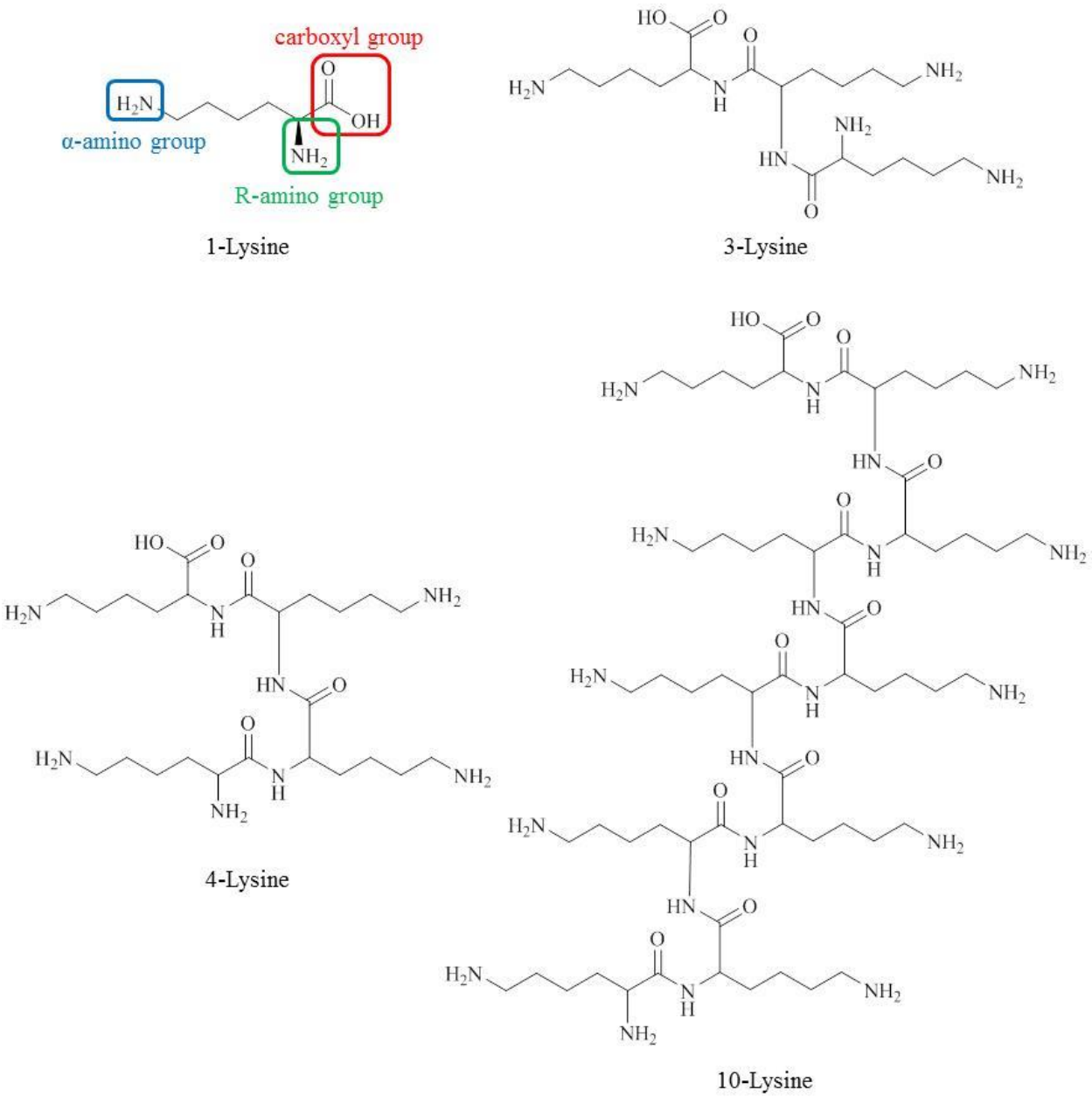

Figure III.1. Molecular structure of the lysine oligomers.

pH values were determined by using a SevenGo Duo pH Meter equipated with an InLab Micro pH electrode sensor by Metter Toledo. Calibration was done using different buffer solutions of pH = 4, 7 and 9. For the different oligomer aqueous solutions (n = 3 to 10), the pH value was around 10. At this pH, the amino acid is in its isoelectric point (pI = 9.75[1-3]) where the α-amino group is uncharged (NH_2), the side chain R-amino group protonated (NH_3^+) and the α-carboxyl

group deprotonated (COO^-), and therefore the net charge is cero. This fact is represented in the lysine titration curve in Figure III.2.

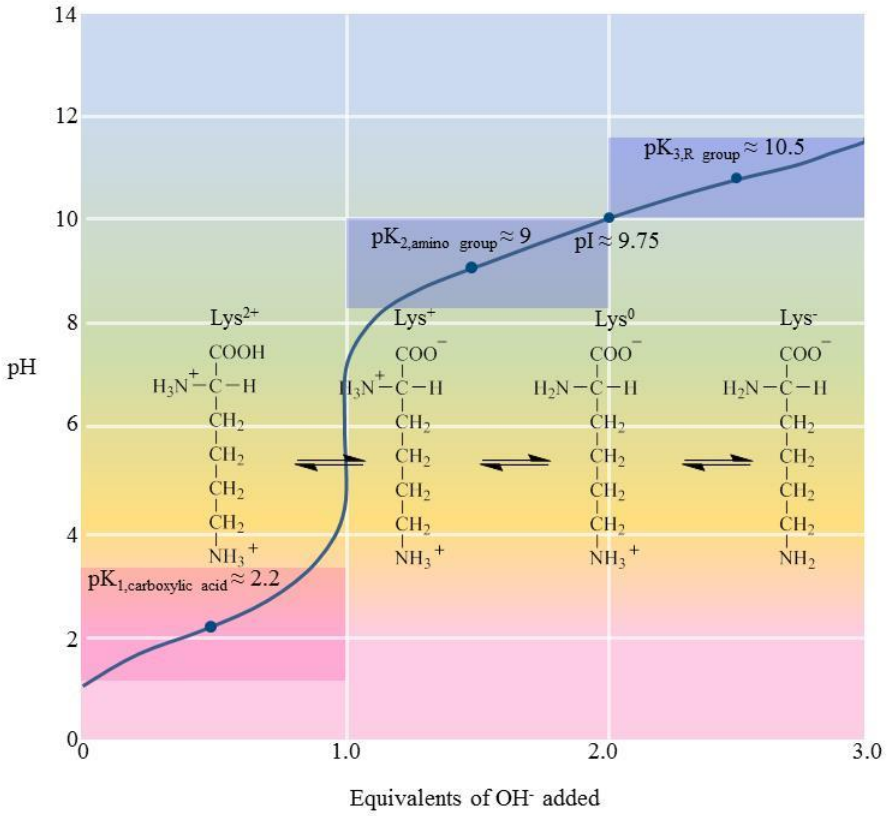

Figure III.2. Lysine titation curve and the different charge states according to the pH values.

General characteristics of *n*-lysine oligomer solutions are shown in Table III. 1. Samples were labeled as *a*-Lys – *b*W, where *a* and *b* indicate the lysine oligomer content and the water content, respectively.

Table III. 1. Samples' general characteristics. c_{lys} and c_w are the weight fraction of lysine and water, and M_w molecular weigth.

Sample	Monomers amount	$c_{n\text{-}lys}$ [wt%]	c_w [wt%]	pH	M_w [g/mol]
60 3-lys – 40W	3	60	40	≈ 10.0	402.5
75 3-lys – 25W	3	75	25	≈ 10.0	402.5
85 3-lys – 15W	3	85	15	-	402.5
90 3-lys – 10W	3	90	10	-	402.5
95 3-lys – 5W	3	95	5	-	402.5
100 3-lys	3	100	0	-	402.5
60 4-lys – 40W	4	60	40	≈ 10.0	530.7
60 10-lys –40W	10	60	40	≈ 10.0	1299.8

The self life (which is the length of time that a product may be stored without becoming unfit for use) of monomers and small peptides in solution is rather limited, so the best approach is to reconstitute the samples for immediate usage. Thus, once homogeneous oligomer aqueous solutions were obtained (after one week of continuous stirring), they were characterizated, and for long term storage they were kept in light-protected flasks at 4 ºC in order to avoid degradation.

1.2. *ε*-Polylysine aqueous solutions

25 wt% *ε*-polylysine aqueous solution (average molecular weight M_w = 4700 g/mol and polydispersity index M_w/M_n = 1.15) was kindly supplied by JNC Corporation (Japan). Its molecular structure is shown in Figure III.3.

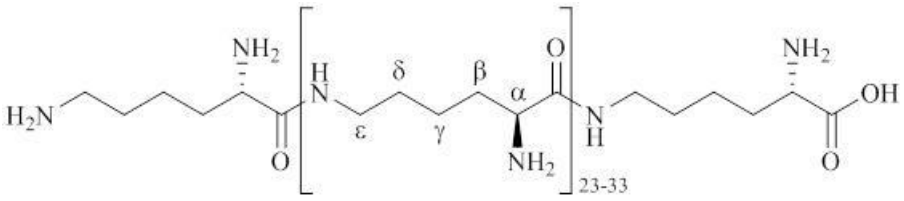

Figure III.3. Molecular structure of *ε*-polylysine.

Different hydration levels were obtained by evaporation of water from the as-received sample at 40 ºC under continuous stirring during several hours depending on the desired c_w content (see the experimental set up for water evaporation in Figure III.4). *ε*-Polylysine's melting point is 172.8 ºC (445.95 K)[4], and it is reported to remain stable even after boiling at 100 ºC for 30 min with no degradation of the material[5-7], so at 40 ºC, the evaporation process ensures no *ε*-polylysine structural damage.

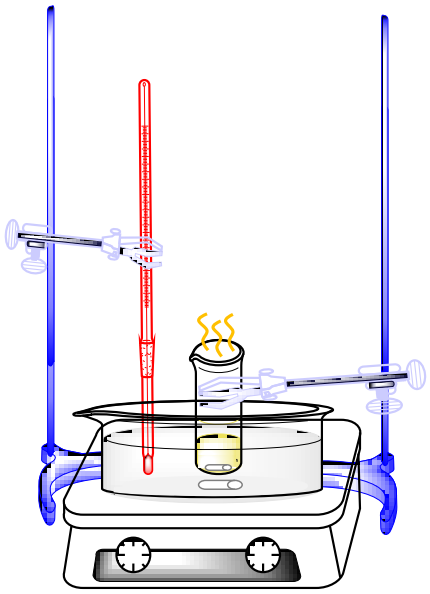

Figure III.4. Experimental set up for water evaporation at 40 ºC under continuous stirring to obtain samples of different hydration levels.

Water contents, shown in Table III. 2, were determined by both thermogravimetry measurements and directly weighting the samples. Samples were labeled as *a*ε-PLL – *b*W_{pHc}, being *a*, *b* and *c* the ε-polylysine content, the water content and the pH value, respectively. Similar to lysine oligomers solutions, samples with c_w from 45 wt% to 35 wt% were clear and transparent solutions by eye inspection. Decreasing the water content, they turned opaque and adopted a gel-like consistency, and the sample with the lowest water level (20 wt%) was considered a hydrated powder.

All the solutions have pH ≈ 10. The isoelectric point for ε-polylysine, with 25 – 35 residues, is found to be at about pI = 9[5,6,8], where the intermediate α-amino groups are uncharged, while the side chain ε-amino and α-carboxyl groups are in a protonated (NH_3^+) and a deprotonated (COO^-) state, respectively (see the ε-polylysine charge states in Figure III.5).

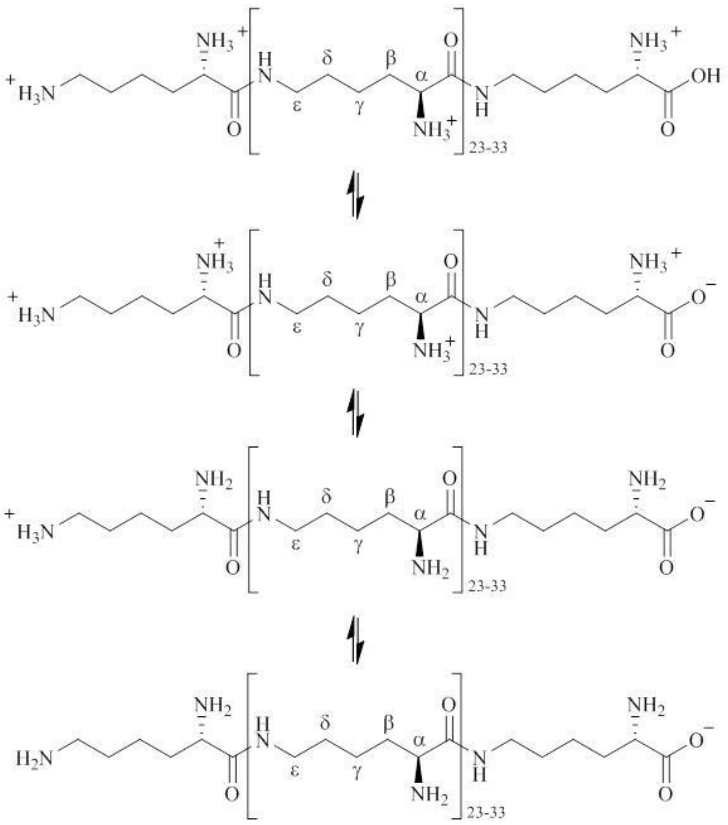

Figure III.5. *ε*-Polylysine charge states according to the different pH values.

In order to study the molecule at pH values differing from its isoelectric point, the pH value was adjusted to lower values by adding HCl (37 wt%) to the c_w = 40 wt% solution (see Table III. 2).

Table III. 2. General characterization of *ε*-PLL (M_w = 4700 g/mol) samples.

Sample	$c_{\varepsilon\text{-}PLL}$ [wt%]	c_w [wt%]	pH
55*ε*-PLL – 45W_{pH10}	55	45	≈ 10.0
60*ε*-PLL – 40W_{pH10}	60	40	≈ 10.0
65*ε*-PLL – 35W_{pH10}	65	35	≈ 10.0
70*ε*-PLL – 30W_{pH10}	70	30	≈ 10.0
80*ε*-PLL – 20W_{pH10}	80	20	-
95*ε*-PLL – 5W_{pH10}	95	5	-
97*ε*-PLL – 3W_{pH10}	97	3	-
98*ε*-PLL – 2W_{pH10}	98	2	-
100*ε*-PLL	100	0	-
60*ε*-PLL – 40W_{pH7}	60	40	≈ 7.0
60*ε*-PLL – 40W_{pH8}	60	40	≈ 8.0
60*ε*-PLL – 40W_{pH9}	60	40	≈ 9.0

Samples were hermetically stored at 4 °C to avoid further water evaporation and possible sample degradation.

1.3. Polyvinylpyrrolidone (PVP) aqueous solutions

Polyvinylpyrrolidone powder (M_w = 55000 g/mol) was supplied by Sigma Aldrich Chemical Co. Inc (see Figure III.6). PVP was purified using an ion transfer resin (AG 501-X8 supplied by Bio-Rad Laboratories) and freeze-dried in vacuum before mixed with water. Deionization for the removal of ionic species from the solutions was carried out by the batch method, which consists in the addition of the resin directly into the sample followed by a stirring process to achieve deionization. In this case, first about 5 g of fresh resin were added for every 100 ml of sample (PVP aqueous solution), and then the mixture was stirred for 1 hour. Finally, samples were filtered from the resin, and freeze-dried to obtain a purified powder. Then, ultrapure water from Aldrich Chemical Co. Inc. was added to the PVP power in order to obtain solutions to different concentrations (see Table III. 3.). Finally, PVP mixtures were left for some days under continuous stirring to achieve homogeneous solutions. For the samples with the lowest hydration levels ($c_w \leq 25$ %wt), it takes a long time, even months, to obtain a uniform water distribution, so in order to accelerate this process, the desired concentration was obtained from diluted solutions. Thus, starting from $c_w = 50$ wt%, water was evaporated by heating the solution to 40 ºC under continuous stirring during several hours (this time is dependent on the desired final c_w content, see experimental set up for the water evaporation in Figure III.4). Final water content was determined by both thermogravimetry measurements and directly by weighting the samples.

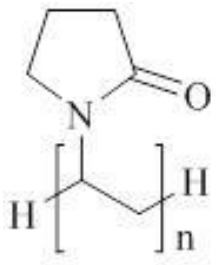

Figure III.6. Molecular structure of PVP.

Samples were labeled as *a*PVP – *b*W, where *a* and *b* indicate the polyvinylpyrrolidone content and water content, respectively. As for the previous *n*-lysine oligomer solutions, samples clearness was lost when decreasing the water content, adopting a gel-like consistency or hydrated powder form for the lowest hydration levels.

Table III. 3. General characterization of PVP (M_w = 55000 g/mol) samples.

Sample	c_{PVP} [wt%]	c_w [wt%]
50PVP – 50W	50	50
55PVP – 45W	55	45
60PVP – 40W	60	40
65PVP – 35W	65	35
70PVP – 30W	70	30
75PVP – 25W	75	25
80PVP – 20W	80	20
85PVP – 15W	85	15
90PVP – 10W	90	10
95PVP – 5W	95	5
98PVP – 2W	98	2
100PVP	100	0

1.4. Aqueous solutions of poyssacharides; dextran and sucrose

Dextran (M_w = 70000 g/mol) and sucrose (M_w = 342.3 g/mol) were supplied by Sigma Aldrich Chemical Co. Inc. Both were purified using an AG 501-X8 ion transfer resing of Bio-Rad Laboratories before mixed with ultrapure water from Aldrich Chemical Co. Inc. For sucrose a unique solution was prepared with c_w = 40 wt% (named as 60sucrose – 40W), while for dextran, solutions of different concentrations were prepared (see Table III. 4.). Dextran samples were labeled as *a*dextran – *b*W, *a* and *b* indicating the dextran and the water content, respectively.

As usual, mixtures were left for some days under continuous stirring to achieve homogeneity. Low hydration level dextran mixtures ($c_w \leq$ 30 %wt) were obtained starting from diluted solutions ($c_w =$ 50 wt%) and evaporating water heating the solutions at 40 ºC under continuous stirring during several hours.

Table III. 4. General characterization of dextran (M_w = 70000 g/mol) samples.

Sample	$C_{dextran}$ [wt%]	c_w [wt%]
50dextran – 50W	50	50
65dextran – 35W	65	35
70dextran – 30W	70	30
80dextran – 20W	80	20
85dextran – 15W	85	15
88dextran – 12W	88	12
90dextran – 10W	90	10
93dextran – 7W	93	7
100dextran	100	0

2. EXPERIMENTAL TECHNIQUES

2.1. Thermal analysis

Thermal analysis comprises a series of techniques as Differential Scanning Calorimetry (DSC), Thermogravimetric Analysis (TGA), Thermomechanical Analysis (TMA), Dynamic Mechanical Analysis (DMA) and Rheology. These techniques can be used to characterize the physical properties of a wide variety of materials and how they change with temperature. In the present work we used DSC and TGA.

2.1.1. Differential scanning calorimetry (DSC)

DSC is a very important analytical tool because all transitions (change in physical properties) involve heat flow. In a DSC experiment, the difference in the amount of heat required to increase the temperature of a sample and an inert reference is measured as a function of the temperature. The sample and the reference are heated at the same rate, and the temperature difference between them is recorded[9]. This temperature difference between the sample and the reference occurs each time the sample goes through an exothermic or endothermic transition. The difference in heat flow caused by the temperature difference between two objects can be expressed by:

$$\frac{dH}{dt} = c_p \frac{dT}{dt} + f(T,t) \qquad \text{(III.1)}$$

where $\frac{dH}{dt}$ is the DSC heat flow signal, c_p is the heat capacity, $\frac{dT}{dt}$ is the heating rate and $f(T,t)$ is the time dependent heat flow at a temperature[10].

Figure III. 7 illustrates the most common type of thermal transitions observed in a DSC experiment.

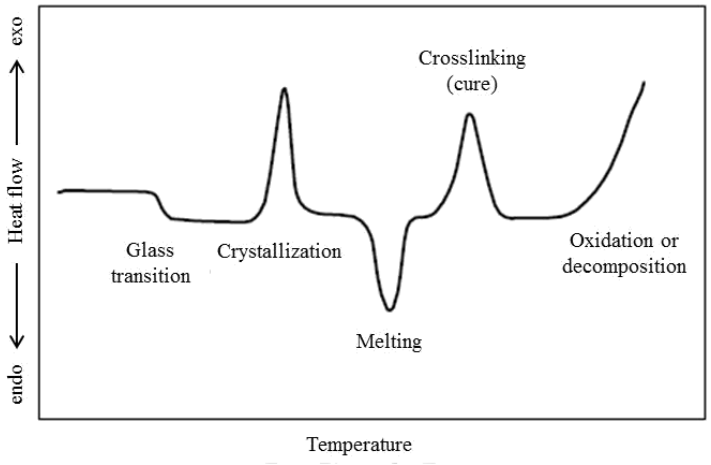

Figure III. 7. Different thermal transitions observed in DSC curves; glass transition as an endothermic shift in the heat flow baseline, crystallization as an exothermic transition which releases energy (heat) (when amorphous to crystalline transition is produced upon a heating cycle, it is often called cold crystallization), and finally, melting process (conversion of crystalline structure to a viscous amorphous structure) as an endothermic transition which absorbs energy.

According to this representation, a liquid that is cooled generally crystallizes somewhat below its melting temperature. Crystallization means that the random moving molecules of the liquid (amorphous state) freeze in positions corresponding to minima in the potential energy resulting in an ordered structure displaying a long range periodicity. Nevertheless, not all liquids crystallize, many polymers (e.g., pure amorphous polymers) are known ever to crystallize, and among those that do crystallize, most of them have both types of structures (amorphous and crystalline) and they are usually referred to as semicrystalline polymers[11] (see Figure III. 8).

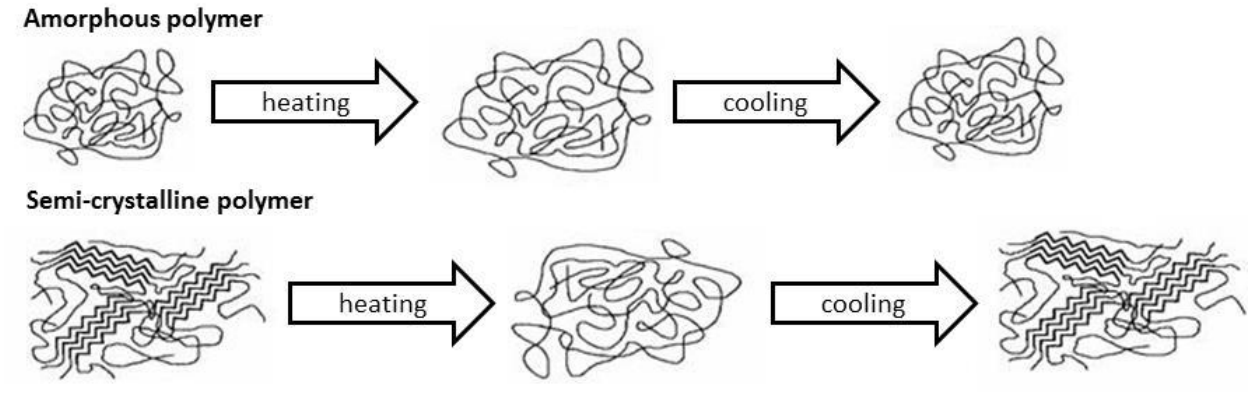

Figure III. 8. Effect of processing on the morphology of amorphous and semy crystalline polymers.

Just below the melting temperature (T_m), the probability of crystallization is maximum, and as the temperature is further reduced, the probability decreases due to the slowing down of molecular motions. Hence, passing the temperature range of high probability of crystallization, near T_m, at a rate faster than that of nucleation, crystallization can be avoided, and the system will then enter in its supercooled state. The resulting supercooled state is thus a disordered state which is meta-stable with respect to the crystalline equilibrium state. In this supercooled regime, the viscosity (η) increases rapidly with decreasing temperature and it is often described by a Vogel-Fulcher-Tammann (VFT)[12,13] behavior:

$$\eta = \eta_0 exp\left(\frac{DT_0}{T-T_0}\right) \quad \text{(III.2)}$$

where D is a uniteless temperature factor and T_0 is the so-called VFT-temperature, which is usually found at several tens (30 - 70 K) below the glass-transition temperature T_g. When the viscosity reaches values above 10^{13} poise (10^{12} Nsm^{-2}), the liquid behaves solid-like and it is termed as a glass[14], having a random structure similar to that of a liquid but no the long range order typical of crystals[15]. So the glass transition temperature (T_g) can be either defined as the temperature where the viscosity reaches a value of 10^{13} poise, or the temperature were other properties of the system change, such as the enthalpy and the volume. This makes material to change form from rubbery and flexible state above T_g to a glassy, rigid structure below T_g[11].

Figure III. 9 shows a typical results of measuring the volume (a) and the heat capacity (b) versus the temperature for a glass-forming liquid.

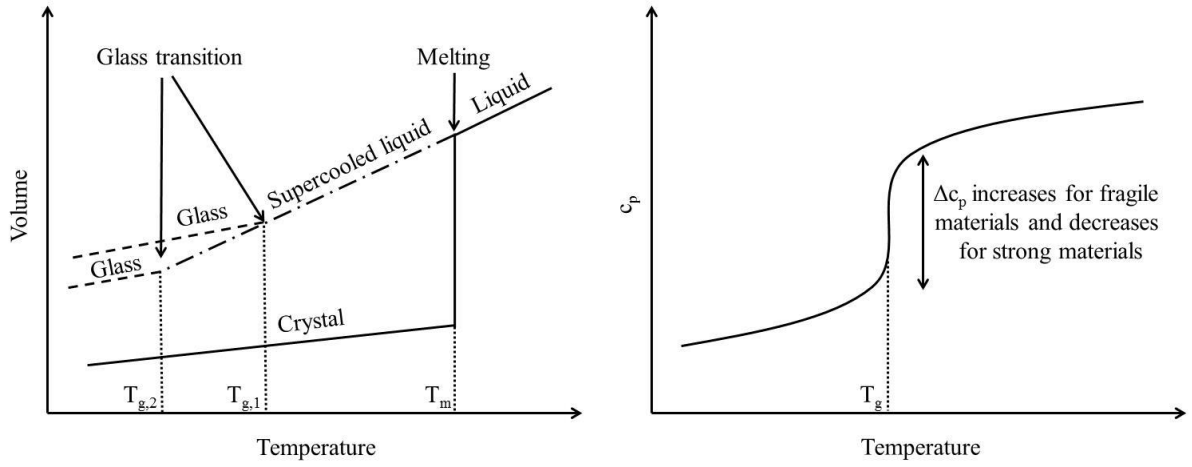

Figure III. 9. Volume (a) and the heat capacity (b) in function of the temperature.

Upon cooling, the volume shows a discontinuity; crystallization. However, as previously explained, if crystallization is avoided, the liquid enters the supercooled state and on further cooling it turns into a glass. For the glass transition, there is a discontinuous change observed for the volume, but rather a change in slope in the region of T_g. This change is accompanied by an often quite sharp drop in the heat capacity[16]. However, as shown in Figure III. 9 (a), the location of the glass transition is sensitive upon cooling rate as the glass transition denoted $T_{g,1}$ is reached by the use of a higher cooling rate than the one denoted as $T_{g,2}$. Hence kinetics is important for the glass transition, and the experimentally observed transition cannot be a pure thermodynamic feature.

In this thesis, a differential scanning calorimeter of TA Instrument Q2000 was used to determine thermal events on all the samples (see in Figure III.10). Samples of about 5 to 10 mg of weight were sealed in aluminum hermetic pans. Repeated cooling and heating cycles at a rate of 10 K/min under nitrogen flow were done. From the heat flow - temperature curves, the glass transition temperature was determined as the onset point of the heat flow step of the heating trace.

Figure III.10. DSC Q2000 from TA Instruments.

2.1.2. Thermogravimetric analysis (TGA)

Thermogravimetric analysis is an analytical technique used to determine the material's thermal stability and the fraction of volatile components by monitoring the weight change that occurs as a specimen is heated[17]. In these experiments, the sample weight is recorded as a function of the temperature in air or in an inert atmosphere, such as Helium or Argon.

In this thesis, the thermogravimetry analysis was performed to determine the water content of the samples using a TA Instruments Q500 thermogravimetric analyzer (see Figure III.11). Samples were placed on the plantinum pan, and heated from room temperature to 1073.15 K with a ramp rate of 5 K/min under a constant N_2 flow of 25 mL/min.

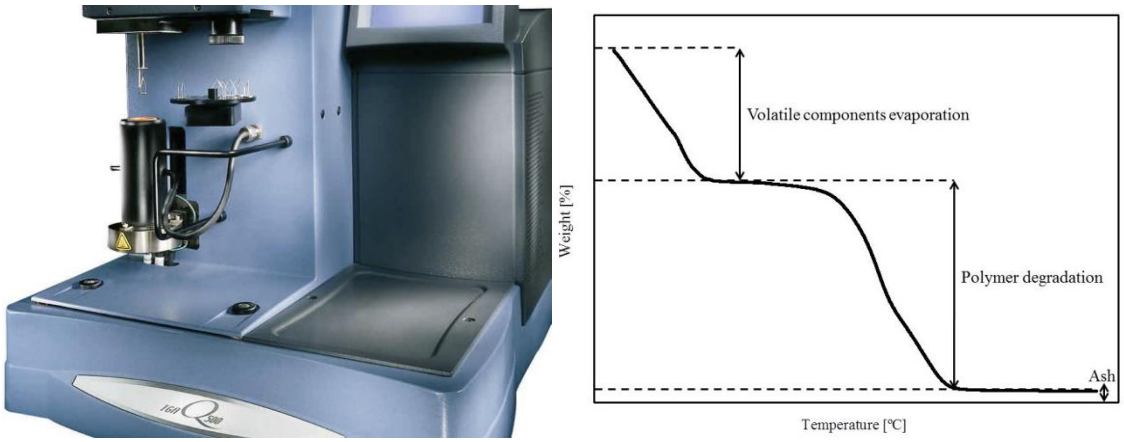

Figure III.11. Q500 thermogravimetric analyzer by TA Instruments employed for the TGA measurements (left) and the lost of weight observed in TGA curves (right).

2.2. Fourier transform infrared spectroscopy (FTIR)

Spectroscopy techniques use the electromagnetic radiation to obtain information about atoms and molecules by means of studying interactions between matter (sample being analyzed) and energy (any portion of the electromagnetic spectrum)[18]. The electromagnetic spectrum extends from high wavelengths (low frequencies) used for modern radio communication, to gamma radiation at short wavelengths (high frequencies), thereby covering wavelengths from thousands of kilometers down to a fraction of the size of an atom. Concerning to the range of infrared region (wavenumber; 12800 - 33 cm^{-1}), it can be divided into near-infrared region (12800 - 4000 cm^{-1}), mid-infrared region (4000 - 200 cm^{-1}) and far-infrared region (200 - 10 cm^{-1})[18] (see Figure III.12).

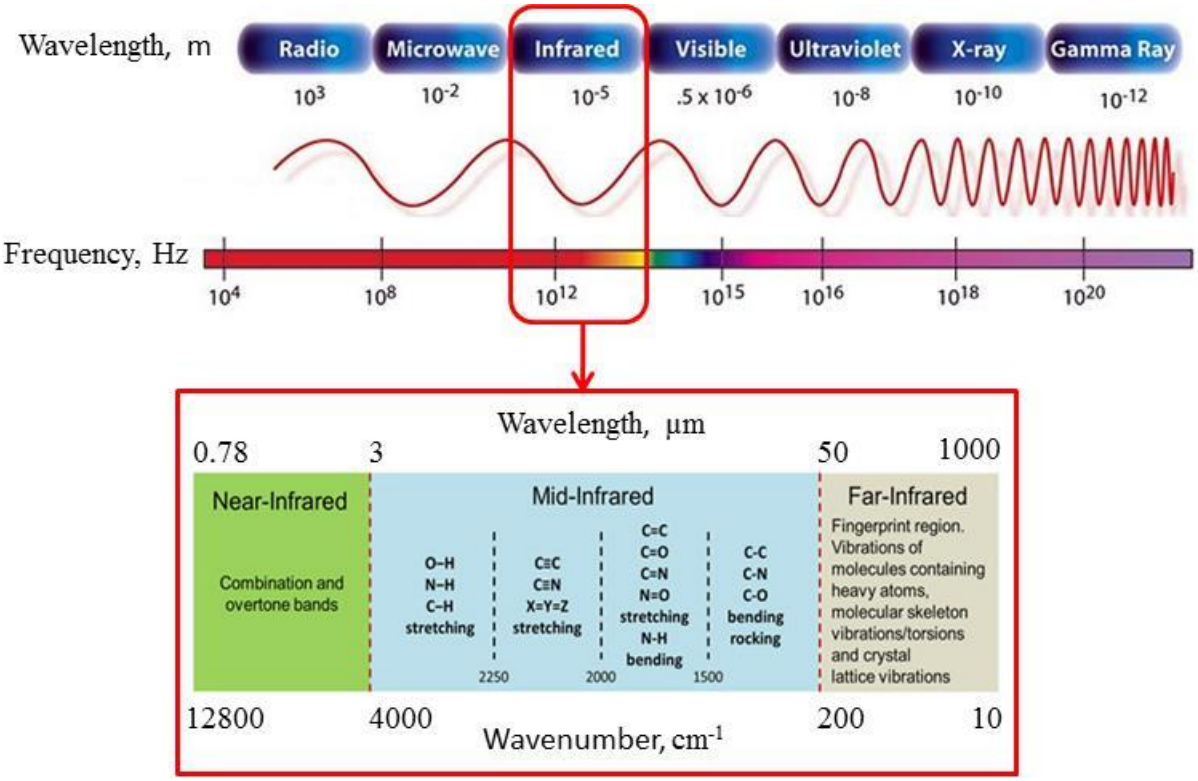

Figure III.12. Electromagnetic spectrum (above). Three infrared regions; near-infrared (12800 - 4000 cm^{-1}), mid-infrared region (4000 - 400 cm^{-1}) and far-infrared region (400 - 33 cm^{-1}) (below).

When the wavelength of the IR radiation is close to the natural frequency of the different molecular vibrations, the radiation is absorbed by the molecule, exciting it to a higher vibrational

state[19]. The resulting IR spectrum is a molecular vibrational spectrum, which represents the wavelength and intensity of the absorption of infrared light by a sample, creating a molecular fingerprint of it. This fingerprint collects the absorption peaks which correspond to the frequencies of vibrations of the bonds of the atoms making up the material and, because each different material is a unique combination of atoms, no two compounds produce the same infrared spectrum. According to this principle, infrared absorption spectroscopy is used in molecular structure characterization to determine their functional groups by means of the characteristic absorption of the infrared radiation.

In this thesis, the infrared spectroscopy technique was mainly used to determine the secondary structures of peptides in H_2O solutions. The most sensitive spectral region of the protein secondary structural components is the amide I band (1700 − 1600 cm^{-1}), which is mainly due to the C=O stretching vibrations of the peptide linkages (approximately 80%), coupled with little in-plane NH bending (< 20%)[20]. Each type of secondary structure results in a different C=O stretching frequency due to unique backbone conformation and hydrogen bonding pattern, making amide I band useful for the analysis of the secondary structure adopted by the peptide chain[20,21]. Amide I band consists of overlapping of various types of protein secondary structures such as α-helices, β-sheets, turns and random structures, and the assignments of the amide I band position to each secondary structure is shown in Table III. 5.

Table III. 5. Spectral ranges of absorption for secondary structures[22].

Secondary structure	**Band position, cm^{-1}**	
	Average	**Range**
α-Helix	1654	1648 – 1657
β-Sheet	1633	1623 – 1641
	1684	1674 – 1695
β-Turns	1672	1662 – 1686
Random coil	1654	1642 - 1657

The infrared spectra were recorded using a Jasco 6300 spectrometer equipped with an attenuated total reflectance (ATR) unit (see Figure III.13), which allows the analysis of the sample with little preparation. In order to study the C=O streching frequency, measurements

were performed at 25 ºC over the mid infrared region (4000 to 600 cm^{-1}) at 2 cm^{-1} resolution and averaging over 50 scans. The baselines were corrected using the Spectra Analysis software from Jasco, and no smoothing of the data was performed. A background spectrum was also measured, which consist of a measurement with no sample in the beam. By subtracting the background spectra from the sample measurements, we obtain the spectrum which has all of the instrumental characteristics removed, and therefore, all spectral features present are strictly due to the sample.

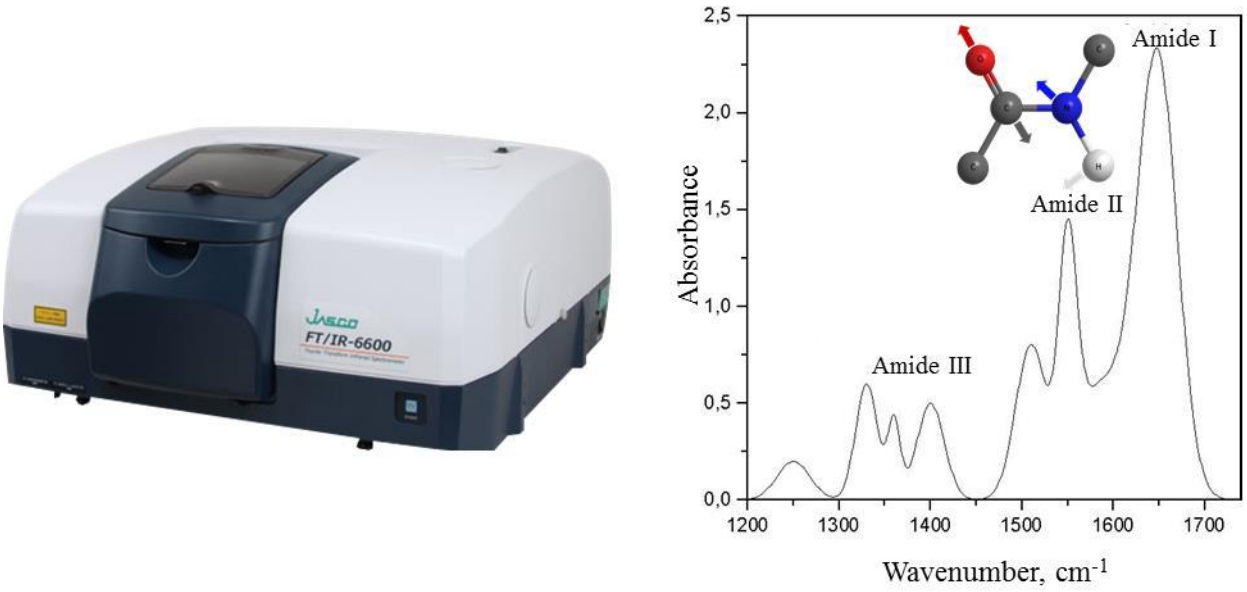

Figure III.13. FTIR spectrometer 6000 series by Jasco employed for FTIR experiments (left) and amide I band vibrational mode in FTIR spectra (rigth).

2.3. X-ray scattering

Scattering methods are a collection of powerful techniques for the evaluation of the molecular organization of materials including polymers[11]. Specifically, in X-ray scattering, radiation has a wavelength comparable to the atomic scale ($\lambda \approx 10^{-10}$ m) being therefore ideal to make the atoms interact with light. When X-rays hit a material, a fraction pass through the sample, and a fraction is scattered into other directions of propagation[23] (see Figure III.14). When X-rays are incident on a sample, the scattered waves interfere with each other, either constructively or destructively, producing a diffraction pattern. Thus, from the knowledge of how the light is scattered when it

impacts on a material, it is possible to deduce information on how the sample components are geometrically arranged[11].

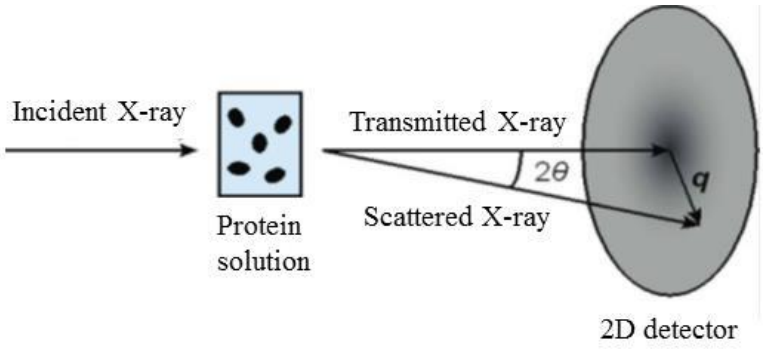

Figure III.14. Basis of the diffraction technique**.**

The angle trough which the beam is scattered determines the structural information. Thus, small angle scattering can be use to determine features on the length scales of several to hundred nanometers, while wide angle examines the features from several nanometers down to angstrom levels, accesing for example information about the polymer chain conformation (e.g. inter and intra chain segments)[11].

In 1910, W.L. Bragg presented an explanation of the diffracted X-ray beams from a cristalline lattice. As it is shown in Figure III.15, incident waves are reflected from parallel planes of the atoms in the crystal, which each plane reflecting the radiation. The difractted waves are reflected specularly, that is, the angle of incidence wave is equal to the angle of reflection wave, so the energy of the X-ray is not changed during reflection (elastic scattering). Considering parallel lattice planes spaced *d* apart, the path difference for rays reflected from adjacent planes is $2dsin\theta$, where *d* is the distance between planes of atoms and θ the reflection angle. Constructive interference of the radiation from successive planes occurs when the path diffrence is an integral number of *n* wavelengths, λ:

$$2dsin\theta = n\lambda \qquad \text{(III.3)}$$

This is the Bragg law[24].

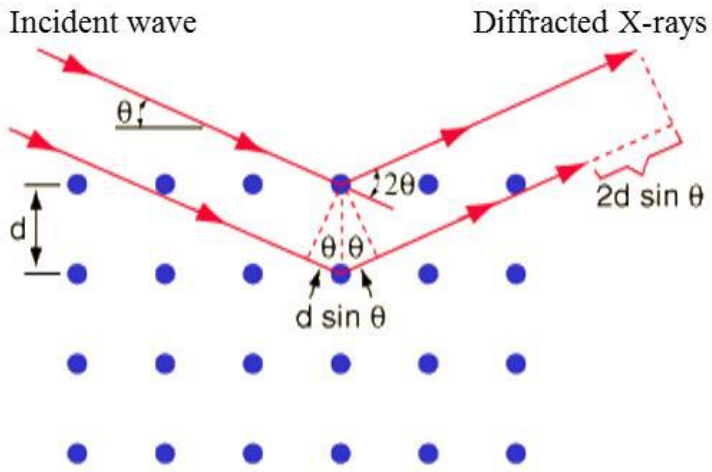

Figure III.15. Bragg law interpretation.

Usually, the scattering pattern represents the intensity of scattered waves as a function of the scattering vector, q, which is described as $q = 4\pi sin\theta / \lambda$[11].

In this thesis, X-ray scattering measurements were carried out in ALBA Synchrotron facilities. ALBA is a complex of electron accelerators to produce 3rd generation Synchrotron Light (3 GeV), which allows the visualization of the atomic structure of matter as well as the study of its properties. The 3 GeV electron beam energy at ALBA is achieved by combining a LInear ACcelerator (LINAC) and an energy booster placed in the same tunnel as the storage ring (see Figure III.16).

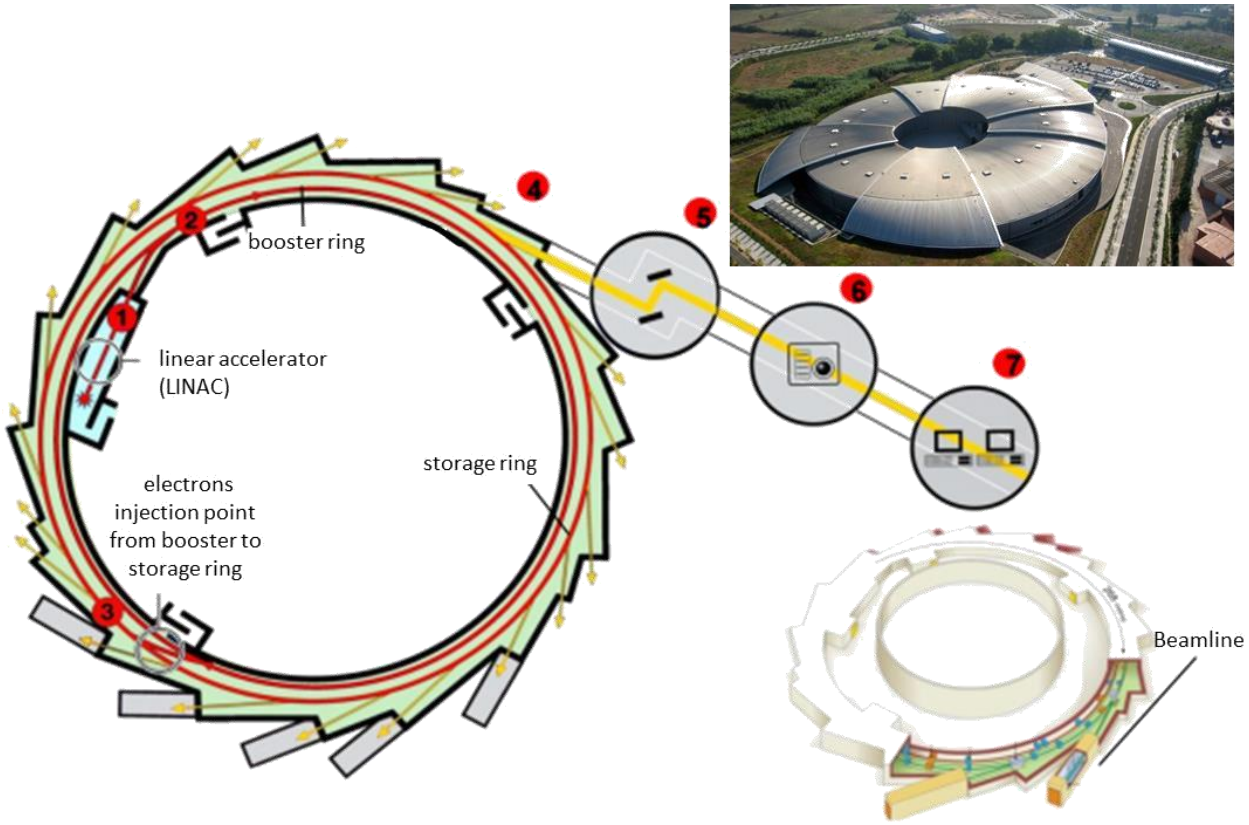

Figure III.16. Aerial view of ALBA Synchrotron facilities and the operation way scheme:
1. Electrons are produced by heating tugsten impregnate in BaO to to extract their surface electrons, and then pre-accelerated up to 100 MeV by electric fields in a linear accelerator (LINAC).
2. In a booster synchrotron electrons are further accelerated up to 3.0 GeV by means of magnetic fields.
3. Electrons are stored and remain circulating at a fixed power (3.0 GeV) within the storage ring using magnetic fields. The booster and the storage ring are located in the same circumference of 249.6 m.
4. Accelerated electrons, when passing through the magnetic fields, they experience a twist that causes the generation of synchrotron light, which is emitted tangentially to the curvature they follow and spreads to the beamlines.
5. In the beamlines (set of optical elements between the light source and the experimental station where the sample is located) the wavelength of interest for each experiment is selected.
6. The synchrotron light illuminates the sample to be analyzed. A detector picks up the image that is generated due to the light-sample interaction.
7. The projected image is scanned, stored and analyzed by computer.

Small Angle X-ray Scattering (SAXS) and Wide Angle X-ray Scattering (WAXS) measurements were carried out using the non-crystalline diffraction beamline (Beamline 11, BL11-NCD), being the SAXS detector supplied by ADSC (Quantum 210r CCD) and the WAXS detector by Rayonix (LX255-HS). ALBA NCD beamline is tunable over a wavelength range of 0.9 Å - 1.9Å (equivalent to an energy range of 6.5 to 13 keV) and delivers a high-photon flux onto the sample. In our case, experiments were performed using a beam energy of 11 keV. Concerning to the beam size at sample position, it determines the brilliance that is directly

related with the contrast of the diffractograms. In NCD, the sample position is movable and therefore the beam size at the sample position is variable. In our case, the distance between the detector and the sample was 6.2 meters and 12 – 13 cm for the small angle and the wide angle scattering respectively. This allowed us to observe a q-range from 0.1 nm^{-1} to 40 nm^{-1}, which according to the equation $d = 2\pi/q$ corresponds to a real space length scale of about 60 to 0.15 nm, to clarify an intramolecular domain correlation of peptides[25].

The diffraction patterns of *n*-lysine (n = 1, 3 and 10) and ε-PLL water solutions at different pH, were investigated to elucidate whether aggregates or larger structural units were formed. Samples were studied in a broad temperature range (from 293 to 153 K using a cooling rate 20 K/min). For these purposes, the beam line is equipped with a HFSX350-CAP linkam stage for 1.5 mm capillaries, a T95 temperature controller and a liquid nitrogen cooling system LNP95 (see Figure III.17).

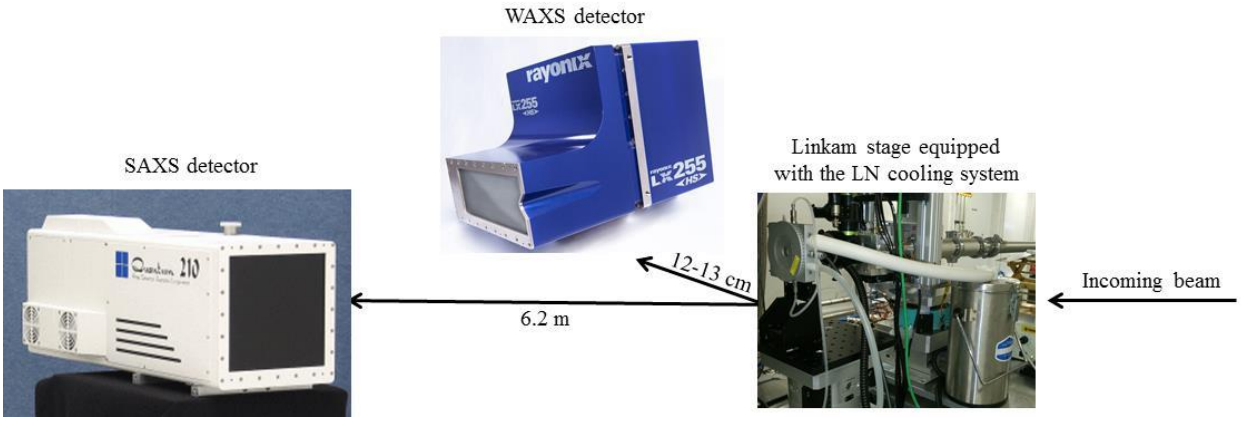

Figure III.17. SAXS and WAXS detectors, together with the HFSX350-CAP linkam stage with the LNP95 pumping system.

2.4. Broadband Dielectric Spectroscopy (BDS)

2.4.1. Basis of dielectric relaxation and polarization mechanisms

Dielectric spectroscopy is a technique mainly used to study the relaxation processes caused by the rotational fluctuations of molecular dipoles. The study of the interaction of electromagnetic waves with matter in the frequency regime between 10^{-6} and 10^{12} Hz is the core of Broadband Dielectric Spectroscopy. The basis of Dielectric Relaxation Spectroscopy as a tool to investigate molecular dynamics is the 'Fluctuation-Dissipation Theorem', which states that the response of a system in thermodynamic equilibrium to a small applied disturbance (linear regime) is the same as its response to a spontaneous fluctuation[26,27].

When materials containing permanent dipoles (with spontaneous fluctuation and randomly oriented due to thermal fluctuations) are placed in an alternating (sinusoidal) external electric field, the latter distorts the arrangement of molecular dipoles which tend to be preferentially oriented in the direction of the field[26]. As it is shown in Figure III.18, the dipolar orientation depends on the frequency of the applied field, and it is related to the dielectric permittivity (ε). This parameter characterizes the dielectric properties of materials containing polar molecules, and it can be interpreted as a measure (on neglecting atomic and electronic polarization) of the number of molecules oriented by an external electric field of unit strength[28]. Dielectric permittivity is usually written as function of the frequency in the complex form[26];

$$\varepsilon^*(\omega) = \varepsilon'(\omega) - i\varepsilon''(\omega) \qquad \text{(III.4)}$$

where ε^* is the complex dielectric permittivity, and ε' and ε'' the real and the imaginary parts, respectively, being $\omega = 2\pi f$.

As shown in Figure III.18, at very high frequencies the relative permittivity assumes a low value (called instant permittivity, ε_∞, which is defined as $\varepsilon_\infty = \lim_{\omega\to\infty} \varepsilon'(\omega)$) but as the frequency of the electric field established inside a dielectric material decreases, the rotation of the pre-existing molecular dipoles increases, which in turn increases the dielectric permittivity.

This is observed as a step in the real part of the complex permitivity, which agrees with a peak in the imaginary part, commonly called "loss peak"[26]. Both, the step in ε' and the loss peak in ε'' are centered at a characteristic frequency. At frequencies low enough, molecular dipoles can follow the electric field with a complete orientation giving rise to a plateau of the dielectric permittivity. This static value in the real part of the complex permittivity is called the static permittivity, ε_S, and is defined as $\varepsilon_s = \lim_{\omega \to 0} \varepsilon'(\omega)$ [26].

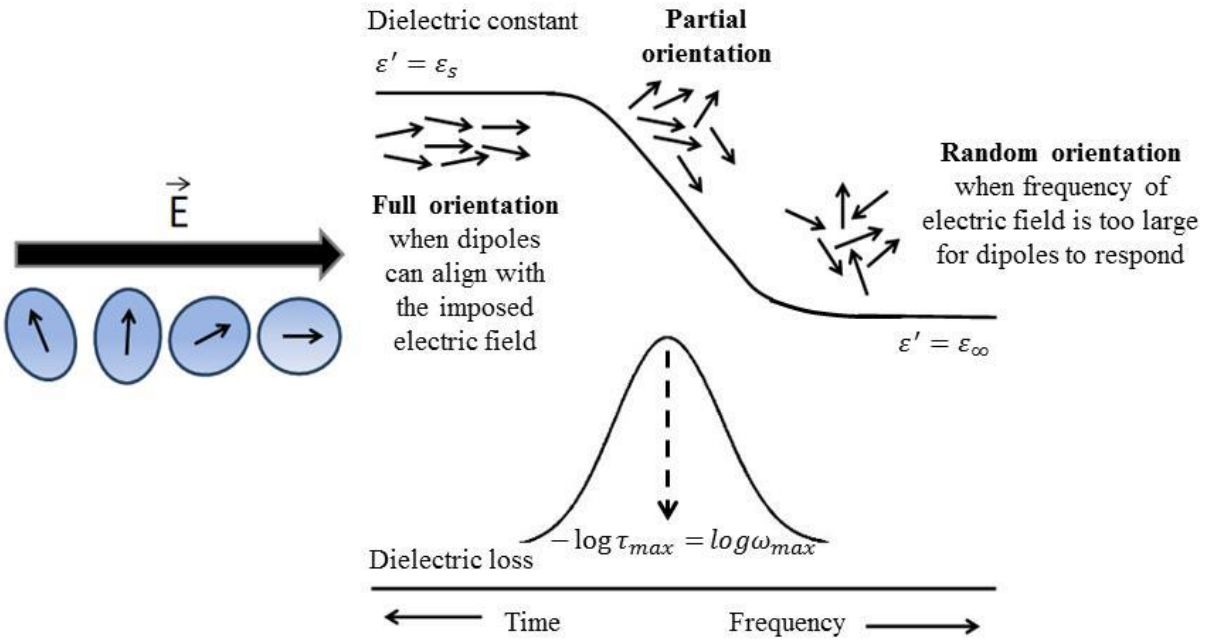

Figure III.18. Scheme of the behavior shown by dipoles when an external electric field is applied.

Thus, the dielectric orientational relaxation time (τ) can then be defined as the time required for dipoles to become field-oriented when applying an electric field[28]. It can be determined from the reciprocal of the loss peak frequency (when the dipolar relaxation reaches its maximum), ranging from several picoseconds, in low viscosity liquids, to hours in glasses and even to years (aging below the glass temperature)[29]. Equation III.5 describes the relaxation time in function of the frequency.

$$\tau_{max} = \frac{1}{2\pi\omega_{max}} \qquad \text{(III.5)}$$

where ω_{max} corresponds with the frequency at the maximum loss.

The mayor drawback of this technique is that within this broad dynamic range, together with dipolar fluctuations, charge transport and interfacial polarization effects also take place[29]. All conductive systems contain dissolved free ions which, under the influence of an electric field, tend to move towards the electrode/sample interface. Interfacial polarization, occurs when charge carriers are trapped at interfaces in heterogeneous systems, or when they are trapped on the electrode surface; namely, electrode polarization[29]. When arriving at the metallic electrodes, free ions are accumulated in thin layers inmediately beneath the sample surface, leading to the development of ionic layers in such regions[30]. Both unwanted effects, ionic conductivity and electrode polarization, lead to difficulties in the interpretation of the dielectric spectra. While ionic conductivity is dominant at low frequencies and high temperatures in the imaginary part of the complex dielectric function, the electrode polarization results in extremely high values of the real part (and imaginary part, however in this interpretation of the complex permittivity, it is not possible to discern between the contribution from the ionic conductivity and from the electrode polarization effect), masking the dielectric response at low frequencies[26]. The real part increases strongly with decreasing frequencies up to very high values which cannot be explained as a molecular relaxation process[26]. Electrode polarization depends on the sample temperature, the structure of the electrodes, their composition and even the roughness of the electrode surface[31].

2.4.2. What is measured in a dielectric experiment?, Debye equation and other empirical models

In a typical dielectric experiment, the sample is placed between two gold plated electrodes creating a parallel plate capacitor with the sample as insulator (see Figure III.19).

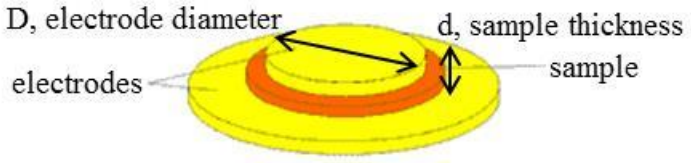

Figure III.19. In typical BDS experiments, the sample is placed between two plane-parallel gold coated electrodes separated by a distance *d* defined by a cross-shaped Teflon spacer which avoid short circuit in a case of a liquid sample.

The electrical capacitance (*C*) of the material, when held between two plane-parallel electrodes of area (*A*) separated by a distance (*d*), is defined by;

$$C = \varepsilon \cdot C_0 = \varepsilon \cdot \varepsilon_o \frac{A}{d} = \varepsilon \cdot \varepsilon_o \frac{\pi D^2}{4d} \quad \text{(III.6)}$$

where *C* is the capacity, C_0 the capacitance of the same arrangement without the sample, ε the dielectric permittivity of the sample, ε_o the permittivity in the vacuum (8.854 pF m^{-1}), *A* the area of the electrodes, *d* the distance between them and *D* the diameter of the upper electrode.

In a dielectric measurement, the capacitor is subjected to a sinusoidal electric field (V = 1 Volt and a frequency $f = \omega/2\pi$), which causes a sinusoidal current of the same frequency. It will generally be a phase shift between the current and the voltage described by the phase angle $\emptyset$. Thus, by considering a sinusoidal excitation, Equation III.6 can be rewritten in the complex form as;

$$C^*(\omega) = \varepsilon^*(\omega) \cdot \varepsilon_o \frac{A}{d} = \varepsilon^*(\omega) \cdot \varepsilon_o \frac{\pi D^2}{4d} \quad \text{(III.7)}$$

The complex permittivity can in turn be described as;

$$\varepsilon^*(\omega) = \varepsilon'(\omega) - i\varepsilon''(\omega) = C^*(\omega) \cdot \frac{d}{\varepsilon_0 A} \quad \text{(III.8)}$$

Moreover, Debye[32] showed that for non interacting molecules with a single relaxation time, the permittivity can be written as;

$$\varepsilon^*(\omega) = \varepsilon'(\omega) - i\varepsilon''(\omega) = \varepsilon_\infty + \frac{\varepsilon_S - \varepsilon_\infty}{1 + i\omega\tau} = \varepsilon_\infty + \frac{\Delta\varepsilon}{1 + i\omega\tau} \quad \text{(III.9)}$$

where $i = (-1)^{1/2}$, $\Delta\varepsilon = \varepsilon_S - \varepsilon_\infty$ is the dielectric relaxation amplitude or dielectric strength, ε_S and ε_∞ refer to the low frequency permittivity and the high frequency permittivity, respectively and τ is the Debye relaxation time. This is the so called Debye equation[32], applicable only for the

case of ideal systems, i.e., systems with a unique time constant (τ), symmetric shape and non interacting dipoles. According to the previous equation, the real part corresponding to the permittivity factor, ε', is given by;

$$\varepsilon'(\omega) = \varepsilon_\infty + \frac{\varepsilon_s - \varepsilon_\infty}{1+\omega^2\tau^2} \qquad \text{(III.10)}$$

And the imaginary component, ε'', known as the dielectric loss factor;

$$\varepsilon''(\omega) = \frac{(\varepsilon_s - \varepsilon_\infty)\omega\tau}{1+\omega^2\tau^2} \qquad \text{(III.11)}$$

ε' is proportional to the energy stored reversibly in the system per period, and ε'' is proportional to the energy dissipated per period, that is, it accounts for the "delay" of the response to the excitation being proportional to the dissipated energy[26]. The Debye relaxation function shows a symmetric loss peak with a narrow width, being the full width at half maximum (FWHM) 1.14 decades in frequency for the dielectric loss[26] (see Figure III.20).

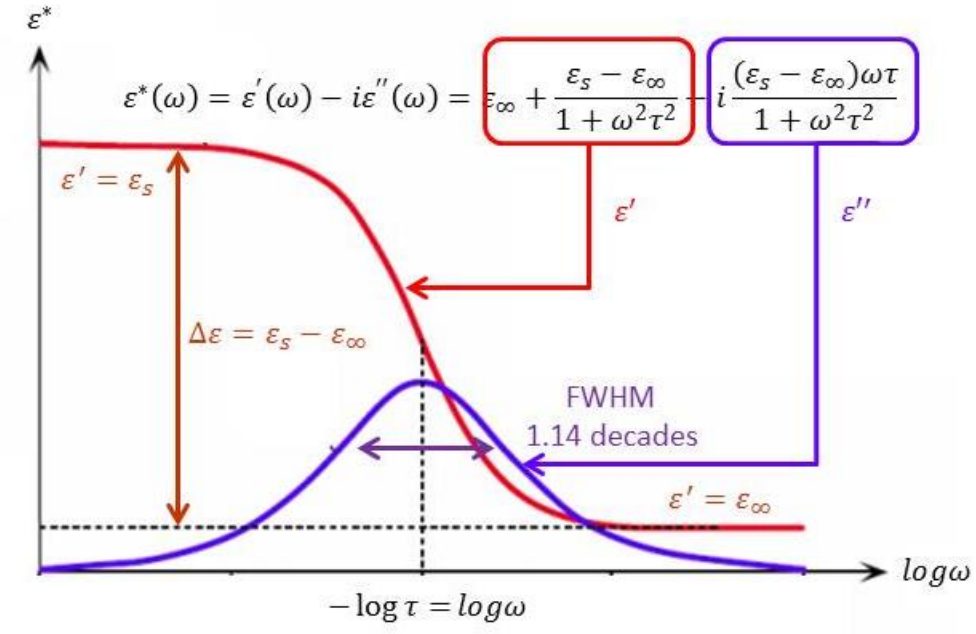

Figure III.20. Frequency variation of the real and imaginary parts of the permittivity.

The Debye equation represents the simplest problem of polarization, as it only considers a single relaxation time, however, this simple behavior is not usually found, and only in rare cases a Debye-like relaxation behavior is observed. So the model fails for describing the relaxation behavior of many materials, which usually present a loss peak significantly broader than the predicted by the Debye function. Moreover, in these cases, the dynamics is somewhat 'spread', making their shape asymmetric, and it is characterized by a distribution of several relaxation times rather than by a single time. This is the so called non-Debye or non-ideal relaxation behavior[26].

There are different empirical equations to account for the broadening and the asymmetry of the relaxation processes by generalizing the Debye function[26]. Among these empirical model functions the most importants are the Cole - Cole (CC)[33], the Cole - Davidson (CD)[34,35] and the Havriliak - Negammi (HN)[36,37] equations in the frequency domain.

Cole-Cole equation

This empirical equation was given by K. S. Cole and R. H. Cole in 1941 to describe $\varepsilon^*(\omega)$. The Cole - Cole equation models a symmetrically-broadened loss curve (ε''), and it is described by the next formulas;

$$\varepsilon*(\omega) = \varepsilon_\infty + \frac{\Delta\varepsilon}{[1+(i\omega\tau cc)^\alpha]} = \varepsilon_\infty + \frac{\varepsilon_s-\varepsilon_\infty}{[1+(i\omega\tau cc)^\alpha]} \quad \text{(III.12)}$$

$$\varepsilon'(\omega) = \varepsilon_\infty + (\varepsilon_S - \varepsilon_\infty)\frac{1+(\omega\tau_{CC})^\alpha sin\frac{1}{2}(1-\alpha)\pi}{1+(\omega\tau_{CC})^\alpha sin\frac{1}{2}(1-\alpha)\pi+(\omega\tau_{CC})^{2\alpha}} \quad \text{(III.13)}$$

$$\varepsilon''(\omega) = (\varepsilon_S - \varepsilon_\infty)\frac{(\omega\tau_{CC})^\alpha cos\frac{1}{2}(1-\alpha)\pi}{1+2(\omega\tau_{CC})^\alpha sin\frac{1}{2}(1-\alpha)\pi+(\omega\tau_{CC})^{2\alpha}} \quad \text{(III.14)}$$

where $\Delta\varepsilon = \varepsilon_0 - \varepsilon_\infty$ is the relaxation strength and α parameter quantifies the symmetrical broadening of the relaxation time distribution around the so-called Cole-Cole relaxation time (τ_{CC}), which gives the position of maximal loss by $\omega = 2\pi f = 1/\tau_{CC}$. α parameter varies from

0 to 1, 0 relating to a widest relaxation and 1 to the narrowest relaxation. This expression reduces to the Debye equation for $\alpha = 1$.

Cole-Davidson equation

In 1950 Davidson and Cole gave another expression for $\varepsilon^*(\omega)$;

$$\varepsilon^*(\omega) = \varepsilon_\infty + \frac{(\varepsilon_S - \varepsilon_\infty)}{(1+i\omega\tau_{CD})^\beta} \quad \text{(III.15)}$$

$$\varepsilon'(\omega) = \varepsilon_\infty + (\varepsilon_S - \varepsilon_\infty) cos\varphi^\beta cos\beta\varphi \quad \text{(III.16)}$$

$$\varepsilon''(\omega) = \varepsilon_\infty + (\varepsilon_S - \varepsilon_\infty) cos\varphi^\beta sin\beta\varphi \quad \text{(III.17)}$$

The parameter β quantifies the asymmetrical broadening of the relaxation function, and it varies from 0 to 1 depending on the skewing of the spectra. This expression reduces to the Debye equation for $\beta = 1$.

The Havriliak-Negami equation

For representing broadened and asymmetrically shaped dispersion and loss curves, the Havriliak - Negami (HN) equation is considered. It is the most versatile fitting function which is in fact a combination of the CC and the CD function:

$$\varepsilon*(\omega) = \varepsilon_\infty + \frac{\Delta\varepsilon}{[1+(i\omega\tau_{HN})^\alpha]^\beta} \quad \text{(III.18)}$$

$$\varepsilon'(\omega) = \varepsilon_\infty + (\varepsilon_S - \varepsilon_\infty) \frac{cos\beta\varphi}{\left[1+2(\omega\tau_{HN})^\alpha sin\frac{1}{2}(1-\alpha)\pi+(\omega\tau_{HN})^{2\alpha}\right]^{\beta/2}} \quad \text{(III.19)}$$

$$\varepsilon''(\omega) = (\varepsilon_S - \varepsilon_\infty) \frac{sin\beta\varphi}{\left[1+2(\omega\tau_{HN})^\alpha sin\frac{1}{2}(1-\alpha)\pi+(\omega\tau_{HN})^{2\alpha}\right]^{\beta/2}} \quad \text{(III.20)}$$

where φ is given by;

$$\varphi = \frac{arctg\left[(\omega\tau_{HN})^\alpha cos\frac{1}{2}\pi(1-\alpha)\right]}{1+(\omega\tau_{HN})^\alpha sin\frac{1}{2}\pi(1-\alpha)} \quad \text{(III.21)}$$

α and β parameters represent the shape of the dielectric spectra. For β = 1 this equation is reduced to a Cole - Cole equation and the Cole - Davidson equation is achieved when α = 1. Moreover, Debye equation is recovered when $\alpha = \beta = 1$.

Usually, more than a single function plus a DC contribution are necessary to fit the experimental loss curves when different relaxation processes contribute to the observed spectra. Moreover, in some cases, the peak at lower frequencies is covered by the strong conductivity contribution, making the direct analysis of the dielectric loss data a formidable task. In this cases, the first derivative of ε' has been suggested to provide a conduction-free ε'' spectrum, which results in a narrower dielectric loss peak[38];

$$\varepsilon''_{der} = -\frac{\pi}{2}\frac{\partial \varepsilon'(\omega)}{\partial \ln\omega} \sim \varepsilon''_{real} \qquad \text{(III.22)}$$

2.4.3. Dielectric relaxations and their temperature dependence

Many experiments in different systems demonstrate that two types of relaxation processes occur, distinguished by their time and temperature dependence[39]. These are the so-called α-and β-relaxation processes. The α-relaxation is a cooperative process involving the main dielectric relaxation[26]. It relates to the structural relaxation of the material and is necessarily of intermolecular nature[26]. β-relaxations are secondary relaxations, attributed to localized rotational fluctuations of the dipole vector, thus, local conformational rearrangements[26]. They describe motions subjected to interactions of both intra and intermolecular nature[26]. By increasing the temperature, these relaxation processes move to higher frequencies (or shorter times) (see Figure III.21). Depending on the temperature dependence of the relaxation times, these processes can be described by the Arrhenius equation or the Vogel - Fulcher - Tammann equation.

The Arrhenius equation

It was originally introduced to describe the variation of the rate constant (k) of a chemical reaction with temperature, based on the idea that particles are pushed by thermal fluctuations to make transitions between two energetic levels where an energy barrier E_a must be overcome. But

it also represents a widely used way for describing the linear temperature dependence of relaxation times;

$$k = Ae^{-E_a/RT} \rightarrow \tau = \tau_0 exp\left(\frac{E_a}{kT}\right) \quad \text{(III.24)}$$

where E_a is the activation energy related to rotational barriers, k is the Boltzmann's constant and τ_0 is related to the relaxation time. In systems which exhibit local molecular mobility below T_g, the processes for the β-relaxations are linear (as in Figure III.21 b), so temperature dependence is well described by the Arrhenius law.

Vogel-Fulcher-Tammann equation (also called super Arrhenius)

The nonlinearity of the relaxation times temperature dependence can be described via the empirical Vogel - Fulcher - Tamman (VFT) equation;

$$k = Ae^{-DT_0/(T-T_0)} \rightarrow \tau = \tau_o exp\left(\frac{DT_o}{T-T_o}\right) \quad \text{(III.25)}$$

where D is the fragility prameter and T_0 denotes the Vogel temperature, sometimes also called ideal glass transition temperature, which is usually found to be approximately 40 K below T_g. At temperatures above T_g where the curved α-relaxations are observed, the VFT expression approximates the data.

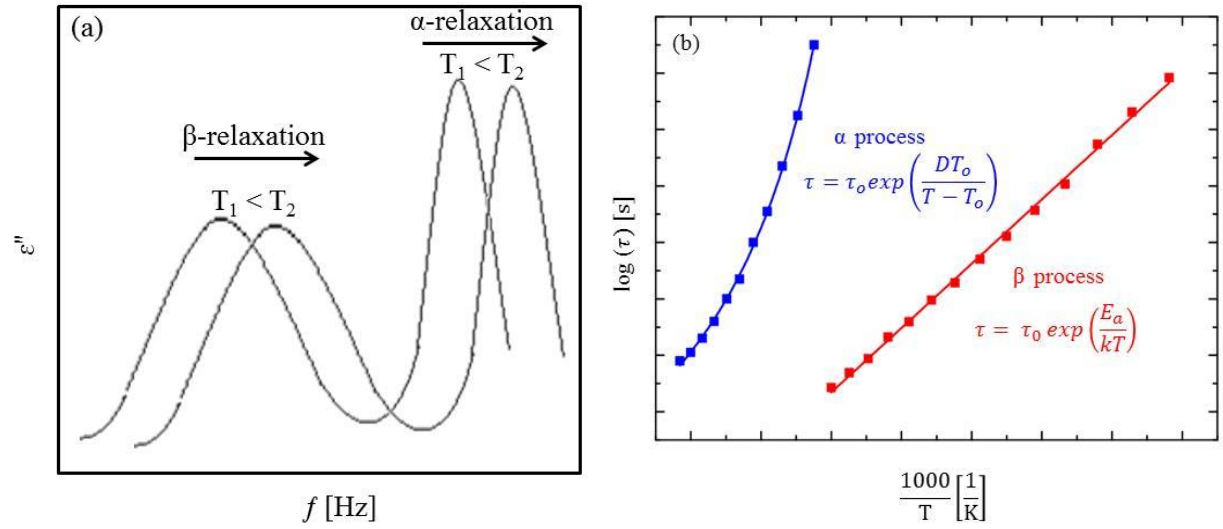

Figure III.21. Relaxation processes movement to higher frequencies when increasing the temperature (left). Relaxation times against the inverse of the temperature. Comparison of the temperature dependence for α- (VFT) and β-processes (Arrhenius) (right).

2.4.4. BDS experimental application to the aqueous solutions studied in this thesis

Accoding to the previous explication about dielectric spectroscopy, being both broadband and sensitive to dipolar motions, it would seem to be eminently suited to the investigation of our samples (*n*-lysine oligomers, PVP and polyssacharides aqueous solutions) due to their polar nature. When the electric field is imposed on such systems, there will be a torque exerted on each water dipole moment so as to induce them to attempt to align along the direction of the field. Moreover, relaxations of polar side groups and vibrations of the solute (lysine oligomers, PVP, sucrose and dextran) backbone will also contribute to the overall polarizability of the system, and orientational relaxations of those molecules will also be observed.

So, our samples properties were characterized in a broad range of temperatures by the complex dielectric permittivity which is accessed measuring the impedance as a function of frequency in a non-invasive way. Dielectric spectroscopy equipments relate the measured impedance (Z^*) with the complex permitivity by means of the next equation[26];

$$Z^*(\omega) = \frac{1}{i\omega\varepsilon^*(\omega)c_0} \qquad \text{(III.26)}$$

The obtained dielectric permittivity results were analyzed fitting simultaneously the real and the imaginary parts of the complex permittivity by means of Novocontrol's WinFIT Curve Fitting Software.

The complex dielectric permittivity was measured in a frequency range from 0.01 Hz to 20 GHz, for which different analyzers were required. For the lowest frequency range, from 10^{-2} to 10^{6} Hz, Novocontrol Alpha Analyzer was used (see Figure III.22), measurements over 10^{6} to 10^{9} Hz frequency range were carried out using an Agilent RF impedance Analyzer 4192B (see Figure III.22), and finally for the GigaHz region, ranging from 0.2 to 20 GHz, a dielectric probe kit Hewlett-Packard (HP) HP- 85070E with an open ended coaxial probe connected to a vector analyzer (VNA) HP-8361 was used (see Figure III.24).

To perform the low frequency dielectric measurements, samples were placed directly between two gold-plated electrodes, with diameters of 20 and 30 mm for the upper and lower electrodes respectively (both with a thickness of 0.4 mm), forming a parallel plate capacitor. A thin cross-shaped spacer of 0.1 mm thick made of Teflon was placed between the electrodes before compressing the sample to avoid short circuit and to determine the sample thickness. For the high frequency dielectric measurements, the capacitor was prepared in the same way, with the only difference in the gold-plated electrodes size, both with a diameter of 10 mm (see Figure III.23). For both, the low and the high frequency range measurements, solutions were placed in their respective sample holders, cooled in liquid nitrogen liquid to 140 K and then heated to 300 K. Isothermal and isocronal frequency scans recording $\varepsilon^*(\omega)$ were performed. For the isothermal measurements data were recorded while heating every 5 K in the low temperature range (140 - 170 K) and every 2.5 K at high temperatures (170 – 300 K). Samples temperature was controlled by a nitrogen gas flow with stability better than ± 0.1 K by Quatro cryosystem (Novocontrol). Concerning to the isocronal measurements, $\varepsilon^*(\omega)$ frequency scans were recorded while heating from 140 to 300 K every 2.5 K at various frequencies; from 10^{-2} to 10^{5} for every decade.

Figure III.22. General perspective of the Agilent RF impedance Analyzer 4192B (left), the Novocontrol Alpha analyzer (rigth) and the nitrogen dewars for temperature control.

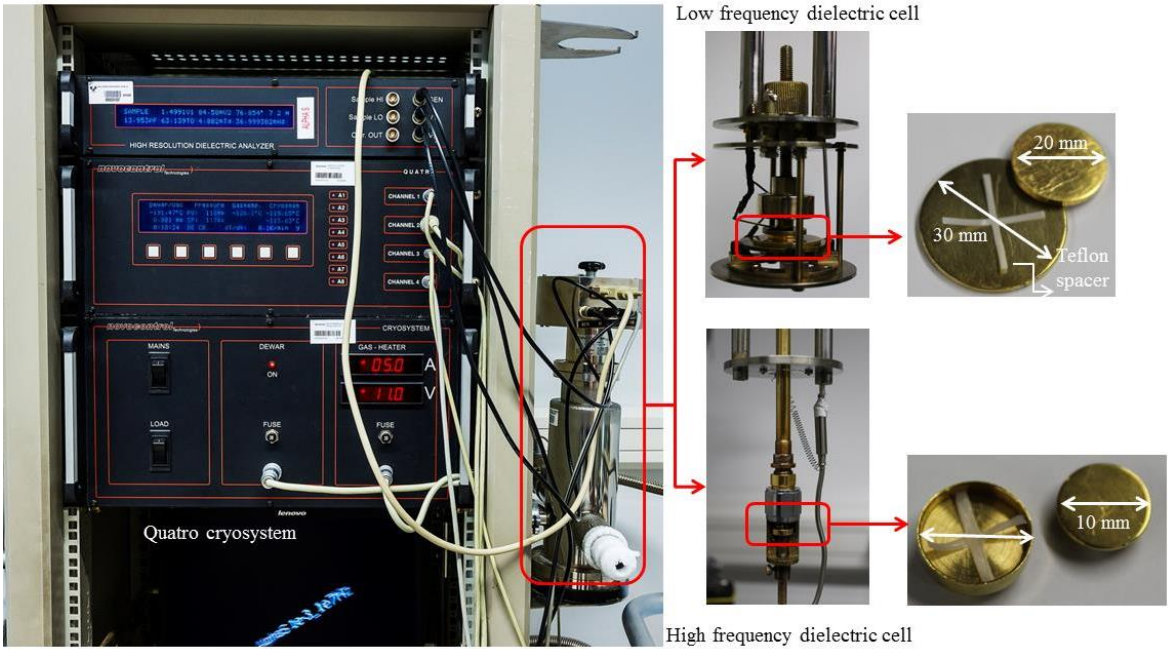

Figure III.23. Quatro cryosystem for the temperature control (left), and samples cells container for low and high frequency measurements (right). Teflon spacers and gold-plated electrodes for low frequency (up) and high frequency dielectric spectroscopy measurements (down).

For the GigaHz domain measurements, solutions were prepared in glass cylindrical containers with a diameter sufficiently wide (20 mm) to permit the access the coaxial probe. Being the minimum thickness required for the measurements of about 1 cm, sample thickness of approximately 2 cm was chosen to ensure correct measurements. To corroborate the accuracy of the solutions results, VNA was calibrated using air, water and short as calibration standards, and for each calibration, measurements on standard liquids as water, ethanol and methanol were also carried out. Finally, isothermal frequency scans recording $\varepsilon^*(\omega)$ were performed at a temperature range from 273 K to 313 K every 5 K, which were controlled using a Quatro controller from Novocontrol as in the Novocontrol Alpha Analyzer and the Agilent RF impedance Analyzer 4192B. In this case, samples temperature was stablized by an ethanol flow (see Figure III.24).

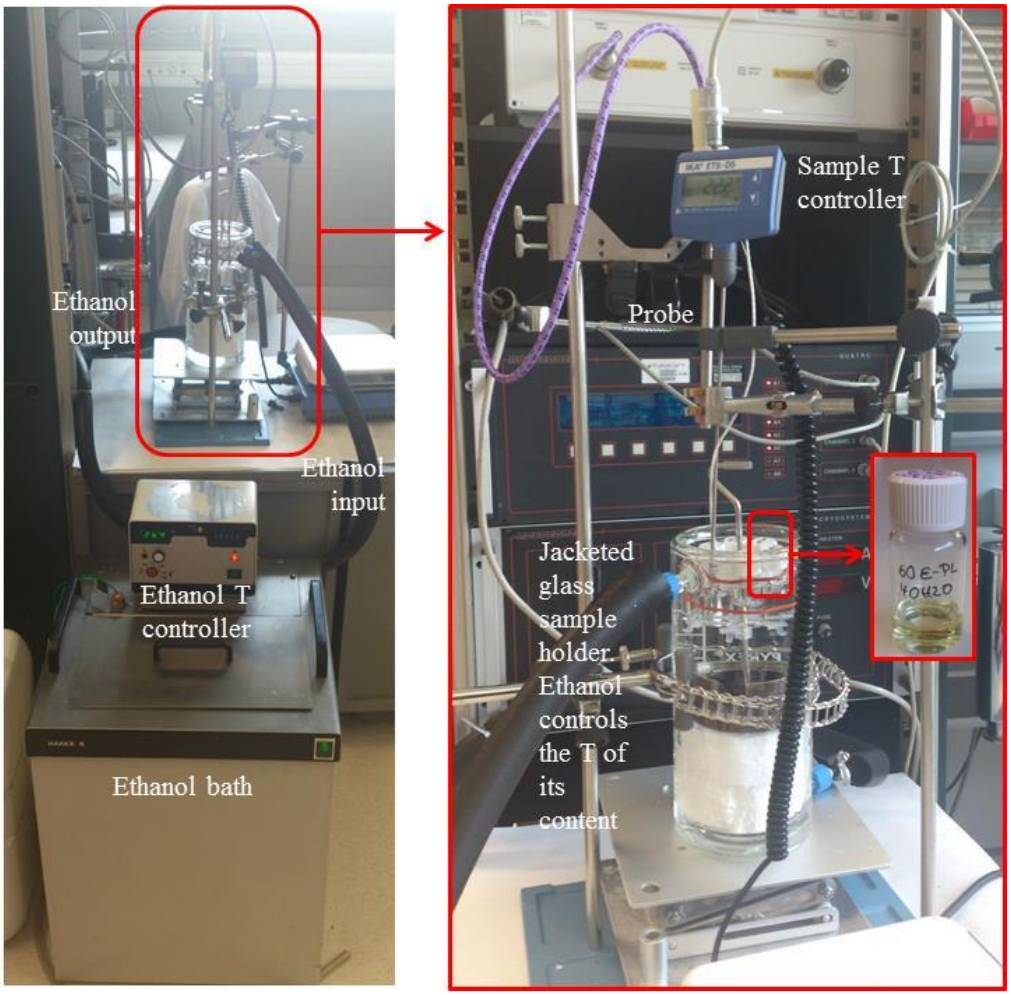

Figure III.24. General perspective of dielectric probe kit Hewlett-Packard (HP) HP- 85070E, the jacketed glass sample container and the ethanol bath for temperature control.

Finally, dielectric spectroscopy measuremets were completed with experiments in the time domain by means of the Thermo Stimulated Depolarization Current (TSDC) technique. TSDC gives access to slow dielectric relaxation processes by measuring the current associated with the depolarization process during the controlled heating of a previously polarized specimen[40]. These measurements were carried out using a Keithley 6517A electrometer, together with a Novocontrol's Quatro temperature controller (see Figure III.25). Concerning to the capacitors preparation, they were prepared as in the low frequency dielectric measurements. Thus, samples were placed between two gold-plated electrodes (20 and 30 mm diameters for the upper and lower electrodes respectively, and 4 mm thicknessess) forming a parallel plate capacitor with a 0.1 mm thick cross-shaped spacer of Teflon between them. Samples were then polarized by applying a 100 V voltage electric field for a short time (3 min), at a temperature (T_{pol}) above the calorimetric glass transition, where dipolar entities are mobile and full orientational polarization is allowed. Then, samples were freezed to 123 K by cooling down with liquid nitrogen with the field still applied. The polarizing voltage was maintained during cooling, in this way, when dipolar entities become frozen the orientational polarization remains. At low temperatures (123 K), the field was switched off and samples were reheated up to 300 K while the discharge current generated due to the thermally stimulated release of the polarization (depolarization current) was measured as a function of the temperature. Depolarization current measurements were performed at heating rates (q) of 0.25, 0.5, 1, 3, 5, 7 and 10 K min^{-1}.

Figure III.25. Keithley 6517A electrometer, together with a Novocontrol's Quatro temperature controller and the nitrogen deward.

3. REFERENCES

1 Nolting, D. *et al.* pH-Induced protonation of lysine in aqueous solution causes chemical shifts in X-ray photoelectron spectroscopy. *Journal of the American Chemical Society* **129**, 14068-14073, doi:10.1021/ja072971l (2007).

2 Kitadai, N., Yokoyama, T. & Nakashima, S. ATR-IR spectroscopic study of L-lysine adsorption on amorphous silica. *Journal of colloid and interface science* **329**, 31-37, doi:10.1016/j.jcis.2008.09.072 (2009).

3 Roddick-Lanzilotta, A. D., Connor, P. A. & McQuillan, A. J. An in situ infrared spectroscopic study of the adsorption of lysine to TiO2 from an aqueous solution. *Langmuir* **14**, 6479-6484, doi:10.1021/la980425n (1998).

4 Maeda, S., Kunimoto, K.-K., Sasaki, C., Kuwae, A. & Hanai, K. Characterization of microbial poly (ε-l-lysine) by FT-IR, Raman and solid state 13C NMR spectroscopies. *Journal of Molecular Structure* **655**, 149-155, doi:10.1016/s0022-2860(03)00218-7 (2003).

5 Bankar, S. B. & Singhal, R. S. Panorama of poly-ε-lysine. *RSC Advances* **3**, 8586, doi:10.1039/c3ra22596h (2013).

6 Yoshida, T. & Nagasawa, T. ε-Poly-L-lysine: microbial production, biodegradation and application potential. *Applied microbiology and biotechnology* **62**, 21-26, doi:10.1007/s00253-003-1312-9 (2003).

7 Shukla, S. C., Singh, A., Pandey, A. K. & Mishra, A. Review on production and medical applications of ε-polylysine. *Biochemical Engineering Journal* **65**, 70-81, doi:10.1016/j.bej.2012.04.001 (2012).

8 Pandey, A. K. & Kumar, A. Improved microbial biosynthesis strategies and multifarious applications of the natural biopolymer ε-poly-l-lysine. *Process Biochemistry* **49**, 496-505, doi:10.1016/j.procbio.2013.12.009 (2014).

9 Pooria Gill, T. T. M., and Bijan Ranjbar. Differential Scanning Calorimetry Techniques: Applications in Biology and Nanoscience. *Journal of Biomolecular Techniques* **21**, 167–193 (2010).

10 Höhne, G., Hemminger, Wolfgang F., Flammersheim, H. *Differential Scanning Calorimetry*. (Springer, 2003).

11 Mitchell, G. R. & Tojeira, A. *Controlling the morphology of polymers. Multiple scales of structure and processing*. (Springer, 2016).

12 Fulcher, G. S. Analysis of recent measurements of the viscosity of glasses. II. *Journal of the American Ceramic Society* **8**, 789-794, doi:10.1111/j.1151-2916.1925.tb18582.x (1925).

13 Tammann, G. & Hesse, W. The dependancy of viscosity on temperature in hypothermic liquids. *Zeitschrift Fur Anorganische Und Allgemeine Chemie* **156** (1926).

14 Angell, C. A. Formation of glasses from liquids and biopolymers *Science* **267**, 1924-1935, doi:10.1126/science.267.5206.1924 (1995).

15 Elliott, S. R. *Physics of amorphous materials*. (Longman Group Ltd., 1990).

16 Debenedetti, P. G. *Metastable Liquids: Concepts and Principles*. (Princeton University Press, 1996).

17 Vyazovkin, S. *Characterization of Materials. Thermogravimetric Analysis*. 2 edn, (John Wiley & Sons, Inc., 2012).

18 Gaffney, J. S., Marley, N. A. & Jones, D. E. *Characterization of Materials. Fourier Transform Infrared (FTIR) Spectroscopy*. 2 edn, (John Wiley & Sons, Inc., 2012).

19 Krimm, S. & Bandekar, J. Vibrational spectroscopy and conformation of peptides, polypeptides and proteins *Advances in Protein Chemistry* **38**, 181-364, doi:10.1016/s0065-3233(08)60528-8 (1986).

20 Kong, J. & Yu, S. Fourier transform infrared spectroscopic analysis of protein secondary structures. *Acta Biochimica Et Biophysica Sinica* **39**, 549-559, doi:10.1111/j.1745-7270.2007.00320.x (2007).

21 Dong, A., Huang, P. & Caughey, W. S. Protein secondary structures in water from 2nd derivative Amide I infrared spectra *Biochemistry* **29**, 3303-3308, doi:10.1021/bi00465a022 (1990).

22 Jia, S. R. *et al.* Fractionation and characterization of ε-poly-l-lysine from Streptomyces albulus CGMCC 1986. *Food Science and Biotechnology* **19**, 361-366, doi:10.1007/s10068-010-0051-9 (2010).

23 Schnablegger, H. & Singh, Y. *The SAXS Guide. Getting acquainted with the principles*. (Anton Paar GmbH, 2011).

24 Kittel, C. *Introduction to Solid State Physics*. (John Wiley & Sons, Inc, 2004).

25 Hirai, M., Iwase, H., Hayakawa, T., Miura, K. & Inoue, K. Structural hierarchy of several proteins observed by wide-angle solution scattering. *Journal of Synchrotron Radiation* **9**, 202-205, doi:10.1107/s0909049502006593 (2002).

26 F.Kremer & Schönhals, A. *Broadband Dielectric Spectroscopy*. (2003).

27 Kubo, R. *The fluctuation-dissipation theorem*. Vol. 29 255-284 (Reports on Progress in Physics, 1966).

28 Gregory, R. B. *Protein-solvent interactions*. (Marcel Dekker, Inc., 1995).

29 Floudas, G. *Polymer Science: A Comprehensive Reference*. Vol. 2 (Elsevier, 2012).

30 Emmert, S. *et al.* Electrode polarization effects in broadband dielectric spectroscopy. *European Physical Journal B* **83**, 157-165, doi:10.1140/epjb/e2011-20439-8 (2011).

31 Ben Ishai, P., Talary, M. S., Caduff, A., Levy, E. & Feldman, Y. Electrode polarization in dielectric measurements: a review. *Measurement Science and Technology* **24**, doi:10.1088/0957-0233/24/10/102001 (2013).

32 Debye, P. *Polar molecules*. Vol. 48 1036–1037 (J. Soc. Chem. Ind., 1929).

33 Cole, K. S. & Cole, R. H. Dispersion and absorption in dielectrics I. Alternating current characteristics. *Journal of Chemical Physics* **9**, 341-351, doi:10.1063/1.1750906 (1941).

34 Davidson, D. W. & Cole, R. H. Dielectric relaxation in glycerine *Journal of Chemical Physics* **18**, 1417-1417, doi:10.1063/1.1747496 (1950).

35 Davidson, D. W. & Cole, R. H. Dielectric relaxation in glycerol, propylene glycol and normal propanol. *Journal of Chemical Physics* **19**, 1484-1490, doi:10.1063/1.1748105 (1951).

36 Havriliak, S. & Negami, S. A complex plane analysis of alpha-dispersions in some polymer systems *Journal of Polymer Science Part C-Polymer Symposium*, 99-+ (1966).

37 Havrilia.S & Negami, S. A complex plane representation of dielectric and mechanical relaxation processes in some polymers *Polymer* **8**, 161-&, doi:10.1016/0032-3861(67)90021-3 (1967).

38 Wubbenhorst, M. & Van Turnhout, J. Analysis of complex dielectric spectra. I. One-dimensional derivative techniques and three-dimensional modelling. *Journal of Non-Crystalline Solids* **305**, 40-49, doi:10.1016/s0022-3093(02)01086-4 (2002).

39 Frauenfelder, H. *The Physics of Proteins: An Introduction to Biological Physics and Molecular Biophysics*. (Springer, 2010).

40 Arbe, A., Genix, A. C., Arrese-Igor, S., Colmenero, J. & Richter, D. Dynamics in Poly(n-alkyl methacrylates): A Neutron Scattering, Calorimetric, and Dielectric Study. *Macromolecules* **43**, 3107-3119, doi:10.1021/ma902833h (2010).

CHAPTER IV

DYNAMICS AND STRUCTURE OF *ε*-POLYLYSINE AQUEOUS SOLUTIONS

In this chapter, we discuss the dynamics of *ε*-polylysine (*ε*-PLL*)* aqueous solution at different hydration levels ($30 \leq c_w$ [wt%] ≤ 45) and different pH values (from 10 to 7). The great advantage of this system compared with proteins is that for most cases water crystallization can be avoided upon both cooling and heating. In the literature, studies of protein dynamics at low temperatures are generally performed on hydrated powders instead of realistic water solutions due to water crystallization. However, by reducing the size of the biomolecules, it is possible to avoid crystallization, enabling study of the dynamics without ice formation.

The main aim of this chapter is to develop an experimental methodology to analyze the very complex dielectric data in a broad temperature and frequency range usually obtained for this type of solution. We first characterize the samples using a combination of different experimental techniques: DSC, FTIR and X-ray spectroscopy. In addition, based on BDS measurement results, the molecular origin of each process in *ε*-polylysine aqueous solutions was determined. Below T_g, three processes (1, 2 and 3) with an Arrhenius temperature dependence and attributed to the dipole reorientations of water molecules were found. It is important to note that the presence of more than one water-related process below T_g (well below the physiological regime) is not commonly observed in other aqueous solutions[1,2] except for protein solutions[3-5]. Above T_g, two main processes were observed (3 and 4) with the very same Vogel–Fulcher–Tammann temperature dependence, although at different time scales. The strong coupling between the two relaxations will be further discussed in Chapter V. At high temperatures, three more processes were observed (processes 5 to 7), which cannot be related to molecular relaxations and were mostly attributed to electrode polarization and high ionic conductivity effects.

1. RESULTS

1.1. Differential scanning calorimetry (DSC)

Figure IV. 1 shows the calorimetric response to cooling and heating at a rate of 10 K/min. For ε-PLL solutions at pH = 10 and different water contents ($c_w \leq 40$ wt%), no crystallization was observed on cooling or heating (see Figure IV. 1a). For c_w = 45 wt%, a small exothermic peak, indicating water cold crystallization, followed by an endothermic peak due to a melting transition at 240 K was observed. Repeated cooling and heating scans from 120 to 310 K gave reproducible DSC signals, indicating that the structure of the ε-PLL was not damaged by either freezing or heating. The glass transition temperature (T_g) was determined from the heat flow as the onset point. Table IV. 1 summarizes the T_g value for each sample. For most of the ε-PLL samples, a narrow glass transition was observed in comparison with proteins, where typically the width of the thermal transition is near 100 ºC[3,5-7]. As expected, T_g shows a strong water content dependence and shifts towards lower temperatures with increasing water concentration. This variation is usually interpreted as plasticization[3,4,6,8] of the ε-PLL chains by water.

By contrast, at pH values lower than 9 (Figure IV. 1b), crystallization peaks were observed upon both cooling and heating. Those crystallizations make it difficult to determine the T_g values of the solutions.

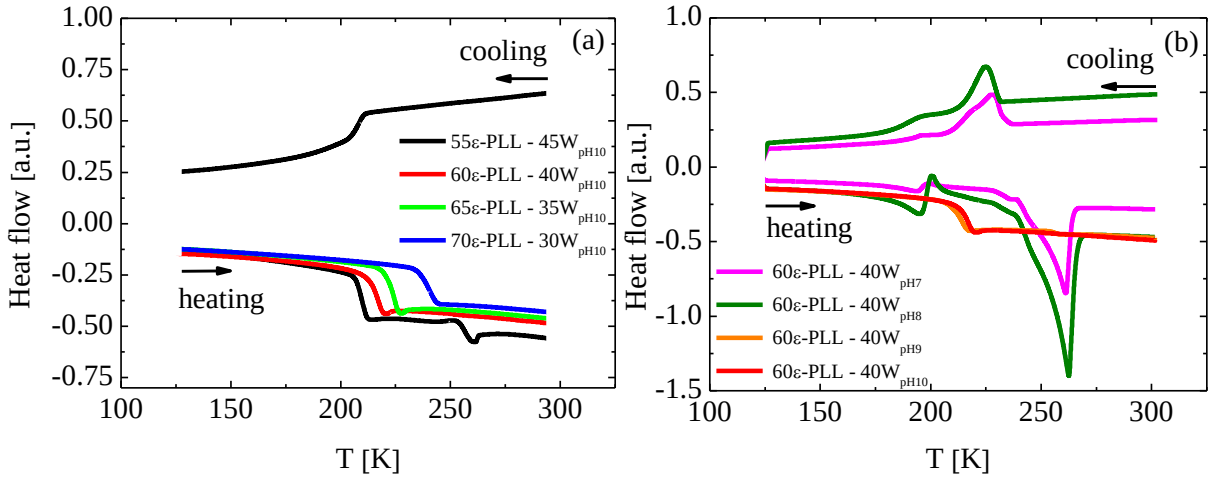

Figure IV. 1. DSC curves upon cooling and heating cycles for samples with different water contents.

Table IV. 1. General characterization of the samples. $c_{\varepsilon\text{-}PLL}$ is the weight fraction of ε-PLL, c_w is the weight fraction of water, and $T_{g,DSC}$ represents the calorimetric glass transition temperature.

Sample	$c_{\varepsilon\text{-}PLL}$ [wt%]	c_w [wt%]	$T_{g,DSC}$ [K]
55ε-PLL – 45W$_{pH10}$	55	45	209.6
60ε-PLL – 40W$_{pH10}$	60	40	212.5
65ε-PLL – 35W$_{pH10}$	65	35	225.0
70ε-PLL – 30W$_{pH10}$	70	30	230.0
60ε-PLL – 40W$_{pH7}$	60	40	190.3
60ε-PLL – 40W$_{pH8}$	60	40	190.9
60ε-PLL – 40W$_{pH9}$	60	40	214.2

1.2. Fourier transform infrared spectroscopy (FTIR)

Figure IV. 2 shows the FTIR spectrum in a wavenumber range from 4000 to 600 cm^{-1} at 2 cm^{-1} resolution and averaging 50 scans per sample at different water contents and pH values. The amide I band, visible in the region of 1700 - 1600 cm^{-1}, is used to determine the conformation of the peptide[9,10]. As previously mentioned in Chapter III, this band arises mainly due to the C=O stretching vibrations of the peptide linkages[9], and therefore each type of secondary structure results in a different C=O stretching frequency due to its unique backbone conformation (see Table III. 4 in Chapter III).

For samples at pH = 10, amide I is located at 1630 cm^{-1} (see pink dotted line in Figure IV. 3), which indicates a β-sheet conformation for all c_w contents. As the pH value decreases, this band splits into two bands located at 1630 and 1665 cm^{-1}, indicating that the conformation is a mix between β-sheets and β-turns. The change of the secondary structure with decreasing pH has been previously studied by several authors[11-18], and the results were in agreement with the ones presented here.

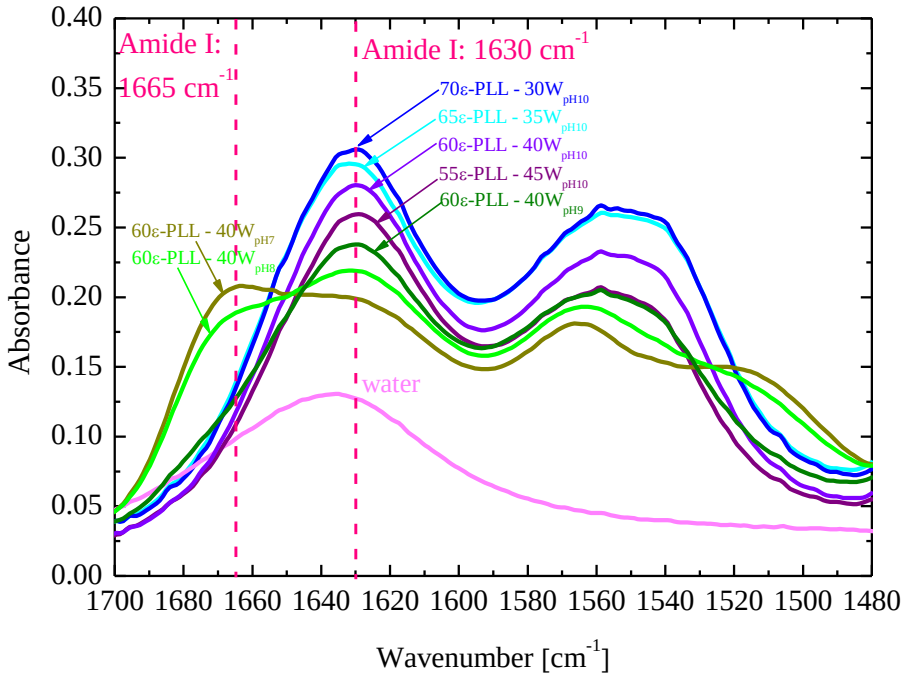

Figure IV. 2. FTIR spectrum for ε-polylysine – water mixtures at various hydration levels and pH values. Pure water spectrum is also shown.

Based on the amide I pH dependence, many authors in the literature have suggested a link between the spectral changes and the ionization of the amino side chain. At basic pH, above pKa of the α-amino group ($pKa_{\alpha\text{-}NH2}$ = 10.5[19]), the α-NH_2 side chains of the ε-PLL are uncharged, but upon reducing the pH value to 7 or below, the FTIR spectral features are different due to the protonation of the side chain α-NH_2 groups. Thus, at alkaline pH, ε-PLL possesses a conformation similar to a pleated β-sheet form. At low pH values, an electrostatically expanded conformation is found because at acidic pH, chain extension in ε-PLL occurs due to repulsion between the charged α-NH_3^+ side-chain groups.

1.3. X-ray scattering (SAXS)

Figure IV. 3 shows the SAXS patterns of the ε-PLL aqueous solutions performed at the BL11 beam line of the Alba Synchrotron. The influence of pH on the scattering behavior in the pH range between 7 and 10 at c_w = 40 wt% was examined to analyze the variation of structural inhomogeneities on a q length scale of 0.1 – 0.3 nm^{-1}. The main aim of this measurement is to

analyze the differences between an amorphous sample (pH = 10) and a sample that exhibits crystallization on cooling (pH = 7). In the latter case, structural inhomogeneities are expected.

It should be noted that the apparent small-angle scattering observed in Figure IV. 3 is not coming from the samples, as evident from the fact that the empty capillary shows the same intensity increase towards low *q*, and therefore it is considered to be a contribution from the direct beam. At pH = 10, no significant small-angle scattering is observed, proving that the sample is homogenous on a length scale from 60 to 20 nm ($d=2\pi/q$), and therefore, no aggregation is observed. On decreasing the pH value, ε-PLL aqueous solution at pH = 7 shows a significant small-angle scattering signal related to aggregation phenomena.

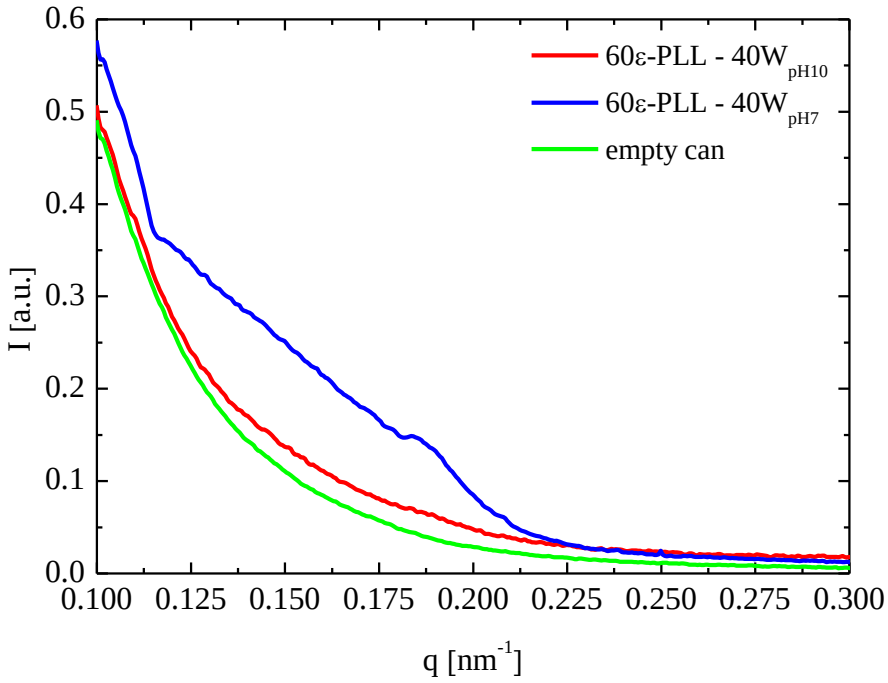

Figure IV. 3. SAXS data for ε-PLL (c_w = 40 wt%) at different pH values.

In addition, the Figure A.1 in Appendix shows the WAXS patterns for ε-PLL aqueous solutions at different hydration levels ($35 \leq c_w$ [wt%] ≤ 45) and pH values (pH = 7 to 9 for samples at c_w = 40 wt%) at selected temperatures from 153 to 293 K.

1.4. Broadband Dielectric Spectroscopy (BDS)

1.4.1. Dielectric results of ε-PLL aqueous solutions at pH = 10 and different hydration levels ($30 \leq c_w$ [wt%] ≤ 45)

In this section, we discuss the dielectric results of samples in the absence of crystallization. We first show the raw data obtained for both components of the complex dielectric permittivity, and we discuss the different strategies used to describe the isothermal dielectric measurements. The fitting procedure is also explained, and the obtained fitting parameters are shown. Finally, we discuss the origin of each of the observed relaxation processes.

Broadband dielectric spectroscopy results

Figure IV. 4 shows both components of the complex dielectric permittivity data for c_w = 40 wt% at pH = 10 at various temperatures below and above T_g. The results for other different hydration levels are shown in the Appendix (see Figure A. 2 to Figure A. 4).

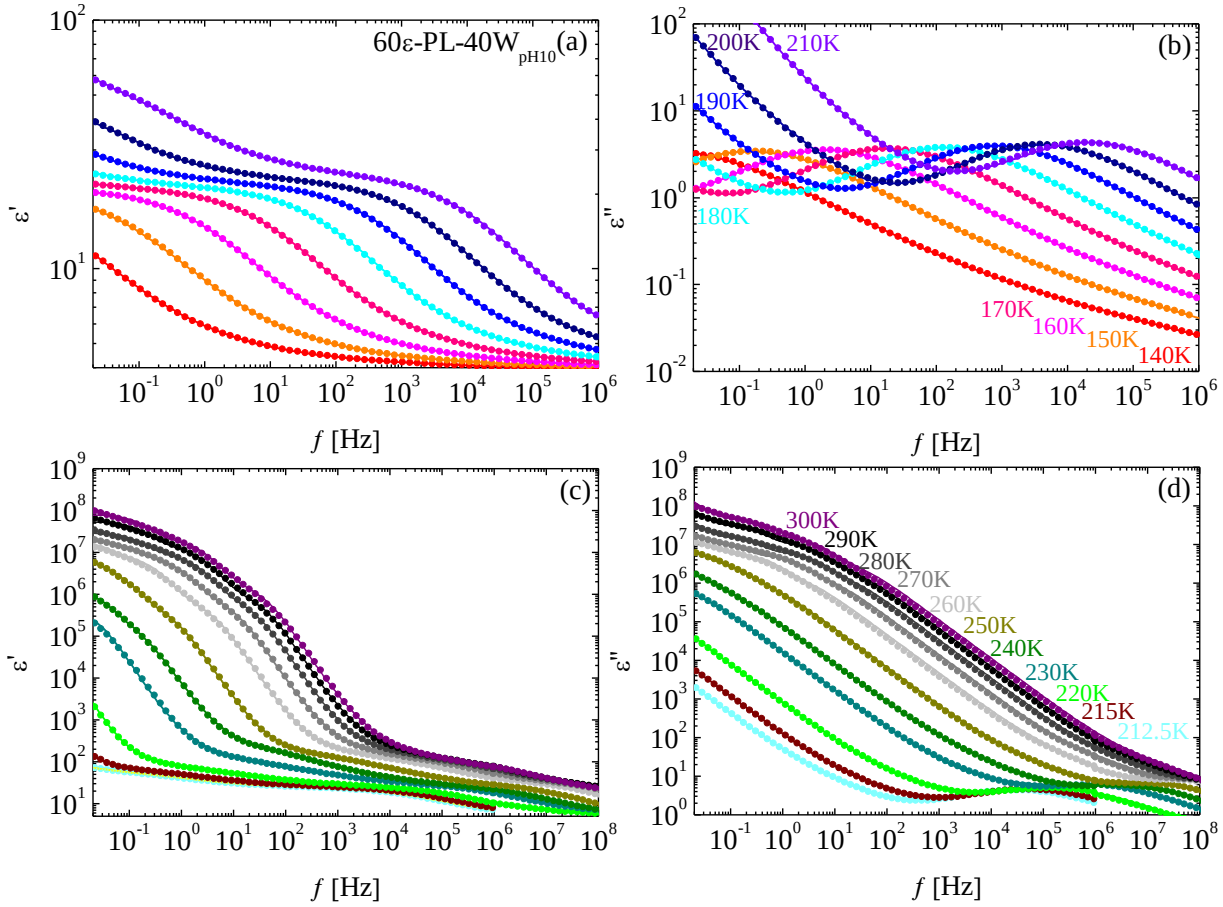

Figure IV. 4. Dielectric data (circle-shaped points) as a function of the frequency for 60ε-PLL – 40W$_{pH10}$ sample at selected temperatures below (a,b) and above (c,d) T_g. The lines represent the obtained fittings.

As typical in biosystems, high ionic conductivity and/or strong electrode polarization dominates the imaginary part of the complex permittivity spectra at lower frequencies[20,21,22,23] and prevents the observation of the dielectric relaxations. Thus, to fit the isothermal dielectric signal, three different procedures were previously performed.

1) **Isochronal measurements** (detailed measurement setup is described in Chapter III): These measurements are more sensitive than isothermal measurements, and therefore they allow the detection of weak relaxations masked in the isothermal scans[24,25]. Isochronal measurements revealed the presence of two relaxation processes at temperatures lower than T_g and a third one above the glass transition temperature (see Figure IV. 5).

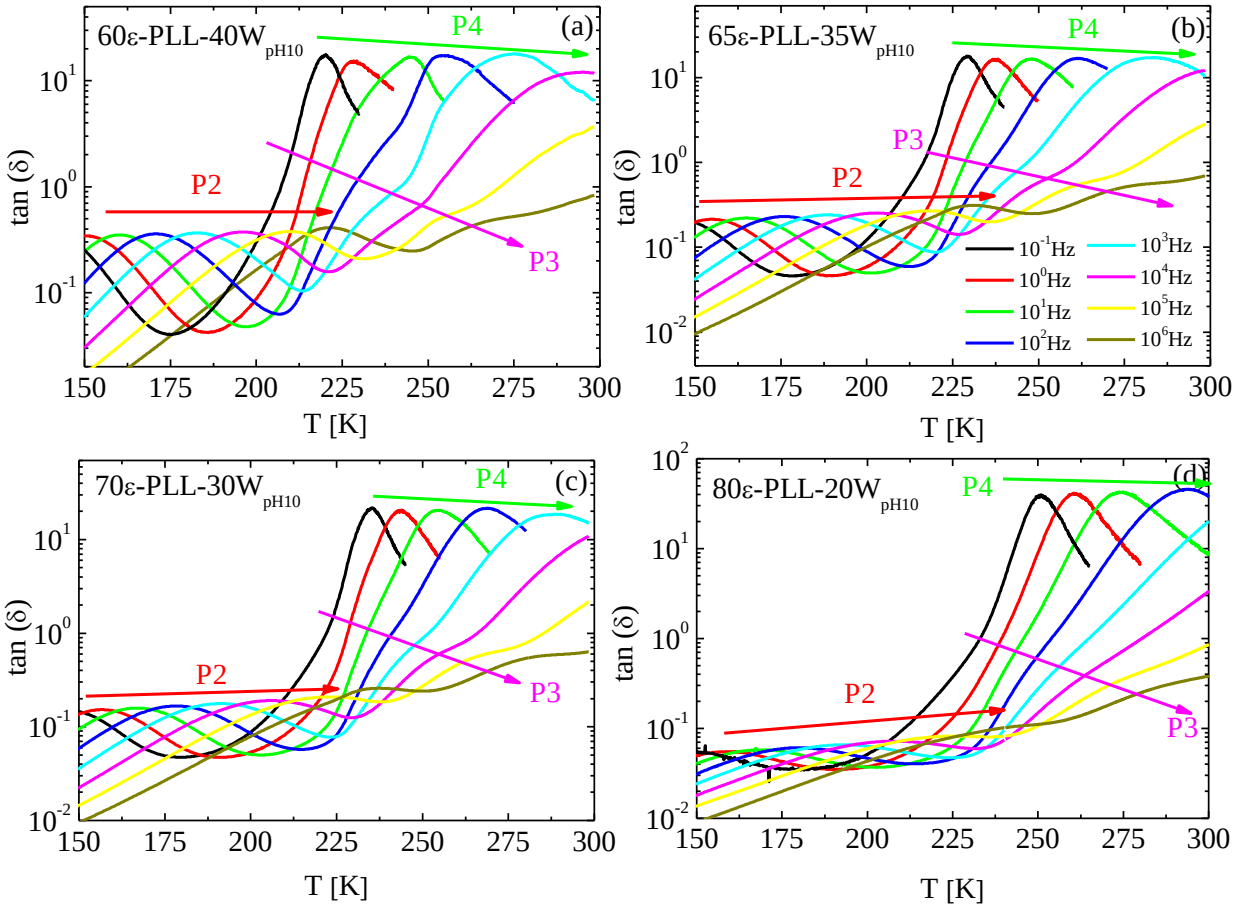

Figure IV. 5. Isochronal dielectric measurements for ε-polylysine aqueous solution at different water contents (from c_w = 40 to 20 wt%). Note that data for ε-polylysine at c_w = 20 wt% are also shown for comparison.

2) **Thermo Stimulated Depolarization Current (TSDC) measurements:** This technique accesses longer relaxation times than the ones observed in isothermal measurements (i.e., times longer than 100 s). In our case, TSDC measurements were performed at various heating rates from 0.25 to 10 K/min (see experimental section in Chapter III). Table IV. 2 summarizes the polarization temperature (T_{pol}) for each sample. Figure IV. 6 shows the TSDC curves, which also revealed the existence of two dynamical processes at temperatures below T_g that are hardly observed in isothermal measurements.

Table IV. 2. Polarization temperature (T_{pol}) value for each sample.

Sample	T_{pol} [K]
55 ε-PLL – 45W$_{pH10}$	216.1
60 ε-PLL – 40W$_{pH10}$	223.1
65 ε-PLL – 35W$_{pH10}$	228.1
70 ε-PLL – 30W$_{pH10}$	230.1

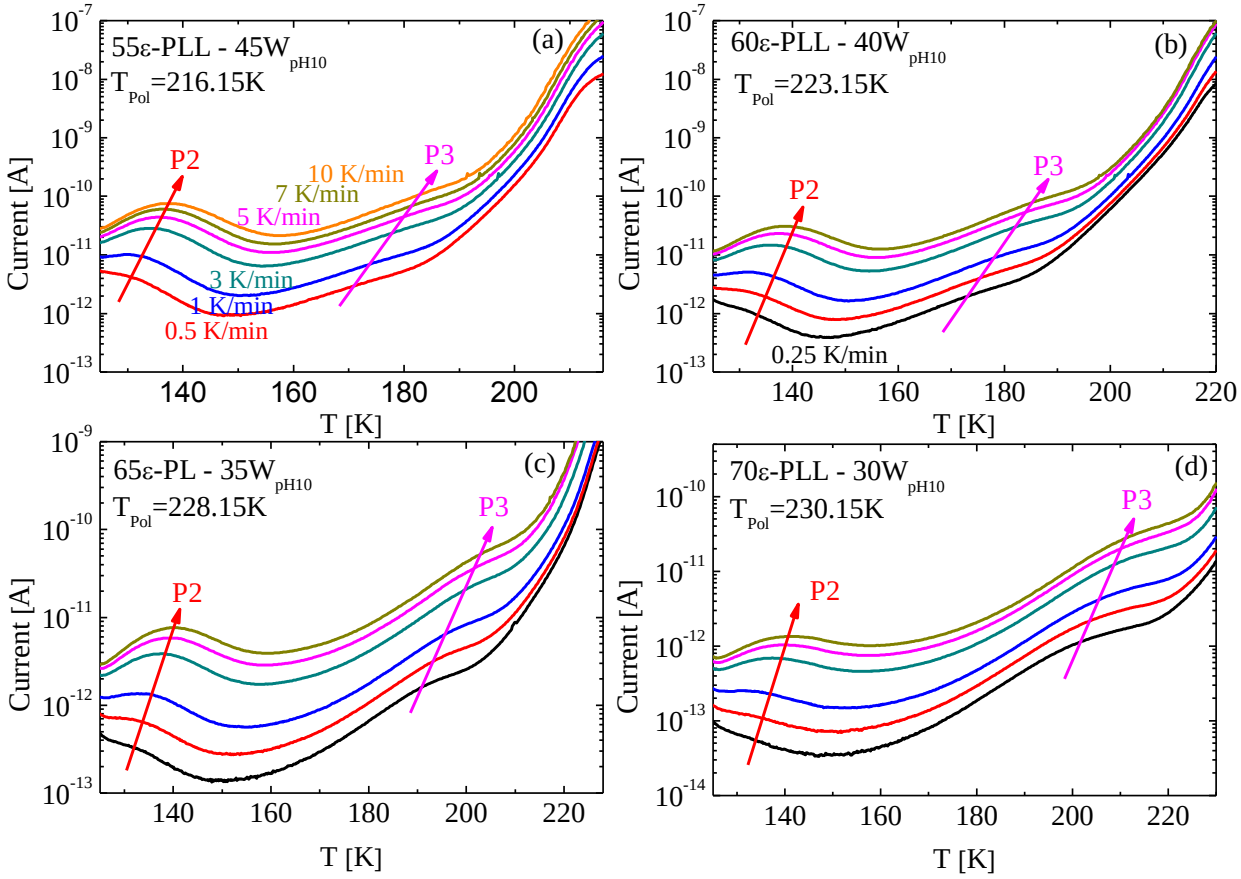

Figure IV. 6. TSDC depolarization current curves of ε-polylysine–water solutions (c_w = 45 - 30 wt%) at different heating rates.

3) **Derivative analysis of the real part of the dielectric permittivity (ε'):** This procedure allows determination of the relaxation times that cannot be clearly observed in the imaginary part of the complex permittivity (ε'') due to the high conductivity of the samples. The derivative analysis was performed directly using the experimental data (no smoothing or other data treatment) following the procedure described by Wübbenhorst et al[26]. As the derivative of the real part of the complex permittivity is practically identical to $\varepsilon''(\omega)$ but not affected by conductivity[26], it is possible to observe the "loss peaks" that are masked by

conductivity in the untreated data. Concerning the logarithmic derivative results observed in Figure IV. 7, two well-defined processes below and above T_g can be observed. The relaxation time for each temperature is obtained from the frequency of the maximum according to the equation $\tau = \frac{1}{2\pi f}$.

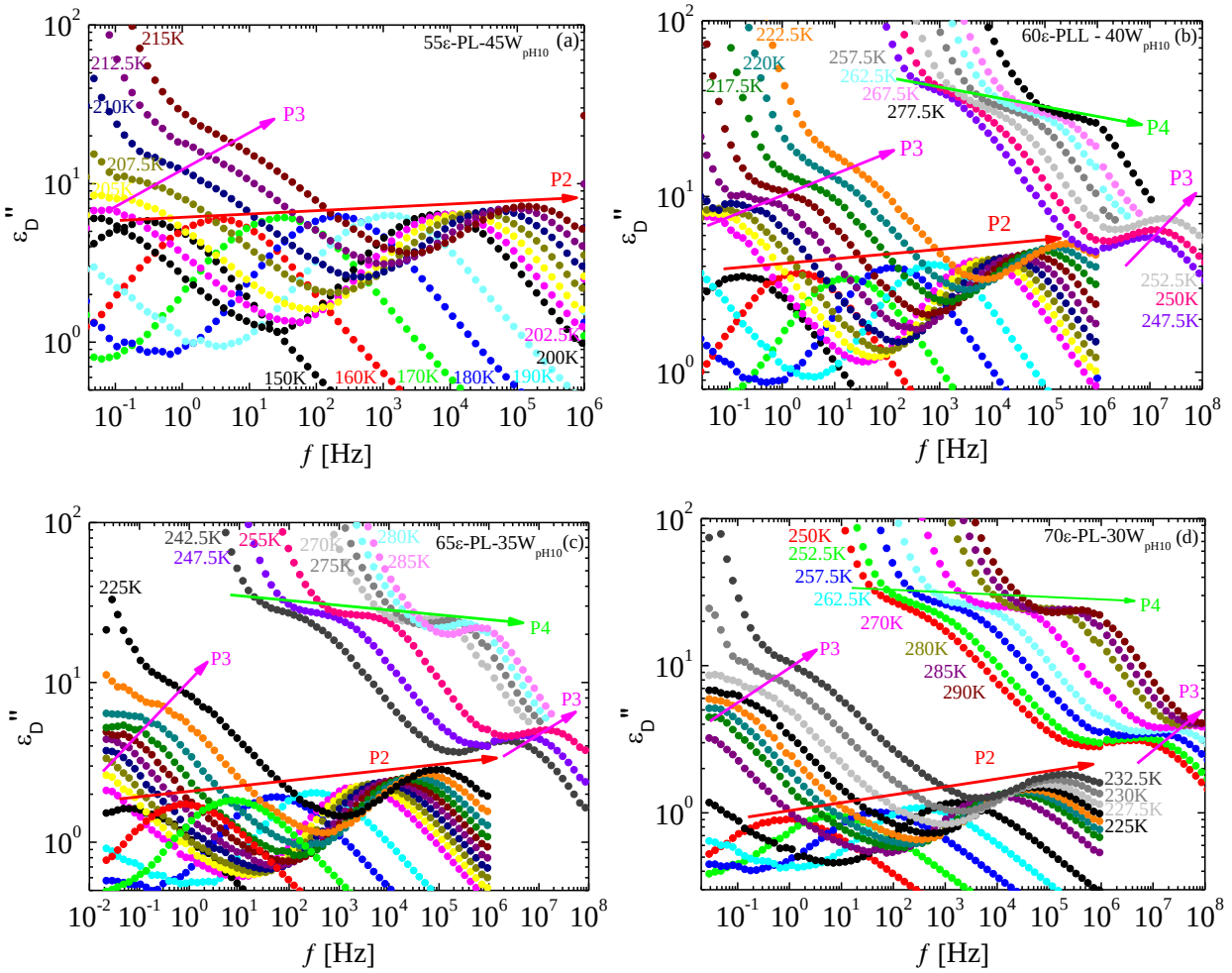

Figure IV. 7. Logarithmic derivative analysis for the different water contents of *ε*-polylysine aqueous solutions.

Fitting procedure

To analyze the complex permittivity (*ε**), simultaneous fittings of both the real (*ε´*) and the imaginary (*ε´´*) components were performed. The dielectric data were described by using the superposition of several standard Cole – Cole functions plus an extra term for the conductivity.

The total fit function was given by;

$$\varepsilon^*(\omega) = \varepsilon_\infty + \sum_j \frac{\Delta\varepsilon_j}{1+(i\omega\tau_j)^{\alpha_j}} - i\left(\frac{\sigma}{\varepsilon_0\omega}\right) \quad \text{(IV.1)}$$

where $\Delta\varepsilon$ is the dielectric strength ($\Delta\varepsilon = \varepsilon_S - \varepsilon_\infty$, being ε_S and ε_∞ the low frequency permittivity and the high frequency permittivity, respectively), ω is the angular frequency ($\omega = 2\pi f$), τ is the relaxation time ($\tau = 1/\omega_{max} = 1/2\pi f_{max}$), α the stretching parameter that determines the symmetric broadening of the peak, ε_0 denotes the vacuum permittivity and σ is the static ionic conductivity.

During the fitting procedure, the relaxation times were fixed based on the values obtained from the derivative analysis and TSDC measurements. Therefore, only two parameters were kept free during the fitting of each Cole - Cole function: the α-parameter, which is related to the shape of the relaxation, and the relaxation strength ($\Delta\varepsilon$), which is related to the number of dipoles participating in the relaxation, their ability to reorient and the absolute value of the dipolar moment.

Figure IV. 8 shows both components of the complex dielectric permittivity for c_w = 40 wt%, together with the different dielectric relaxation processes used to fit ε' and ε''. The results for other different hydration levels are shown in the Appendix (see Figure A. 7 to Figure A. 9).

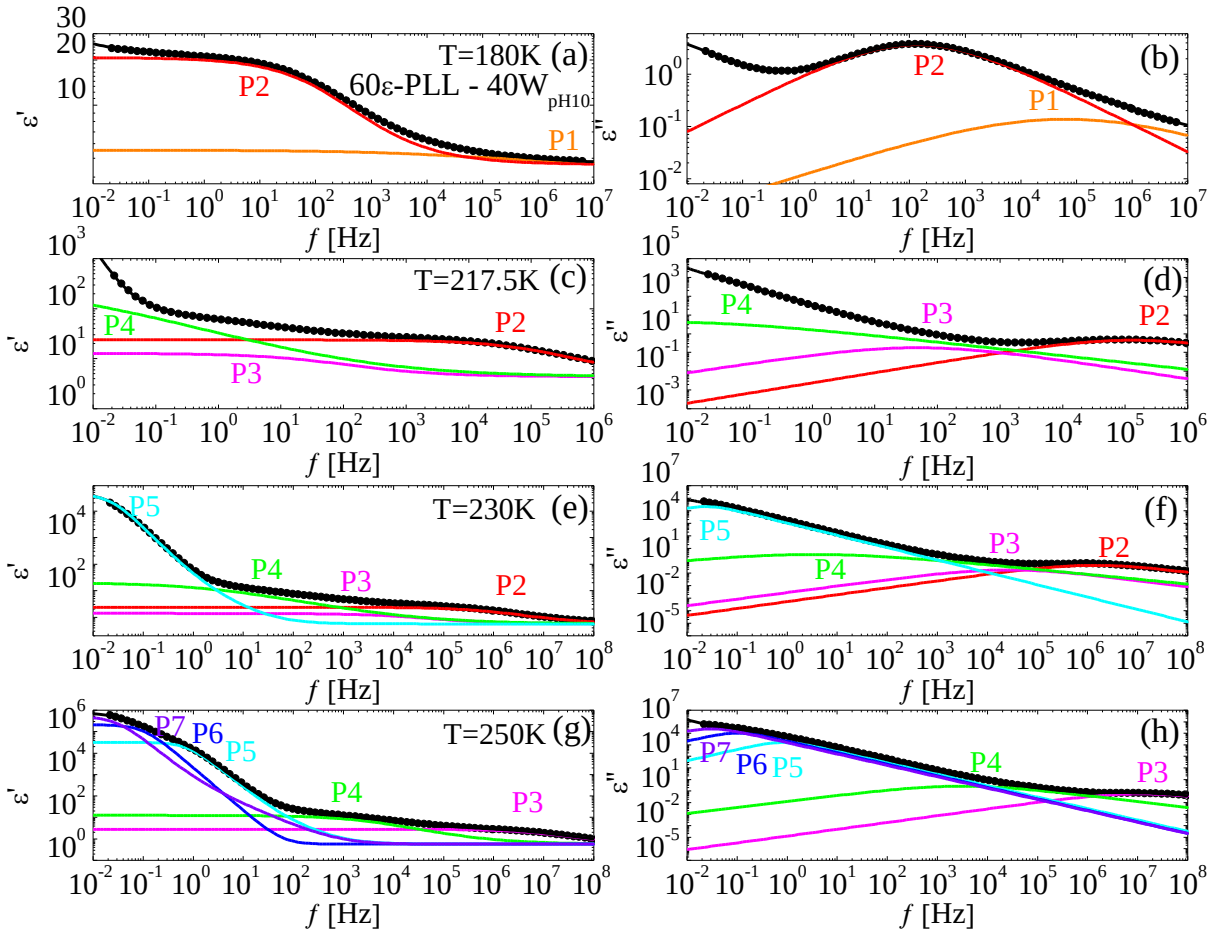

Figure IV. 8. Real (a) and imaginary (b) parts of the complex dielectric permittivity of ε-polylysine water solution (c_w = 40 wt%) at four different temperatures: T = 180, 217.5, 230 and 250 K.

Figure IV. 8 shows that below T_g (from 140 to 217.5 K), two main dielectric processes, called processes 2 and 3 (P2 and P3), are found. Up to 202.5 K, another process, process 1 (P1), is necessary to obtain a proper fitting of the experimental data. However, its intensity is extremely low, and it is barely observed in isothermal BDS measurements (undetectable in isochronal and TSDC measurements, and the derivative analysis). Above T_g, from 217.5 to 235 K, along with processes 2 and 3, two more relaxations are observed, processes 4 and 5 (P4 and P5). Finally, at high temperatures, above 235 K, process 2 is no longer detectable in the dynamic window, and together with P3, P4 and P5, two extra processes (P6 and P7) are needed to fit the dielectric data.

To compare the BDS results at different water contents of pH = 10, Figure IV. 9 shows the frequency dependence of the real and imaginary parts of the dielectric permittivity at two

representative temperatures (below T_g, T = 180K and above T_g, T = 250 K) together with the fitting functions.

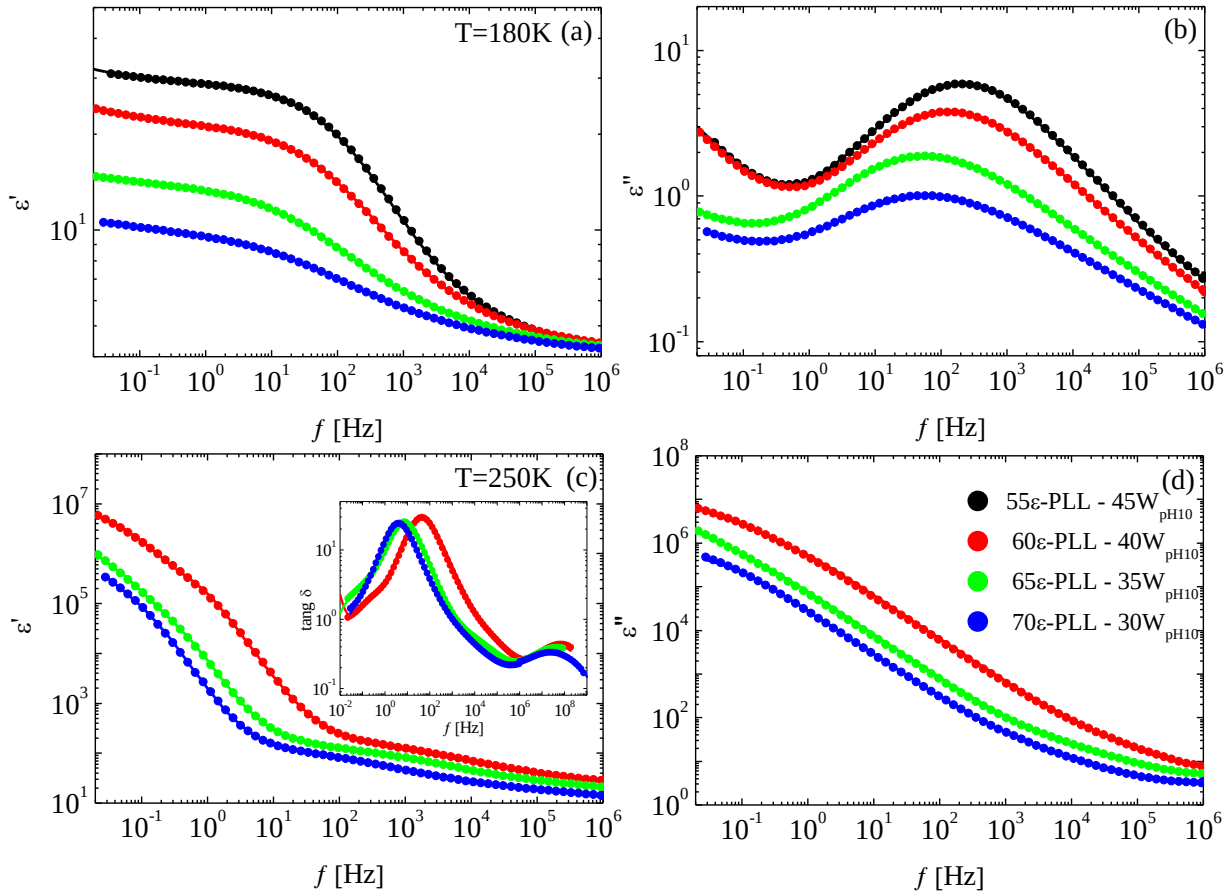

Figure IV. 9. Real (ε') and imaginary (ε'') parts of the complex permittivity of different contents of ε-PLL aqueous solutions at 180 and 250 K. At 250 K dependence of tang $\boldsymbol{\delta} = {}^{\varepsilon'}/_{\varepsilon''}$ with the frequency is also included. Symbols show experimental data, and lines represent the total fitting function.

Fitting parameters

The temperature dependences of relaxation times, relaxation strengths and shape parameters were extracted from the fitted signals. The temperature dependence of relaxation times for 60 ε-PLL – $40W_{pH10}$ is shown in Figure IV. 10, which also includes the relaxation times obtained from TSDC experiments (open star-shaped points) and logarithmic derivative analysis (open circle point).

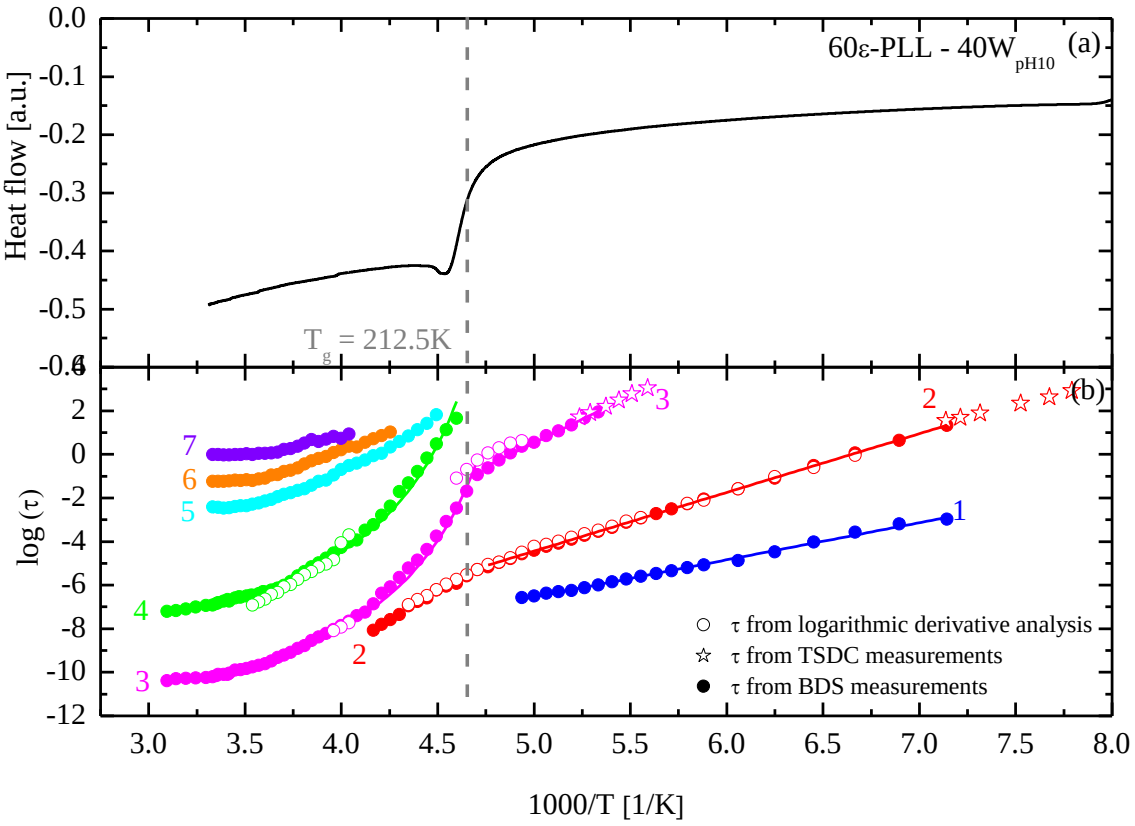

Figure IV. 10. Temperature dependence of the relaxation times for 40 wt% water content sample at pH = 10 (b). Close circle points represent results obtained from fitted signals, open star-shaped points TSDC experiment results, and open circle points the logarithmic derivative results. Additionally, the DSC curve upon heating cycles is also included (a).

As shown in Figure IV. 10, below T_g, three processes (1, 2 and 3) with an Arrhenius temperature dependence are found ($\tau = \tau_0 \exp\left(\frac{E_a}{k_B T}\right)$)[22], where E_a represents the activation energy, k the Boltzmann constant, and τ_0 is the relaxation time extrapolated to infinite temperature. P3 at T_g presents a crossover from low-temperature Arrhenius behavior to high-temperature non-Arrhenius behavior. Above T_g, four more processes are observed (4 to 7), which follow a Vogel – Fulcher – Tammann temperature dependence ($\tau = \tau_0 \exp\left[\frac{DT_0}{T-T_0}\right]$)[22,27,28] where T_0 is the temperature when it would diverge to infinite time and D parameter is the so called dynamic fragility; $\frac{d\, log\tau}{d\,(T_g/T)}$.

Figure IV. 11 shows the concentration dependence of the relaxation times of processes 1 to 4. In Figure A. 11 in the Appendix, the same information is shown, but including the relaxation times obtained from the TSDC experiments and the logarithmic derivative analysis. For the most

hydrated sample (c_w = 45 wt%), we only report the results at few degrees above T_g because water crystallization prevents observation of the relaxation of amorphous water.

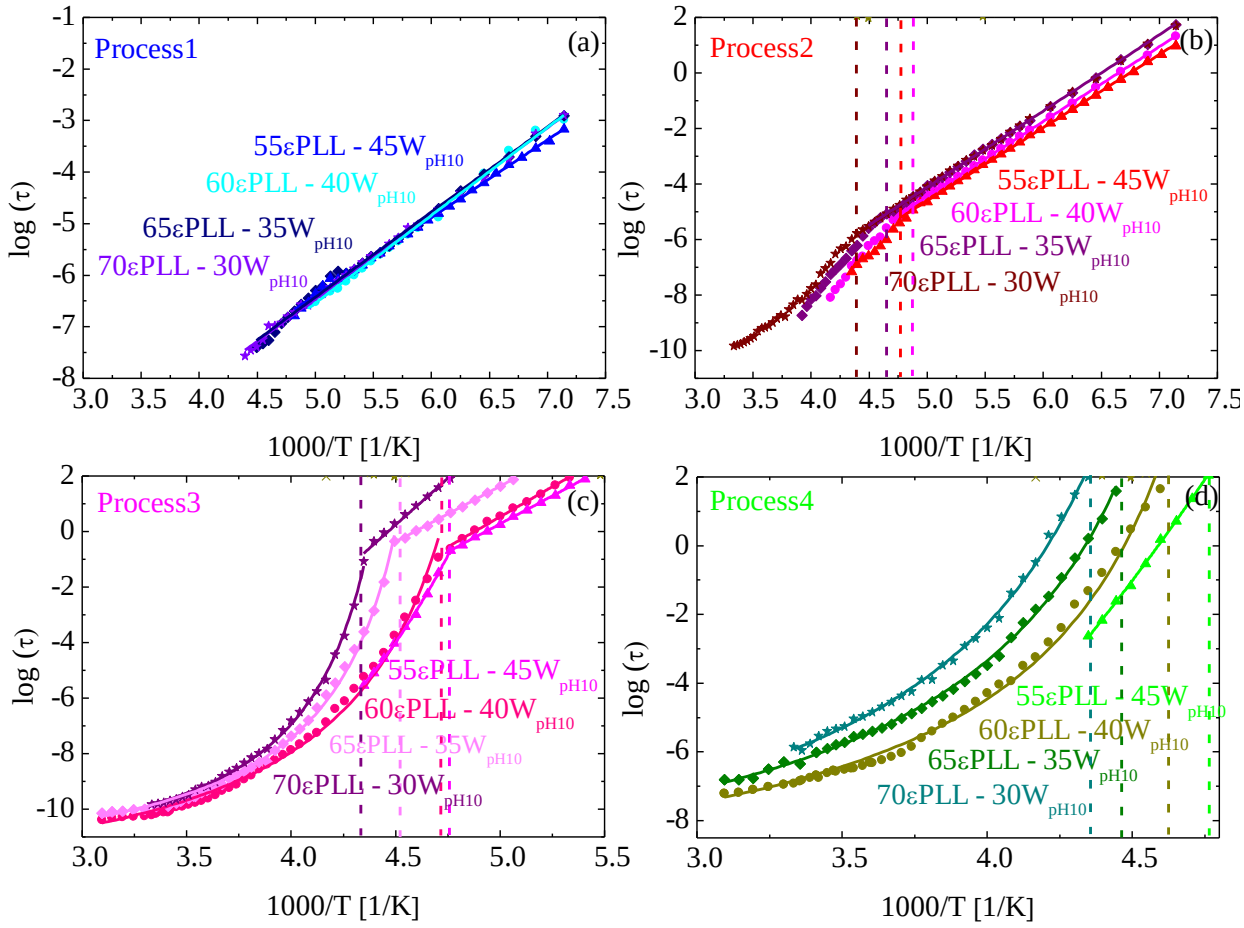

Figure IV. 11. Comparison of the temperature dependence of the relaxation times for 1 to 4 processes at different water contents. Vertical dashed lines indicate $T_{g,DSC.}$

In the range where the relaxation times show an Arrhenius-like temperature dependence, the activation energies (E_a) and $log(\tau_0)$ were calculated, and the values are shown in Table IV. 3 for processes 1 to 3. Above T_g, where the relaxation times have a VFT temperature dependence, the $log(\tau_0)$, D and T_0 values were calculated, and these values are shown in Table IV. 4 for processes 3 and 4.

Table IV. 3. Activation energy (E_a) and $log(\tau_0)$ values obtained from the Arrhenius fittings at low temperatures for ε-PLL solutions at different hydration levels.

c_w [wt%]	P1		P2		P3	
	E_a [eV]	$log(\tau_0)$	E_a [eV]	$log(\tau_0)$	E_a [eV]	$log(\tau_0)$
45	0.3	-13.9	0.5	-17.8	0.8	-19.9
40	0.3	-15.0	0.5	-17.9	0.9	-21.2
35	0.3	-14.7	0.5	-17.8	0.8	-18.6
30	0.3	-14.7	0.5	-17.7	1.2	-27.4

Table IV. 4. $Log(\tau_0)$, D and T_0 values from Vogel – Fulcher - Tammann fittings at high temperatures for ε-PLL solutions at different water contents.

c_w [wt%]	P3			P4		
	$log(\tau_0)$	D	T_0 [K]	$log(\tau_0)$	D	T_0 [K]
45	-12.0	4.0	182.4	-9.0	4.0	182.0
40	-12.6	3.4	191.2	-9.8	3.4	195.6
35	-12.0	2.3	205.3	-8.3	2.3	205.5
30	-12.1	2.1	212.0	-7.6	2.1	211.2

Figure IV. 12 shows the temperature dependence of the dielectric strength ($\Delta\varepsilon$) for processes 1 to 4 at c_w = 40 wt%. Below T_g, the relaxation strength of processes 1 to 3 increases with temperature, as is typical of local relaxations[4,22]. At temperatures above the glass transition, the $\Delta\varepsilon$ value decreases with temperature for processes 3 and 4. This behavior is typically observed for a cooperative process such as the α-relaxation[4,22]. However, for process 3, we prefer to understand this relaxation as a collective motion of water molecules. At T_g, the dielectric strength of process 3 changes the temperature dependence, which implies that the physical nature of the relaxation is altered at this temperature, coinciding with the crossover from non-Arrhenius to Arrhenius behavior observed for the relaxation times in Figure IV. 10.

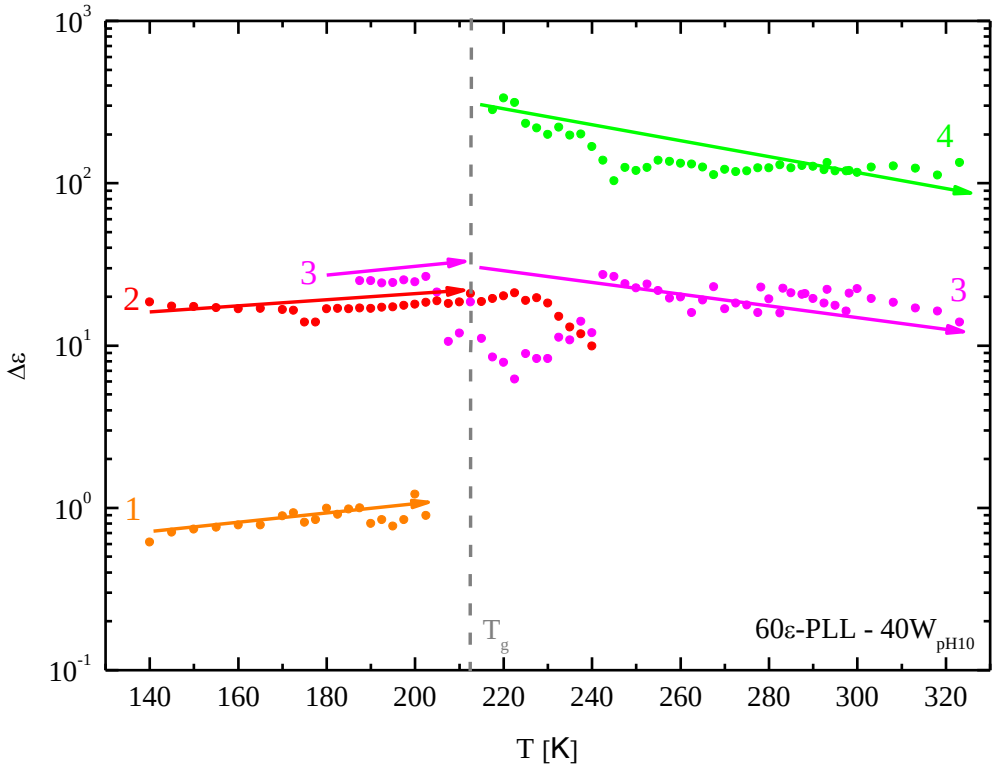

Figure IV. 12. Temperature dependence of the dielectric strengths of processes 1 to 4 of *ε*-polylysine aqueous solution at c_w = 40 wt%.

Figure IV. 13 displays the relaxation strength of P2 (a) and P4 (b) as a function of temperature for samples at different hydration levels. For P2, the relaxation strength increases with hydration level ($\Delta\varepsilon_{P3}$ follows the same dependence on the water content). The dielectric strength of P4 decreases with increasing water content, i.e., increases with *ε*-PLL concentration. This behavior indicates that P2 and P3 are related to the water molecule relaxation, whereas P4 is related to *ε*-PLL reorientation. In addition, the dielectric strength as a function of the hydration level for processes 3 and 4 is shown in Figure IV. 14. The value of $\Delta\varepsilon_{P4}$ decreases with increasing water content, whereas $\Delta\varepsilon_{P3}$ increases with water content.

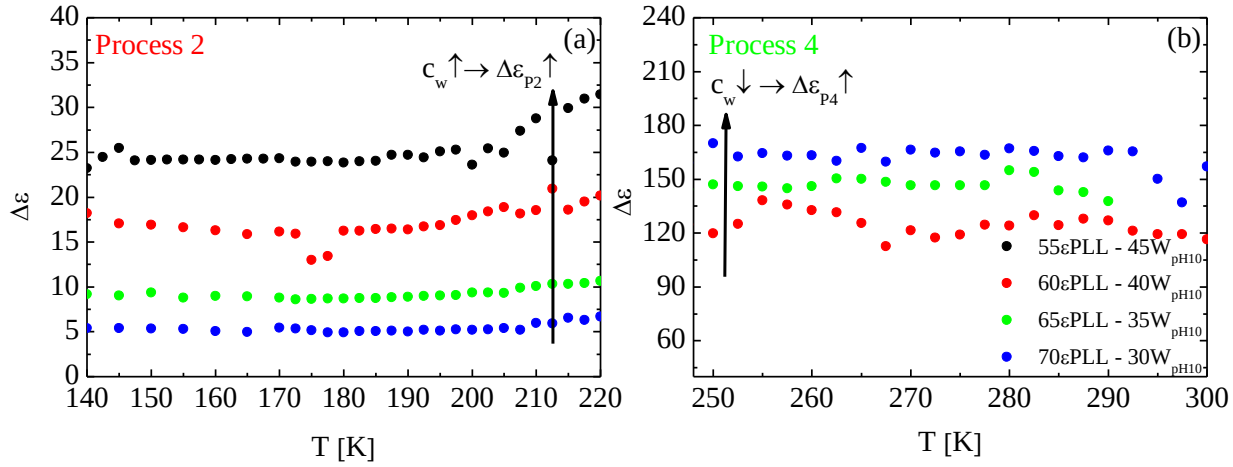

Figure IV. 13. Relaxation strength for process 2 (a) and process 4 (b) as a function of temperature for different hydration levels for *ε*-PLL - water system.

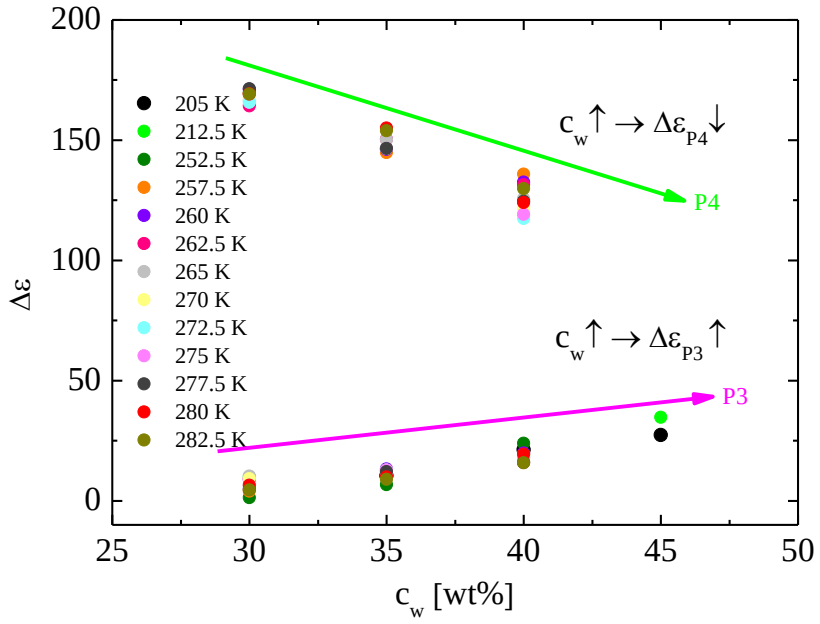

Figure IV. 14. Dielectric strength (*Δε*) as a function of water content for processes 3 and 4.

Molecular origin of the relaxation processes (P1 to P4)

According to Figure IV. 10 and Figure IV. 11, the dynamics of *ε*-PLL aqueous solutions revealed the presence of several dynamic phenomena arising from the water and the *ε*-PLL molecules. Considering the number of processes, the dielectric response has the same characteristics for samples with $30 \leq c_w$ [wt%] ≤ 45 wt%. In the following pages, the general interpretation of the different processes is summarized.

Process 1

This process is commonly observed in different types of water-containing systems, such as water confined in hydrophilic matrices[29] and hydrated proteins[4,30], but its origin is not fully clear. M. Monasterio et al[29] attempted to relate this process to the reorientation of hydroxyl groups, since the low activation energy that they found for this process was very close to the energy required to break a single hydrogen bond (0.22 eV). A. Panagopoulou et al[4] also observed this relaxation in low-hydration BSA protein - water mixtures (c_w = 2 wt%). They speculate that the origin of this process could be the reorientation of water molecules that are completely isolated from each other. Finally, a process of similar E_a has been observed for lysozyme - water mixtures with high water contents studied by NMR and assigned to a particular relaxation of water[30]. In this case, this process is not well defined (no peak is observed in the imaginary part of the permittivity), and therefore a large uncertainty is expected in the determination of the relaxation time and shape parameters. Nevertheless, since this process is not the main focus of our work, we will not engage in the controversy associated with its molecular interpretation.

Process 2

Figure IV. 13a shows the relaxation strength of P2 ($\Delta\varepsilon_{P2}$) as a function of water content. $\Delta\varepsilon_{P2}$ increases with water content, which is an indication that this process originates from the motion of water molecules.

The temperature dependence of the relaxation time shows Arrhenius behavior below T_g, and the time scale is independent of water concentration (see Figure IV. 11 a). The activation energy of this process is 0.5 eV (see Table IV. 3), which agrees with the universal activation energy for water molecules in several solutions (E_a = 0.45 – 0.55 eV)[2,4,24,31]. In addition, the relaxation strength increases slightly with temperature (see Figure IV. 12). All these experimental findings are frequently found in so-called secondary- or β-relaxations of glass-forming materials[4,31], and therefore these characteristics strongly suggest that P2 can be identified as a β-like relaxation of water molecules.

In Figure IV. 15, we compare the temperature dependence of the relaxation time of process 2 (ε-PLL, c_w = 40 and 45 wt%) with of water in different solutions (mixtures of PVP[32], PVME[33],

myoglobin[3], elastin[34] and BSA[4]) at similar water content. As shown in Figure IV. 15, the relaxation time of water in ε-PLL is similar (slightly slower) to all these systems. Another similarity between ε-PLL and all these systems is that the relaxation times depend weakly on water content. However, this case does not hold for water in PVME, where the relaxation time depends on water content. Consequently, process 2 shares the same characteristics in ε-PLL, PVP and proteins (myoglobin, elastin and BSA) but differs from other aqueous solutions such as PVME – water mixtures.

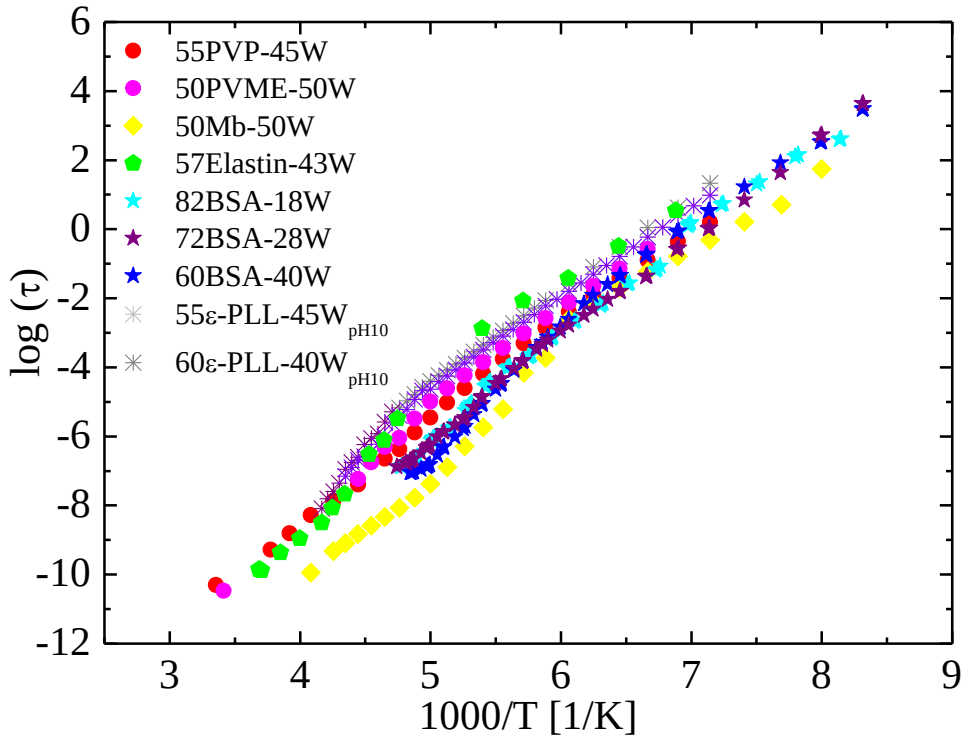

Figure IV. 15. Temperature dependence of the relaxation times of process 2 in aqueous solutions (PVP and PVME), solvated proteins (myoglobin, elastin and BSA) and 60ε-PLL – 40W.

Process 3

The value of $\Delta\varepsilon_{P3}$ increases with water content (see Figure IV. 14), indicating that this relaxation is also due to the relaxation of water molecules in the solution. Process 3 is the slowest relaxation of water molecules observed in ε-PLL aqueous solutions below T_g. The presence of two water relaxations is not common in other ordinary water solutions (e.g., PVME – water mixtures), where a single water relaxation is observed[2]. However, the presence of at least two water relaxations below T_g has already been observed in protein - water mixtures[3-5] and in small

peptides[24,35,36]. Note that ε-PLL can be classified as an ordinary solution, and therefore finding more than one water relaxation is a very significant feature.

At high temperatures ($T >> T_g$), process 3 follows a VFT behavior up to the temperature corresponding to the T_g of the solution, and at lower temperatures ($T < T_g$), it becomes Arrhenius. The VFT behavior of process 3 extends up to 0.1 sec ($\log \tau = -1$), and at longer times it becomes Arrhenius. As the relaxation time does not reach 100 s, process 3 is not responsible for the glass transition observed by DSC, which implies that this relaxation cannot be identified as the structural α-relaxation of the solution. Above T_g, $\Delta\varepsilon_{P3}$ decreases with temperature (see Figure IV. 12), and the relaxation times have VFT temperature dependence; therefore, we are observing the collective motion of water molecules, although it is not related to the calorimetric T_g of the solution.

The crossover from a high-temperature non-Arrhenius to low-temperature Arrhenius behavior has previously been observed in several aqueous solutions[2,4,5,24,37-39]. Different interpretations of this crossover can be found in the literature, and nowadays its physical origin is still not fully understood. Nevertheless, all interpretations agree that the nature of the water dynamics changes from a cooperative α-like relaxation above the crossover temperature to a more local β-like relaxation below the crossover temperature[2,4,5,24,39]. From our perspective[40], as this crossover occurs in the temperature range where DSC measurements show the glass transition, it might be associated with the freezing of the mixture at this temperature. At temperatures above T_g, water reorientation can be expected to be coupled to the cooperative motions involved in the global α-like relaxation process of the system (P4 in our system). When the temperature is decreased toward T_g, the viscosity of the global dynamics increases, and at T_g the global dynamics become frozen. Below T_g, water molecules are somehow trapped in the frozen matrix, but they still have significant mobility. Their motions are restricted, similarly to a secondary β-process in a simple glass. As a consequence, the temperature dependence of the relaxation times is Arrhenius-like. This interpretation is supported by the fact that water dynamics in well-defined geometrical confinements, such as molecular sieves[2,41], show a similar crossover. Moreover, this kind of crossover from liquid-like dynamics towards confined-like behavior has also been reported for the dynamics of the fast component in asymmetric polymer blends, i.e., blends where the two

components exhibit different mobilities[2,42,43], and in solid electrolyte systems[2,44], where again the ion mobility is much higher than the matrix mobility. Thus, the crossover observed for process 3 seems likely to be due to confinement effects caused by the freezing of the molecular movements of ε-PLL. However, this explanation does not apply to process 2, in which the dynamics also shows a change in the behavior at the glass transition temperature. If we assume that process 2 is the local relaxation of water molecules, then the speeding up of the relaxation time when the system reaches T_g is a normal observation in other secondary relaxations.

With regard to the concentration dependence, below T_g, P3 becomes faster with increasing water content until c_w = 40 wt%, whereas the further addition of water causes no change in the time scale of the relaxation (see Figure IV. 11 c). At temperatures near T_g, we still find the same concentration dependence, but well above T_g, the time scale of the relaxation becomes very similar for all water contents. This behavior of process 3 resembles the concentration dependence of water in ordinary solutions and determines the main difference from process 2 (not water dependent, see Figure IV. 11 b) apart from the different time scale.

We wonder why two water relaxations (P2 and P3) are observed in this system, whereas for other ordinary solutions, only one water peak is observed. We do not have an exact answer, but we believe that a "singular cluster" of water molecules is formed in this system. In this context, "singular cluster" means a cluster big enough to let the water molecules relax collectively. Therefore, we also wonder if this relaxation (P3) needs a minimum number of water molecules to be observed. To answer this question, we have measured a sample with c_w = 5 wt%. At this low hydration level, the sample is a hydrated powder instead of a solution, and process 3 is no longer observed. Thus, this result is in agreement with the indication that we need a certain critical water concentration to observe process 3.

Therefore, we can conclude that to observe P3 requires a minimum quantity of water molecules, and at water contents higher than 30 wt%, this process is due to a collective relaxation of water molecules. It is also important to note that the distribution of water in both ε-PLL and protein – water mixtures should be similar because two water relaxations can be observed only for these systems.

Process 4

In contrast to processes 2 and 3, the relaxation strength of process 4 increases with increasing ε-PLL content (see Figure IV. 13b and Figure IV. 14), which indicates that P4 is due to the reorientation of ε-PLL molecules. In addition, process 4 shows VFT temperature dependence for all the water contents analyzed (see Table IV. 4). The temperature at which this VFT equation extrapolates to 100 s is defined as the dielectric glass transition temperature ($T_{g,\,100\,s}$). This value agrees with the one obtained by DSC (T_g), indicating that the relaxation origin can be attributed to the α-relaxation of the solution. However, we must mention that not only P4 but also process 5 extrapolates to 100 s at T_g. Thus, process 5 can also be responsible for the glass transition observed by DSC, and therefore, they can both be related to the glass transition phenomenon. Nevertheless, we believe that process 5 is related to ionic conductivity and electrode polarization effects and therefore not related to the glass transition phenomena. To probe that possibility, ε-PLL was purified using an ion transfer resin by the batch method (AG 501-X8 supplied by Bio-Rad Laboratories) to remove ionic species from the solution. In this way, both dc conductivity and electrode polarization effects can be reduced.

The purified ε-PLL solution was measured by BDS to compare the dielectric results with the non-deionized sample at the same hydration level (c_w = 40 wt%). Figure IV. 16 shows both components of the complex dielectric permittivity data for the non-purified and the deionized ε-PLL solution at various temperatures below (a, b) and above (c, d) T_g. Figure IV. 17 also shows the different dielectric relaxation processes used to fit ε' and ε''. Processes 1 to 4 remain very similar after deonization, whereas the intensity of high-temperature processes (processes 5 to 7) is reduced after deionization. This result indicates that processes 1 to 4 are not affected by ionic species, whereas P5 is strongly affected. After deonization, the relaxation time of process 5 does not extrapolate to 100 s at T_g, and therefore P4, and not P5, is related to the glass transition phenomena.

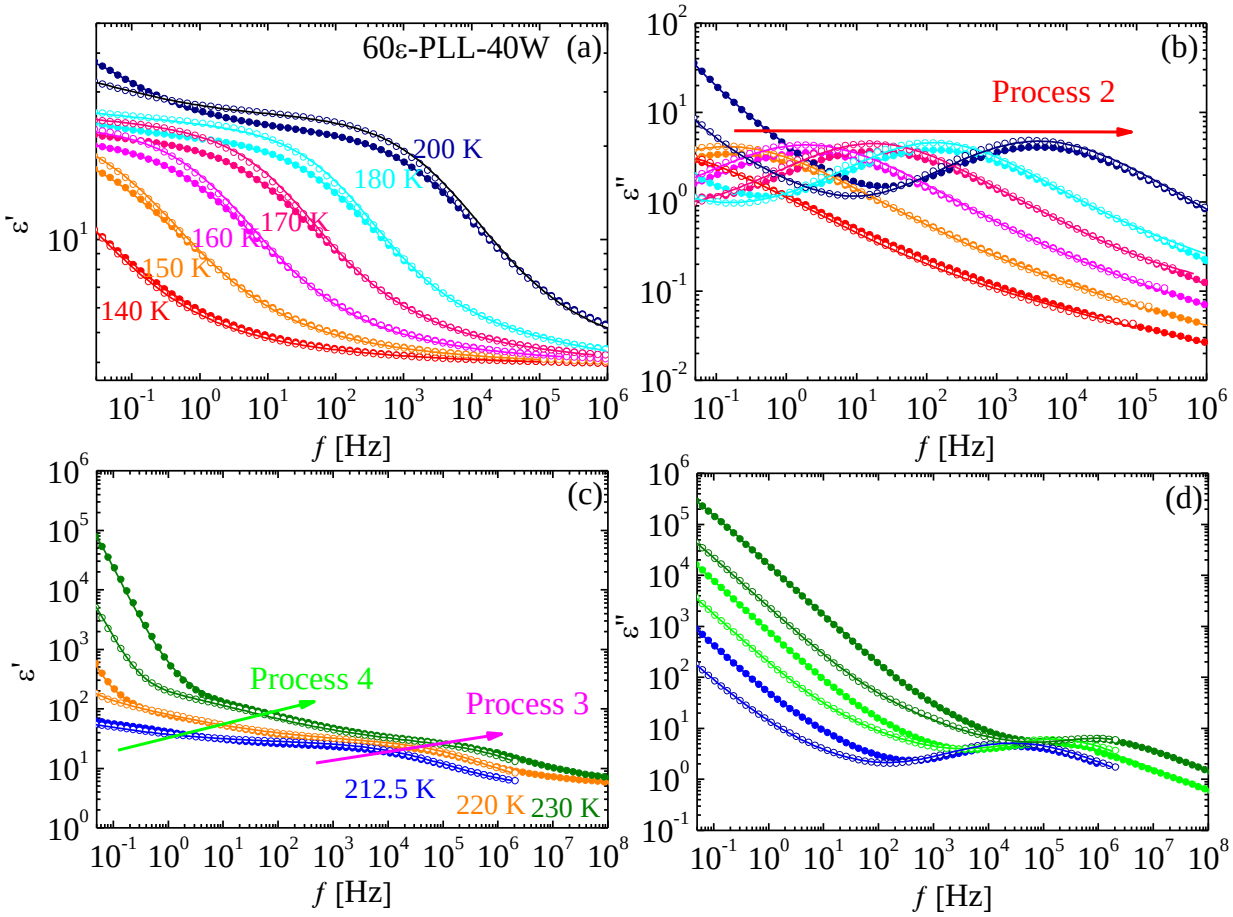

Figure IV. 16. Real (ε') and imaginary (ε'') parts of the complex permittivity of 60ε-PLL – 40W solution at various temperatures below (a,b) and above T_g (c,d). Closed symbols show experimental data for the non-deionized sample, whereas open symbols represent the experimental data for the purified ε-PLL solution.

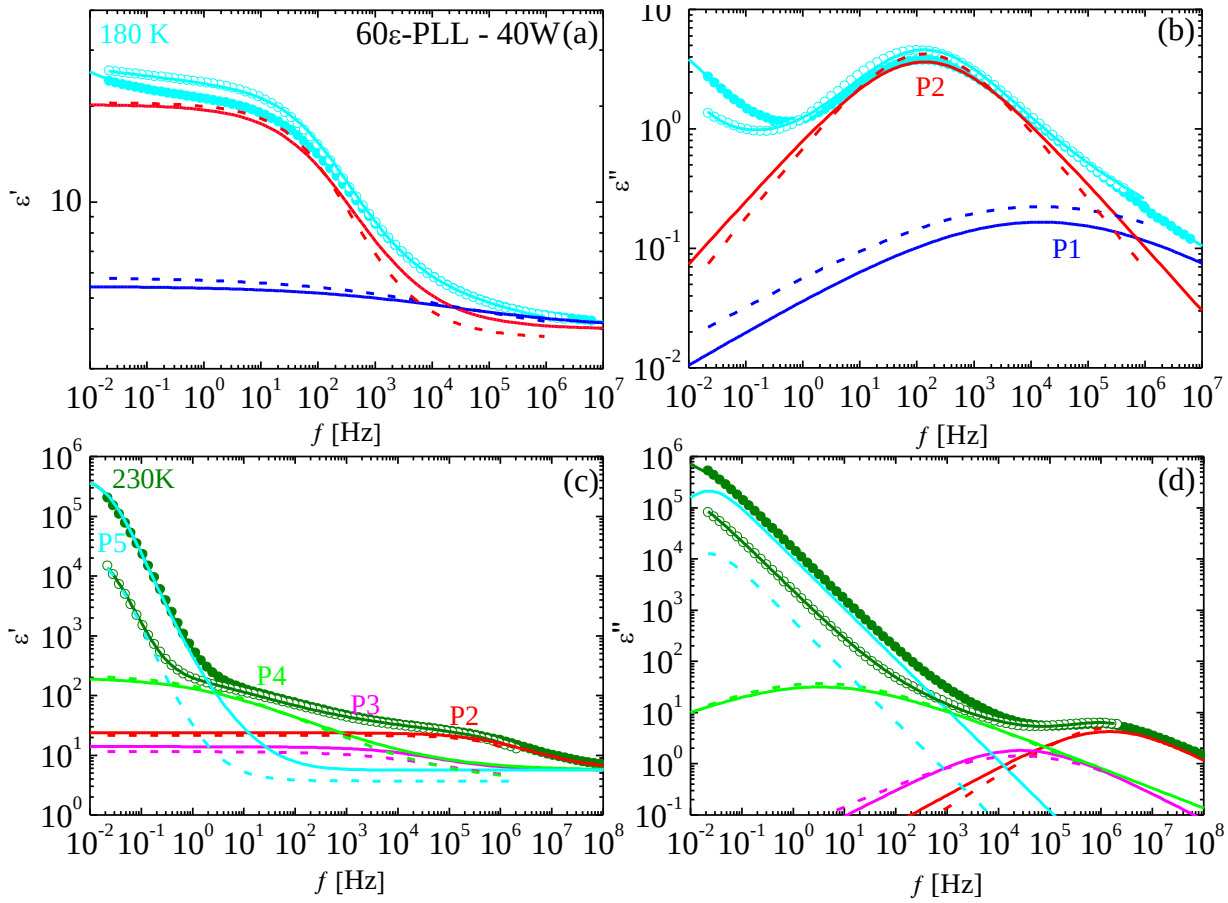

Figure IV. 17. Real (ε') and imaginary (ε'') parts of the complex permittivity of 60εPLL – 40W sample at two temperatures below (a,b) and above T_g (c,d). Closed and open symbols show experimental data for the non-purified sample and the purified ε-polylysine solution, respectively. Lines over the symbols represent the total fitting function, whereas lines below the symbols represent the dielectric relaxation processes. Among them, straight lines show the non-purified sample relaxations, while dotted lines show the relaxations for the deionized sample.

As it is shown in Figure IV. 11 d, the relaxation time of process 4 becomes faster with hydration level, and therefore the speeding up of the dynamics is induced by water.

Finally, we should mention that processes 4 and 3 both display the same VFT temperature dependence (see Figure IV. 18), suggesting a strong coupling between the two relaxation mechanisms. Nevertheless, this phenomenon will be further discussed in Chapter V.

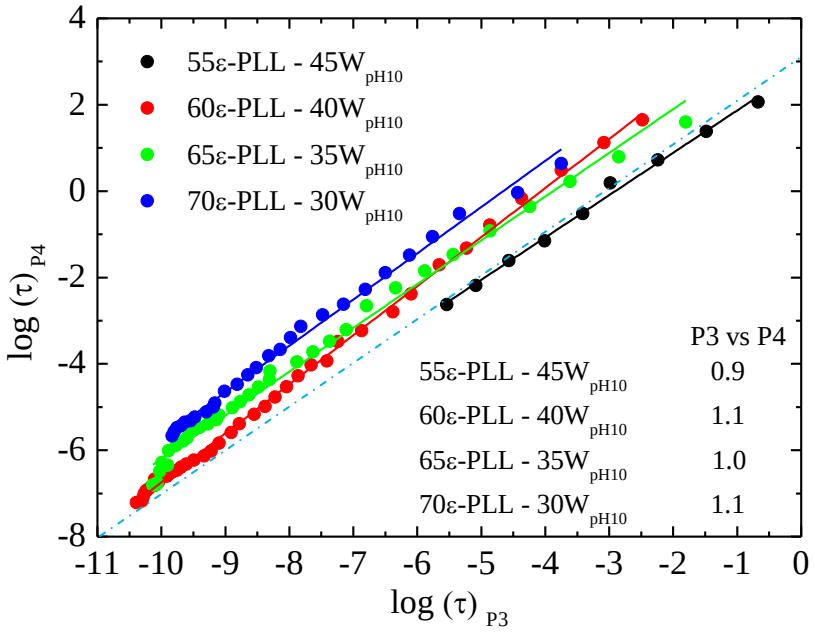

Figure IV. 18. Relaxation times of process 4 as a function of relaxation times for process 3. An almost perfect linear dependence, with a slope of one, is observed. Dashed blue line represents a line of slope 1.

High-temperature processes (P5 to P7)

Concerning processes 5 to 7, although they may also contain some dipolar reorientations, they are mostly attributed to electrode polarization effects and an overlapping high ionic conductivity. Thus, the origin of these processes is not related to molecular relaxations.

In aqueous systems such as our *ε*-PLL solutions, water molecules can be dissociated, giving free ions (H_3O^+ and OH^-). When placed in an external field, these ions can flow in the direction of the applied field but cannot "pass into" the metal electrodes, so they are accumulated at the electrode surface[20,21]. Due to this phenomenon, two major polarization mechanisms are observed: the ionic polarization due to charge migrations (e.g., free ions resulting from water molecule dissociation or impurities present in the solution) and the dielectric polarization current, caused by the orientation of permanent dipoles (water and *ε*-PLL polar molecules in our case). Moreover, the large dielectric intensities ($\Delta\varepsilon > 10^4$) of these processes show that they cannot be attributed to standard relaxation[24,45], as there is no dipolar species that can cause a relaxation process with such high intensity (see *Δε* differences among P3 to P7 in Figure IV. 19).

In addition, as previously shown in Figure IV. 18, these three processes are largely affected by the ion content in the samples.

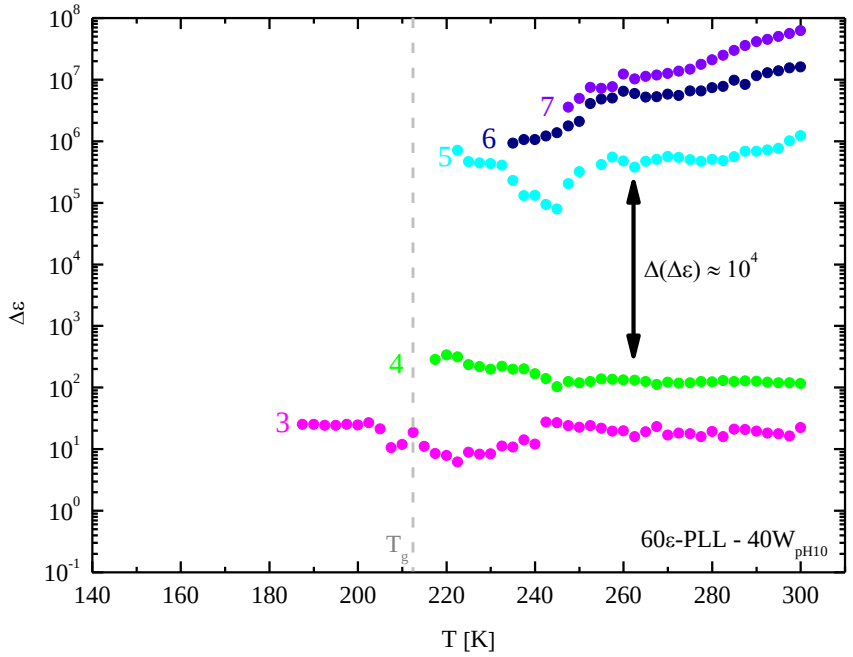

Figure IV. 19. Dielectric intensity temperature dependence of processes 3 to 7 for 60ε-PLL – 40W_{pH10} solution.

1.4.2. Dielectric results of ε-PLL aqueous solutions at c_w = 40 wt% at different pH

Broadband dielectric spectroscopy results

Figure IV. 20 shows both components of the complex dielectric permittivity at various temperatures below and above T_g for the 60ε-PLL – 40W sample at pH = 8 (data for samples at pH= 9 and 7 are shown in the Appendix, Figure A. 5 and Figure A. 6). As shown in Figure IV. 1, samples with pH values of 7 and 8 crystallize on cooling and were therefore quenched to 120 K to prevent crystallization. The dielectric study was limited to 200 K because cold crystallization starts at this temperature. In addition, we have performed TSCD measurements (Table IV. 5 shows polarization temperature, T_{pol}, values**)**, and the data analysis also includes the derivative of the real part of the dielectric permittivity. Figure IV. 21a shows the obtained TSDC results of ε-PLL at pH = 9, where two dynamical processes below T_g are observed, whereas at pH = 8 (Figure IV. 21 b), only one process is observed. Figure IV. 22 shows the logarithmic derivative

analysis for the samples at the three different pH values (9, 8 and 7). At pH = 9, two processes are observed below the glass transition temperature, and at lower pH, only one process is clearly discerned.

Table IV. 5. Polarization temperature (T_{pol}) value for each sample.

Sample	T_{pol} [K]
60 ε-PLL – 40W$_{pH8}$	196.1
60 ε-PLL – 40W$_{pH9}$	248.1

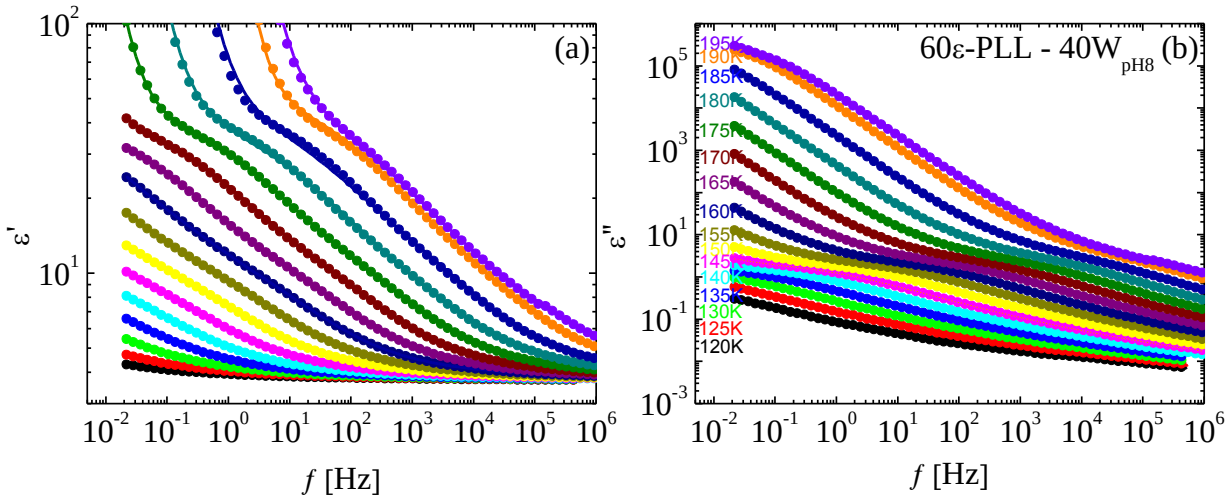

Figure IV. 20. Dielectric data as a function of frequency for 60ε-PLL – 40W samples at pH 8 at selected temperatures below and above T_g. Closed symbols show experimental data, and lines over the symbols represent the total fitting function.

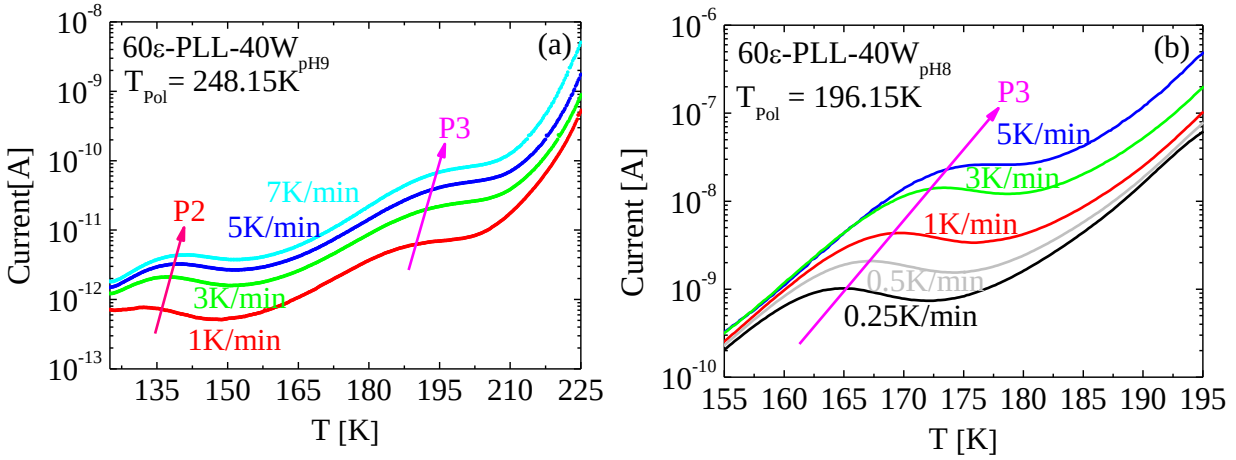

Figure IV. 21. TSDC depolarization current curves of ε-polylysine – water solutions (c_w = 40 wt%) at various pH values at different heating rates.

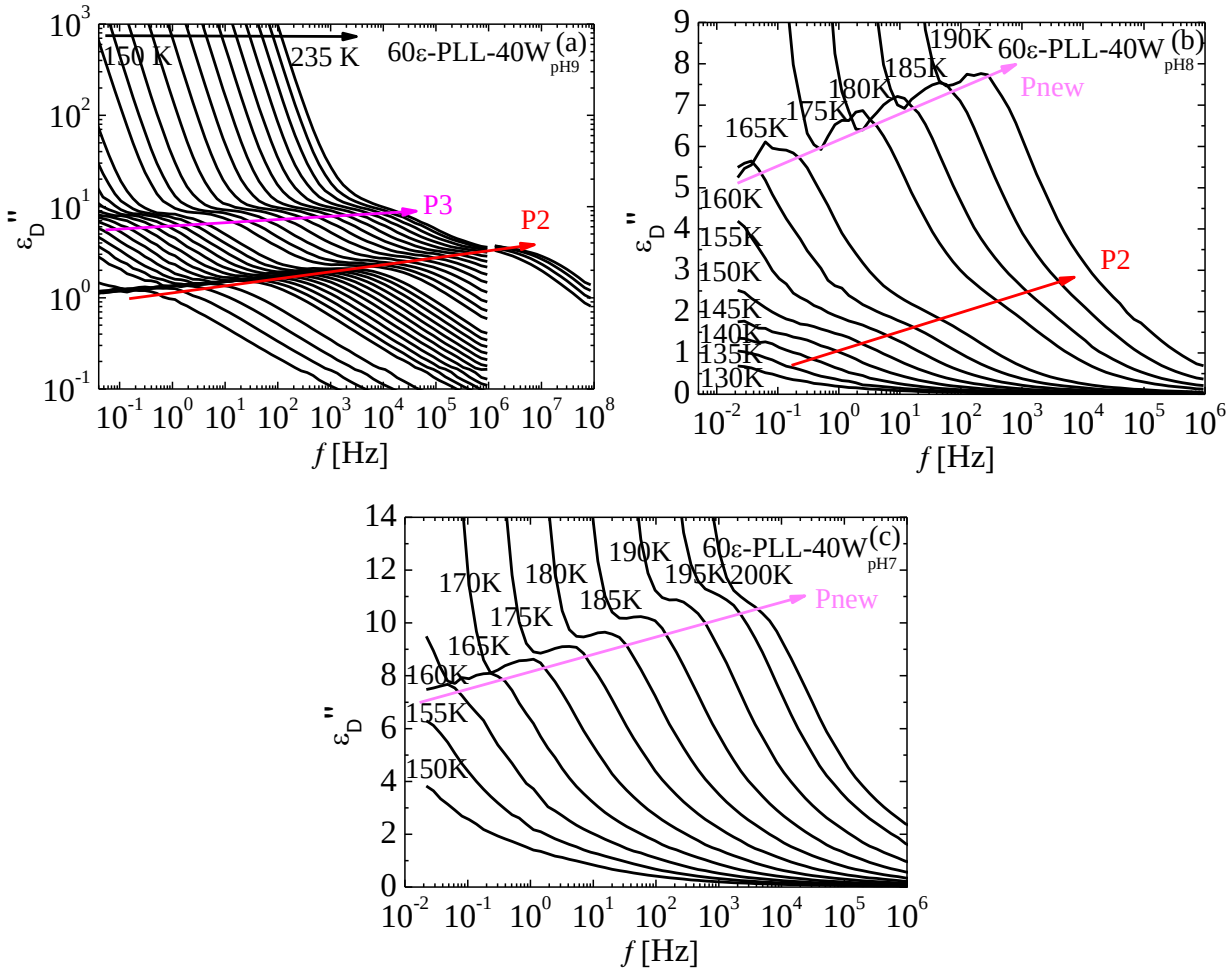

Figure IV. 22. Logarithmic derivative analysis for samples with different pH at water contents of c_w = 40 wt%.

Fitting procedure

To analyze the complex permittivity (ε^*), simultaneous fittings of both the real (ε') and imaginary (ε'') components were performed. The dielectric response was described using the superposition of several standard Cole - Cole functions plus an extra term for the conductivity (see Equation IV.1). In Figure IV. 23, the different dielectric relaxation processes used to fit ε' and ε'' are shown for the sample at pH = 8. The results for pH values of 7 and 9 are shown in the Appendix section (see Figure A. 10). Figure IV. 24 compares the dielectric signal at different pH at 180 K together with the fitting functions. As the pH is decreased, the conductivity is enhanced, and therefore the fitting is more difficult.

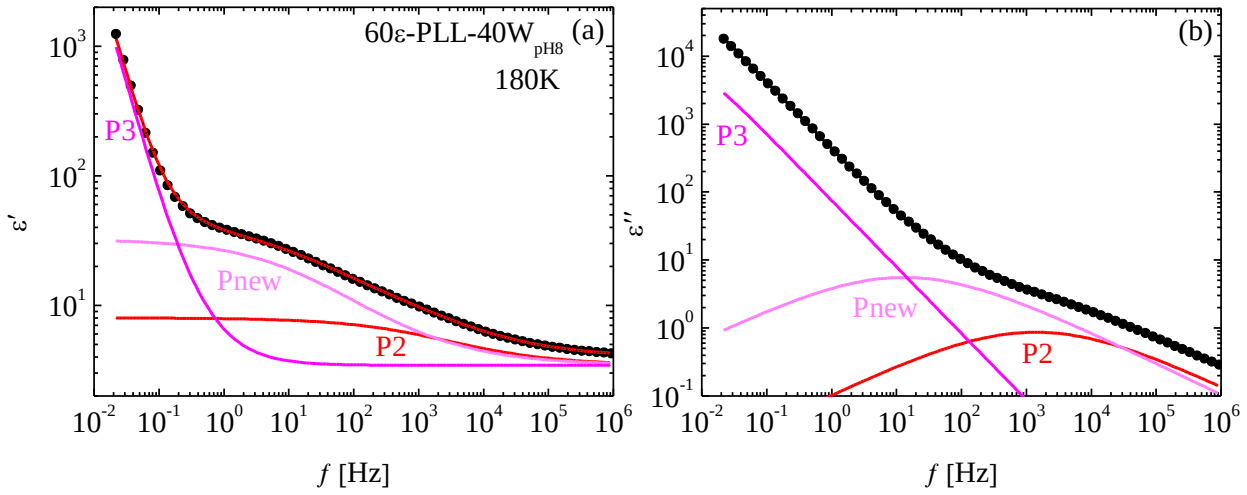

Figure IV. 23. Real (a) and imaginary (b) parts of the complex dielectric permittivity of ε-PLL water solution (c_w = 40 wt%) at pH = 8 and 180 K. Different relaxation processed used to fit ε´ and ε´´ are shown in colored lines.

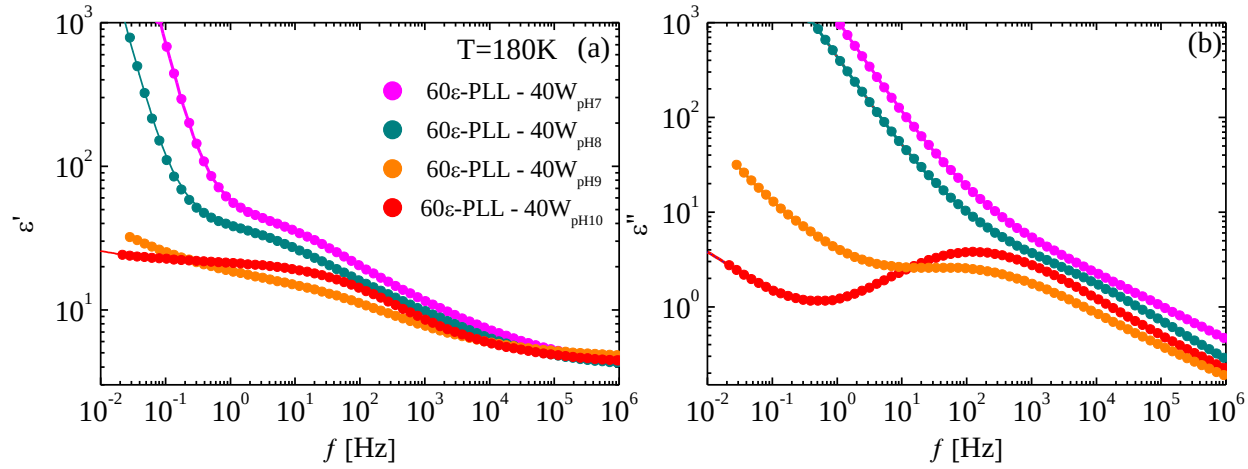

Figure IV. 24. Real (ε´) and imaginary (ε´´) parts of the complex permittivity for 40 wt% water samples at 180 K and different pH values. The solid line through the data points represents the fit to the experimental data.

Fitting parameters

From the fittings, we obtained the relaxation times and their temperature dependence, as shown in Figure IV. 25 for 60ε-PLL-40W samples at different pH values. The results for the previously analyzed sample at pH = 10 are also shown for comparison. Moreover, relaxation times obtained from TSDC measurements and the logarithmic derivative analysis are also included.

At low pH values (7 and 8), four processes are observed below T_g, one more than in the case of a fully amorphous system. This new dielectric process is called P_{new}, and similar to processes 1 to 3, it follows an Arrhenius temperature dependence behavior. The activation energy (E_a) and $log(\tau_0)$ values at various pH are shown in Table IV. 6.

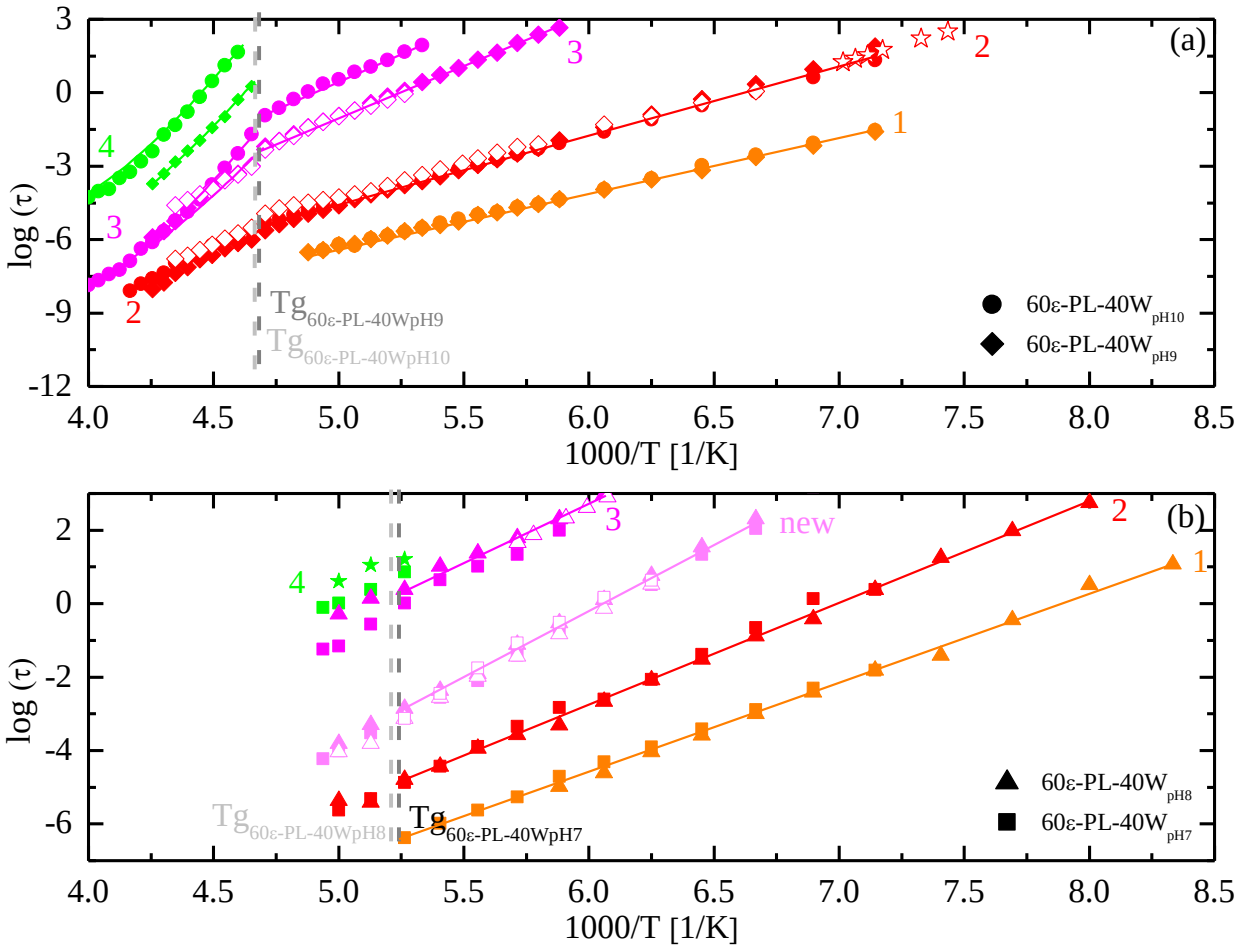

Figure IV. 25. Temperature dependence of the relaxation times for 40 wt% water content sample at various pH values (pH = 10 and 9 (a) and pH = 8 and 7 (b)). Temperature dependences of the relaxation times obtained by LF experiments are shown by closed circles for the c_w = 40 wt% pH = 10 sample, closed diamonds for the pH = 9 sample, closed triangles for pH = 8 and closed squares for pH = 7. Open red and dark pink diamond-shaped points and light pink open triangle and square points represent the logarithmic derivative results for the pH = 9, 8 and 7 samples respectively, while open red stars and open triangles in dark pink represent TSDC experiment results for the pH = 9 and 8 samples, respectively.

Table IV. 6. Activation energy *(E_a)* and *log(τ_0)* values obtained from the Arrhenius fittings for *ε*-PLL aqueous solutions at various pH.

pH	P1		P2		Pnew		P3	
	E_a	$log(\tau_0)$	E_a [eV]	$log(\tau_0)$	E_a [eV]	$log(\tau_0)$	E_a [eV]	$log(\tau_0)$
7	0.5	-19.2	0.6	-19.8	0.7	-22.6	0.6	-15.7
8	0.5	-19.8	0.5	-19.6	0.7	-22.4	0.6	-15.2
9	0.4	-17.1	0.6	-19.5	-	-	0.8	-21.6

Molecular origin of the dynamics at lower pH values

When the pH is decreased from 10 to 9, no significant differences are observed in the dynamics of the solutions (see Figure IV. 25 a), since at pH = 9, we find almost the same dynamic as at pH = 10. Only processes 3 and 4 become slightly faster at pH = 9.

Larger differences are visible upon decreasing the pH from 10 to 8 or 7. Process 2 becomes faster, and a new relaxation process (P_{new}) is observed between P2 and P3 (see Figure IV. 25b). As the samples at pH = 7 and 8 showed crystallization, to analyze this new relaxation, in Figure IV. 26 we compare the relaxation times of P_{new} with the relaxation of some ices observed in a BSA – water mixture[4]. Note that the two contributions related to the relaxation of ice in Figure IV. 26 have similar activation energy but different time scales. The relaxation time of P_{new} is between the two "ice" relaxations found in BSA-water mixtures. However, it is well known that the relaxation of ice is dependent on the concentration of defects in the crystals[4], and therefore, the time scale could depend on the way ice is formed in each system.

On the other hand, process 2 in *ε*-PLL aqueous solutions at pH = 7 and 8, which is consistent with the *ν*-process found in the BSA – water system (Figure IV. 26) and assigned to the main relaxation of water[4], becomes faster upon decreasing the pH from 10 to 7 or 8. At lower pH, the solution has more ion content (as also reflected in the strong conductivity), which could affect the relaxation of the local water via process 2. However, this possibility is only a speculation, and we cannot verify this reason for a faster process 2. We also note that *ε*-PLL has different conformations at pH = 7 and 8. At lower pH, the conformation is a mix between *β*-sheets and *β*-

turns instead of a pure β-sheet as at pH = 9 or 10. Thus, a different distribution of water molecules because of the different conformation of ε-PLL could be another reason for a faster relaxation.

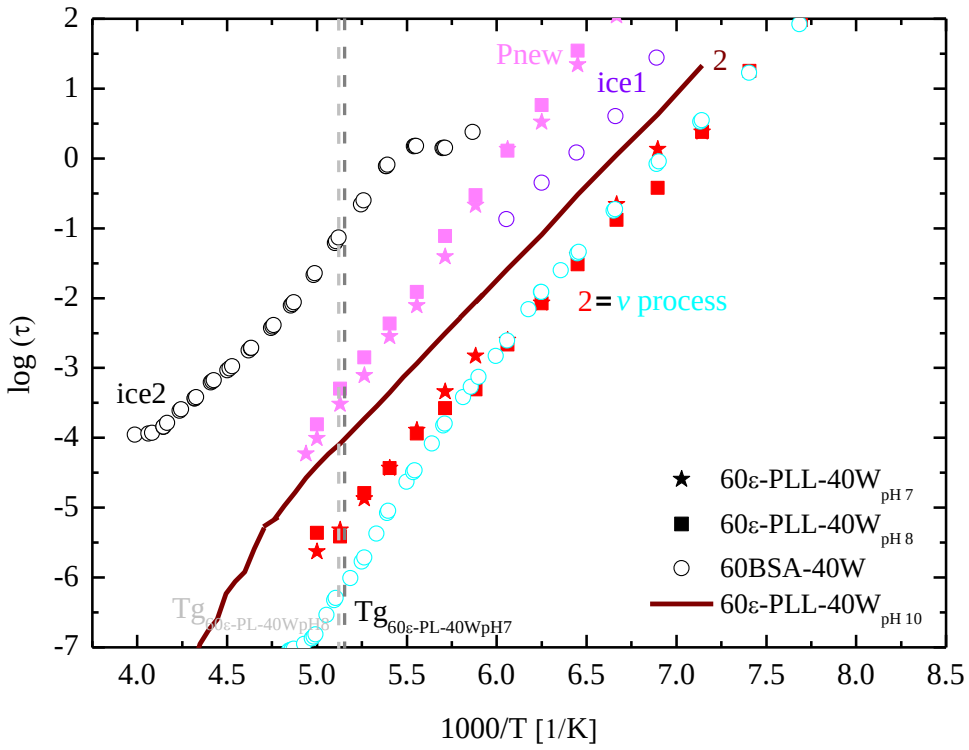

Figure IV. 26. Temperature dependence of P2 and P_{new} relaxation times for 40 wt% water content sample at pH = 7 and 8. Additionally, relaxation times for ice1, ice2 (violet and black open circle-shaped points, respectively), *v* process (light blue open circle-shaped points) from A. Panagopoulou et al[4] for BSA-water mixture at 40 % hydration level and P2 relaxation times temperature dependence for 60ε-PLL-40W at pH = 10 (brown line) are also included.

2. CONCLUSIONS

The dynamics of hydrated biosystems analyzed in broad temperature and frequency ranges is very complex, showing several relaxation processes. The analysis of these data is extremely difficult, and therefore no clear interpretation of the dynamics can be performed. In addition, proteins in solution show the crystallization of water at low temperatures, which masks the relaxations of the fraction of amorphous water.

Taking advantage of the fact that ε-PLL is a homogeneous solution and has no crystallization of water up to c_w = 40 wt%, we have developed an experimental strategy to analyze the dielectric data in a broad frequency and temperature range. This strategy includes different experimental techniques (isothermal, isochronal and TSDC measurements). In addition, we have shown that the dielectric signal should be analyzed using the derivative of the real permittivity.

Using this approach, we have analyzed the dynamics of ε-PLL for different c_w ($30 \leq c_w$ [wt%] ≤ 45) and pH values (from 10 to 7). In the absence of crystallization, a rich dynamic was observed, and in addition, an analysis of the origin of each relaxation processes can also be performed. The most relevant results are as follows:

1) Below T_g, two main relaxations (P2 and P3) were observed with an Arrhenius temperature dependence of the relaxation times. Both Arrhenius processes have different activation energies. The dynamics of process 3 depends on water content, whereas the dynamics of process 2 not. Thus, the fact that the time scale of P2 is independent of water content (i.e. solute content) indicates that this dynamic is not affected by the solute.

2) Above T_g, two main processes (P3 and P4) were detected, the faster one due to a collective relaxation of water molecules and the slower one related to the calorimetric glass transition. The fact that the time scale of P3 depends on water or solute content indicates that the collective motion of water molecules represented by process 3 is affected by the presence of the solute. In addition, the dynamics of the solute molecules (P4) also depends on water. Thus, our results suggest that both dynamics (solvent and solute) influence each other.

3) The dynamics of P3 and P4 are extremely closely coupled to each other, resembling the "slaving behavior" observed in proteins. This behavior will be discussed in the next chapter.

4) Also above T_g, the slowest processes 5 to 7 were observed and attributed to ionic conductivity and/or electrode polarization. This observation was made through the deionization of the samples.

The presence of more than one water-related process below T_g is not commonly observed in aqueous solutions other than protein solutions. The reason for the existence of process 3 is probably that a special cluster of water molecules is present in this system. At a very low water content (c_w = 5 wt%), only the β-relaxation (P2) of water was observed, and at higher water contents ($c_w \geq$ 30 wt%), this β-relaxation is complemented by process 3, which below T_g should be caused by the β-like relaxation of the remaining water, i.e., the water that is too much influenced by the solute molecules, both structurally and dynamically, to participate in the β-relaxation of water (P2).

3. REFERENCES

1 Swenson, J. & Cerveny, S. Dynamics of Deeply Supercooled Interfacial Water. *J. Phys.: Condens. Matter* **27**, 033102 (2015).

2 Cerveny, S., Alegria, A. & Colmenero, J. Universal features of water dynamics in solutions of hydrophilic polymers, biopolymers, and small glass-forming materials. *Physical review. E, Statistical, nonlinear, and soft matter physics* **77**, 031803, doi:10.1103/PhysRevE.77.031803 (2008).

3 Jansson, H. & Swenson, J. The protein glass transition as measured by dielectric spectroscopy and differential scanning calorimetry. *Biochimica et biophysica acta* **1804**, 20-26, doi:10.1016/j.bbapap.2009.06.026 (2010).

4 Panagopoulou, A., Kyritsis, A., Shinyashiki, N. & Pissis, P. Protein and water dynamics in bovine serum albumin-water mixtures over wide ranges of composition. *The journal of physical chemistry. B* **116**, 4593-4602, doi:10.1021/jp2105727 (2012).

5 Jansson, H., Bergman, R. & Swenson, J. Role of solvent for the dynamics and the glass transition of proteins. *The journal of physical chemistry. B* **115**, 4099-4109, doi:10.1021/jp1089867 (2011).

6 Miyazaki, Y., Matsuo, T. & Suga, H. Low-temperature heat capacity and glassy behavior of lysozyme crystal. *Journal of Physical Chemistry B* **104**, 8044-8052, doi:10.1021/jp0007686 (2000).

7 Panagopoulou, A. *et al.* Glass transition and dynamics in BSA-water mixtures over wide ranges of composition studied by thermal and dielectric techniques. *Biochimica Et Biophysica Acta-Proteins and Proteomics* **1814**, 1984-1996, doi:10.1016/j.bbapap.2011.07.014 (2011).

8 Panagopoulou, A. *et al.* Glass Transition and Dynamics in Lysozyme-Water Mixtures Over Wide Ranges of Composition. *Food Biophysics* **6**, 199-209, doi:10.1007/s11483-010-9201-0 (2011).

9 Kong, J. & Yu, S. Fourier transform infrared spectroscopic analysis of protein secondary structures. *Acta Biochimica Et Biophysica Sinica* **39**, 549-559, doi:10.1111/j.1745-7270.2007.00320.x (2007).

10 Dong, A., Huang, P. & Caughey, W. S. Protein secondary structures in water from 2nd derivative Amide I infrared spectra *Biochemistry* **29**, 3303-3308, doi:10.1021/bi00465a022 (1990).

11 Maeda, S., Kunimoto, K.-K., Sasaki, C., Kuwae, A. & Hanai, K. Characterization of microbial poly (ε-l-lysine) by FT-IR, Raman and solid state 13C NMR spectroscopies. *Journal of Molecular Structure* **655**, 149-155, doi:10.1016/s0022-2860(03)00218-7 (2003).

12 Maeda, S., Oumae, S., Kaneko, S. & Kunimoto, K.-K. Formation of carbamates and cross-linking of microbial poly(ε-l-lysine) studied by 13C and 15N solid-state NMR. *Polymer Bulletin* **68**, 745-754, doi:10.1007/s00289-011-0580-2 (2011).

13 Maeda, S., Fujiwara, Y., Sasaki, C. & Kunimoto, K.-K. Structural analysis of microbial poly(ε-L-lysine)/poly(acrylic acid) complex by FT-IR, DSC, and solid-state 13C and 15N NMR. *Polymer Journal* **44**, 200-203, doi:10.1038/pj.2011.108 (2011).

14 Shukla, S. C., Singh, A., Pandey, A. K. & Mishra, A. Review on production and medical applications of ε-polylysine. *Biochemical Engineering Journal* **65**, 70-81, doi:10.1016/j.bej.2012.04.001 (2012).

15 Shih, I. L., Shen, M. H. & Van, Y. T. Microbial synthesis of poly(ε-lysine) and its various applications. *Bioresource technology* **97**, 1148-1159, doi:10.1016/j.biortech.2004.08.012 (2006).

16 Lee, H.-H. *et al.* Synthesis and Conformation of Monodispersed Oligo(ε-L-Lysine)mers Studied by Cd and IR Spectroscopies. *Spectroscopy Letters* **28**, 177-190, doi:10.1080/00387019508010070 (1995).

17 Kushwaha, D. R. S., Mathur, K. B. & Balasubramanian, D. Poly(ε-l-lysine) synthesis and conformation. *Biopolymers* **19**, 219-229, doi:10.1002/bip.1980.360190202 (1980).

18 Maeda, S., Sasaki, C. & Kunimoto, K. K. in *Nmr Spectroscopy of Polymers: Innovative Strategies for Complex Macromolecules* Vol. 1077 *ACS Symposium Series* (eds H. N. Cheng, T. Asakura, & A. D. English) 317-335 (2011).

19 Grimsley, G. R., Scholtz, J. M. & Pace, C. N. A summary of the measured pK values of the ionizable groups in folded proteins. *Protein Science* **18**, 247-251, doi:10.1002/pro.19 (2009).

20 Ben Ishai, P., Talary, M. S., Caduff, A., Levy, E. & Feldman, Y. Electrode polarization in dielectric measurements: a review. *Measurement Science and Technology* **24**, doi:10.1088/0957-0233/24/10/102001 (2013).

21 Emmert, S. *et al.* Electrode polarization effects in broadband dielectric spectroscopy. *European Physical Journal B* **83**, 157-165, doi:10.1140/epjb/e2011-20439-8 (2011).

22 F.Kremer & Schönhals, A. *Broadband Dielectric Spectroscopy*. (2003).

23 Floudas, G. *Polymer Science: A Comprehensive Reference*. Vol. 2 (Elsevier, 2012).

24 Cerveny, S. & Swenson, J. Dynamics of supercooled water in a biological model system of the amino acid L-lysine. *Physical Chemistry Chemical Physics* **16**, 22382-22390, doi:10.1039/c4cp02487g (2014).

25 Samouillan, V., Tintar, D. & Lacabanne, C. Hydrated elastin: Dynamics of water and protein followed by dielectric spectroscopies. *Chemical Physics* **385**, 19-26, doi:10.1016/j.chemphys.2011.04.016 (2011).

26 Wübbenhorst, M. & van Turnhout, J. Analysis of complex dielectric spectra. I. One-dimensional derivative techniques and three-dimensional modelling. *Journal of Non-Crystalline Solids* **305**, 40-49, doi:http://dx.doi.org/10.1016/S0022-3093(02)01086-4 (2002).

27 Fulcher, G. S. Analysis of recent measurements of the viscosity of glasses. II. *Journal of the American Ceramic Society* **8**, 789-794, doi:10.1111/j.1151-2916.1925.tb18582.x (1925).

28 Tammann, G. & Hesse, W. The dependancy of viscosity on temperature in hypothermic liquids. *Zeitschrift Fur Anorganische Und Allgemeine Chemie* **156** (1926).

29 Monasterio, M., Jansson, H., Gaitero, J. J., Dolado, J. S. & Cerveny, S. Cause of the fragile-to-strong transition observed in water confined in C-S-H gel. *Journal of Chemical Physics* **139**, doi:10.1063/1.4826638 (2013).

30 Khodadadi, S. *et al.* The origin of the dynamic transition in proteins. *Journal of Chemical Physics* **128**, doi:10.1063/1.2927871 (2008).

31 Ngai, K. L., Capaccioli, S., Ancherbak, S. & Shinyashiki, N. Resolving the ambiguity of the dynamics of water and clarifying its role in hydrated proteins. *Philosophical Magazine* **91**, 1809-1835, doi:10.1080/14786435.2010.523716 (2011).

32 Cerveny, S., Alegria, A. & Colmenero, J. Broadband dielectric investigation on poly(vinyl pyrrolidone) and its water mixtures. *Journal of Chemical Physics* **128**, doi:10.1063/1.2822332 (2008).

33 Cerveny, S., Colmenero, J. & Alegria, A. Dielectric investigation of the low-temperature water dynamics in the poly(vinyl methyl ether)/H2O system. *Macromolecules* **38**, 7056-7063, doi:10.1021/ma050811t (2005).

34 Lusceac, S. A. *et al.* NMR and dielectric studies of hydrated collagen and elastin: Evidence for a delocalized secondary relaxation. *Journal of Non-Crystalline Solids* **357**, 655-663, doi:10.1016/j.jnoncrysol.2010.07.035 (2011).

35 Pagnotta, S. E., Cerveny, S., Alegria, A. & Colmenero, J. The dynamical behavior of hydrated glutathione: a model for protein-water interactions. *Physical Chemistry Chemical Physics* **12**, 10512-10517, doi:10.1039/c003493b (2010).

36 Cerveny, S., Combarro-Palacios, I. & Swenson, J. Evidence of Coupling between the Motions of Water and Peptides. *Journal of Physical Chemistry Letters* **7**, 4093-4098, doi:10.1021/acs.jpclett.6b01864 (2016).

37 Vogel, M. Temperature-Dependent Mechanisms for the Dynamics of Protein-Hydration Waters: A Molecular Dynamics Simulation Study. *Journal of Physical Chemistry B* **113**, 9386-9392, doi:10.1021/jp901531a (2009).

38 Vogel, M. Origins of apparent fragile-to-strong transitions of protein hydration waters. *Physical review letters* **101**, 225701, doi:10.1103/PhysRevLett.101.225701 (2008).

39 Swenson, J., Jansson, H. & Bergman, R. Relaxation processes in supercooled confined water and implications for protein dynamics. *Physical review letters* **96**, 247802, doi:10.1103/PhysRevLett.96.247802 (2006).

40 Cerveny, S., Mallamace, F., Swenson, J., Vogel, M. & Xu, L. M. Confined Water as Model of Supercooled Water. *Chemical Reviews* **116**, 7608-7625, doi:10.1021/acs.chemrev.5b00609 (2016).

41 Jansson, H. & Swenson, J. Dynamics of water in molecular sieves by dielectric spectroscopy. *European Physical Journal E* **12**, S51-S54, doi:10.1140/epjed/e2003-01-013-5 (2003).

42 Genix, A. C. *et al.* Dynamics of poly(ethylene oxide) in a blend with poly(methyl methacrylate): A quasielastic neutron scattering and molecular dynamics simulations study. *Physical Review E* **72**, doi:10.1103/PhysRevE.72.031808 (2005).

43 Schwartz, G. A., Colmenero, J. & Alegria, A. Single component dynamics in miscible poly(vinyl methyl ether)/polystyrene blends under hydrostatic pressure. *Macromolecules* **40**, 3246-3255, doi:10.1021/ma062609b (2007).

44 Mizuno, F. *et al.* Highly decoupled ionic and protonic solid electrolyte systems, in relation to other relaxing systems and their energy landscapes. *Journal of Non-Crystalline Solids* **352**, 5147-5155, doi:10.1016/j.jnoncrysol.2006.06.006 (2006).

45 Serghei, A., Tress, M., Sangoro, J. R. & Kremer, F. Electrode polarization and charge transport at solid interfaces. *Physical Review B* **80**, doi:10.1103/PhysRevB.80.184301 (2009).

CHAPTER V

COUPLING BETWEEN THE MOTIONS OF WATER AND PEPTIDES

In this chapter, we discuss the dynamics of *n*-lysine oligomers (*n* = 1, 3, 4, 10 and 32) fully dissolved in water (c_w = 40 wt%). As shown in Chapter IV for ε-PLL, *n*-lysine oligomers at c_w = 40 wt% also do not show crystallization upon cooling or heating. The dielectric relaxation data show that the glass transition-related dynamics of the oligomers is coupled to water dynamics, in a way similar to previous observations for solvated proteins. We will show that this finding supports the idea of a slaving behavior of the oligomer-related process (here called process 4) by the water-related process (process 3). This result implies that the crucial role of water for protein dynamics can be extended to other types of macromolecular systems, where water is also able to determine their conformational fluctuations (e.g., peptide – water systems and ordinary aqueous solutions).

1. RESULTS

1.1. Differential scanning calorimetry (DSC)

Figure V. 1 shows the calorimetric response during a heating run at a rate of 10 K/min where no sign of crystallization was found, except for 10-lysine aqueous solution, which crystallized in the range of 210 – 230 K. Moreover, a single narrow glass transition temperature (T_g) was observed for all the samples. Table V. 1 shows the molecular weight of its oligomer (M_w), the calorimetric glass transition temperature ($T_{g,DSC}$), the width of the transition (ΔT_g), and the pH values. Note that T_g does not show a monotone molecular weight dependence for the sample with four monomer units.

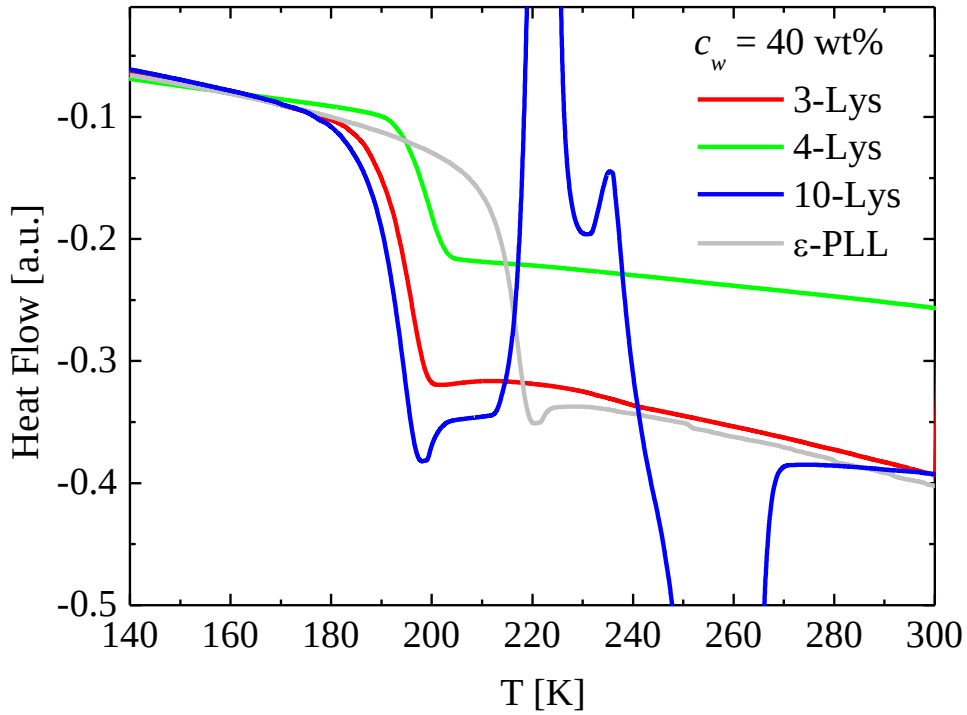

Figure V. 1. Heat flow vs. temperature for oligomers of lysine (*n*-lys, n = 3, 4 and 10) and ε-PLL (n = 32). 10-lysine crystallizes on heating in the range of 210 – 230 K.

Table V. 1. General characterization of *n*-lysine samples at c_w = 40 wt%, where M_w is the molecular weight of each oligomer, $T_{g,DSC}$ represents the calorimetric glass transition temperature, and ΔT_g is the width of the transition.

c_w = 40 wt%					
Sample	**Monomer amount**	M_w **[g/mol]**	$T_{g,DSC}$ **[K]**	ΔT_g**[K]**	**pH**
3-lys	3	402.5	190.0	9	≈ 10
4-lys	4	530.7	186.0	6	≈ 10
10-lys	10	1300.0	194.6	7	≈ 10
ε-PLL	32	4090.0	219.5	6	≈ 10

1.2. Fourier transform infrared spectroscopy (FTIR)

Figure V. 2 shows the infrared spectra in the 1800 – 1300 cm^{-1} region at 2 cm^{-1} resolution and averaging 50 scans per sample. This range contains the amide I band, which is a sign of the peptide conformation[1,2]. For ε-PLL, amide I is at 1630 cm^{-1} and indicates a β-sheet conformation, whereas for 10-lysine, this band is located at 1646 cm^{-1} and indicates an α-helix conformation. However, for the rest of the oligomers (n = 3, and 4), there are too few monomers to adopt any specific conformation. Moreover, their amide I bands are shifted to lower frequencies (see brown dotted line) close to the bending mode of water (1642 cm^{-1}, see brown dotted line), indicating that they are correlated to water and thus not to any specific conformation. In addition, the appearance of the band at 1402 cm^{-1} for *n*-lysine is assigned to the COO^- stretching. This band is absent in ε-PLL aqueous solutions because increasing the length of the chain decreases the number of carboxyl groups.

The chosen systems have the advantage of having chain-length dependent conformations (ε-PLL has a β-sheet secondary structure, and 10-lysine has an α-helix conformation, whereas the short peptides, 3- and 4-lysine, have no defined secondary structure for this concentration), and therefore, the possible influence on the dynamics can be studied. Moreover, the platelet β-sheet of ε-PLL differs from the β-sheet conformation of proteins in the number of carbon atoms in the main chain.

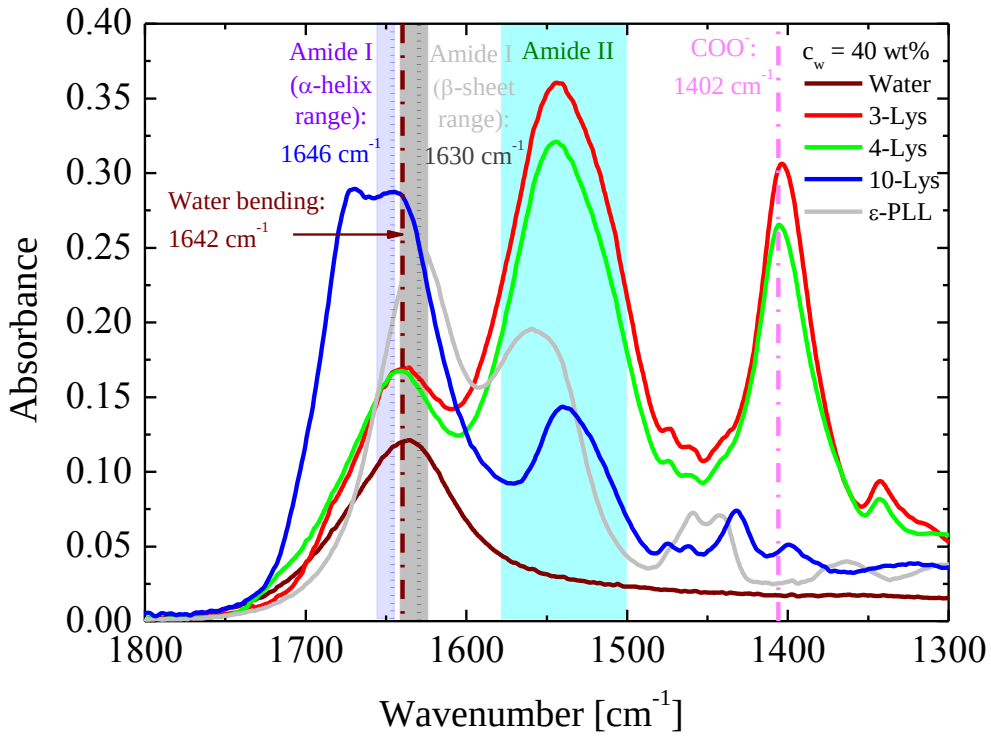

Figure V. 2. FTIR-ATR spectra of water solutions of *n*-lysine (c_w = 40 wt%) and ε-PLL at 25 ºC. Pure water spectrum is also added for comparison. Colored areas indicate the amide I α-helix or β-sheet bands and amide II band. Brown and pink dotted lines indicate the bending band of water and the symmetric stretching of COO^-, respectively.

1.3. Broadband dielectric spectroscopy (BDS)

BDS was used to study the dynamics of the aqueous solutions of *n*-lysine (*n* = 1, 3, 4 and 10). The ε-PLL (*n* = 32) results discussed in the previous chapter are also shown for comparison. Figure V.3 a - d and Figure V. 4 a and b shows both components of the complex dielectric permittivity together with the fitting data for *n* = 3 and 10 lysine oligomers water solution at some temperatures below and above T_g. To analyze the complex permittivity (ε^*), the simultaneous fitting of both the real (ε') and imaginary (ε'') components were performed by the superposition of several symmetric Cole - Cole functions plus an extra term for the conductivity (see Equation V. 1):

$$\varepsilon^*(\omega) = \varepsilon_\infty + \sum_j \frac{\Delta\varepsilon_j}{1+(i\omega\tau_j)^{\alpha_j}} - i\left(\frac{\sigma}{\varepsilon_0\omega}\right) \qquad \text{(V. 1)}$$

where $\Delta\varepsilon$ is the dielectric strength ($\Delta\varepsilon = \varepsilon_S - \varepsilon_\infty$, being ε_S and ε_∞ the low frequency and high frequency permittivity, respectively), ε_0 the the vacuum permittivity, ω the angular frequency ($\omega = 2\pi f$), τ the relaxation time ($\tau = 1/\omega_{max} = 1/2\pi f_{max}$), α the stretching parameter and σ the static ionic conductivity.

The derivative of the real part of the complex permittivity, which is practically identical to $\varepsilon''(\omega)$ but not affected by conductivity[3] is also shown in Figure V.3 e and f for n = 3 and in Figure V. 4 c and d for n = 10 samples. n= 4 oligomer show very similar behavior to what is shown here for 3-lysine. In the previous chapter, we showed and discussed the fitting procedure of ε-PLL aqueous solutions. The protocol to analyze the shorter oligomers is the same as the one used in Chapter IV, and therefore the fitting procedure is not described in greater detail here.

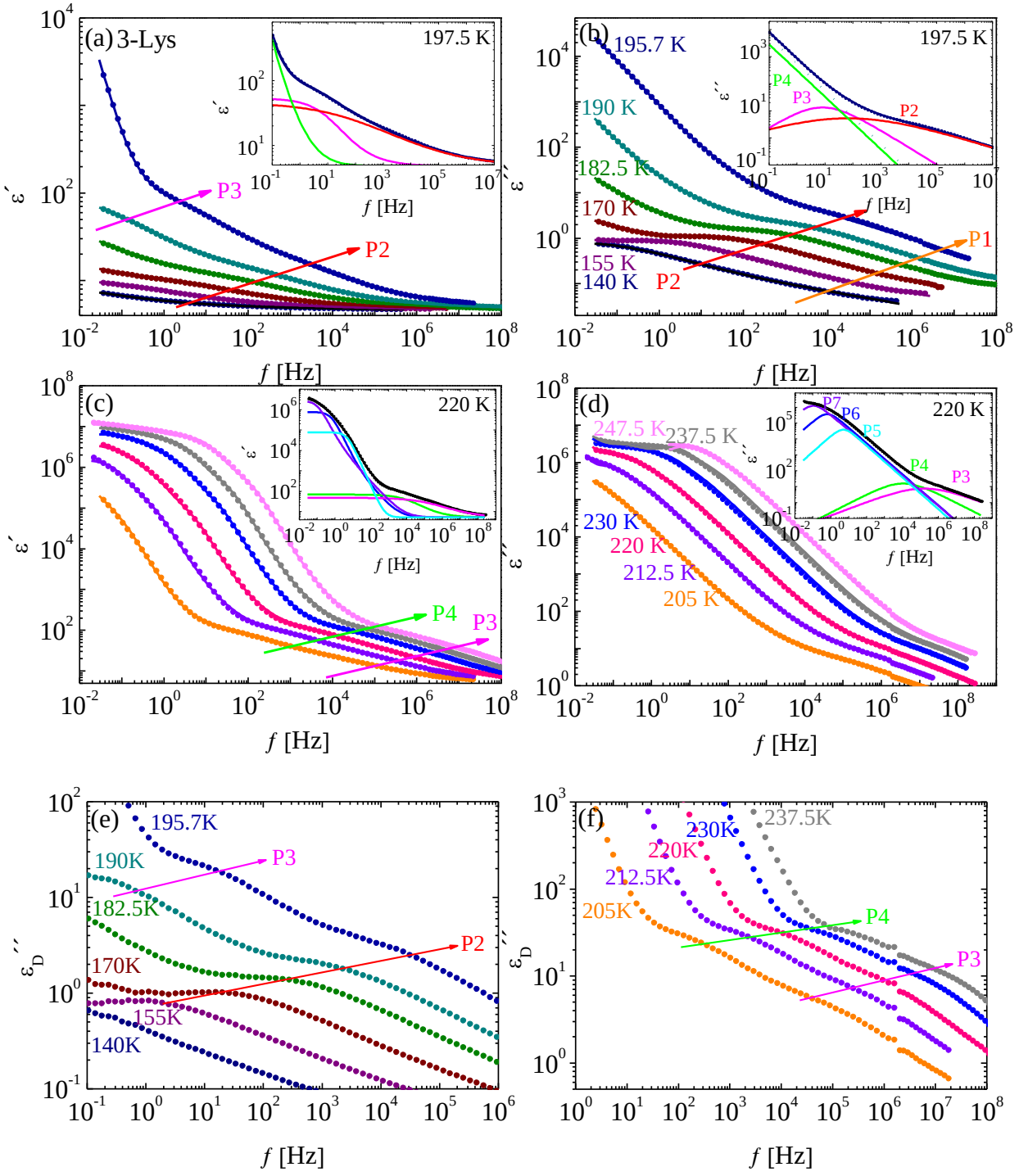

Figure V.3. (a, b) Real and imaginary part of the complex dielectric permittivity of the 3-lysine water solution (c_w = 40 wt%) at temperatures lower than T_g. Solid lines through the data points represent fits to the experimental data. (c, d) Same as in (a, b) at temperatures higher than T_g. (e, f) $\varepsilon_D''(\omega)$ calculated from the derivative of $\varepsilon'(\omega)$ at some temperatures below and above T_g, respectively.

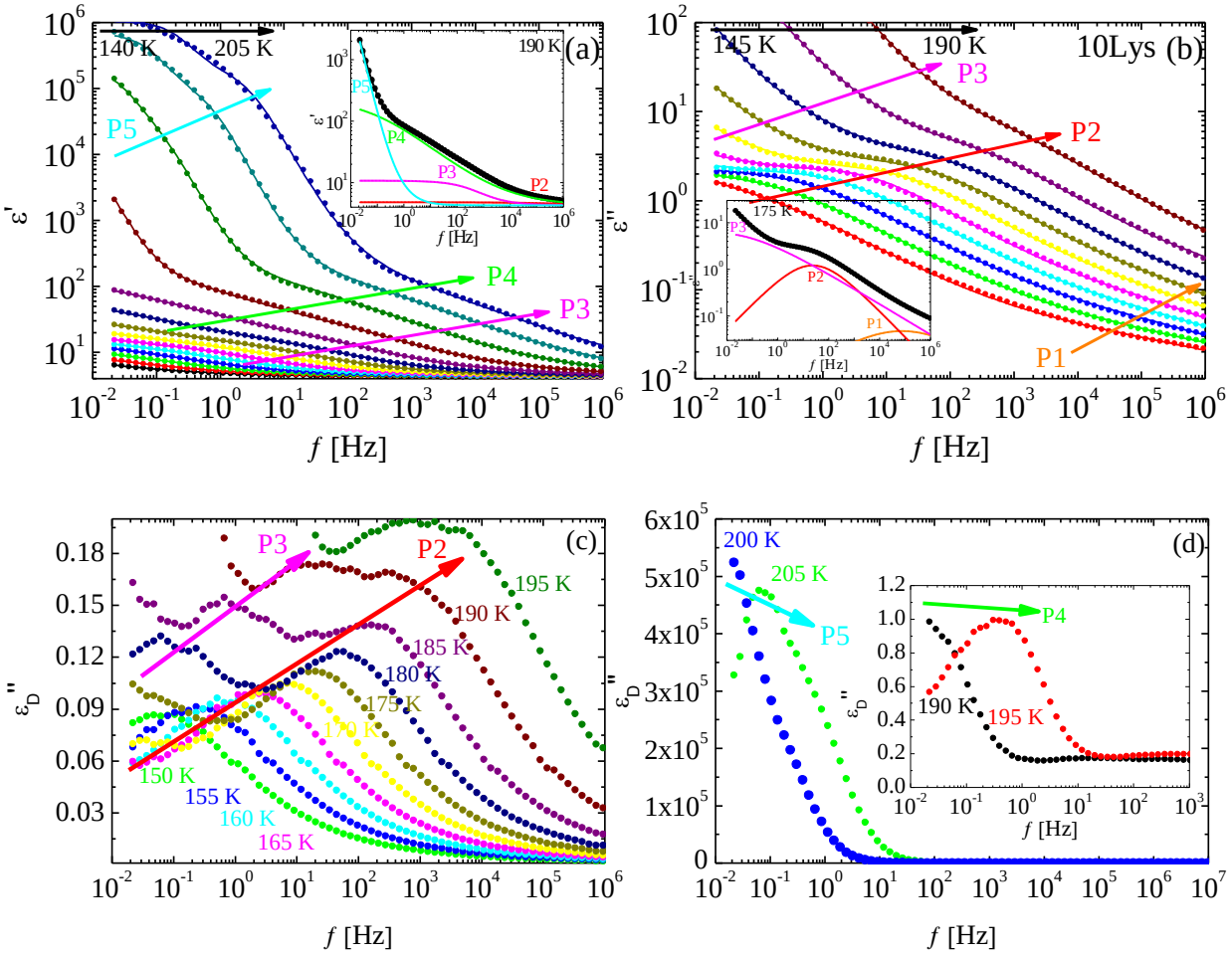

Figure V. 4. (a, b) Real and imaginary part of the complex dielectric permittivity of 10-lysine water solution (c_w = 40 wt%) at some temperatures below and above T_g. Solid lines through data points represent fits to the experimental data. $\varepsilon_D''(\omega)$ calculated from the derivative of $\varepsilon'(\omega)$ at selected temperatures below and above T_g are also included in (c and d) respectively.

As shown in Figure V.3 and Figure V. 4, the imaginary part of the permittivity at temperatures higher than T_g does not show clear dielectric processes (i.e., "peaks"). However, in the real part of the permittivity, we can observe the typical step associated with a relaxation. Nevertheless, the fitting strategy includes the simultaneous fit of the real and imaginary part of the dielectric permittivity, as well as other complementary measurements and data treatment to ensure the reliability of the fitting procedure. Thus, the performed experiments and data treatments include the following:

1) **Isochronal measurements** (at fixed frequencies from 10^{-2} to 10^{6} every decade) to establish the presence of processes 2, 3 and 4.

2) **Analysis of the derivative of the real part of the dielectric permittivity (ε´).** As the derivative of the real part of the complex permittivity is practically identical to ε´´(ω) but not affected by conductivity, it was possible to observe the "loss peak" corresponding to processes 2 – 4, which are masked by conductivity in the raw data.

3) Finally, **Thermo Stimulated Depolarization Current (TSDC) measurements** were performed to obtain relaxation times at longer times than the ones observed in typical isothermal measurements (> 100 s). In this case, TSCD measurements were performed at various heating rates, from 0.5 to 7 K/min, to determine the relaxation times of processes 2, 3 and 4 at longer times.

Thus, using the information obtained from the above experiments, the measured dielectric signals were fitted using fixed values of the relaxation times obtained from the derivate analysis and TSDC measurements (lines through data points in Figure V.3 and Figure V. 4 represent the fittings to experimental data).

The temperature dependences of the relaxation times obtained from the fittings for 3-lysine, 10-lysine and ε-PLL at c_w = 40 wt% are shown in Figure V. 5, where we can distinguish three different temperature regions:

1) Below T_g (from 140 to 220 K), two main dielectric processes called processes 2 and 3 were found. Another process, called process 1, was necessary to obtain a correct fitting of the experimental data, but to date, its origin is not fully understood. As previously explained, in the fitting procedure, the relaxation times were fixed and determined from the derivative analysis, along with the data obtained from TSDC. Thus, two parameters, the shape of the relaxation (α-parameter) and the intensity ($\Delta\varepsilon$), were kept free during the fitting for each CC function.

2) Above T_g (from 225 to 235 K), four dielectric processes, 2 to 5, were found. As in the previous temperature range, the relaxation times were fixed, whereas α and $\Delta\varepsilon$ were free parameters in the fitting procedure.

3) Finally, at high temperatures, above 235 K, two extra processes (6 and 7) were needed to fit the dielectric data. Thus, in this region, up to five dielectric processes coexist (processes 3 to 7).

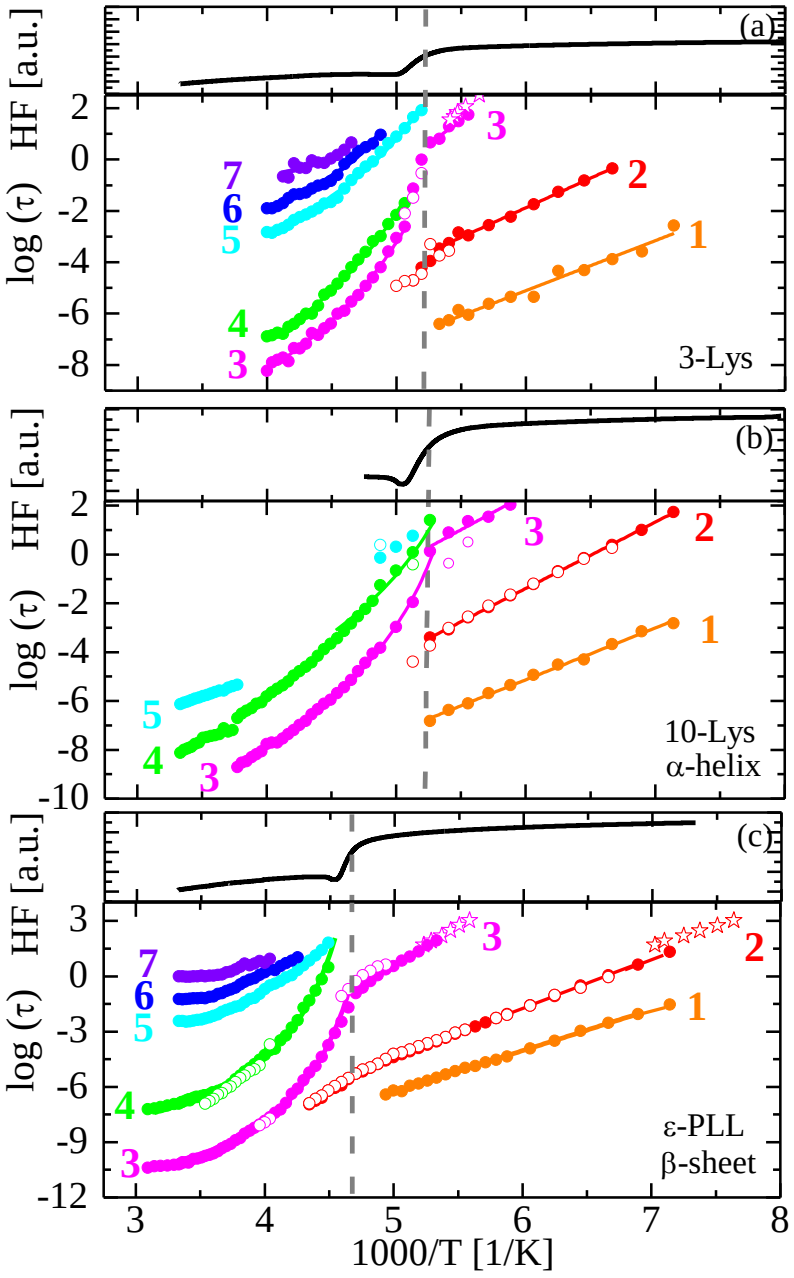

Figure V. 5. Temperature dependences of relaxation times of 3-lysine, 10-lysine and ε-PLL (c_w = 40 wt%). Vertical dashed lines represent the glass transition. Data obtained from TSDC experiments are shown in open star-shaped points and open circle-shaped points from the derivative analysis. The straight lines below T_g represent fits to the experimental data by the Arrhenius equation, whereas above T_g, the full lines represent VFT fits to the experimental data. The upper panel in each figure represents the heat flow measured by DSC of 3-lysine, 10-lysine and ε-PLL (c_w = 40 wt%) respectively. The average errors in the determinations of τ_1, τ_3 and τ_4 are 10%, 5% and 4%, respectively. For τ_2, the average error is approximately the same as the size of the symbols.

The dynamics of water in ε-PLL solutions at different water concentrations (c_w = 35 to 45 wt%) were previously analyzed in Chapter IV. For short chains of lysine (n = 3, 4 and 10), a rich dynamical behavior was also found, with the appearance of seven different relaxations. Below the glass transition temperature, three dynamical processes (1, 2 and 3) were observed, following an Arrhenius temperature dependence. Their activation energies and pre-exponential factor values are shown in Table V. 2. At temperatures above T_g, the dielectric data showed as many as five dynamical processes (3 to 7), although we mainly focus on the behaviors of processes 3 and 4. Table V. 3 shows all the fit parameters of the Vogel–Fulcher–Tammann (VFT) equations used to describe the temperature dependences of the relaxation times of processes 3 and 4 for the different oligomers. For both processes, the fragility-associated parameter (D) is the same, providing evidence that the relaxation times of processes 3 and 4 follow the same temperature dependence.

Table V. 2. Activation energy (E_a) and pre-exponential factor ($log(\tau_0)$) from the Arrhenius equation applied to the data in Figure V. 5.

	Process 1		**Process 2**	
Sample	$\boldsymbol{log(\tau_0)}$	$\boldsymbol{E_a}$ **[eV]**	$\boldsymbol{log(\tau_0)}$	$\boldsymbol{E_a}$ **[eV]**
3-lys	-16.8	0.4	-15.7	0.5
4-lys	-15.0	0.4	-17.8	0.5
10-lys	-15.0	0.4	-17.4	0.5
ε-PLL	-15.0	0.3	-17.9	0.5

Table V. 3. VFT parameters ($log\ (\boldsymbol{\tau}) = log\ (\boldsymbol{\tau_0})\ exp\ (DT_0 / (T-T_0))$) for processes 3 and 4 above T_g, where T_0 is a pre-exponential factor, D is a parameter related to fragility, and To is the temperature at which the relaxation time extrapolates to infinity.

Sample	**Process 3**			**Process 4**		
	$\boldsymbol{D}$	$\boldsymbol{T_0}$ **[K]**	$\boldsymbol{log(\tau_0)}$	$\boldsymbol{D}$	$\boldsymbol{T_0}$ **[K]**	$\boldsymbol{log(\tau_0)}$
3-lys	7.9	149.0	-13.2	7.9	149.0	-12.1
4-lys	7.9	148.5	-13.3	7.9	149.6	-12.5
10-lys	12.1	136.5	-14.2	12.1	138.8	-12.5
ε-PLL	3.4	191.2	-12.6	3.4	195.6	-9.8

1.3.1. Molecular origin of the dielectric relaxation of *n*-lysine oligomers

Comparing these results to the ε-PLL studied in Chapter IV, the molecular origin of each process in the *n*-lysine oligomers was determined. The dielectric response for the shorter lysine chains revealed the same relaxation processes as in ε-PLL, and therefore they can be attributed to the same molecular origin.

Processes 5 to 7

These three processes (5 to 7) have large dielectric amplitudes ($\Delta\varepsilon > 10^4$), and therefore it is difficult to explain them as standard relaxation processes[4]. Instead, P5 to P7 seem to be related to ionic conductivity and electrode polarization (EP) effects. In fact, Floudas et at[5] proposed a detailed analysis to determine the frequency at which ionic conductivity and electrode polarization begin. In a 'master curve' of the complex permittivity (ε*), the complex electric modulus (M^*) and the complex conductivity (σ^*) at the same reference temperature (T_{ref}) (Figure V. 6 and Figure V. 7 for 3-lysine and ε-PLL, respectively) the crossing points of the real and imaginary parts of ε^*, M^* and σ^* occur at the same frequency (f_e). This frequency determines the beginning of the ionic mobility.

In a dielectric experiment, the complex conductivity is determined by the complex permittivity through the Maxwell relation[6];

$$\sigma^*(\omega) = i2\pi f \varepsilon_0 \varepsilon^*(f) \qquad \text{(V. 2)}$$

where f is the frequency, and ε_0 is the vacuum permittivity.

The complex electric modulus $M^*(f)$ is related to $\varepsilon^*(f)$ by[6]

$$M^*(f) = 1/\varepsilon^*(f) \qquad \text{(V. 2)}$$

This parameters above demonstrate that $\varepsilon^*(f)$, $\sigma^*(f)$, and $M^*(f)$ are interchangeable representations of the same macroscopic dielectric relaxation data.

At frequencies higher than f_e, dipolar motions are dominant, but at lower frequencies, ionic movements become relevant. Below f_e, the frequency dependence of ε'' displays a slope of 1, while ε' remains constant. In a wide frequency range covering approximately 11 orders of magnitude, the spectral dependence of the electrode polarization effects leads to changes of approximately 6 orders of magnitude in the intensity of the dielectric response. These values (as for instance $\varepsilon' > 10^6$) lack any direct molecular interpretation but reflect the net impedance of the measured cell, where the contribution of the interfaces must be added to the contribution of the bulk[4].

At frequencies below f_e, the M' and M'' data display slopes of 2 and 1, respectively[5]. However, electrode polarization effects arise at a much lower frequency, when $f = f_{on}$ (f_{on} is the onset frequency of the electrode polarization, EP). At this point, ε' increases with decreasing frequency. Moreover, this steep increase in ε' corresponds to a minimum in σ''[7]. Further increases in ε' and ε'' are due to the electrode polarization process. On the other hand, the σ^* representation emphasizes the transition from high-frequency ac conductivity (which strongly depends on the frequency of the external electric field) to dc conductivity (which is static and independent of frequency) at lower frequencies[5]. The transition again occurs near the crossing of σ' with σ''.

For systems with high ion content and/or very mobile ions, electrode polarization is the dominant mechanism at lower frequencies. At $f = f_{max}$, full development of the electrode polarization is detected in the dielectric spectra by another crossing of the real and imaginary parts at low frequencies[7]. At this point, a plateau in the real part of the permittivity begins to develop, corresponding to a maximum peak in σ''[7].

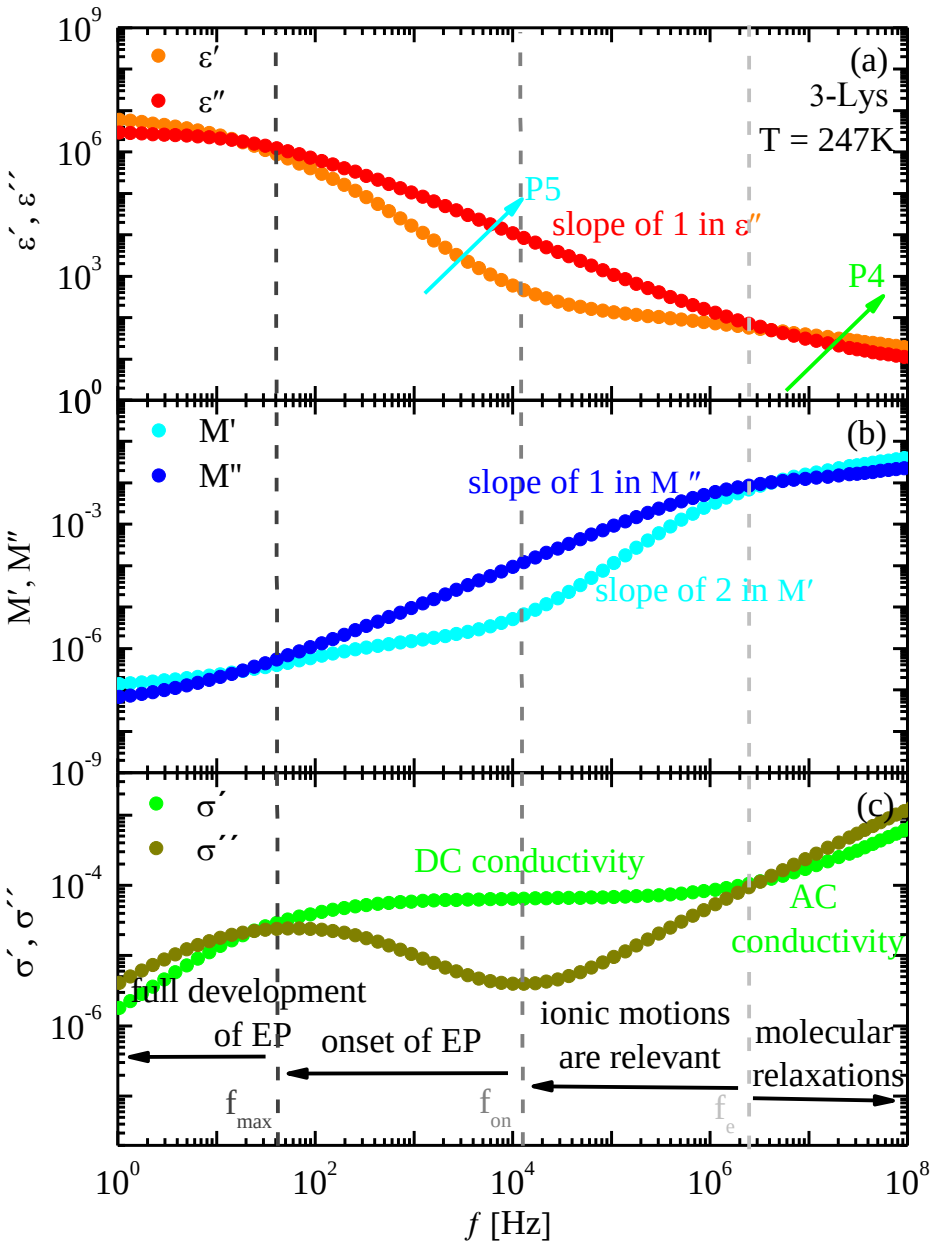

Figure V. 6. Real and imaginary parts of the complex dielectric permittivity, ε*; the electric modulus, M*; and the conductivity, σ*, for 3-lysine (c_w = 40 wt%) at a reference temperature of 247 K. The dashed vertical line indicates the process due to ion mobility and electrode polarization.

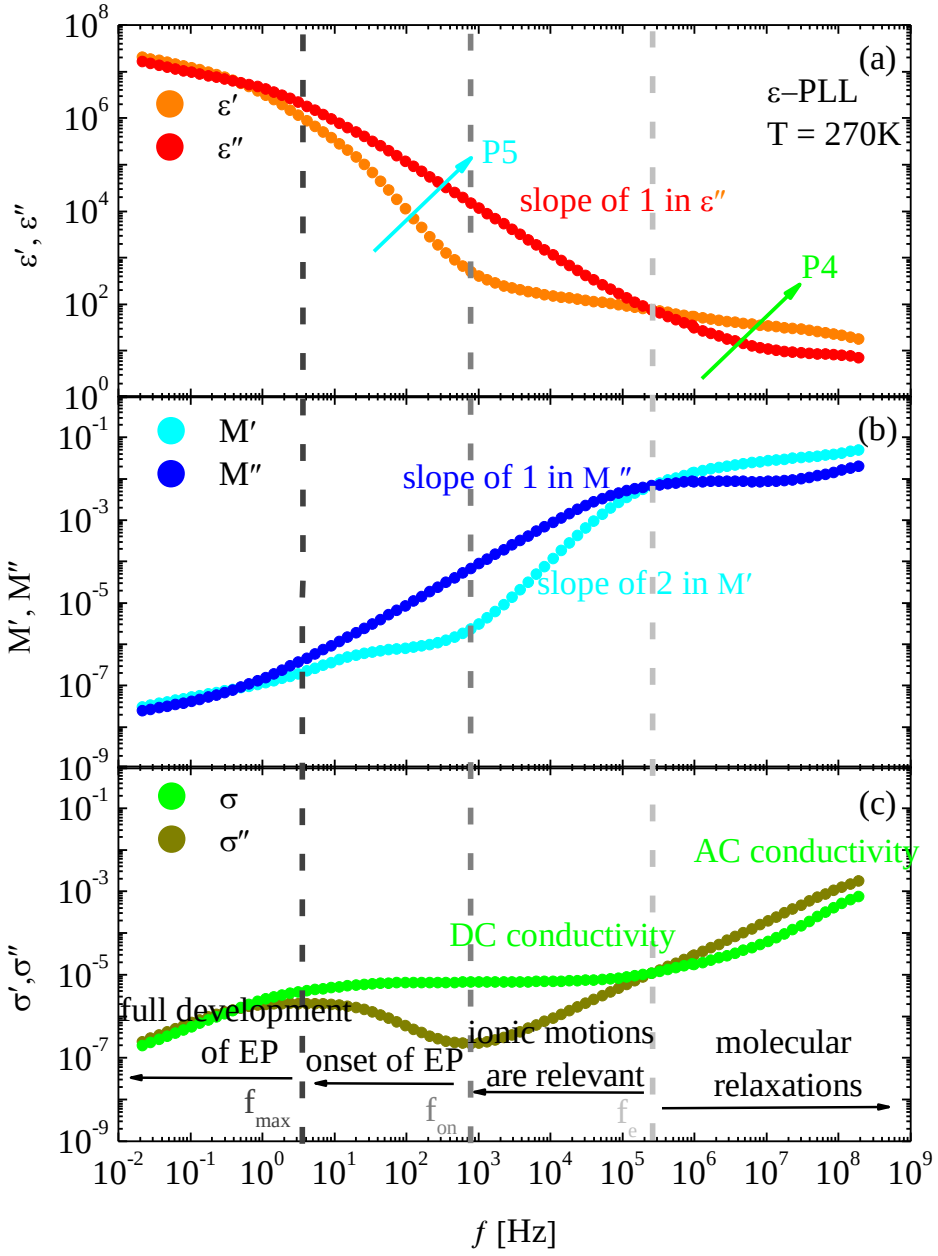

Figure V. 7. Composite plot of the dielectric permittivity (top), the electric modulus (middle), and the ionic conductivity (bottom) shifted to a temperature of 270 K for 60ε-PLL - 40H_2O_{pH10}. The vertical dashed lines mark the locations of the ionic and segmental relaxations, respectively.

Thus, according to the analysis above, the slowest processes, 5 to 7, are coupled to ionic conductivity and electrode polarization effects. On the other hand, some authors identify P5 in protein solution as the glass transition relaxation[8]. The temperature at which the structural α-relaxation time extrapolates to 100 s defines a temperature usually called the dielectric glass transition temperature, $T_{g,100s}$. For 3-lysine, τ_4 reaches 100 s at 192 K, whereas τ_5 reaches 100 s at

200 K. Considering the width of the glass transition (9 K, see Table V. 1), these values are both in good agreement with the calorimetric T_g (191 K), and both processes can therefore be related to the glass transition phenomenon. Nevertheless, in accordance to the previous analysis and the large dielectric amplitude values ($\Delta\varepsilon > 10^4$) of process 5, its identification as a glass transition-related process is not straightforward. Processes 6 and 7 were also detected in protein solutions and attributed to electrode polarization[9].

Processes 1 to 4

Now, we will focus on processes 1 to 4, which are related to the dynamics of the dipolar entities. Processes 1 to 3 observed in lysine oligomers, which are similar to the ones shown for ε-PLL solutions, are caused by dipole reorientations of water molecules. Nevertheless, it is important to note that the presence of more than one water-related process below T_g (well below the physiological regime) is not commonly observed in aqueous solutions[10,11] other than protein solutions[12-14].

The main characteristic of process 3 is that it follows an Arrhenius temperature dependence below the glass transition temperature, but at higher temperatures, a dynamic crossover appears, and it goes through a high-temperature Vogel – Fulcher – Tammann (VFT) dependence. Its physical origin is still not fully understood, and different interpretations of the α to β-relaxation crossover can be found in the literature. As explained in previous Chapter IV, from our perspective, the crossover is associated with the freezing of the mixture at T_g[15]. Above T_g, water reorientation (process 3) is coupled to the motions involved in the global α-like relaxation (process 4) process of the system. When the temperature is decreased toward T_g, however, the α-like relaxation process becomes frozen, and water molecules are trapped in a frozen matrix. Nevertheless, they still have significant mobility, and its dynamics can be described as a typical secondary β-process[15]. According to the previous interpretation for process 4 in ε-PLL aqueous solutions, process 4 for n = 3, 4 and 10 can also be related to reorientational motions of the oligomer molecules. In addition, the values of τ_4 extrapolated for all the oligomers to 100 s are in agreement with the calorimetric glass transition temperature.

Figure V. 8 a and b shows the temperature dependence of the relaxation strengths of processes 3 and 4 for the n = 3 and 10 oligomers, respectively. Above T_g, for both processes 3 and 4, $\Delta\varepsilon$ decreases with increasing temperature. In the case of polymers, these characteristics are strong indications that such relaxations are caused by cooperative motions, as is typical for the glass transition-related structural α-relaxation[16,17]. However, in this case, the cooperative character of process 4 comes from the cooperativity of the water relaxation (process 3). Therefore, process 4 should be denoted as collective rather than cooperative, although it is responsible for the observed glass transition. Concerning process 3, below T_g, $\Delta\varepsilon$ increases with increasing temperature, as is typical for local relaxations[16,17]. Thus, process 3 presents a transition from a collective α-like relaxation above the crossover temperature to a more local β-like relaxation below the crossover temperature, as also seen in the relaxation times temperature dependence.

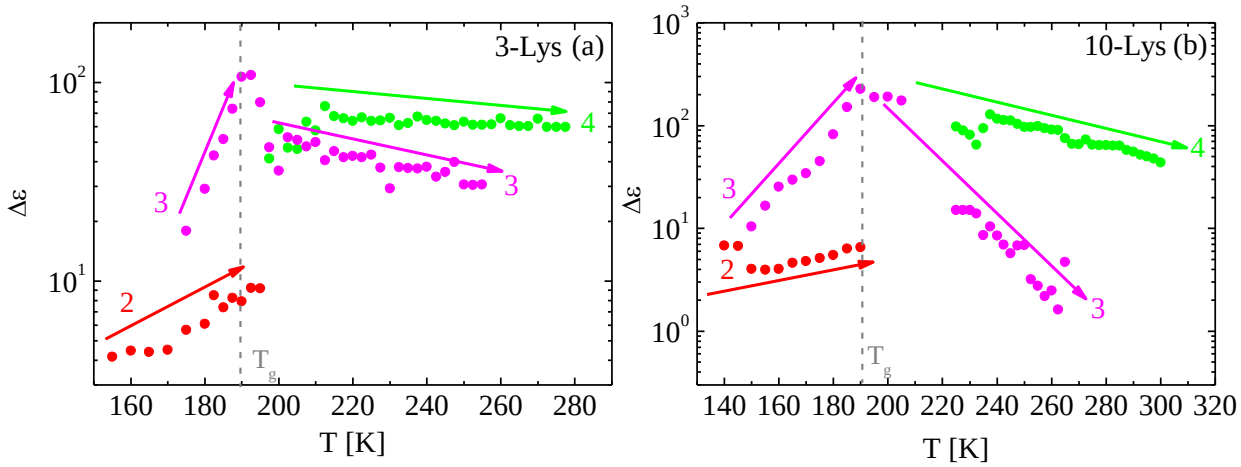

Figure V. 8. Temperature dependence of the relaxation strengths of processes 2, 3 and 4 for n = 3 (a) and 10 (b) lysine oligomers.

1.3.2. Discussion of temperature dependence of the relaxation times for processes 3 and 4

Figure V.9 a and b shows the chain-length dependences of the relaxation time of processes 3 and 4, respectively. The water relaxation (process 3) is almost unaffected by the chain-length, except for the ε-PLL solution at temperatures lower than 235 K. At this temperature, it becomes considerably slower than for the shorter oligomers. This observation further suggests that the water molecules in the solution of ε-PLL form larger and more bulk-like clusters than in the solutions of the shorter oligomers, probably because the relatively large β-sheets of ε-PLL cannot be mixed with the water molecules on a short length scale as the smaller n-lysine molecules.

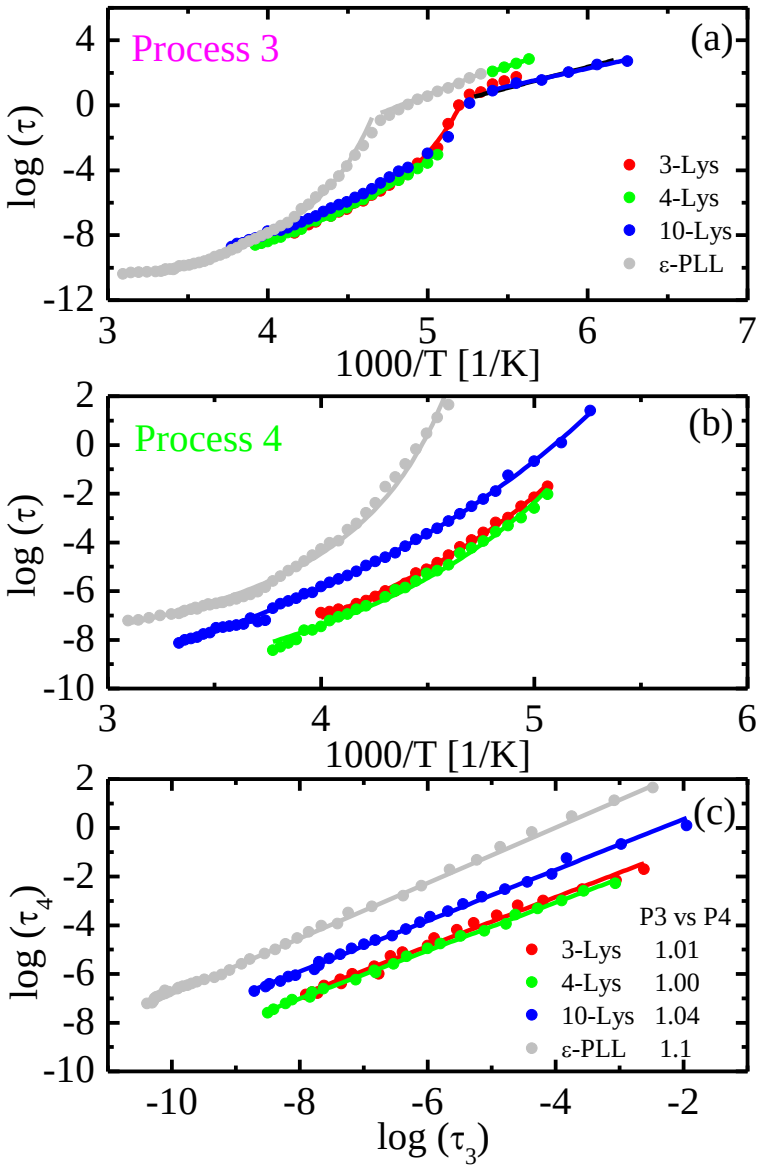

Figure V.9. (a) and (b) Temperature dependences of the relaxation time for processes 3 and 4, respectively. Solid lines through the data symbols represent VFT fits above T_g and Arrhenius fits below T_g (see text). (c) Relaxation times of process 4 as a function of the relaxation times for process 3. An almost perfect linear dependence, with a slope of one, is found for all the oligomers.

Since process 4 is slaved by process 3, it can be seen in Figure V.9 b that process 4 of the ε-PLL solution also slows down much more rapidly at low temperatures, compared to the same process in solutions of the shorter oligomers.

An anomalous molecular weight dependence is observed in the sample with 4 monomer units, where process 4 is faster than the rest of the oligomers. The assignment of process 4 to the

structural α-relaxation of the oligomers comes from the calorimetric glass transition temperature values presented in Table V. 1, where it is seen that T_g increases with increasing chain length, except for the 4-lysine sample, which is consistent with the corresponding dielectric relaxation process. Thus, it is evident that except for the n = 4 sample, the aqueous solutions of *n*-lysine follow the expected molecular weight dependence observed for other aqueous solutions (e.g., *n*-ethylene glycol oligomers[18]), where a clear correlation between the relaxation times and the molecular weight is observed. We have no explanation for the loss of the monotonous molecular weight dependence of T_g for 4-lysine solutions, but this anomalous molecular weight dependence is also observed in the dry n = 4 lysine oligomer.

Finally, Figure V.9 c shows how the relaxation times of processes 3 and 4 follow the very same non-Arrhenius temperature dependence, leading the concept of "slaving," which states that the solvent drives the protein motions[19]. This idea is further explained in the next section.

1.3.3. Comparison with proteins and slaving phenomena

A large difference between the *n*-lysine-water solutions studied here and previous protein solution studies is that *n*-lysine-water mixtures exhibit a narrow glass transition, (see Table V. 1, ΔT_g) in contrast to proteins, which display a glass transition that extends over a large temperature range (more than 70 K has been reported for myoglobin[12] and other proteins as lysozyme[20-22] and BSA[23,24]). The reason for this difference is that for proteins, the glass transition is due to the "freezing in" of a wide range of different types of relaxations (conformational fluctuations, electrostatic interactions, rotations of small side groups, motions of the full chain, and so on) that occur on very different time scales at a given temperature[12,25], whereas for the *n*-lysine-water systems, we expect a substantially reduced number of intra-molecular motions to be present because of the smaller size of the oligomers and their lower degree of structural complexity compared to proteins. In fact, as mentioned above, only one relaxation (process 4) is clearly due to molecular motions of *n*-lysine. The important role of water in this relaxation process, as further discussed below, is also supported by the fact that it is undetectable for low-hydration ε-polylysine powders (c_w = 5 wt%). This result implies that it is the water molecules that give rise to these *n*-lysine motions that freeze in at T_g and follow the same temperature dependence as

water dynamics but at different time scales. The same role of water (or solvent) has also been observed by N. Shinyashiki et al for hydrated bovine serum albumin[24] and by H. Jansson et al for myoglobin[14].

In view of our results, it is now interesting to elucidate the relationship between processes 3 and 4 in the same way as has previously been done for protein and solvent motions, where the important role of water in protein dynamics (and related biological activities) has been linked to the observation that structural protein fluctuations are determined or "slaved" by motions in the surrounding solvent[14,24,26-30]. This slaving means that the protein and solvent relaxations exhibit the same temperature dependence but occur on different time scales. Tests of the slaving model are shown in Figure V.9 c, where it can be seen that processes 3 and 4 exhibit almost identical temperature dependences. Thus, Figure V.9 c provides evidence that the observed structural relaxation of *n*-lysine (process 4) is slaved by the α-like water relaxation (process 3). This behavior has previously been observed only for proteins with a surrounding solvent[14,24,26-30] and not for other types of aqueous solutions[11,31]. This finding thereby shows that the solvent plays the same important role in the dynamics of oligomers of amino acids as in protein dynamics, and that the biological functions of amino acids are also crucially dependent on the surrounding water. For both types of systems, the solvent-slaved relaxations (α-relaxation) involve both conformational intra-chain fluctuations and inter-chain motions. Furthermore, since the small oligomers (3- and 4-lysine) lack the three-dimensional structure observed in folded proteins, it is evident that the slaving behavior is not directly dependent on the topology of the system.

2. CONCLUSIONS

For the solutions of *n*-lysine and water studied here, it is clear that the glass transition-related conformational fluctuations of the oligomers (process 4) exhibit the same temperature dependence as the α-like water relaxation (process 3), although the time scale of these fluctuations is considerably slower, as also observed for protein solutions. This case holds even if the timescale of the water dynamics (see Figure V.9 a) is affected by the structure of the solute molecules and the interactions between the two components.

The similar role of water found here in the dynamics of peptides may have important implications for both the general understanding of the role of water in biological systems and of how proteins work. In fact, our findings suggest that the observed slaving behavior is not limited to biological systems but can also be present in non-biological systems if their conformational motions can only occur due to motions in the surrounding solvent. This suggestion is studied in Chapter VI.

3. REFERENCES

1 Kong, J. & Yu, S. Fourier transform infrared spectroscopic analysis of protein secondary structures. *Acta Biochimica Et Biophysica Sinica* **39**, 549-559, doi:10.1111/j.1745-7270.2007.00320.x (2007).

2 Dong, A., Huang, P. & Caughey, W. S. Protein secondary structures in water from 2nd derivative Amide I infrared spectra *Biochemistry* **29**, 3303-3308, doi:10.1021/bi00465a022 (1990).

3 Wubbenhorst, M. & Van Turnhout, J. Analysis of complex dielectric spectra. I. One-dimensional derivative techniques and three-dimensional modelling. *Journal of Non-Crystalline Solids* **305**, 40-49, doi:10.1016/s0022-3093(02)01086-4 (2002).

4 Serghei, A., Tress, M., Sangoro, J. R. & Kremer, F. Electrode polarization and charge transport at solid interfaces. *Physical Review B* **80**, doi:10.1103/PhysRevB.80.184301 (2009).

5 Floudas, G. in *Polymer Science: A Comprehensive Reference* (ed Krzysztof MatyjaszewskiMartin Möller) 825-845 (Elsevier, 2012).

6 Ngai, K. L. & Rendell, R. W. Interpreting the real part of the dielectric permittivity contributed by mobile ions in ionically conducting materials. *Physical Review B* **61**, 9393-9398, doi:10.1103/PhysRevB.61.9393 (2000).

7 Samet, M. *et al.* Electrode polarization vs. Maxwell-Wagner-Sillars interfacial polarization in dielectric spectra of materials: Characteristic frequencies and scaling laws. *Journal of Chemical Physics* **142**, doi:10.1063/1.4919877 (2015).

8 Khodadadi, S. & Sokolov, A. P. Protein dynamics: from rattling in a cage to structural relaxation. *Soft matter* **11**, 4984-4998, doi:10.1039/c5sm00636h (2015).

9 Kundu, S. K. *et al.* Relaxation dynamics of liposomes in an aqueous solution. *Physical Chemistry Chemical Physics* **17**, 18449-18455, doi:10.1039/c5cp01334h (2015).

10 Swenson, J. & Cerveny, S. Dynamics of deeply supercooled interfacial water. *Journal of Physics-Condensed Matter* **27**, doi:10.1088/0953-8984/27/3/033102 (2015).

11 Cerveny, S., Alegria, A. & Colmenero, J. Universal features of water dynamics in solutions of hydrophilic polymers, biopolymers, and small glass-forming materials. *Physical review. E, Statistical, nonlinear, and soft matter physics* **77**, 031803, doi:10.1103/PhysRevE.77.031803 (2008).

12 Jansson, H. & Swenson, J. The protein glass transition as measured by dielectric spectroscopy and differential scanning calorimetry. *Biochimica et biophysica acta* **1804**, 20-26, doi:10.1016/j.bbapap.2009.06.026 (2010).

13 Panagopoulou, A., Kyritsis, A., Shinyashiki, N. & Pissis, P. Protein and water dynamics in bovine serum albumin-water mixtures over wide ranges of composition. *The journal of physical chemistry. B* **116**, 4593-4602, doi:10.1021/jp2105727 (2012).

14 Jansson, H., Bergman, R. & Swenson, J. Role of solvent for the dynamics and the glass transition of proteins. *The journal of physical chemistry. B* **115**, 4099-4109, doi:10.1021/jp1089867 (2011).

15 Cerveny, S., Mallamace, F., Swenson, J., Vogel, M. & Xu, L. M. Confined Water as Model of Supercooled Water. *Chemical Reviews* **116**, 7608-7625, doi:10.1021/acs.chemrev.5b00609 (2016).

16 Ngai, K. L. *Relaxation and Diffusion in Complex Systems (Partially Ordered Systems)*. (Springer, 2011).
17 Kremer, F. & Schönhals, A. *Broadband Dielectric Spectroscopy*. (Springer Berlin Heidelberg, 2003).
18 Capaccioli, S., Ngai, K. L. & Shinyashiki, N. The Johari-Goldstein beta-relaxation of water. *Journal of Physical Chemistry B* **111**, 8197-8209, doi:10.1021/jp071857m (2007).
19 Frauenfelder, H. *The Physics of Proteins: An Introduction to Biological Physics and Molecular Biophysics*. (Springer, 2010).
20 Khodadadi, S., Malkovskiy, A., Kisliuk, A. & Sokolov, A. P. A broad glass transition in hydrated proteins. *Biochimica et biophysica acta* **1804**, 15-19, doi:10.1016/j.bbapap.2009.05.006 (2010).
21 Miyazaki, Y., Matsuo, T. & Suga, H. Low-temperature heat capacity and glassy behavior of lysozyme crystal. *Journal of Physical Chemistry B* **104**, 8044-8052, doi:10.1021/jp0007686 (2000).
22 Panagopoulou, A. *et al.* Glass Transition and Dynamics in Lysozyme-Water Mixtures Over Wide Ranges of Composition. *Food Biophysics* **6**, 199-209, doi:10.1007/s11483-010-9201-0 (2011).
23 Panagopoulou, A., Kyritsis, A., Shinyashiki, N. & Pissis, P. Protein and Water Dynamics in Bovine Serum Albumin-Water Mixtures over Wide Ranges of Composition. *Journal of Physical Chemistry B* **116**, 4593-4602, doi:10.1021/jp2105727 (2012).
24 Shinyashiki, N. *et al.* Glass Transitions in Aqueous Solutions of Protein (Bovine Serum Albumin). *Journal of Physical Chemistry B* **113**, 14448-14456, doi:10.1021/jp905511w (2009).
25 Doster, W. The protein-solvent glass transition. *Biochimica Et Biophysica Acta-Proteins and Proteomics* **1804**, 3-14, doi:10.1016/j.bbapap.2009.06.019 (2010).
26 Fenimore, P. W., Frauenfelder, H., McMahon, B. H. & Young, R. D. Bulk-solvent and hydration-shell fluctuations, similar to alpha- and beta-fluctuations in glasses, control protein motions and functions. *Proceedings of the National Academy of Sciences of the United States of America* **101**, 14408-14413, doi:10.1073/pnas.0405573101 (2004).
27 Frauenfelder, H. *et al.* A unified model of protein dynamics. *Proceedings of the National Academy of Sciences of the United States of America* **106**, 5129-5134, doi:10.1073/pnas.0900336106 (2009).
28 Beece, D. *et al.* Solvent viscosity and protein dynamics. *Biochemistry* **19**, 5147-5157, doi:10.1021/bi00564a001 (1980).
29 Swenson, J., Jansson, H. & Bergman, R. Relaxation processes in supercooled confined water and implications for protein dynamics. *Physical review letters* **96**, 247802, doi:10.1103/PhysRevLett.96.247802 (2006).
30 Finkelstein, I. J., Massari, A. M. & Fayer, M. D. Viscosity-dependent protein dynamics. *Biophysical Journal* **92**, 3652-3662, doi:10.1529/biophysj.106.093708 (2007).
31 Cerveny, S., Colmenero, J. & Alegria, A. Dynamics of confined water in different environments. *European Physical Journal-Special Topics* **141**, 49-52, doi:10.1140/epjst/e2007-00015-1 (2007).

CHAPTER VI

WATER PLASTICIZATION VERSUS SLAVING PHENOMENA

In this chapter we analyze the occurrence of the slaving dynamics, typically observed in protein solutions, in non-biological solutions. In addition, we also investigated the phenomena of plasticization by water molecules on the glass transition of different aqueous solutions.

First, we review the typical dynamical behavior observed in the literature of aqueous solutions. In this case, we have used the results of tripropylene glycol (3PG) aqueous solutions and we have compared the dynamics with the results obtained for 3-lysine solutions in the previous chapter. To understand the dynamical differences among both systems, we have measured and compared the concentration dependence of the glass transition temperature of these aqueous solutions and other systems such as poly(vinyl pyrrolidone) (PVP), ε-polylysine and dextran as well as many other solutes taken from the literature (some synthetic polymers, polysaccharides and proteins). We find that the concentration dependence of T_g is different for the different solutions, and we concluded that the T_g dependence can be classified following three different types of behaviors. For the solutions with a strong T_g concentration dependence (PVP, 3-lysine, ε-polylysine and dextran) we find that at very low hydration levels, water acts as a plasticizer of the solute molecules. Nevertheless, increasing the water content, differences between these solutions and the typical aqueous solutions previously studied in the literature (e.g., 3PG) become apparent. Analyzing the dynamics of all these solutions, BDS results evidence the slaving behavior between the molecular motions of PVP, *n*-lysine or dextran and the water molecules at high hydration levels. In these cases, water does not act as a normal plasticizer (as it does in typical aqueous solutions) but it manages the solute motions as previously observed in protein solutions. As far as we are aware, this is the first time that the slaving dynamics has been observed in other solutions than proteins or peptides, and allow us to conclude that this phenomena is not only restricted to biological systems. Finally, the mutual influence of these solute

molecules (PVP, dextran and *n*-lysine oligomers) and their hydration water was also analyzed.

1. PLASTICIZATION

Plasticization, refers to a change in the thermal and mechanical properties of a given system which involves lowering of the viscosity in the case of polymer - solvent mixtures[1,2]. This occurs because the plasticizer reduces the inter- and intra-macromolecular interactions, facilitating segmental molecular motions and reducing the internal friction in the material[2]. The glass transition temperature is also decreased[2] approximately proportional to the plasticizer concentration in the polymeric material[1]. The plasticizing effect is usually described by the dependence of the glass transition temperature (T_g) on either the weight or volume fraction (C) of the solvent[2] $T_g = f(C)$, and the shift of the glass transition temperature is a measure of plasticizer efficiency[1].

In polymer - solvent mixtures, a good plasticizer has therefore to be miscible with the polymer. To achieve good compatibility, polar plasticizers must be used with polymers containing polar groups. The smaller the distance between the polar groups along the polymer chain, the higher must be the plasticizer polarity to overcome the forces between the polymer molecules. However, if the forces among the plasticizer molecules become stronger than the plasticizer polymer interactions, then no plasticization occurs[1]. Additionally, plasticizers must have a much lower viscosity and T_g than those of the polymer to be plasticized[2]. Water is a great plasticizer, and the key property for its plasticizing activity is its capability to strongly interact with other polar molecules via the hydrogen bonding[2]. One more contributory factor is its low T_g value[2].

There are two main groups of plasticizers; internal and external plasticizers. Internal plasticizers are actually a part of the polymer molecule. They are inherent parts of the polymer molecules and become part of the product, e.g., a second monomer copolymerized into the polymer structure[1,3]. External plasticizers are low volatile substances that are added to polymers. In this case, plasticizer molecules interact with polymer chains, but are not chemically attached to them by primary bonds and can, therefore, be lost by evaporation[1,3]. Furthermore, a distinction should be made between primary plasticizers and secondary plasticizers. With a crystalline or semi-crystalline polymer, there are some compounds which enter both the crystalline (ordered) and the amorphous (disordered) regions, called primary plasticizers. Nevertheless, other

compounds only penetrate in the amorphous regions and they are considered as secondary plasticizers or softeners[1].

1.1 Dynamics of triropylene glycol (3PG) water solutions. Water plasticization

We now discuss the plasticization phenomenon using as example the results of 3propylene glycol aqueous solutions[4]. Figure VI. 1 shows the dielectric loss of 3PG - water mixture with c_w = 50 wt%, at different temperatures where two relaxation processes (I and II) are observed. The temperature dependence of the relaxation times is shown in Figure VI. 2 (a) for this solution, and in Figure VI. 2 (b and c) the concentration dependence is shown for processes I and II, respectively.

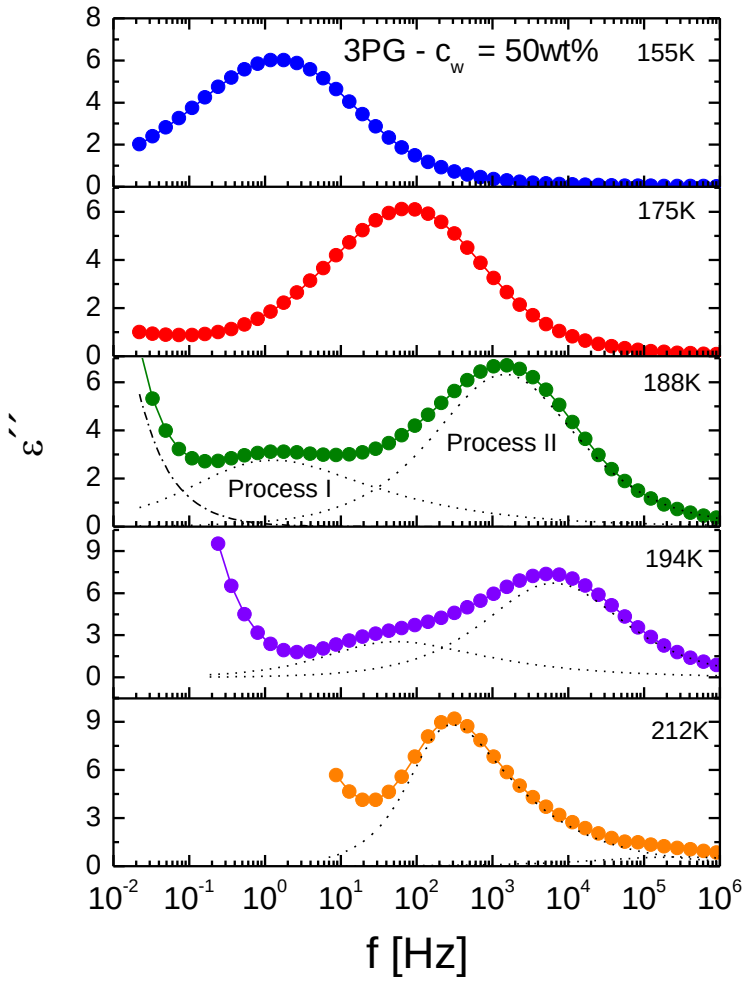

Figure VI. 1. Loss component of the complex dielectric permittivity of 3PG-water solution with c_w = 50 wt% at some temperatures[4]. At 188 K an example of the fitting procedure is shown. The solid line through the data points represents the total fitting.

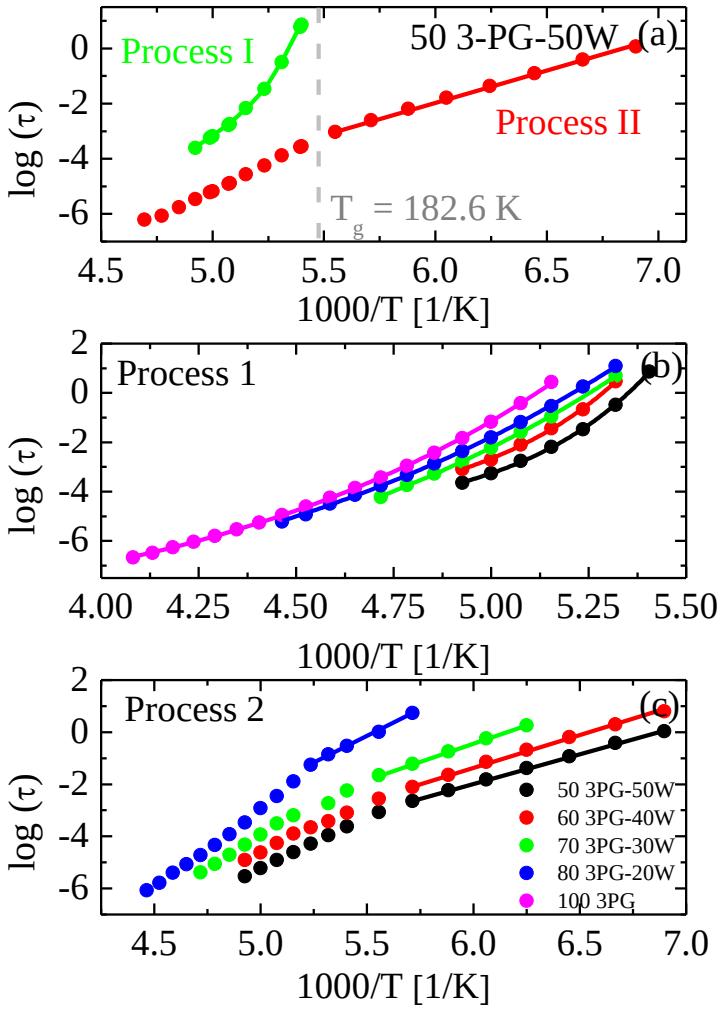

Figure VI. 2. Temperature dependence of relaxation times for 3PG at c_w = 50 wt% (a). Temperature dependence of relaxation times of process I (b) and process II (c) for various 3PG - water solutions. Fittings of VFT and Arrhenius functions to the data are shown with solid lines.

The slowest process I is related to the α-relaxation of the solution, whereas the faster process II is associated to the relaxation of water molecules in the solution[4]. The α-relaxation becomes faster when increasing water content, as usual for other water solutions (e.g., ethanol, ethylene glycol and glycerol aqueous solutions[5-7]) and the T_g value decreases with increasing the hydration level (see Figure VI. 3). This fact evidences that water facilitates the motion of 3PG, acting as a plasticizer; the bigger the c_w, the lower the T_g value. This behavior can be interpreted as simple plasticization of the solute due to the presence of water molecules which reduce the intermolecular interactions facilitating the segmental motions of the solute. We notice that the T_g value varies from 191 K in the dry system to 182.6 K for 3PG with c_w = 50 wt%. This represents 8 degrees of variation increasing 50 wt% of water.

The relaxation times for the faster process, process (II), show an Arrhenius behavior for temperatures lower than T_g, consistent with a local process. Nevertheless, at high temperatures, above the solution's T_g, the relaxation times change their temperature dependence deviating from the low temperature Arrhenius behavior (see Figure VI. 2 (b)). This behavior has been extensively discussed in the literature[8].

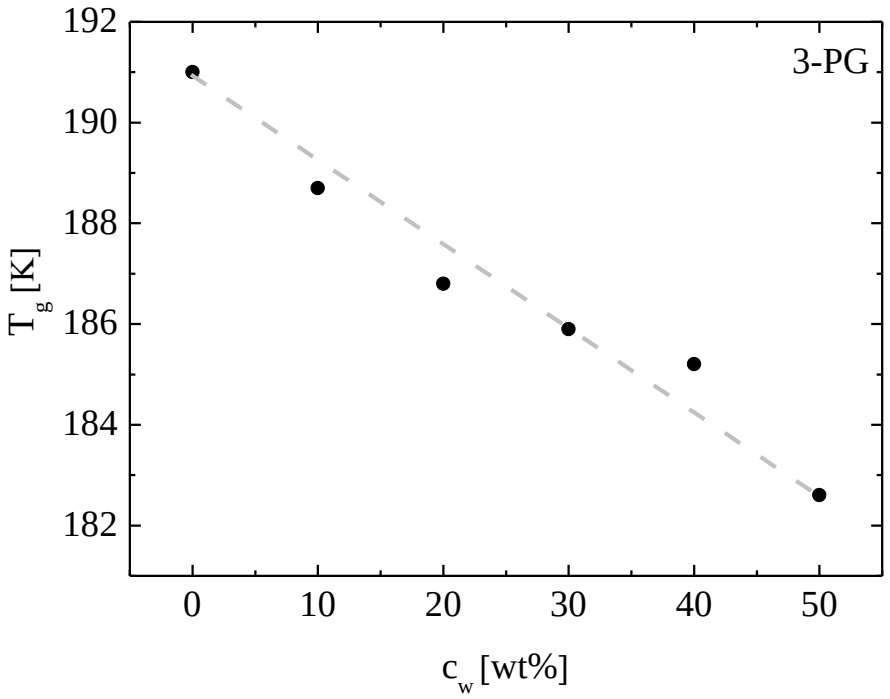

Figure VI. 3. Concentration dependence of the glass transition temperature of 3PG water mixtures.

1.2 Dynamics of 3-lysine versus 3PG aqueous solutions

Now we discuss the differences between the dynamics of 3PG and 3-lysine aqueous solutions. Figure VI. 4 shows the temperature dependence of the relaxation times for both systems at c_w = 40 wt%. 3PG water mixture shows two relaxation processes (I and II), whereas for 3-lysine aqueous solutions three main relaxations (2, 3 and 4) were observed as discussed in the Chapter V.

Process I in 3PG and process 4 in 3-lysine aqueous solutions are both related to the α-relaxation of the solutions since in both cases, the relaxation time at 100 s extrapolates to the calorimetric T_g. By contrast, considering the water relaxations, the main difference is the number of water processes we can observed by BDS. 3PG only shows one water related peak (process II), whereas in the case of 3-lysine two main water

relaxations are observed (processes 2 and 3). Therefore, the main difference between these two aqueous solutions is the presence a different number of relaxations related to water molecules. Another important difference is that the dynamics of both processes 3 and 4 observed in 3-lysine are coupled, whereas process I and II of 3PG are independent to each other.

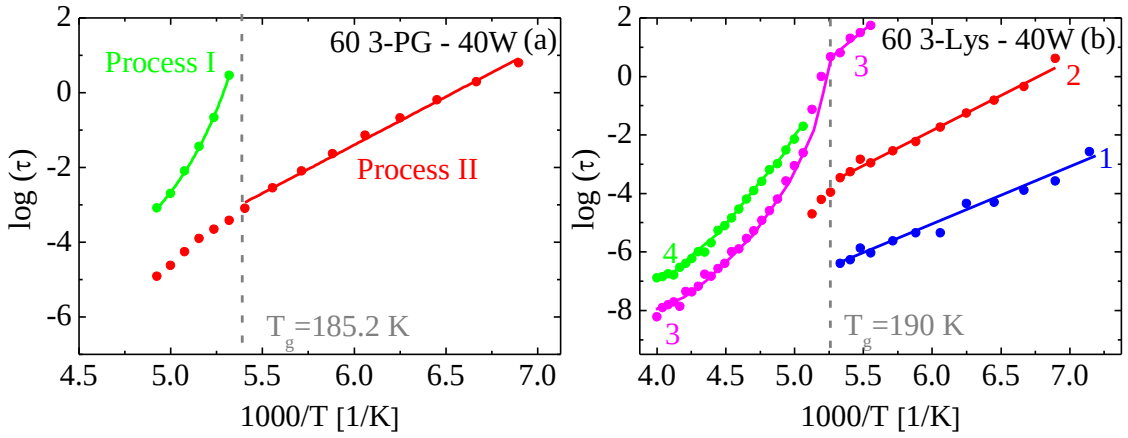

Figure VI. 4. Temperature dependence of relaxation times of 3PG and 3-lysine aqueous solutions at c_w = 40 wt%. Solid lines represent the fits of VFT and Arrhenius equations respectively.

We wonder why this difference is found when comparing these aqueous solutions. Therefore, we decided to compare and to revise the variation of T_g in a broad hydration range for many different aqueous solutions.

2. CALORIMETRIC RESULTS

2.1 Concentration dependence of the glass transition temperature of water solutions

As previously mentioned, the T_g of a material is reduced by the addition of low molecular weight miscible plasticizers. The low molecular size of a plasticizer allows it to occupy intermolecular spaces between polymer chains. These molecules change the three-dimensional molecular organization of polymers, reducing the energy required for molecular motion and promote the formation of hydrogen bonding between the chains. As a consequence, an increase in the free volume and, hence, in the molecular mobility is observed[3]. It has also been experimentally showed that when the T_g of the solvent is

much lower than that of the neat solute, the T_g of the solution decreases to a greater extent.

In this section we first analyze the concentration dependence of the calorimetric glass transition temperature for several systems analyzed in the literature as poly(vinyl methyl ether) (PVME)[9], *n*-propylene glycol (PG[10], 2PG[10] and 3PG[4] and PPG[11]), 5-ethylene glycol (5EG), some polysaccharides (fructose[12], glucose[13], sucrose[14] and trehalose[14]) and some proteins (BSA[15], elastine[16], collagen[16], gelatin[17], gluten[18], cellulose[16], gliadin[18], glutenin[18] and lysozyme[19]) aqueous solutions. These solutions have been chosen since no crystallization on cooling was observed and therefore the determination of T_g can be reliably done. In addition, we also prepared and measured new calorimetric data of solutions of poly(vinyl pyrrolidone), dextran, ε-PLL and 3-lysine studied in a very broad concentration range (see DSC curves in Appendix, see Figure A. 12 and Figure A. 13).

Figure VI. 5 shows the water concentration dependence of T_g for all these solutions. We observe that T_g decreases almost linearly with increasing hydration for PVME, *n*PG and 5EG aqueous solutions (see Figure VI. 5 (a)), while for polysaccharides the variation of the T_g loses its almost linear dependence due to the high T_g values at low hydration levels (see Figure VI. 5 b). Finally, we observe a stronger variation of T_g with concentration in the case of PVP, ε-PLL, 3-lysine and some polysaccharides as dextran and trehalose aqueous solutions (see Figure VI. 5 c). In the first case (for PVME, *n*PG and 5EG) by adding 50 wt% of water T_g decreases as much as 50 degrees (for PPG, 5EG and PVME the value goes down in 4 K, 13 K and 48 K, respectively), whereas for most of the polysaccharides, panel (b), T_g decreases as much as 190 degrees (ΔT_g = 95 K for fructose and ΔT_g = 190 K for trehalose water mixtures). Finally, in the last panel (c), we can observe a much stronger variation of T_g: ΔT_g = 223 K for PVP, ΔT_g = 169 K for ε-PLL and ΔT_g = 124 K for 3-lysine.

We also note that for protein solutions (see Figure VI. 6) the concentration dependence of T_g is more similar to that observed in Figure VI. 5 (b or c), although at high water contents the T_g dependence is more flat that in non-biological solutions. The T_g of pure and dry proteins (dashed region in Figure VI. 6) is unknown because the impossibility of preparing a glass (proteins cannot be melted without degradation)[20].

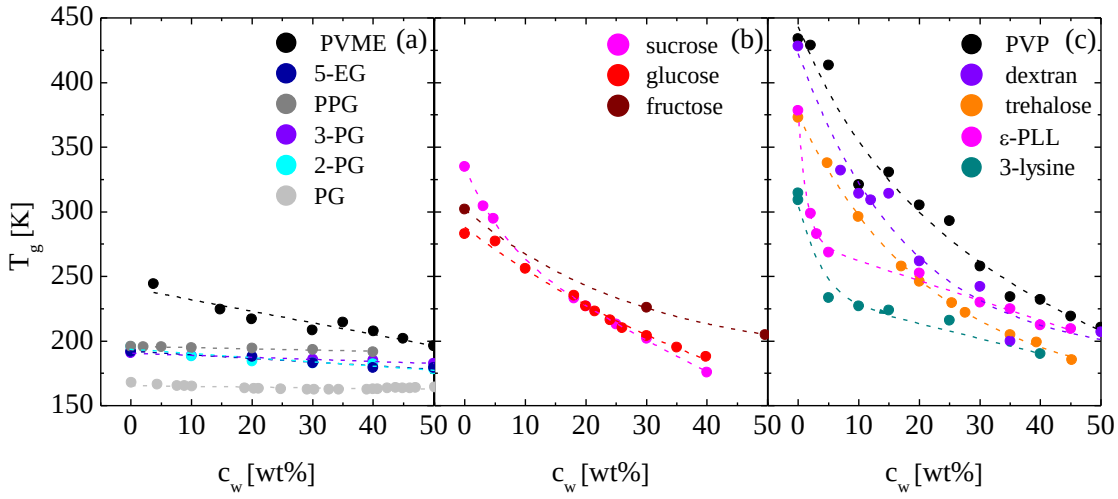

Figure VI. 5. Concentration dependence of T_g for PVME, 5EG, PPG, 3PG, 2PG and PG (a), sucrose, glucose and fructose (b) and PVP, dextran, trehalose, ε-PLL, and 3-lysine aqueous solutions (c). Dashed lines are given as guides to the eye.

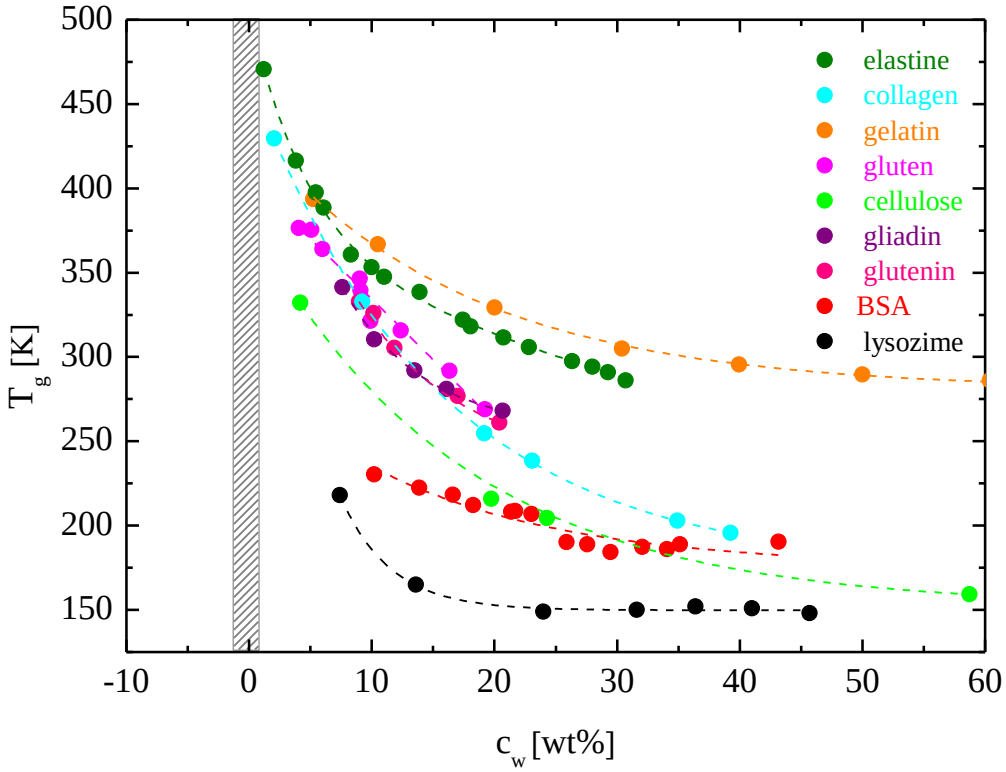

Figure VI. 6. Concentration dependence of T_g for elastin, collagen, gelatin, gluten, cellulose, gliadin, glutenin, BSA and lysozyme aqueous solutions. Dashed lines are given as guides to the eye. The dashed area represents the unknown area of T_g of dried proteins.

As previously mentioned, it is remarkable that the glass transition of hydrated proteins is exceptionally broad[21] (it covers a large temperature (range). However, this does not occur for PVP and *n*-lysine oligomers. Instead, the broadness of the T_g in PVP and *n*-

lysine oligomer solutions and in the dry state is almost the same covering a narrow temperature range.

Several attempts have been proposed to predict the concentration dependence of T_g of amorphous mixtures. One of the most used is the Fox equation[22,23];

$$\frac{1}{T_g} = \frac{x_1}{T_{g,1}} + \frac{1-x_1}{T_{g,2}} \quad \text{(VI. 1)}$$

where T_g represents the glass transition temperature of the mixture, $T_{g,1}$ and $T_{g,2}$ (in K) are the glass transition temperatures of the pure components with the lower and higher T_g, respectively, and x represents the mass fraction of the higher T_g component. Equation (VI. 1) is symmetric with respect to the components and it should be applied if the components have similar properties. Another possible description is the so-called Gordon and Taylor (GT) equation[22,23] normally used for miscible blends with relative weak intermolecular interactions. In this case, a parameter k was introduced to represent the unequal contributions of components in a mixture to the final T_g;

$$T_g = \frac{x_1 T_{g,1} + k(1-x_1) T_{g,2}}{x_1 + k(1-x_1)} \quad \text{(VI. 2)}$$

All these models (Fox or GT equations) assume that the free volume of a liquid can be added to that of the solute to obtain the free volume of a mixture and that the free volume of all the substances at T_g are equal.

For the solutions in Figure VI. 5 (a) the T_g concentration dependence can be described using the Fox equation, whereas for the rest of the materials the Gordon and Taylor equation should be used (with $k \sim 0.2$ and $T_{g,water} = 170$ K). Figure VI. 7 shows the obtained fittings for all the solutions in spite of the fact that the use of this equation can be controversial since, for instance, the T_g value of bulk water is unknown.

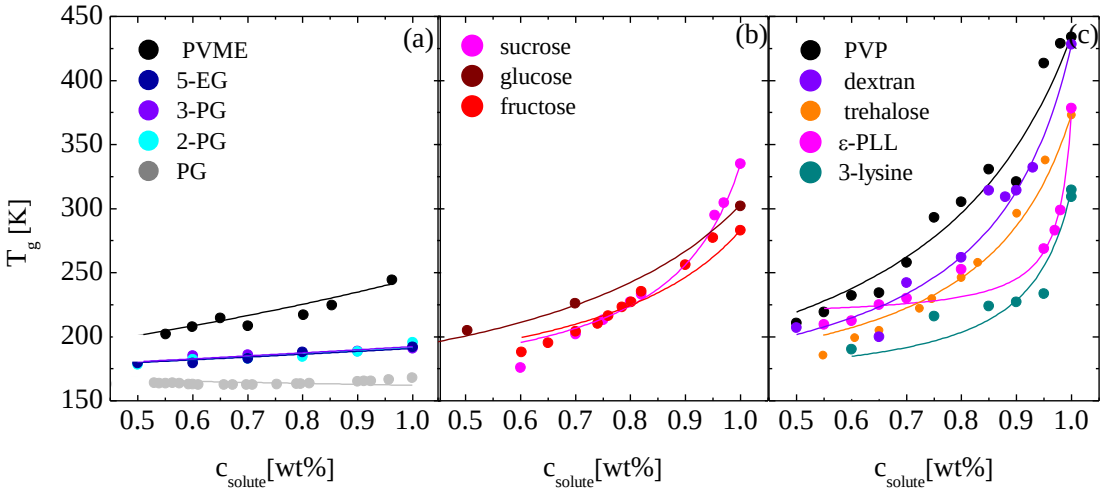

Figure VI. 7. T_g as a function of solute concentration for the systems analyzed in Figure VI.5. In (a) the data were fitted using the Fox equation and in (b and c) the Gordon and Taylor equation was used.

It is clear that for all these solutions, the water molecules directly interact with the different hydrophilic groups in the solute (for instance -OH, CO-, COOH, etc.) by forming hydrogen bonds. In addition, the presence of water molecules increases the available free volume of the solute molecules removing barriers and increasing the chain mobility in comparison to the dry state. However, this effect is much stronger for PVP, dextran or ε-PLL than for PVME or 3PG, and we think that the observed T_g variation (~200 K) cannot be explained as the simple raise of the free volume available. On the other hand, we wonder whether these solutions, with a strong T_g variation, have a different structure or if there is some phase separation between the water and the solute and this could be the cause of this strong T_g variation. However, as previously discussed in Chapter IV for ε-polylysine, we showed that no phase separation was found for these materials. In addition, although ε-PLL in solution has a specific conformation (β-sheet[24]), this is not the case for polysaccharides, 3-lysine or PVP. Therefore, the observed T_g variation cannot be due to a specific conformation of the solute in aqueous solutions. A formation of a water cluster could be the reason for this difference in the T_g behavior. However, we do not know how big the water cluster formed in both types of systems is, i.e., we have no evidence whether water molecules form larger and more bulk-like clusters for solutions of Figure VI. 5 (c) than in solutions of Figure VI. 5 (a).

As discussed in the section 1.2, the dynamical behavior is also different for 3PG solutions compared to *n*-lysine solutions. Therefore, in the following we analyze the dynamical behavior of these solutions with this strong T_g variation. In particular, we

have revised and re-measured the dynamics of PVP, some polysaccharides (dextran and sucrose) and *n*-lysine oligomers at different hydration levels. First, we present the data of the calorimetric results and then, BDS results are shown and discussed.

2.2 Calorimetric results of PVP, 3-lysine and ε-PLL in a broad concentration range

Figure VI. 8 and Table VI. 1 show T_g values of PVP-water mixtures for different hydration levels. In the Appendix (Figure A. 12), the heat flow as a function of the temperature for some water contents analyzed is shown.

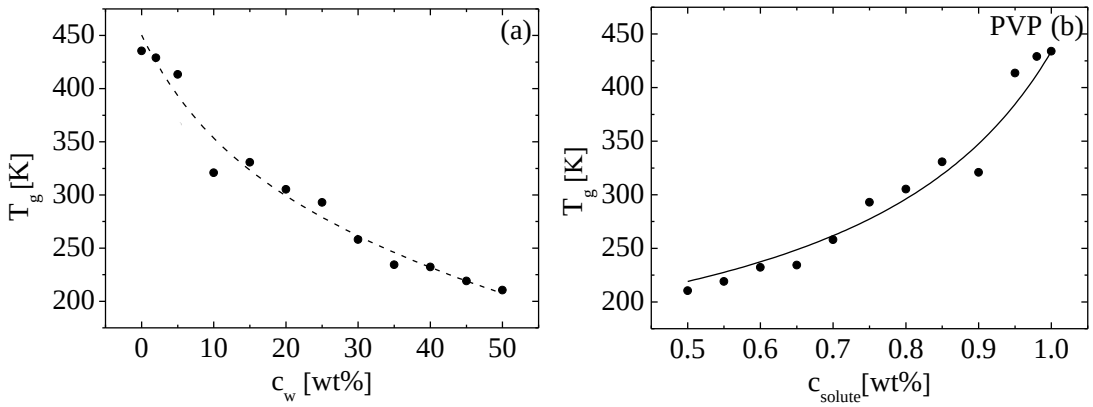

Figure VI. 8. (a) Water concentration dependence of the T_g for PVP. Dashed lines are given as guides to the eye. (b) T_g as a function of solute concentration. Data fitting to the Gordon and Taylor equation is also included.

Table VI. 1. Samples of PVP (M_w = 55,000 g/mol) water mixtures, where c_{solute} and c_w are the PVP and the water content, respectively, and $T_{g,DSC}$ represents the calorimetric glass transition temperature.

Sample	c_{solute} [wt%]	c_w [wt%]	$T_{g,DSC}$ [K]
50PVP – 50W	50	50	210.4
55PVP – 45W	55	45	219.1
60PVP – 40W	60	40	232.2
65PVP – 35W	65	35	234.3
70PVP – 30W	70	30	257.9
75PVP – 25W	75	25	292.9
80PVP – 20W	80	20	305.2
85PVP – 15W	85	15	330.6
90PVP – 10W	90	10	320.8
95PVP – 5W	95	5	413.5
98PVP – 2W	98	2	429.0
100PVP	100	0	433.9

Following the results in Table VI.1 we observed that increasing the hydration level only in 10 wt%, T_g strongly decreases (almost 115 degrees). With a further increase of the water content, T_g still decreases even more (e.g., from c_w = 10 wt% to 50 wt%, T_g

decreases 110 degrees). Therefore for PVP, adding 50 wt% of water, T_g decreases around 225 degrees.

The same huge T_g variation as here described for PVP is observed in 3-lysine and ε-PLL solutions studied in broad water concentration range (see calorimetric data in the Appendix, Figure A. 13). Figure VI. 9 and Table VI. 2 show the glass transition temperature values for both systems. The monotonous T_g dependence with the hydration level is broken in both cases at around c_w = 5 wt%.

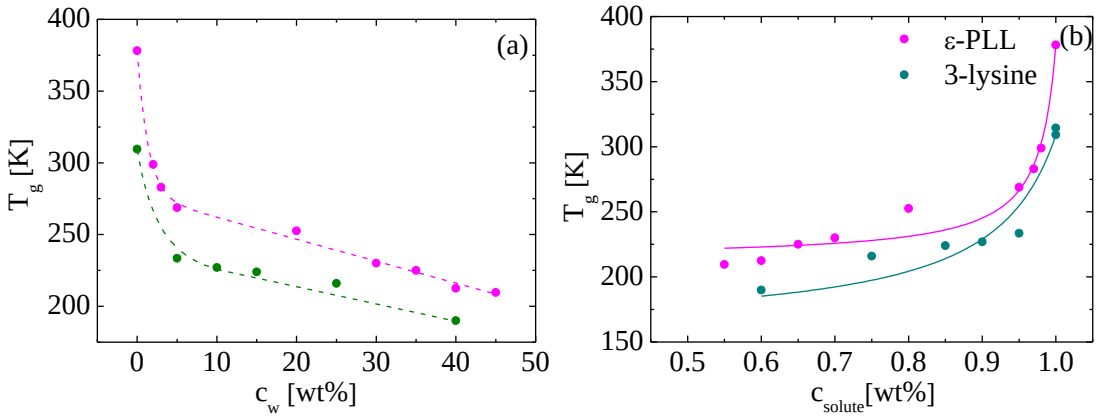

Figure VI. 9. (a) Glass transition temperature values in function of the water content for 3-lysine and ε-PLL. Dashed lines are given as guides to the eye. (b) T_g as a function of solute concentration. Data fitting to the Gordon and Taylor equation is also included.

Table VI. 2. Samples of 3-lysine (M_w = 402.5 g/mol) and ε-PLL (M_w = 4700 g/mol) aqueous solutions, where c_w represent the water content and $T_{g,DSC}$ the calorimetric glass transition temperature.

Sample	c_{solute} [wt%]	c_w [wt%]	$T_{g,DSC}$ [K]
60 3-lys - 40W	60	40	190.0
75 3-lys -25W	75	25	215.9
85 3-lys - 15W	85	15	224.0
90 3-lys -10W	90	10	227.0
95 3-lys - 5W	95	5	233.5
100 3-lys	100	0	309.2
55 ε-PLL – 45W	55	45	209.6
60 ε-PLL – 40W	60	40	212.5
65 ε-PLL – 35W	65	35	225.0
70 ε-PLL – 30W	70	30	230.0
80 ε-PLL – 20W	80	20	252.5
95 ε-PLL – 5W	95	5	268.7
97 ε-PLL – 3W	97	3	282.9
98 ε-PLL – 2W	98	2	298.9
100 ε-PLL	100	0	378.1

As previously analyzed, the glass transition of PVP, 3-lysine and ε-PLL solutions studied from the dry state to c_w = 50 wt% show an extremely T_g variation with the water concentration dependence compared to other aqueous solutions of synthetic polymers such as PVME[9] or 3PG[4]. This strong variation and anomalous concentration dependence of T_g was also observed in other types of materials as polystyrene (PS) in solution with toluene[25]. This system also showed two descending curves which come together in a cusp.

3. DYNAMICS OF SOLUTIONS WITH A BROAD T_G CONCENTRATION DEPENDENCE

3.1 Dynamics of 3-lysine aqueous solutions

At the light of these results, we first analyze the dynamics of 3-lysine at different hydration levels from the dry state to c_w = 40 wt%. The dynamics was studied by means of BDS using the methodology explained in Chapter IV. Both the real (ε') and imaginary (ε'') components of the complex permittivity were simultaneously fitted using the superposition of symmetric Cole-Cole functions plus an extra term for the conductivity (see Equation IV. I in Chapter IV).

We have studied the following water concentrations: 0, < 1, 10, 15 and 40 wt% to analyze the α-relaxation of 3-lysine in aqueous solutions. Figure VI. 10 (a - c) shows the relaxation times and shape factors corresponding to the α-relaxation. At very low hydration levels (< 1 wt%), the α-relaxation of the solution is similar to that of the dry 3-lysine. The relaxation times become slightly faster in agreement with the change of T_g, the relaxation strength is a little bit lower but the relaxation become narrow. This sample (< 1 wt%) has ~0.07 water molecules per 3-lysine molecule and this behavior can be explained as plasticization of the 3-lysine molecules by water. However, when we analyzed a sample with c_w = 10 wt% (~0.8 water molecules per 3-lysine molecule), we find that the α-relaxation becomes strongly faster (almost 6 decades), the intensity increases (in spite of the fact that the quantity of 3-lysine is lower than in previous sample) and the relaxation is even narrower. Increasing the water content to 15 wt%, we

find two relaxations instead of only one: the slower one extrapolates at 100 s to the calorimetric T_g and the faster one can be related to the relaxation of water molecules (in agreement with that discussed in Chapter V). At this hydration level the sample has 1.3 water molecules per 3-lysine molecule. This behavior is even more clear increasing the water content to 40 wt% (5 water molecules per 3-lysine molecule). As discussed in the previous chapter, at this water content two relaxations (processes 3 and 4) are observed and both dynamics are strongly coupled to each other (i.e., the slaving behavior).

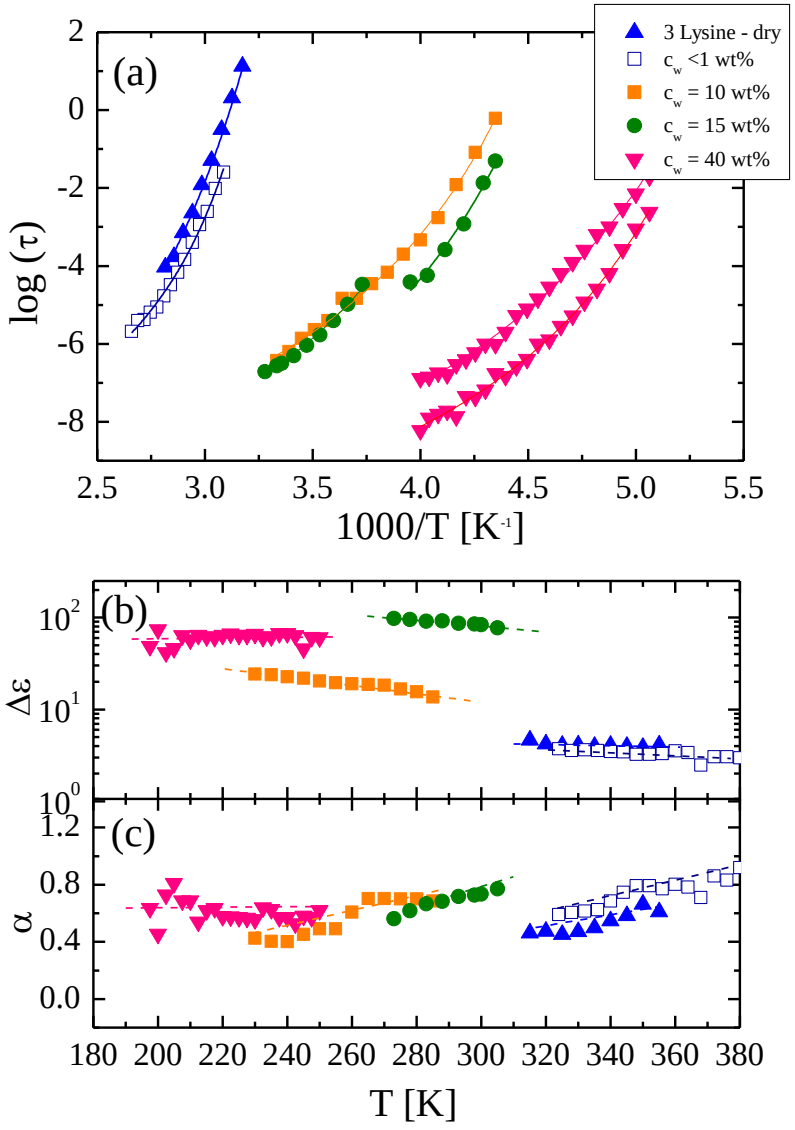

Figure VI. 10. Temperature dependence of relaxation times of 3-lysine aqueous solutions at different hydration levels (a). Dielectric strength and α parameter of the α-relaxation in function of the temperature (b) and (c), respectively.

The phenomenological behavior showed here for 3-lysine is also observed for other materials shown in Figure VI. 5 c (see PVP and ε-PLL results in the Appendix, Figure

A. 14 and Figure A. 15) when studied at different hydration levels from the most diluted solutions to the non-hydrated samples. Therefore, from these results we can conclude that increasing the water content, the dynamics corresponding to the solute molecules undergoes profound changes due to the interaction with water molecules which cannot be explained as simple plasticization as previously showed for 3PG.

In the following we will compare the dynamics of other systems in Figure VI. 5 (b and c) at c_w = 40 wt%.

3.2 The slaving behavior observed in PVP, *n*-lysine, sucrose and dextran at c_w = 40 wt%

The temperature dependence of the main relaxation times (processes 2, 3 and 4) for the PVP aqueous solution, 3-lysine and ε-PLL are shown in Figure VI. 11. Figure A. 16 in Appendix shows PVP aqueous solution results from isochronal measurements and the derivative analysis corroborating the presence of processes 2 to 4. Based on the previous dynamical studies on *n*-lysine oligomers, process 2 and 3 in PVP solutions can be related with the water molecules reorientation, while the origin of process 4 is correlated with the calorimetric glass transition. Table VI. 3 shows the Arrhenius and VFT parameters used to fit the data in Figure VI. 11.

Table VI. 3. Activation energies (E_a) and pre-exponential factors ($log\ (\tau_0)$) from the Arrhenius equation below T_g and VFT parameters ($log\ (\tau) = log\ (\tau_0)\ exp\ (DT_0/(T-T_0))$ for processes 3 and 4 above T_g.

Sample	Process 2		Process 3 (below T_g)	
	$log(\tau_0)$	E_a [eV]	$log(\tau_0)$	E_a [eV]
60PVP-40W	-18.8	0.5	-17.4	0.7
60ε-PLL-40W	-17.9	0.5	-21.2	0.9
60 3lys-40W	-15.7	0.5	-19.8	0.8

Sample	Process 3 (above T_g)			Process 4		
	D	T_0 [K]	$log(\tau_0)$	D	T_0 [K]	$log(\tau_0)$
60PVP-40W	8.9	178.7	-15.5	8.9	179.5	-10.9
60ε-PLL-40W	3.4	191.2	-12.6	3.4	195.6	-9.8
60 3lys-40W	7.9	149.0	-13.2	7.9	149.0	-12.1

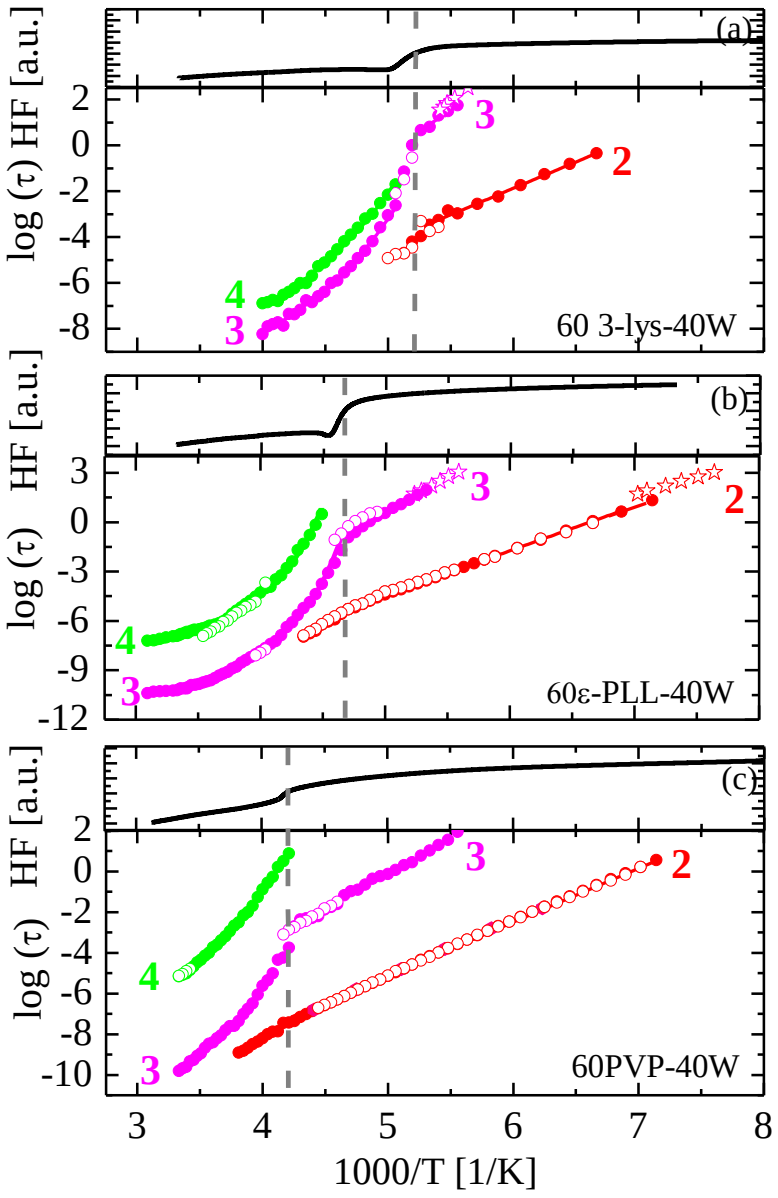

Figure VI. 11. Temperature dependence of relaxation times for 3-lysine (a), ε-PLL (b) and PVP (c) at c_w = 40 wt%. Open stars-shaped points represent TSDC experiments results and open circle points the logarithmic derivative results. Solid lines are fits of the VFT and Arrhenius equations.

The relaxation maps corresponding to the different solutions have strong similarities. Process 2 has the same activation energy and time scale for all the solutions, process 3 shows a crossover at T_g and process 4 can be related with the calorimetric T_g. Moreover, the relaxation times of processes 3 and 4 follow the very same non-Arrhenius temperature dependence for all the materials. It seems that there is a relationship between the observation of two relaxations strongly coupled and the strong concentration dependence of T_g showed in Figure VI.5 c. We wonder whether this is also the case of materials in Figure VI. 5 (b) (polysaccharides) and therefore, we have

also analyzed the dynamics of sucrose and dextran at the highest water content before water crystallization. The results are showed in Figure VI. 12 (a) for sucrose at c_w = 30 wt% and Figure VI. 12 (b) for dextran at c_w = 35 wt%. Temperature and frequency dependence of the components of the complex dielectric permittivity and the analysis of the derivative of the real part of the dielectric permittivity for sucrose and dextran aqueous solutions are shown in Figure A. 17 and Figure A. 18 in the Appendix, respectively. As in the case of PVP, 3-lysine and ε-PLL, we find two relaxations due to water molecules (processes 2 and 3).

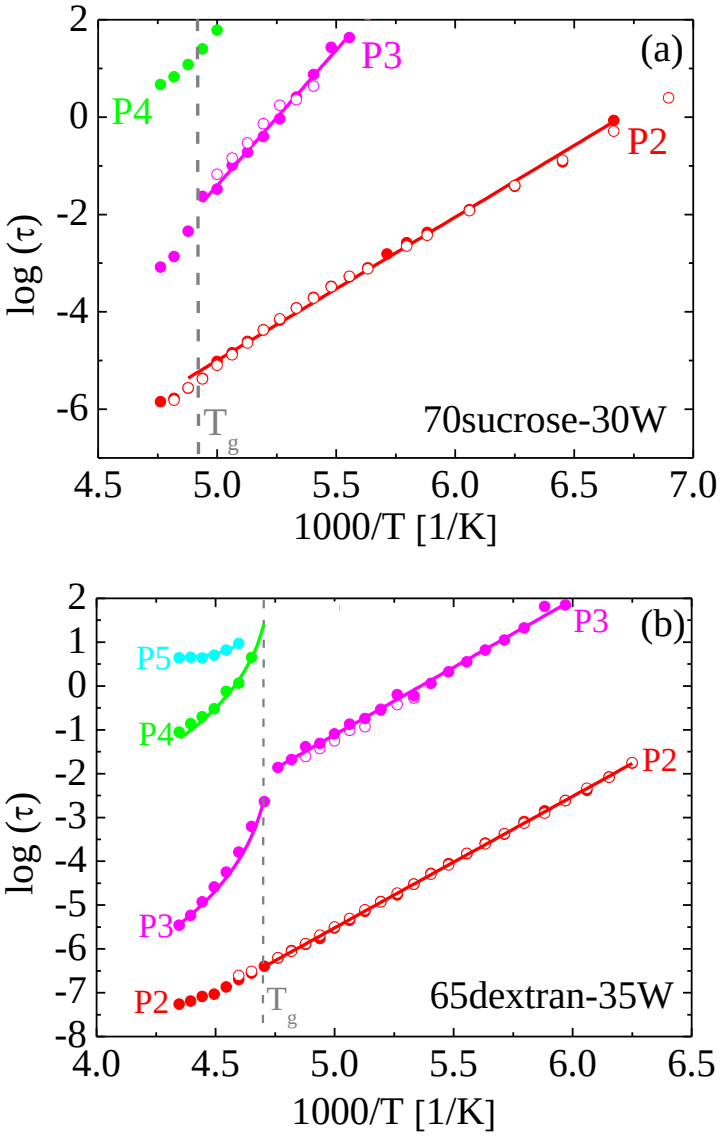

Figure VI. 12 Temperature dependence of relaxation times for sucrose at c_w = 30 wt% (a) and dextran (b) at c_w = 35 wt%. As usual, open circle points represent the logarithmic derivative results, solid lines are fits of the VFT and Arrhenius equations and vertical dashed lines indicate $T_{g,DSC}$.

We should mention that the dielectric behavior of solutions of PVP[26] and sucrose[27] were previously analyzed in the literature, and in those cases the here called process 3 was not observed. This is mainly because here we previously deionized the samples using a resin for the removal of ionic species from the solution. This procedure was carried out by the batch method as explained in Chapter III, and in this way, conductivity and electrode polarization effects can be reduced. In addition, we have fitted both ε´ and ε´´ instead of only ε´´ as usual in the literature.

4. DISCUSSION

H. Frauenfelder et al[28] proposed that the solvent "slaves" the protein, in the sense that not only the dynamics but also the protein activity follow the solvent dynamics. This view was supported by different simulations and experiments which showed a strong coupling between protein and solvent dynamics[29-31]. These results led to the idea that the solvent dynamics controls the dynamics of the biological macromolecule although the mechanism of this coupling remains the subject of discussion. For instance, M. Tarek and D. J. Tobias[32] using simulations of the globular protein Ribonuclease A (Rnase-A) showed that the structural relaxation of the protein requires relaxation of the hydrogen bond network. S. Khodadadi et al[33], by experimentally studying the dynamics of different biomolecules in similar environments, analyzed the influence of the biological molecules on the dynamics of the surrounding solvent. They conclude that the dynamics of the biomolecules is not simply slaved by the dynamics of the hydration water. This idea is based on the fact that the timescale of water dynamics is different in different biomolecules (DNA, lysozyme and tRNA). They also argue that the chemical and three-dimensional structures of the biomolecules play an important role. Moreover, according to the authors, the biomolecule affects the dynamics of the hydration water and therefore the concept of slaving dynamics should be reconsidered[33].

Figure VI.13a shows the relaxation time of process 3 in three different environments (PVP, ε-PLL and 3-lysine at the same hydration level, c_w = 40 wt%). Clearly, the timescale of water is different for the different environment's and therefore, we can observe that water dynamics is also affected by the solute presence as Khodadadi et al

also analyze for DNA, lysozyme and tRNA[33]. However, at low temperatures (below T_g) where the dynamical movements of the solute are frozen, we can observe that water dynamics is very similar for these three different systems. Moreover, the dynamics of process 2 (see Figure VI. 13 b) is almost the same for all the different environments. This strongly indicates that this dynamics corresponds to a local process of water molecules. The same behavior is observed for sucrose and dextran in Figure VI. 13 (c and d) although at a slightly different water contents (c_w = 30 wt% for sucrose and c_w = 35 wt% for dextran). From these results we can conclude that the solute affects the dynamics of water (process 3) but not the dynamics of the local process 2.

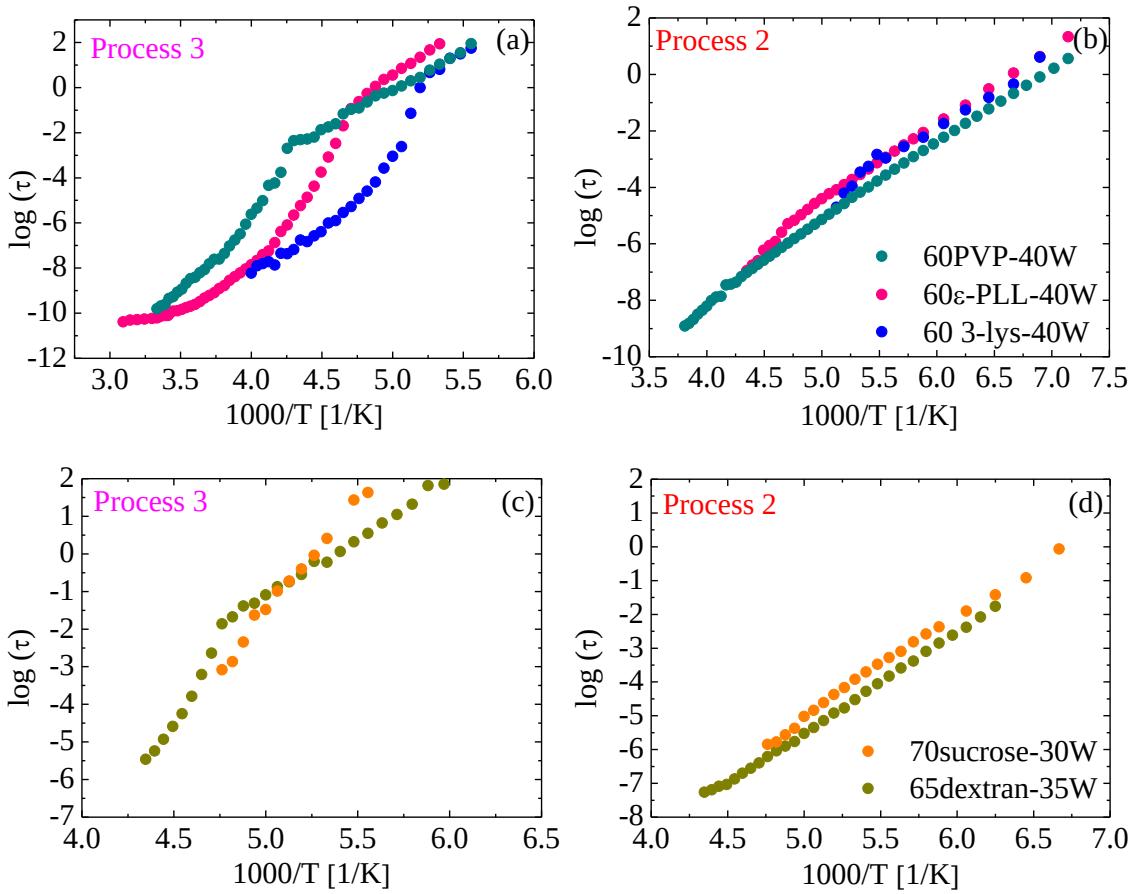

Figure VI. 13. (a and b) Relaxation time of processes 2 and 3 (water moelcules) of ε-PLL, PVP and 3-lysine in a solution with c_w = 40 wt%. (c and d) the same as in (a and b) for sucrose c_w = 30wt% and dextran c_w = 35wt%.

Now we analyze the relationship between processes 3 and 4 in the same way as has been done previously for *n*-lysine in the Chapter V. The slaving model is showed in Figure VI. 14, where it, indeed, can be seen that processes 3 and 4 exhibit almost identical temperature dependences. Thus, these results provide evidence that the observed structural relaxation of PVP and dextran is also slaved by the α-like water

relaxation as previously showed for *n*-lysine oligomers. This phenomenon cannot be seen for sucrose aqueous solution since there are a very limited data above T_g due to water crystallization.

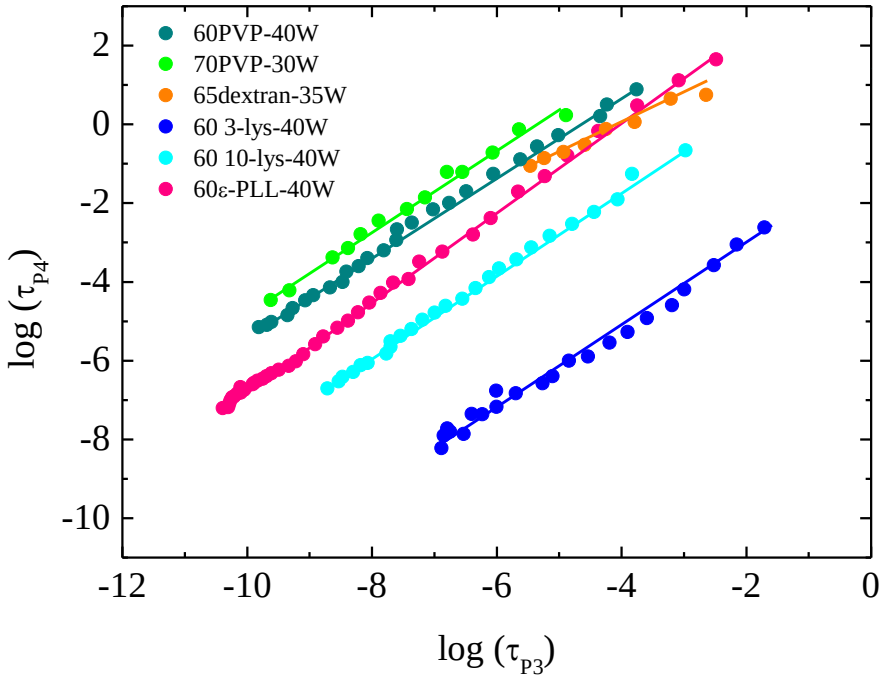

Figure VI. 14. Relaxation time of process 3 versus relaxation time of process 4 of ε -PLL and 3-lysine in a solution with c_w = 40 wt%, PVP in a solution with c_w = 30 and 40 wt%, and dextran in a solution with c_w = 35 wt%.

On the other hand, it was also suggested that the three-dimensional structure of folded proteins plays an important role in the slaving picture[33]. However, here we show that the structure cannot be related with the observation of the slaving behavior because PVP, 3-lysine or dextran has not structure in the sense as the biomolecules have, but the slaving behavior is still observed.

Now we discuss the results in Figure VI. 10a where the temperature dependence of relaxation times of 3-lysine aqueous solutions at different hydration levels are shown. As previously mentioned, to observe the two coupled dynamics it is necessary at least a minimum water content in the solutions. For 3-lysine at c_w = 10 wt% we still observe only a single relaxation (process 4) but at c_w = 15 wt% we can observe the two slaved dynamics. For ε-PLL this water content is also around c_w = 10 wt%. These results indicate that a minimum water cluster is necessary to observe the two coupled dynamics.

From all these results, we can conclude that the slaving phenomenon is not unique of protein solutions. We have observed it in a synthetic polymer (PVP), in a polysaccharide (dextran), and finally in several lysine oligomers. They all have the same dynamical behavior as proteins have, evidencing a slaving behavior between the solute molecules and the water molecules motions. In terms of *n*-lysine oligomers, this similarity with the protein dynamics could be more understandable since the solute in both cases is composed of amino acids. However, we wonder why the slaving behavior is observed for instance in PVP but not in PVME or 3PG solutions, being all of them synthetic polymers. Concerning to the hydrogen interactions, in the case of the PVP, water molecules interact with the amide group of the solute (N-C=O), while for PVME and 3PG, interactions are through the alcohol (-OH) and the ether (-O-) groups, respectively. Thus, due to the heterogeneity concerning to the solute groups that interact with the water molecules, we cannot relate this interaction with the presence or absence of the slaving phenomenon. Moreover, PVP, PVME and 3PG systems, have no specific conformation as ε-PLL (β-sheet) does. Thus, the differences among them cannot be related with structural differences. Another possible explanation could be that in solutions of 3PG the α-like water relaxation (process 3) is masked by the α-relaxation of the solution. To study this alternative we analyzed the temperature dependence of the relaxation strength of the α-relaxation of 3PG-water solutions[4] at different water contents (see Figure VI. 15). According to this plot, if process I would include the α-like water relaxation (process3), then $\Delta\varepsilon$ value should increase with the hydration level among the different solutions. However, as evident from Figure VI. 15, this does not happen. Therefore, we can conclude that process I is not a combination of both processes, and thus, the α-like water relaxation (process 3) does not occur in 3PG aqueous solutions. Instead, we believe that the very high glass transition temperature in materials as PVP, *n*-lysine oligomers and dextran is the most important variable to observe the slaving behavior. The motions of water promote and facilitate the motions of the solute at low temperatures. In addition, we believe that some special cluster of water is necessary to observe the α-like water relaxation (process 3). These conditions are also required in protein solutions.

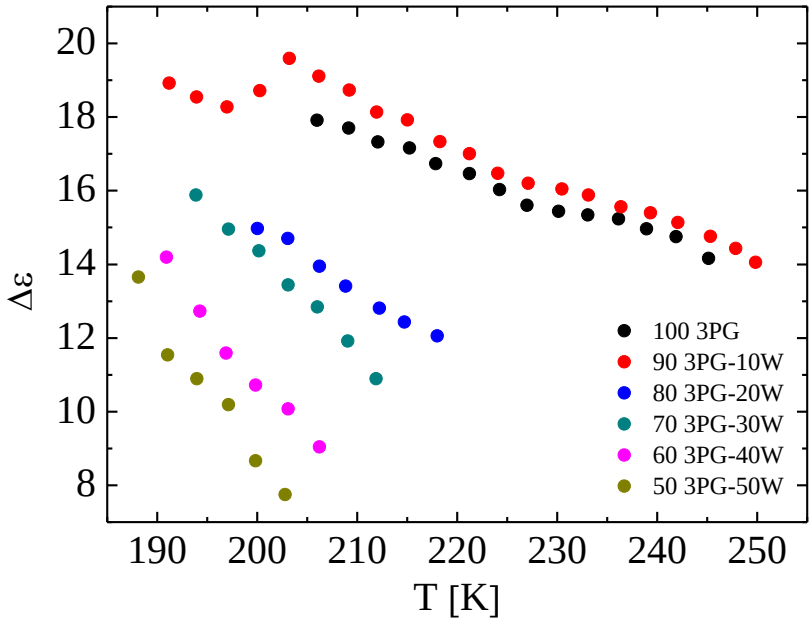

Figure VI. 15. Temperature dependence of the relaxation strength ($\Delta\varepsilon$) of process I (α-relaxation) of 3PG-water solutions at different water contents.

5. CONCLUSIONS

The calorimetric results for the very different systems analyzed evidenced that the glass transition temperature behavior varies among the different solutes. In all the cases T_g depends on the hydration level increasing its value as the hydration level is reduced. Nevertheless, the increment in the T_g (ΔT_g) is not common for all those systems. For example the T_g variation of 3PG is of 6 degrees increasing the water content in 40 wt%. However, for PVP, dextran and *n*-lysine oligomers, the differences in T_g values between the dried and 40 wt% samples are much more broad. Furthermore, in these systems, the concentration dependence is not monotonous and the T_g value increases much faster than expected at low hydration levels. This behavior has already been observed in aqueous solutions of polysaccharides and proteins.

Differences in the dynamical behaviour between different ordinary aqueous solutions are also remarkable. While ethylene-glycol oligomer solutions show only a single relaxation of water molecules, the dynamics of PVP, dextran and *n*-lysine solutions at high water contents evidences the presence of two main water dynamics (processes 2 and 3). In Chapters IV and V, we already mentioned the unusual presence of two main

simultaneous water dynamics below T_g for the *n*-lysine oligomers together with a solvent-slaved relaxation (α-like relaxation) above T_g, but among the results presented in this chapter we have extended the previous finding to other water solutions. The simultaneous presence of processes 2 and 3 below T_g in aqueous solutions of PVP, sucrose and dextran at high water contents is also an uncommon behaviour since for other solutions normally a single water relaxation is observed.

In addition for these solutions above T_g we observed two slaved relaxations; the α-like water relaxation (P3) and the glass transition related conformational relaxation (P4). Moreover, the relaxation time of processes 3 and 4 in PVP and dextran water mixtures follow the same temperature dependence. This is the most significant feature of these water solutions, since even being ordinary solutions the α-relaxation seems to be slaved to the water dynamics. Thus, along with the PVP, dextran and *n*-lysine oligomers dynamics results, we have established that the slaving behaviour is not limited to biological systems (proteins). Instead, it is also observed in non-biological solutions at sufficiently high hydration level if T_g is high enough.

6. REFERENCES

1 Immergut, E. H. & Mark, H. F. Platzer; Plasticization and Plasticizer Processes. *Advances in Chemistry; American Chemical Society*, doi:10.1021/ba-1965-0048.ch001 (1965).

2 Matveev, Y. I., Grinberg, V. Y. & Tolstoguzov, V. B. The plasticizing effect of water on proteins, polysaccharides and their mixtures. Glassy state of biopolymers, food and seeds. *Food Hydrocolloids* **14**, 425-437, doi:10.1016/s0268-005x(00)00020-5 (2000).

3 Vieira, M. G. A., da Silva, M. A., dos Santos, L. O. & Beppu, M. M. Natural-based plasticizers and biopolymer films: A review. *European Polymer Journal* **47**, 254-263, doi:10.1016/j.eurpolymj.2010.12.011 (2011).

4 Cerveny, S., Schwartz, G. A., Alegria, A., Bergman, R. & Swenson, J. Water dynamics in n-propylene glycol aqueous solutions. *Journal of Chemical Physics* **124**, doi:10.1063/1.2198206 (2006).

5 Sato, T. & Buchner, R. Dielectric relaxation processes in ethanol/water mixtures. *Journal of Physical Chemistry A* **108**, 5007-5015, doi:10.1021/jp035255o (2004).

6 Kumbharkhane, A. C., Puranik, S. M. & Mehrotra, S. C. Temperature dependent dielectric relaxation study of ethylene glycol-water mixtures. *Journal of Solution Chemistry* **21**, 201-212, doi:10.1007/bf00647008 (1992).

7 Hayashi, Y., Puzenko, A., Balin, I., Ryabov, Y. E. & Feldman, Y. Relaxation dynamics in glycerol-water mixtures. 2. Mesoscopic feature in water rich mixtures. *Journal of Physical Chemistry B* **109**, 9174-9177, doi:10.1021/jp050425d (2005).

8 Cerveny, S., Mallamace, F., Swenson, J., Vogel, M. & Xu, L. M. Confined Water as Model of Supercooled Water. *Chemical Reviews* **116**, 7608-7625, doi:10.1021/acs.chemrev.5b00609 (2016).

9 Cerveny, S., Colmenero, J. & Alegria, A. Dielectric investigation of the low-temperature water dynamics in the poly(vinyl methyl ether)/H2O system. *Macromolecules* **38**, 7056-7063, doi:10.1021/ma050811t (2005).

10 Sjostrom, J. *et al.* Dielectric secondary relaxation of water in aqueous binary glass-formers. *Physical Chemistry Chemical Physics* **12**, 10452-10456, doi:10.1039/c001275k (2010).

11 Singh, L. P., Cerveny, S., Alegria, A. & Colmenero, J. Dynamics of Water in Supercooled Aqueous Solutions of Poly(propylene glycol) As Studied by Broadband Dielectric Spectroscopy and Low-Temperature FTIR-ATR Spectroscopy. *Journal of Physical Chemistry B* **115**, 13817-13827, doi:10.1021/jp2073705 (2011).

12 Ablett, S., Izzard, M. J., Lillford, P. J., Arvanitoyannis, I. & Blanshard, J. M. V. Calorimetric study of the glass transition ocurring in fructose solutions *Carbohydrate Research* **246**, 13-22, doi:10.1016/0008-6215(93)84020-7 (1993).

13 Caffarena, E. R. & Grigera, J. R. Glass transition in aqueous solutions of glucose. Molecular dynamics simulation. *Carbohydrate Research* **300**, 51-57, doi:10.1016/s0008-6215(97)00029-3 (1997).

14 Frank, G. A. Measurement analysis of glass transition temperature for sucrose and trehalose aqueous solutions. *Journal of Physical and Chemical Reference Data* **36**, 1279-1285, doi:10.1063/1.2779330 (2007).

15 Panagopoulou, A. *et al.* Glass transition and dynamics in BSA-water mixtures over wide ranges of composition studied by thermal and dielectric techniques. *Biochimica Et Biophysica Acta-Proteins and Proteomics* **1814**, 1984-1996, doi:10.1016/j.bbapap.2011.07.014 (2011).

16 Batzer, H. & Kreibich, U. T. Influence of water on thermal transitions in natural polymers amnd synthetic polyamides *Polymer Bulletin* **5**, 585-590 (1981).

17 Gennadios, A. *Protein based films and coatings*. (2002).

18 Kalichevsky, M. T., Jaroszkiewicz, E. M. & Blanshard, J. M. V. Glass-transition of gluten. Gluten and gluten sugar mixtures *International Journal of Biological Macromolecules* **14**, 257-266, doi:10.1016/s0141-8130(05)80038-8 (1992).

19 Miyazaki, Y., Matsuo, T. & Suga, H. Low-temperature heat capacity and glassy behavior of lysozyme crystal. *Journal of Physical Chemistry B* **104**, 8044-8052, doi:10.1021/jp0007686 (2000).

20 Pikal, M. J., Rigsbee, D. R. & Roy, M. L. Solid state chemistry of proteins: I. Glass transition behavior in freeze dried disaccharide formulations of human growth hormone (hGH). *Journal of pharmaceutical sciences* **96**, 2765-2776, doi:10.1002/jps.20960 (2007).

21 Jansson, H. & Swenson, J. The protein glass transition as measured by dielectric spectroscopy and differential scanning calorimetry. *Biochimica et biophysica acta* **1804**, 20-26, doi:10.1016/j.bbapap.2009.06.026 (2010).

22 Brostow, W., Chiu, R., Kalogeras, I. M. & Vassilikou-Dova, A. Prediction of glass transition temperatures: Binary blends and copolymers. *Materials Letters* **62**, 3152-3155, doi:10.1016/j.matlet.2008.02.008 (2008).

23 Weng, L. D., Vijayaraghavan, R., MacFarlane, D. R. & Elliott, G. D. Application of the Kwei equation to model the Tg behavior of binary blends of sugars and salts. *Cryobiology* **68**, 155-158, doi:10.1016/j.cryobiol.2013.12.005 (2014).

24 Maeda, S., Kunimoto, K.-K., Sasaki, C., Kuwae, A. & Hanai, K. Characterization of microbial poly (ε-l-lysine) by FT-IR, Raman and solid state 13C NMR spectroscopies. *Journal of Molecular Structure* **655**, 149-155, doi:10.1016/s0022-2860(03)00218-7 (2003).

25 Floudas, G., Steffen, W. & Fischer, E. W. Solvent and polymer dynamics in concentrated polystyrene toluene solutions *Journal of Chemical Physics* **99**, 695-703, doi:10.1063/1.465742 (1993).

26 Sasaki, K. *et al.* Glass Transition and Dynamics of the Polymer and Water in the Poly(vinylpyrrolidone)-Water Mixtures Studied by Dielectric Relaxation Spectroscopy. *Journal of Physical Chemistry B* **120**, 6882-6889, doi:10.1021/acs.jpcb.6b05347 (2016).

27 Jansson, H., Bergman, R. & Swenson, J. Dynamics of sugar solutions as studied by dielectric spectroscopy. *Journal of Non-Crystalline Solids* **351**, 2858-2863, doi:10.1016/j.jnoncrysol.2005.04.086 (2005).

28 Frauenfelder, H., Fenimore, P. W. & McMahon, B. H. Hydration, slaving and protein function. *Biophysical chemistry* **98**, 35-48, doi:10.1016/s0301-4622(02)00083-2 (2002).

29 Caliskan, G. *et al.* Protein and solvent dynamics: How strongly are they coupled? *Journal of Chemical Physics* **121**, 1978-1983, doi:10.1063/1.1764491 (2004).

30 Tarek, M. & Tobias, D. J. Role of protein-water hydrogen bond dynamics in the protein dynamical transition. *Physical review letters* **88**, doi:10.1103/PhysRevLett.88.138101 (2002).

31 Frauenfelder, H. *et al.* A unified model of protein dynamics. *Proceedings of the National Academy of Sciences of the United States of America* **106**, 5129-5134, doi:10.1073/pnas.0900336106 (2009).

32 Tarek, M. & Tobias, D. J. The dynamics of protein hydration water: A quantitative comparison of molecular dynamics simulations and neutron-scattering experiments. *Biophysical journal* **79**, 3244-3257 (2000).

33 Khodadadi, S. *et al.* Dynamics of biological macromolecules: not a simple slaving by hydration water. *Biophysical journal* **98**, 1321-1326, doi:10.1016/j.bpj.2009.12.4284 (2010).

CHAPTER VII

CONCLUDING REMARKS

In this thesis, we have performed a detailed study of the dynamics of water in different biological and non-biological aqueous solutions. Nowadays, it is well known that a "working protein" does not consist solely of the folded chain of amino acids but requires the surrounding solvent to be biologically active and perform its biological functions. Nevertheless, the debate in the literature is open, and to date it is not fully clear whether water guides the protein dynamics or both protein and water dynamics affect each other. Studies on proteins dynamics are numerous. In particular, BDS experiments must be performed at low temperatures to well split the different relaxation processes. However, to obtain a proper solution in the case of a protein, a large quantity of water is required, which crystallizes on cooling, thus hindering the dynamical study. Therefore, to avoid crystallization, most reported literature studies are on hydrated protein powders instead of diluted solutions which represent more realistic cases. To overcome these drawbacks, we studied small peptides. They share many properties with proteins, but with the great advantage that they do not crystallize up to water concentrations of 40 – 45 wt%.

We first studied the dynamics of ε-polylysine (ε-PLL). Although it has no specific biological function, ε-PLL has a well-defined β-sheet structure, which makes it comparable with biologically active proteins. To obtain a complete understanding of the dynamics, ε-PLL solutions of various concentrations and pH values were studied over a wide range of frequency and temperature values using BDS. These results give evidence for the presence of two main Arrhenius-like relaxation processes (called P2 and P3) below the glass transition temperature of the solution related to the water molecules. Each of these relaxations has a distinct molecular origin. P2 is the universal β-relaxation of water found in every aqueous solution (soft and hard confinements), whereas P3 is a "new'' water-related relaxation not previously observed in other aqueous solutions. At the glass transition temperature, this process showed a crossover from Arrhenius temperature dependence to VFT temperature dependence above T_g. Above T_g, two main relaxations were also detected. The already mentioned P3 attributed to the α-like water

relaxation, and P4 related to the reorientation of ε-PLL molecules and responsible for the glass transition. Three more slow processes were observed at high temperatures, but due to their high dielectric strength, they were considered to originate from electrode polarization and ionic conductivity effects and not molecular relaxations. In addition, the temperature dependence of the relaxation times of P3 and P4 showed a very similar VFT dependence, suggesting a strong coupling between them. This coupling has been observed in other protein solutions but never in a non-biological system, so we pursued this finding and studied it in other *n*-lysine oligomers.

Aqueous solutions of n = 3, 4 and 10 also showed the coupling between the water and peptide dynamics above T_g, and the dynamics of the solute was described as "slaved" by the relaxation of the solvent. Oligomers of 3- and 4-lysine residues showed no specific conformation, whereas 10-lysine and the ε-PLL had α-helix and β-sheet conformations, respectively. Thus, the slaving phenomenon was also proven among systems with different structures.

Using the BDS results obtained for the lysine peptides, we can conceive how the dynamics of a protein solution should behave in the absence of ice. We therefore propose that, as seen by dielectric spectroscopy, the dynamics of a protein solution should appear as shown in Figure VII. 1 in a broad temperature range above and below T_g.

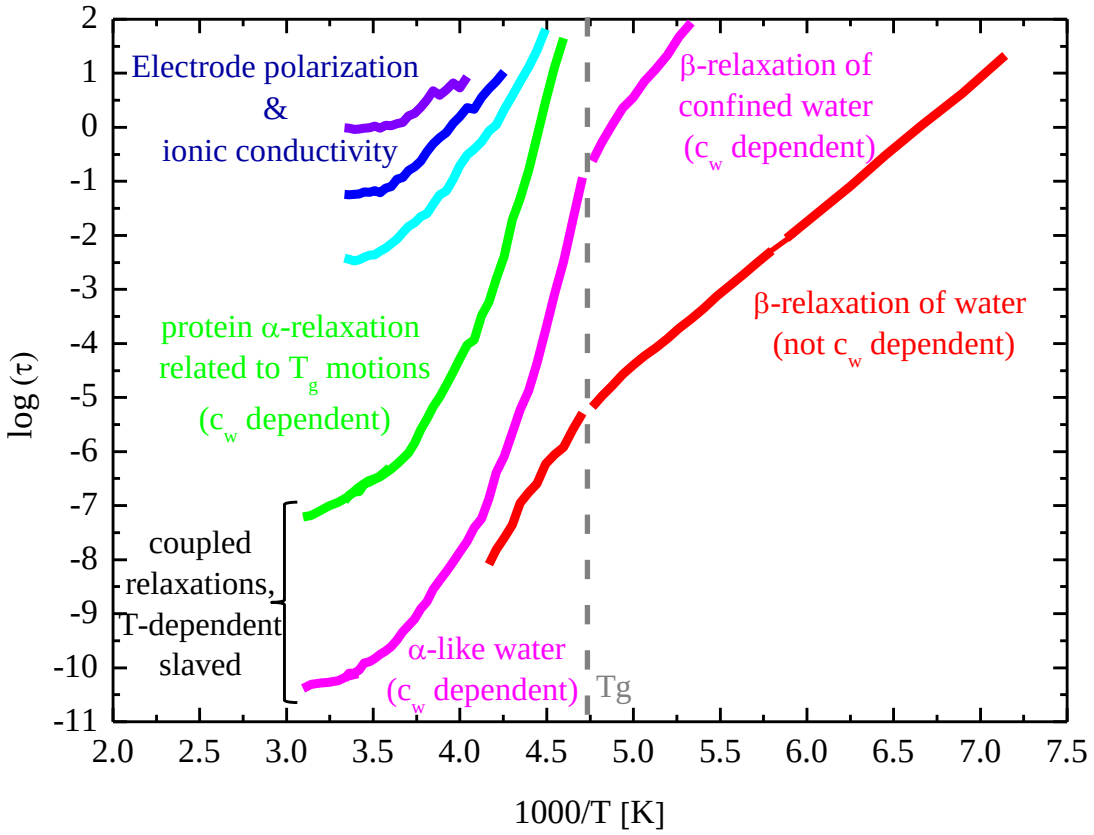

Figure VII. 1. The proposal for protein dynamics seen by dielectric spectroscopy.

Finally, we have been able to generalize the concept of slaved dynamics to other types of molecules than proteins and peptides. For this, we have studied aqueous solutions of polyvinyl pyrrolidone (PVP), a synthetic polymer, and some polysaccharides such as sucrose and dextran. To differentiate between the slaving phenomenon and the plasticization effect, a broad range of hydration levels were analyzed from the non-hydrated to solutions of c_w = 40 wt%. In addition, 3-lysine and ε-PLL in the dry state and in very different hydration levels were also studied. The calorimetric results were compared with that observed in many synthetic polymers, polysaccharides and proteins from the literature. Finally, the dynamical behavior of *n*-lysine oligomers, PVP, sucrose and dextran was compared with a typical ordinary solution as tripropylene glycol (3PG) water mixture. We observed that in materials with a strong variation of T_g with the water content and high hydration levels (PVP, ε-PLL, 3-lysine and dextran), BDS results evidenced a slaving behavior between the α-like water relaxation and the α-relaxation of the solution (processes 3 and 4, respectively). In these solutions, water allows the solute molecule reorientation and enables the glass transition-related relaxation. Nevertheless, at low

hydration levels, process 3 was vanished, and similarities in the behavior of PVP and *n*-lysine oligomers water mixtures with ordinary aqueous solutions of 3PG became evident. Therefore, at very low water concentrations, the effect of water in PVP and lysine oligomers was described as a plasticizer.

According to the relation between the calorimetric and BDS results, we concluded that the extremely broad T_g variation observed in these materials could be one of the most important variables to observe the slaving behavior. Moreover, as far as we are aware, it is the first time that the slaving phenomenon has been observed in non-biological solutions such as synthetic polymers, polysaccharides and *n*-lysine oligomers, and allow us to conclude that the slaved dynamics can be extended to other systems than proteins as believed so far.

APPENDIX

1. CHAPTER IV. DYNAMICS AND STRUCTURE OF ε-PLL AQUEOUS SOLUTIONS

1.1. X-ray scattering

Figure A. 1 shows the WAXS patterns of the ε-PLL aqueous solutions at different water contents (a – d) and different pH values (d –f) at various temperatures from 153 to 293 K on a q length scale of 5 to 40 nm^{-1}.

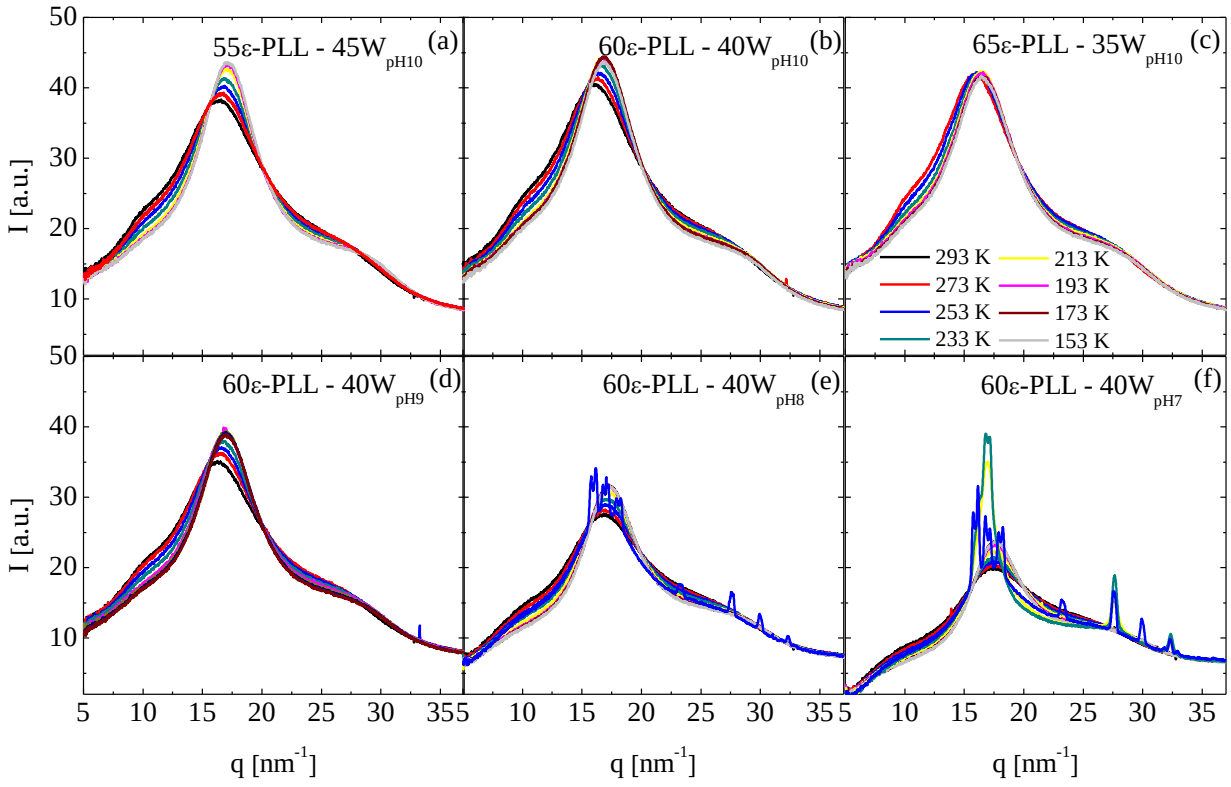

Figure A. 1. WAXS patterns of the ε-PLL – water mixtures at different hydration levels (a – d) and pH values (d –f).

We are not going to comment much on these scattering results, they are only presented in order to show that samples at pH = 10 and different hydration levels ($45 \leq c_w$ [wt%] ≤ 55 wt%) do not

crystallize in the broad temperature range analyzed. Neither does the ε-PLL solution with a pH of 9, while samples with lower pH values show crystallization peaks at the same temperatures observed by DSC measurements.

1.2. Broadband dielectric spectroscopy

Figure A. 2 to Figure A. 6 show both components of the complex dielectric permittivity data for the different water content and pH mixtures at various temperatures, below and above T_g.

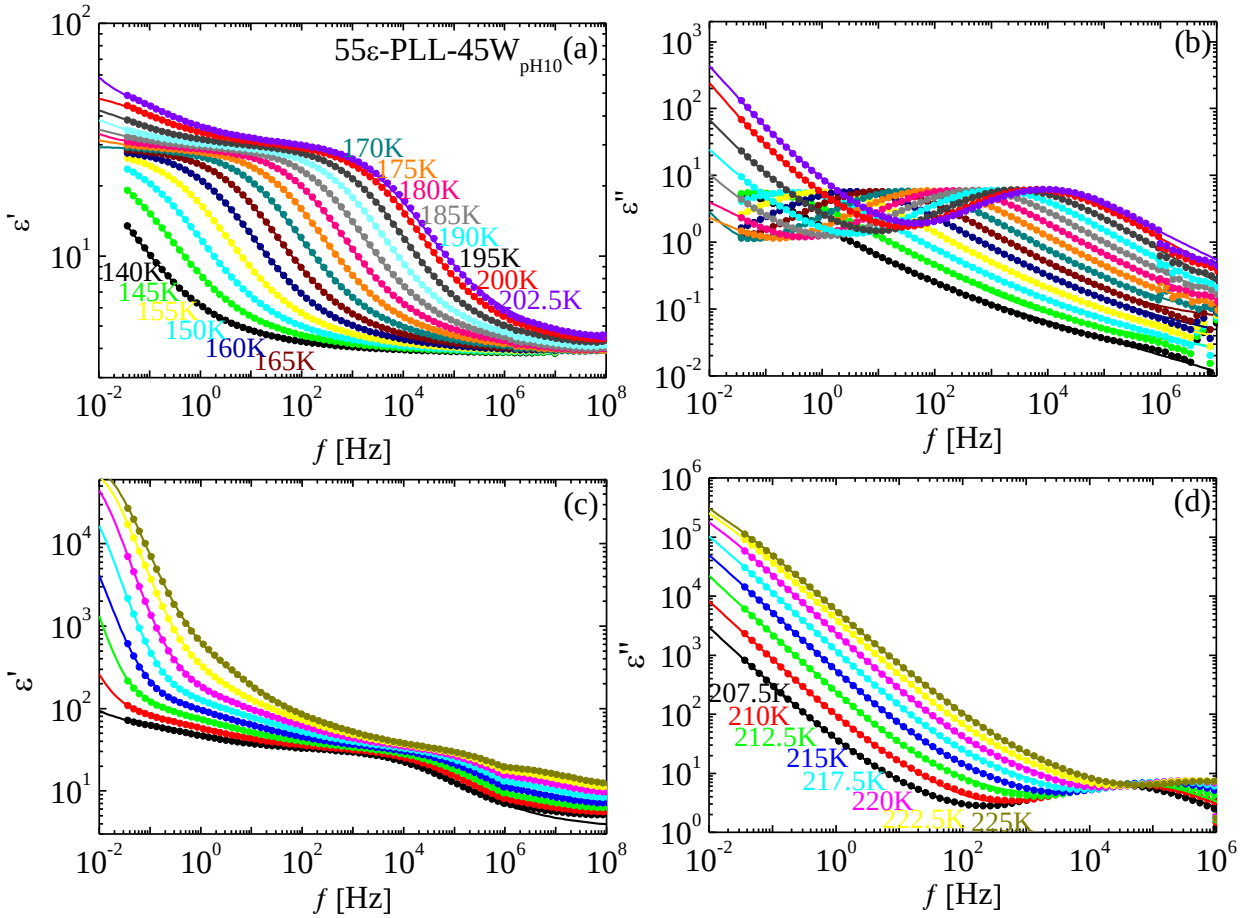

Figure A. 2. Dielectric data in function of the frequency for 55ε-PLL – 45W$_{pH10}$ sample at some temperatures below (a,b) and above (c,d) T_g. Close symbols show experimental data and lines over the symbols represent the total fitting function.

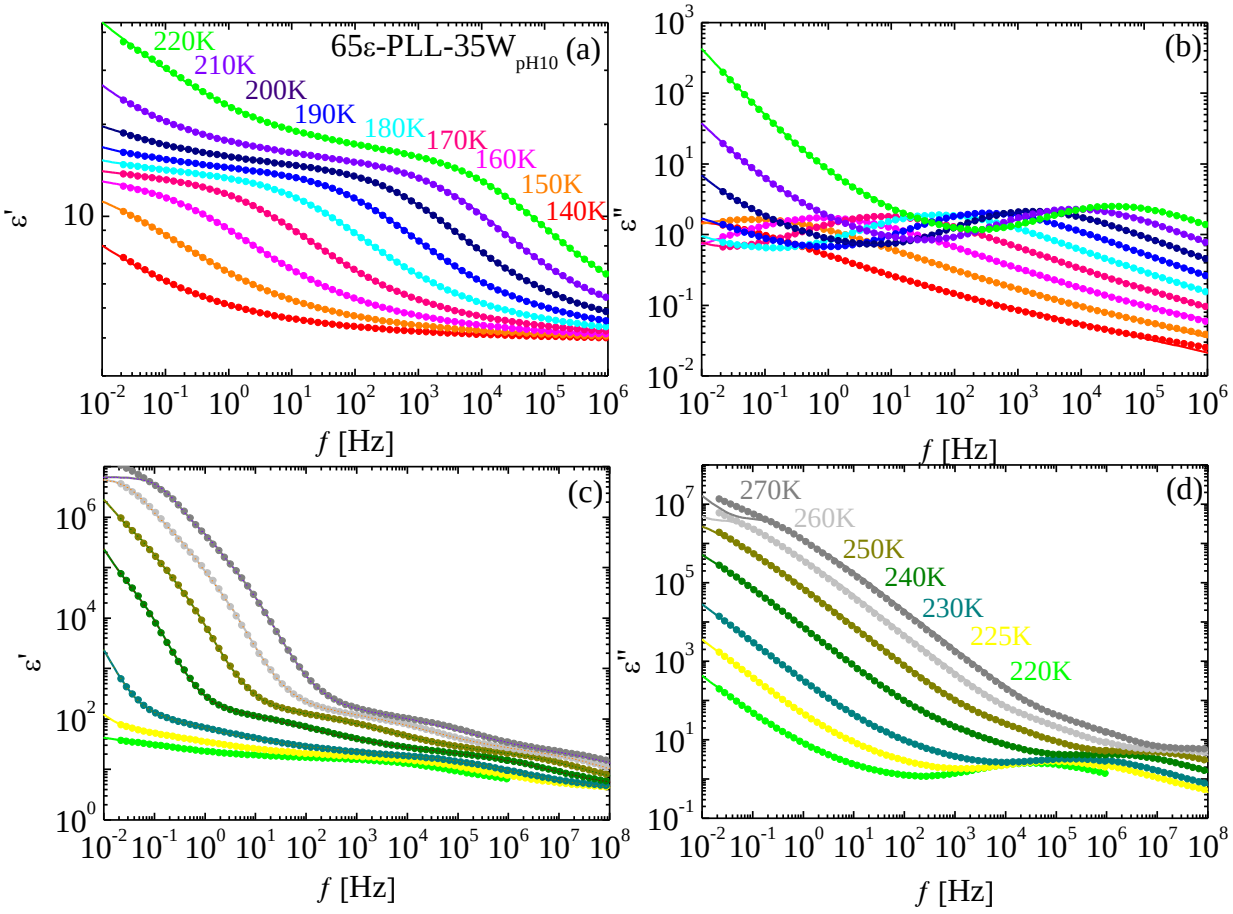

Figure A. 3. Dielectric data in function of the frequency for 65ε-PLL – 35W_{pH10} sample at some temperatures below (a,b) and above (c,d) T_g.

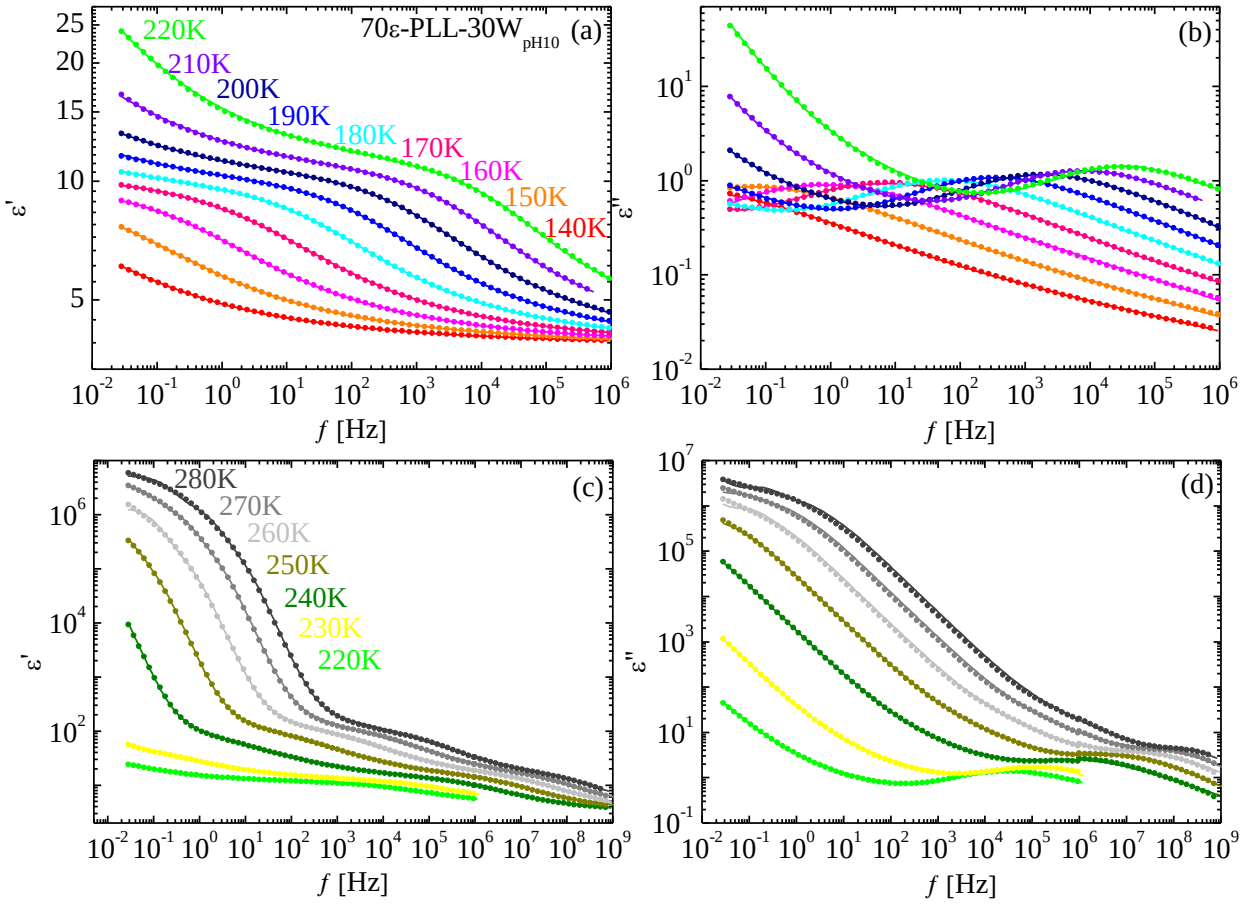

Figure A. 4. Dielectric data in function of the frequency for 70ε-PLL – 30W$_{pH10}$ sample at some temperatures below (a,b) and above (c,d) T_g.

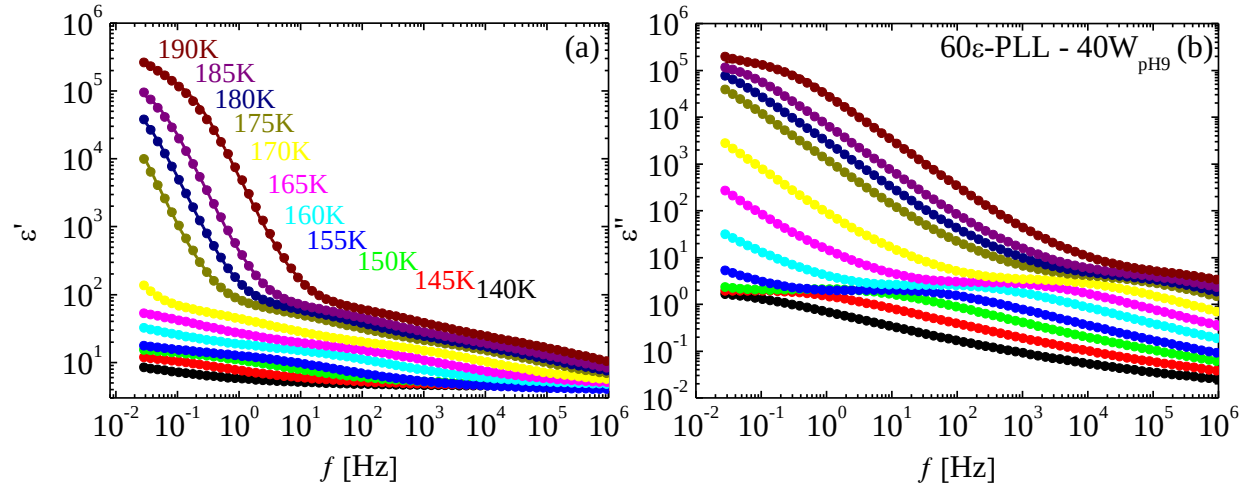

Figure A. 5. Dielectric data in function of the frequency for 60ε-PLL – 40W sample at pH = 9 at some temperatures below (a) and above T_g (b). Close symbols show experimental data and lines over the symbols represent the total fitting function.

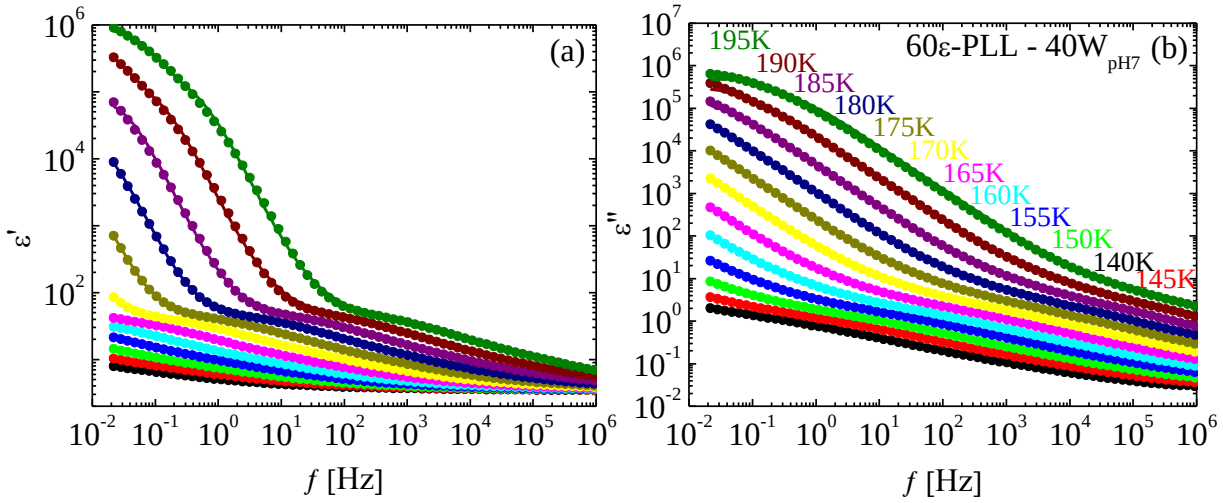

Figure A. 6. Dielectric data in function of the frequency for 60ε-PLL – 40W sample at pH = 7 at some temperatures below (a) and above T_g (b).

In Figure A. 7 to Figure A. 10 the different dielectric relaxation processes used to fit ε' and ε'' are also shown.

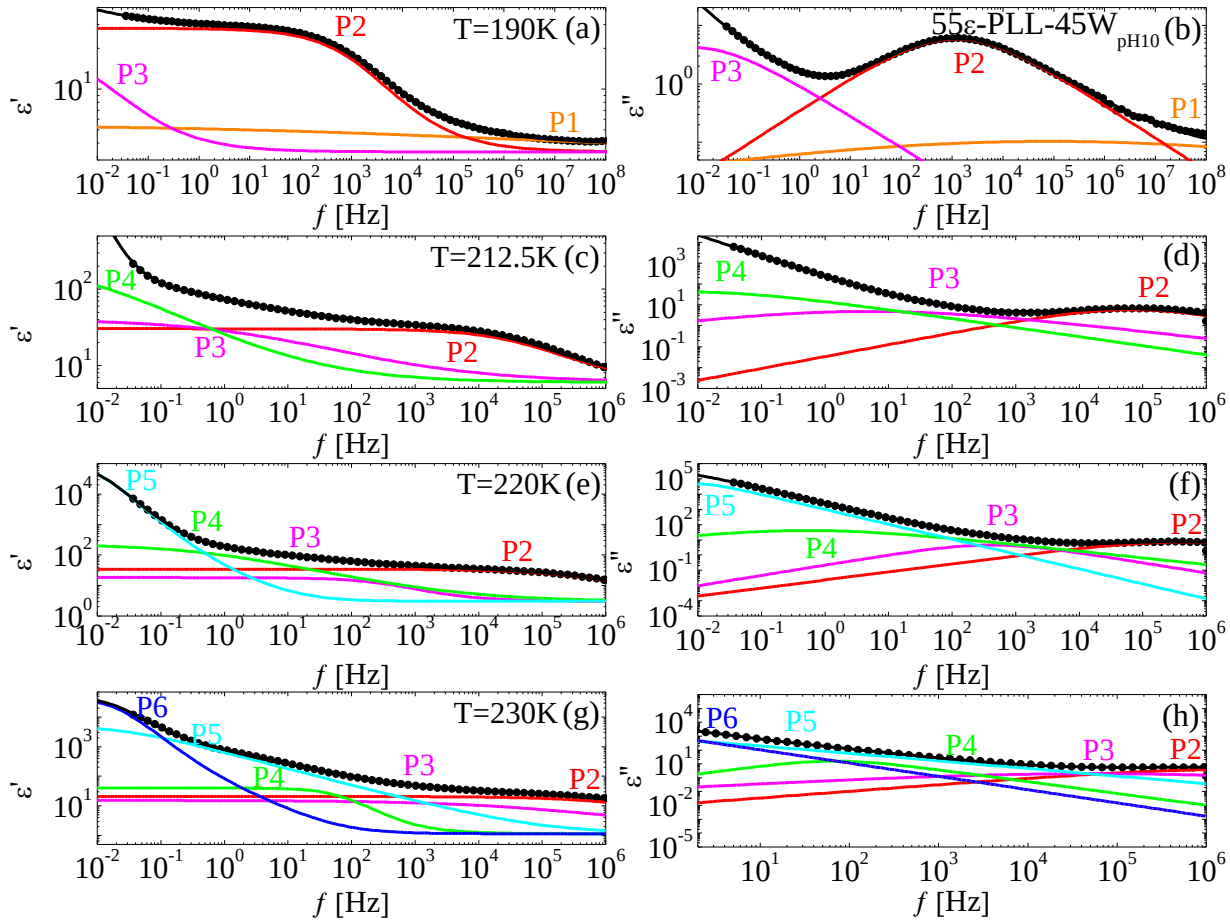

Figure A. 7. Real (a) and imaginary (b) parts of the complex dielectric permittivity of ε-polylysine water solution (c_w = 45 wt%) at four different temperatures: T = 180, 212.5, 220 and 230 K. Solid lines through the data points represent the fits to the experimental data.

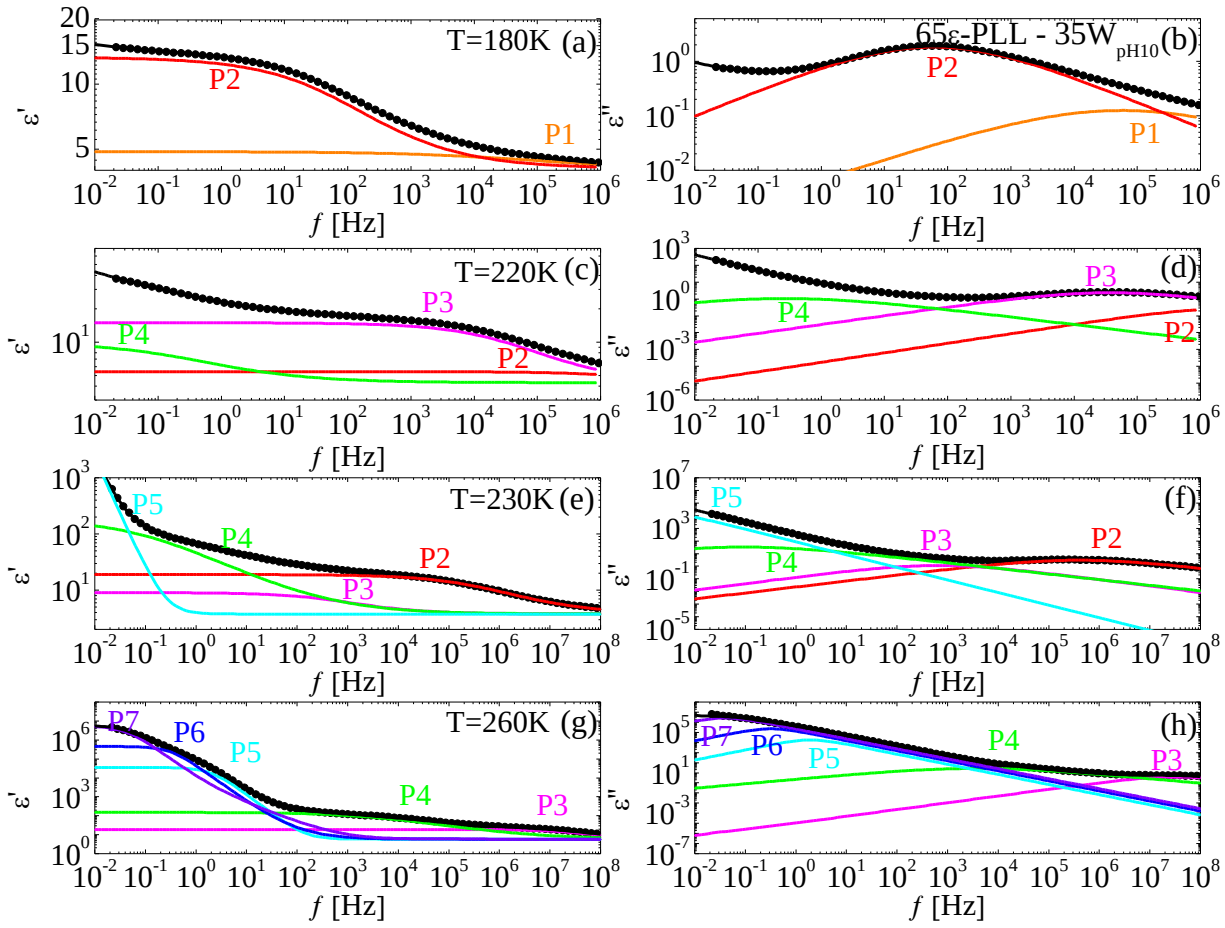

Figure A. 8. . Real (a) and imaginary (b) parts of the complex dielectric permittivity of ε-polylysine water solution (c_w = 35 wt%) at four different temperatures: T = 180, 220, 230 and 260 K.

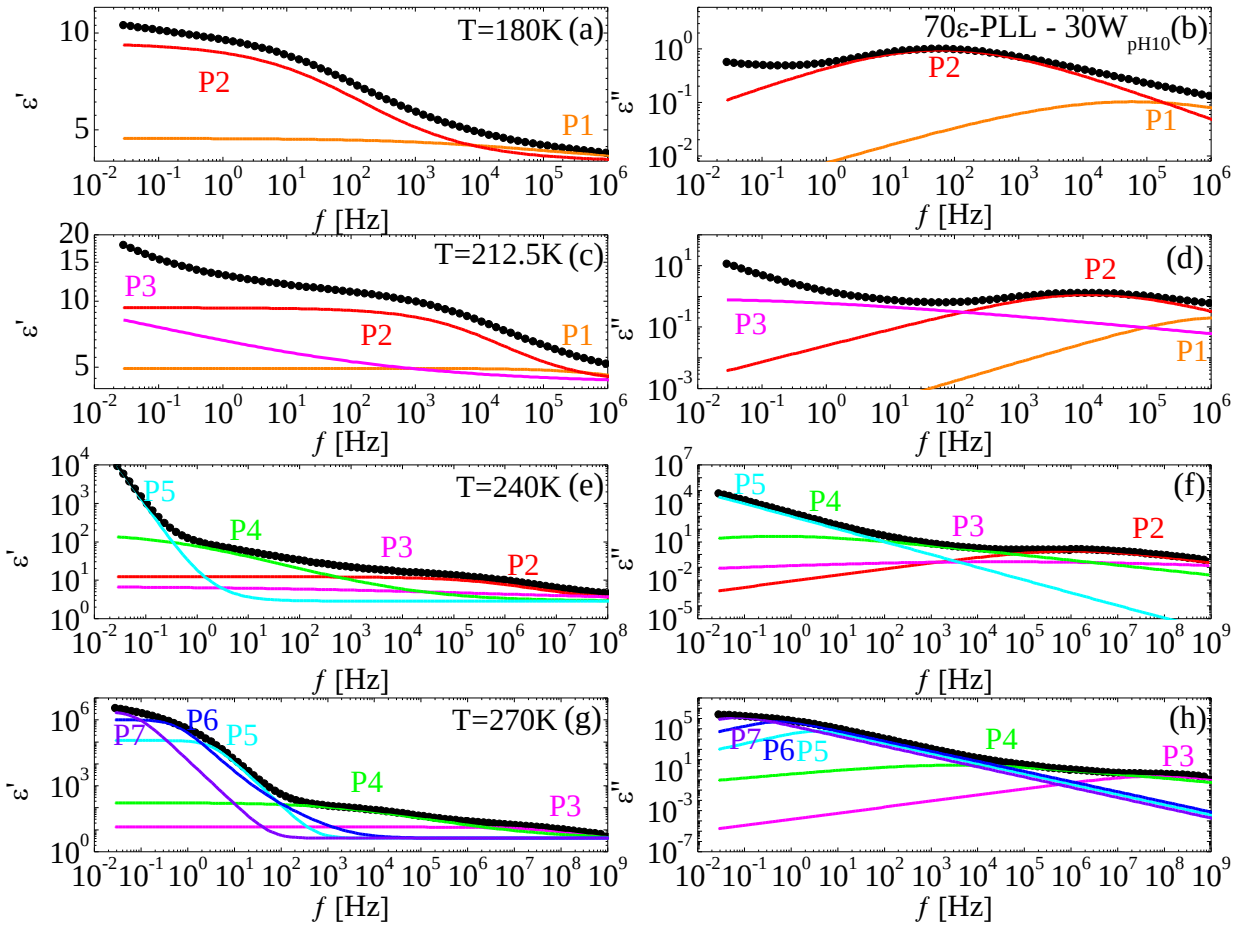

Figure A. 9. Real (a) and imaginary (b) parts of the complex dielectric permittivity of ε-polylysine water solution (c_w = 30 wt%) at four different temperatures: T = 180, 212.5, 240 and 270 K.

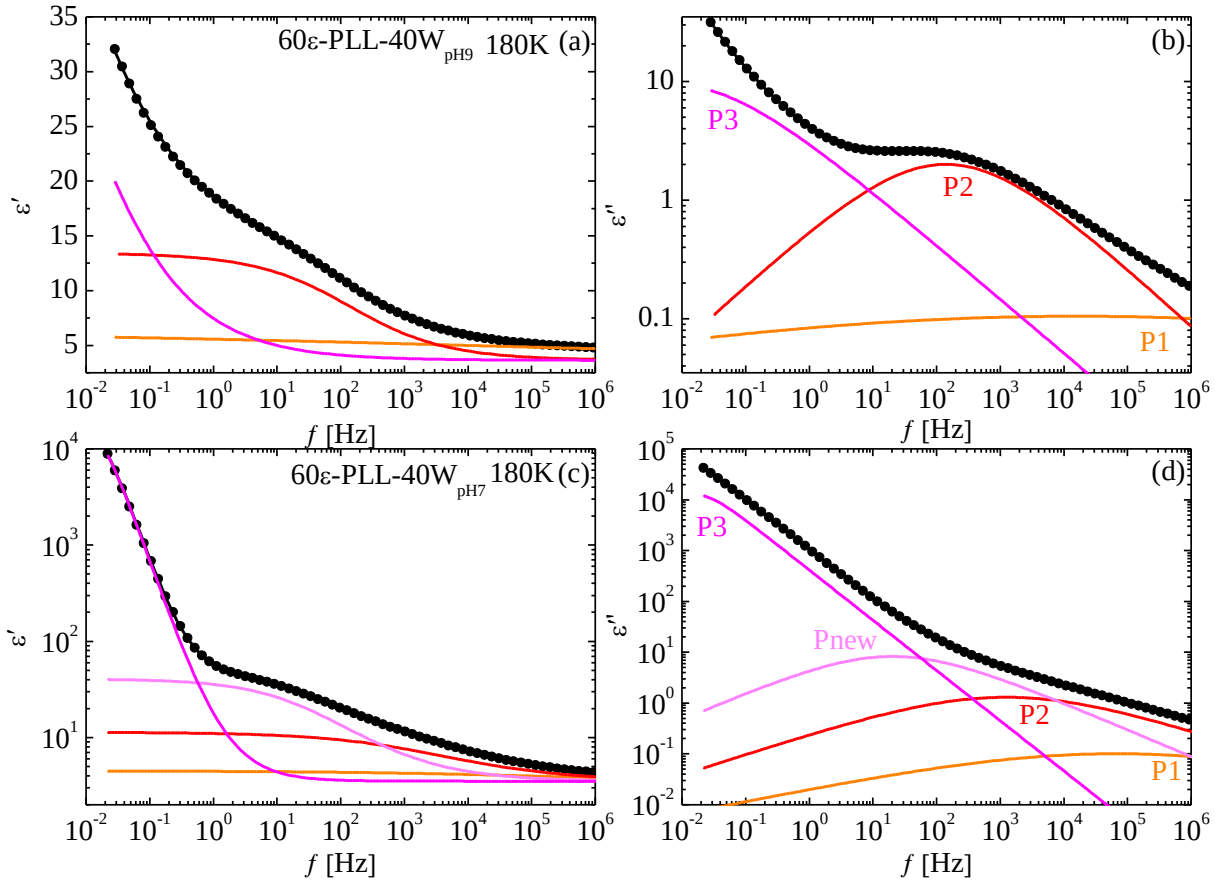

Figure A. 10. Real (a and c) and imaginary (b and d) parts of the complex dielectric permittivity of ε-polylysine water solution (c_w = 40 wt%) at pH = 9 and 7 for T = 180 K.

Figure A. 11 shows the temperature dependence of the relaxation times for processes 2 and 3 at the different hydration levels, the relaxation times obtained from isochronal and TSDC measurements, and the logarithmic derivative analysis are also included.

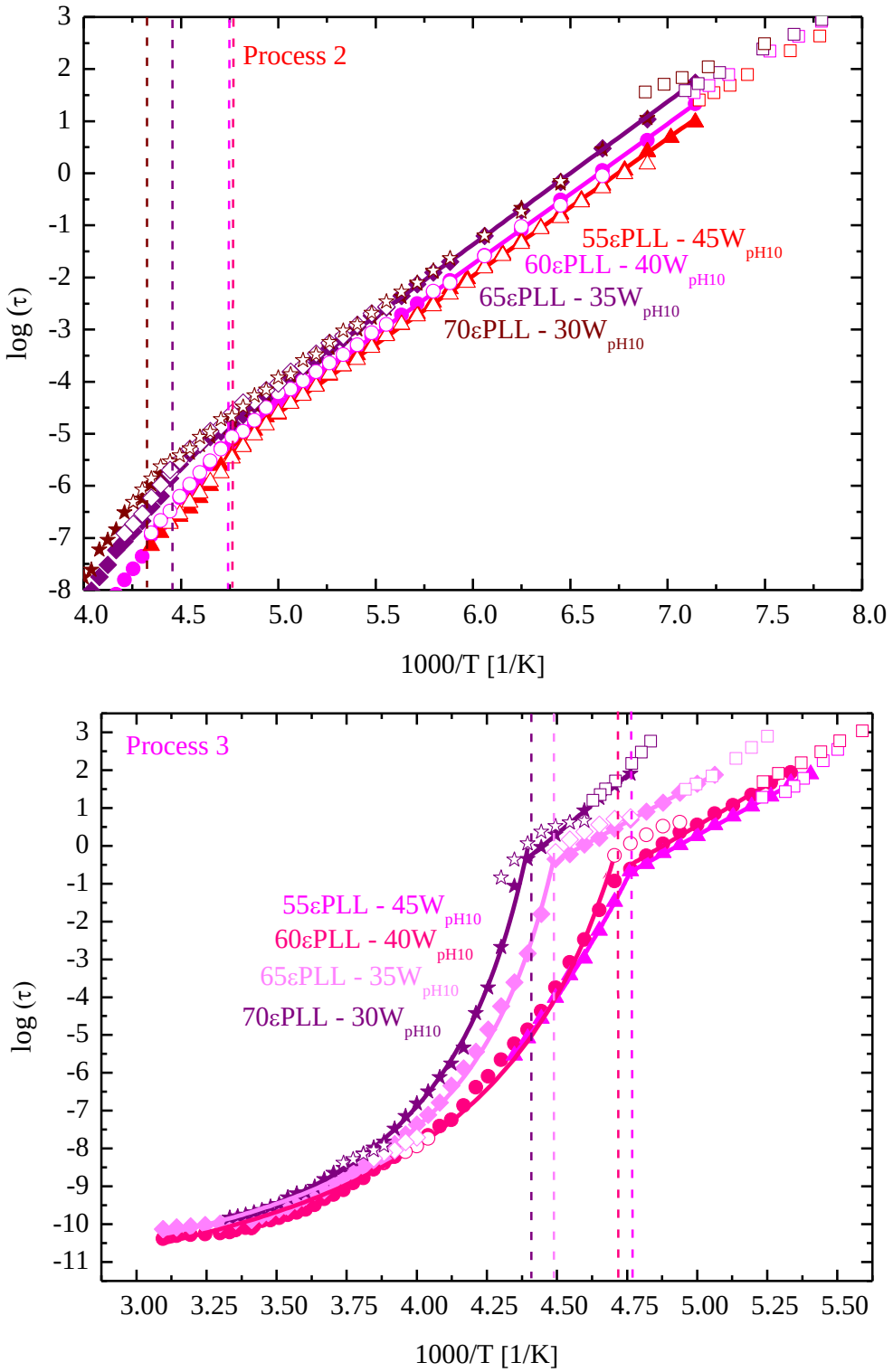

Figure A. 11. Comparison of the temperature dependence of the relaxation times for processes 2 and 3 at the different water contents. Close triangles represent ε-PLL sample at c_w = 45 wt%, close circles c_w = 40 wt% sample, close diamons c_w = 35 wt% sample and close stars c_w = 30 wt% sample. Open triangles, circles, diamonds and stars represent the relaxation times obtained from the logarithmic derivative analysis, and open square points relaxation times from TSDC measurements. Finally, as in previous representations, vertical dash lines represent the glass transition temperatures for each sample.

2. CHAPTER VI. WATER PLASTICIZATION VERSUS SLAVING PHENOMENA

2.1. Concentration dependence of the glass transition temperature of water solutions

Figure A. 12 shows the DSC curves for several PVP aqueous solutions upon cooling at heating rates of 10 K/min from 175 to 500 K. No sign of crystallization was found, neither on cooling nor on heating. Moreover, a single and narrow glass transition temperature (T_g) was observed for all the samples, which values increases decreasing c_w, consistent with the plasticizing effect that water has on the flexibility of PVP.

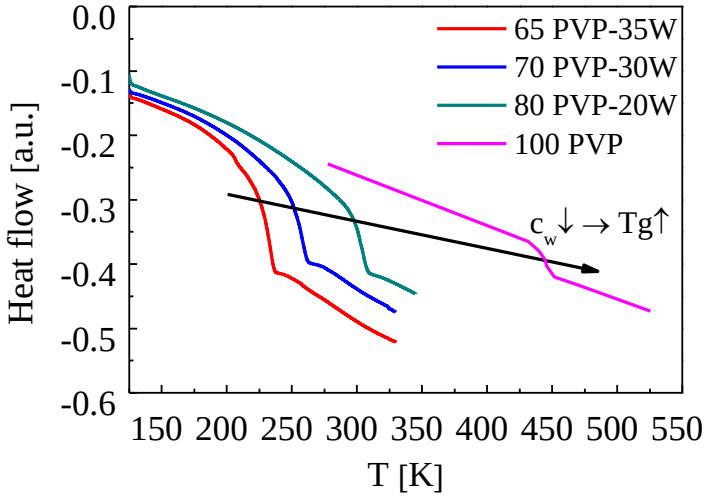

Figure A. 12. DSC curves upon heating cycles for several PVP (M_w = 55000 g/mol) aqueous solutions

Figure A. 13 (a and b) shows the DSC curves for some 3-lysine and ε-PLL aqueous solutions, respectively, upon cooling and heating rates of 10 K/min from 150 to 350 K.

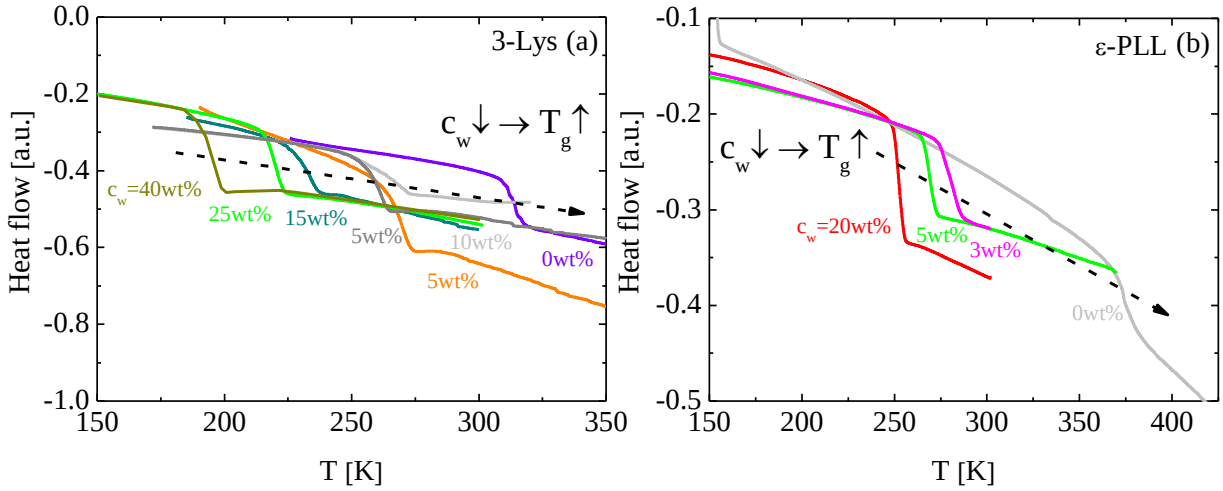

Figure A. 13. DSC curves for different water contents of 3-lysine (a) and ε-PLL (b) samples.

2.2. Dynamics of 3-lysine aqueous solutions

Figure A. 14 shows a comparative of the relaxation times temperature dependence of the glass transition related relaxation and the α-like water process for PVP (a) and ε-PLL (b) systems at different hydration levels, from the most diluted solutions (c_w = 40 – 45 wt%) to the non-hydrated samples.

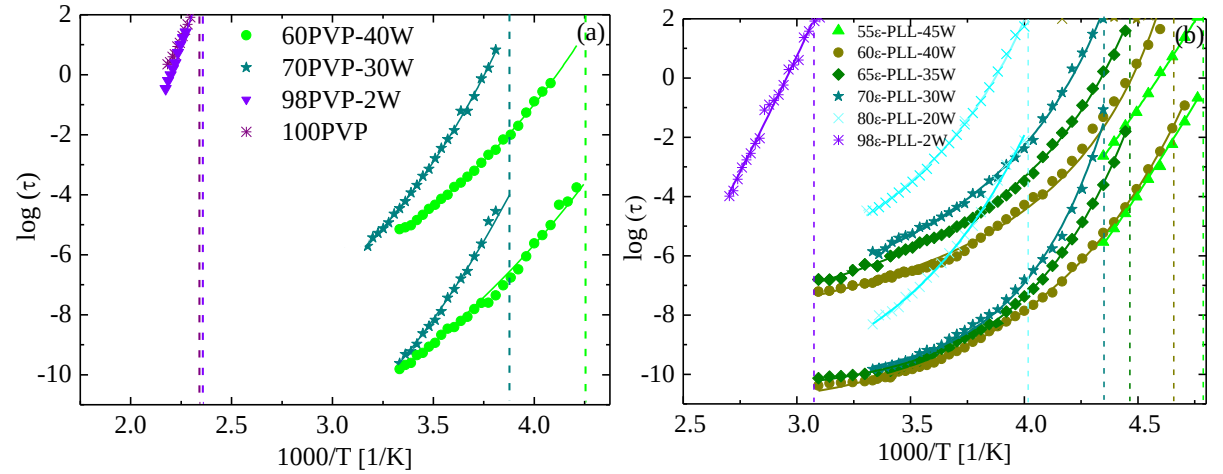

Figure A. 14. Temperature dependence of the glass transition related relaxation times for PVP (a) and ε-PLL (b) samples at different hydration levels. Dashed vertical lines represent the T_g value of each sample.

Figure A. 15 shows the temperature dependence of $\Delta\varepsilon$ for process 4 in PVP (a) and ε-PLL (b) at various water contents.

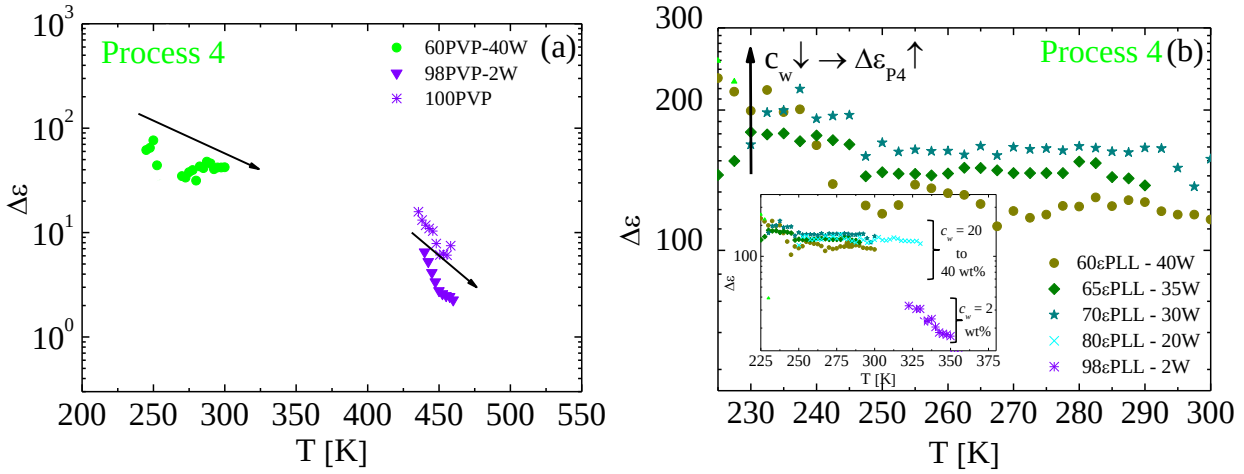

Figure A. 15. Temperature dependence of process 4 $\Delta\varepsilon$ for PVP (a) and ε-PLL (b) at various water contents.

2.3. The slaving behavior observed in PVP, *n*-lysine, sucrose and dextran at c_w = 40 wt%

Figure A. 16 a and b shows the isochronal measurements (at fixed frequencies from 10^{-1} to 10^{6} every decade from 150 to 300 K) and the analysis of the derivative of the real part of the dielectric permittivity, respectively. Both, isochronal measurements and the derivative analysis corroborate the presence of two relaxation processes below T_g (P2 and P3), and one more at high temperaturas (P4).

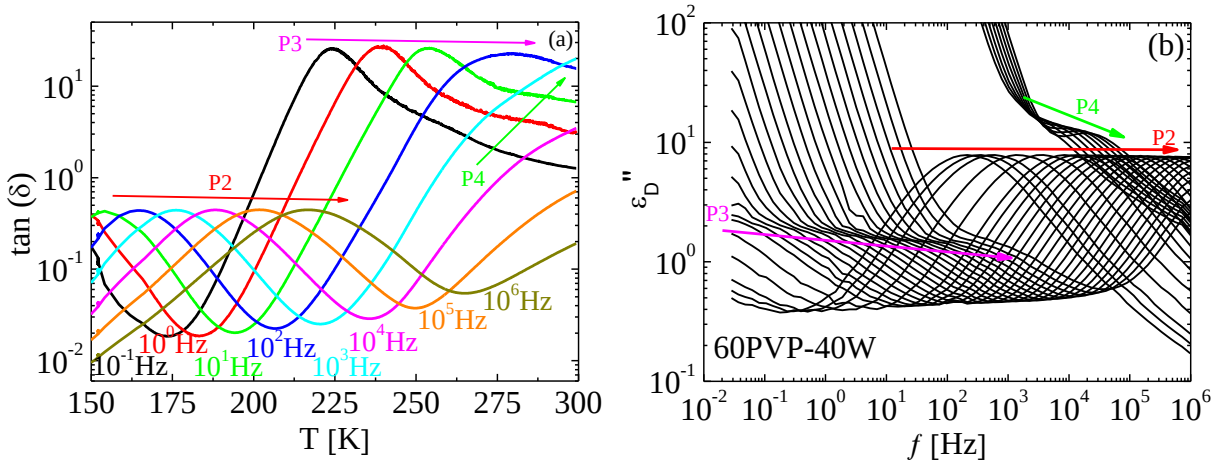

Figure A. 16. Isochronal measurements results (a) and analysis of the derivative of the real part of the dielectric permittivity (b) for PVP at c_w = 40 wt%.

Figure A. 17 show the real and the imaginary parts of the complex dielectric permittivity at various temperatures for sucrose (a and b) and dextran (c and d) aqueous solutions.

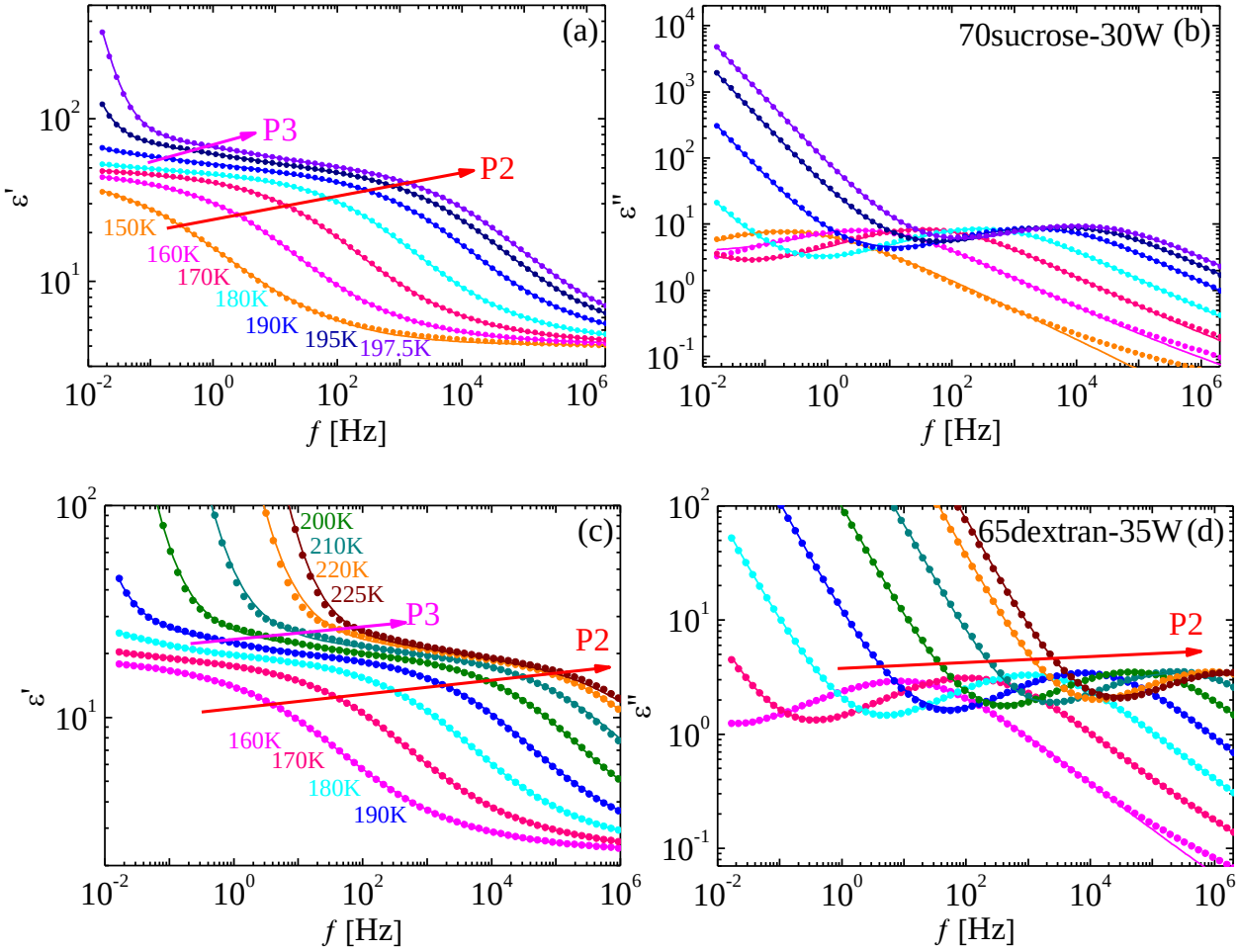

Figure A. 17. Real (a and c) and imaginary (b and d) parts of the complex dielectric permittivity of sucrose aqueous solution (c_w = 30 wt%) and dextran aqueous solution (c_w = 35 wt%) at various temperatures. Solid lines through the data points represent the fits to the experimental data.

Figure A. 18 (a and b) show the analysis of the derivative of the real part of the dielectric permittivity for sucrose and dextran aqueous solutions, respectively.

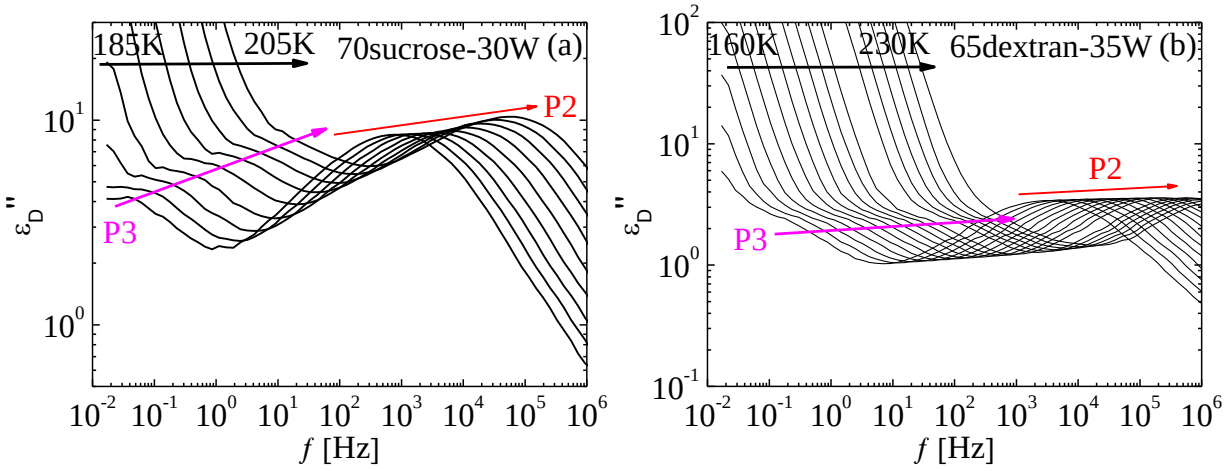

Figure A. 18. Analysis of the derivative of the real part of the dielectric permittivity for sucrose (a) and dextran (b).

LIST OF PUBLICATIONS

This thesis has contributed to the following publications:

Evidence of coupling between the motions of water and peptides

Silvina Cerveny, Izaskun Combarro-Palacios and Jan Swenson

The Journal of Physical Chemistry Letters, **2016**, *7* (20), 4093-4098 DOI: 10.1021/acs.jpclett.6b01864

Dynamics and structure of ε-polylysine aqueous solutions at different pH

Manuscript in preparation (2017)

Generalization of the slaved dynamics to non-biological solutions

Manuscript in preparation (2017)

ACKNOWLEDGMENTS

AGRADECIMIENTOS

Antes que a nadie me gustaría agradecer la ayuda que me han brindado durante estos tres años a mis directores de tesis Silvina Cerveny y Ángel Alegría. Su apoyo ha sido imprescindible no solo para llevar a cabo este trabajo, sino también para mi formación como investigadora. También quisiera agradecer al Prof. Juan Colmenero el haberme acogido en el grupo "Polymers and Soft Matter''.

David merece una mención especial, por escucharme, aconsejarme, apoyarme y acompañarme en este trabajo. Su paciencia ha sido infinita. Aunque ellos han vivido esta experiencia más de lejos, también tengo que agradecer todo el apoyo que me han dado a mi familia; mi ama, mi aita, mi hermano, mi tía Pili y por supuesto mi prima Jone, todo un referente como investigadora, que siempre ha estado interesada en este proyecto, apoyándome y animándome en la aventura de la tesis doctoral.

Además, esta tesis no hubiera sido posible sin la ayuda de muchas otras personas que me han acompañado en el día a día. Comienzo con Natalia, la única compañera de despacho que he mantenido desde los inicios, a ella tengo que agradecerte que haya estado a mi lado durante estos tres años, sacándome una sonrisa incluso en los malos momentos. Sin duda Lucía ha sido otra de las personas clave, compartiendo conmigo innumerables tazas de té, conversaciones y buenos momentos. Gracias a las dos por vuestra simpatía.

Por supuesto tengo que dar las gracias al resto de compañeros de grupo; a Dani, por sus visitas diarias al despacho preocupándose por el estado de la tesis, a Amaia por su ayuda con los las figuras, gracias por todo el tiempo que me has dedicado, a Isabel y Alex por su ayuda en el laboratorio, el pHmetro se me hubiera resistido sin ellos, a mi compañero de despacho Thomas por los buenos momentos conversando sobre monte y atletismo, y a Beatriz, por interesarse por el trabajo y ofrecerme su ayuda en la recta final de la tesis. Gracias también al resto de los compañeros como Jon, Marina, Ana Lucia, Paula, Edurne, Gerardo, Guido, Maud y Jordan por haberme prestado vuestro apoyo cuando lo he necesitado.

No me puedo olvidar de los que ya no están en el grupo pero que tanto me ayudaron en los comienzos de esta tesis; Luisa, Irma y Ana. Y por supuesto Manuel, que desde China ha seguido interesándose por el trascurso de la tesis. Ya no les veo, pero el agradecimiento es el mismo. Asimismo, quiero agradecer al resto de los compañeros del "Polymers and Soft Matter Group'' que en algún momento u otro me han prestado su ayuda.

I would also like to thank Christoffer Olsson for being always ready to help me even from Sweden.

Una vez más, gracias, esta tesis lleva un poquito de todos vosotros.

Por último, quisiera agradecer el apoyo financiero obtenido por la Universidad del País Vasco (UPV / EHU) para el cumplimiento del programa de doctorado.